



**UNIVERSIDADE ESTADUAL DE FEIRA DE
SANTANA
PROGRAMA DE PÓS-GRADUAÇÃO EM
BIOTECNOLOGIA**



CÁSSIO SANTANA MEIRA

**INVESTIGAÇÃO DA ATIVIDADE ANTI-*Trypanosoma cruzi*
DE ESTEROIDES ISOLADOS DE PLANTAS E
DERIVADOS SINTÉTICOS**

Feira de Santana, BA
2014

CÁSSIO SANTANA MEIRA

**INVESTIGAÇÃO DA ATIVIDADE ANTI-*Trypanosoma cruzi*
DE ESTEROIDES ISOLADOS DE PLANTAS E
DERIVADOS SINTÉTICOS**

Dissertação apresentada ao Programa de Pós-graduação em Biotecnologia, da Universidade Estadual de Feira de Santana como requisito parcial para obtenção do título de Mestre em Biotecnologia.

Orientadora: Prof^a. Dr^a. Milena Botelho Pereira Soares

Feira de Santana, BA
2014

AGRADECIMENTOS

Gostaria de agradecer inicialmente a minha família e amigos, pelo apoio, incentivo para superar os obstáculos e amor que sempre me foram dados, em especial a **minha mãe Waldimara Silva Santana**, que está sempre vibrando a cada conquista minha e, acima de tudo, estendendo a mão em cada momento difícil.

À **Luana Muniz Ribeiro Rodrigues** por sempre estar ao meu lado, nos momentos alegres ou tristes, e por me estimular a sempre fazer o meu melhor.

A minha orientadora, **Dra. Milena Botelho Pereira Soares**, por acreditar no meu potencial e contribuir de forma significativa para meu crescimento científico e pessoal.

À **Dra. Elisalva Teixeira Guimarães** (CPqGM) e ao **Dr. Diogo Rodrigo Magalhães Moreira** (CBTC/HSR), por estarem sempre à disposição para ajudar em todos os momentos e por terem contribuído para a minha formação científica durante o mestrado.

À **Dra. Simone Garcia Macambira** (CPqGM) e a **Dra. Fabiana Regina Nonato** (CPqQBA) por terem apostado em mim a todo o momento e pelo incentivo dado ao longo do tempo.

A todos os meus amigos do LETI, em especial algumas pessoas que os laços de amizade foram mais fortes: **Tanira Matutino, Jamyle Santos e Juliana Leal** por estarem sempre à disposição para ajudar em todos os momentos, principalmente nos experimentos; **Afrânio Evangelista, Nanashara Carvalho, Taís Macedo, Vinícius Rocha, Gisele Leite e Kelly Gama** pela amizade e pelos momentos de conversas nada científicas.

À **Dra. Adriana Lanfredi Rangel** (CPqGM) e a **Dra. Maria Lúcia Vieira Moreno** (CPqGM) pelos ensinamentos passados e pela amizade.

Aos **colegas** da Pós- graduação em Biotecnologia.

Ao secretário da PPgBiotec, **Helton Ricardo**, pela paciência e dedicação para com os alunos do programa.

À **Universidade Estadual de Feira de Santana**, por ter me proporcionado um ensino de qualidade.

Ao **Centro de Pesquisas Gonçalo Moniz**, pela estrutura que proporcionou a minha participação em diversos projetos de pesquisa.

À **FAPESB** pela concessão da bolsa, imprescindível para a realização deste trabalho.

“Você nasceu para vencer, mas para ser um vencedor você precisa planejar para vencer, se preparar para vencer, e esperar vencer.”

Zig Zglar

RESUMO

A doença de Chagas é uma zoonose causada pelo protozoário hemoflagelado *Trypanosoma cruzi*, que afeta milhões de pessoas na América Latina. O tratamento dessa enfermidade se baseia na utilização de dois fármacos, o benzonidazol e o nifurtimox, que possuem baixa taxa de cura na fase crônica da doença, além de gerarem uma série de efeitos colaterais. Nesse contexto, o surgimento de novos medicamentos para uma quimioterapia mais adequada da doença de Chagas torna-se necessário. Neste estudo investigamos o potencial anti-*T. cruzi* de esteroides isolados de plantas, fisalinas e ácido betulínico, assim como de derivados sintéticos deste último, em ensaios *in vitro*. Nossos resultados demonstram uma elevada atividade tripanocida das fisalinas B e F e do derivado BA5 contra formas tripomastigotas e sobre os processos de invasão e desenvolvimento destas em macrófagos peritoneais. Através de ensaios de microscopia eletrônica foi possível observar que o tratamento com a fisalina B ou com o derivado BA5 causa alterações ultraestruturais na membrana plasmática, complexo de Golgi, cinetoplasto e retículo endoplasmático das formas tripomastigotas, além da formação de vacúolos atípicos e o aparecimento de figuras mielínicas, que foram marcadas com MDC para confirmar a sua identidade como vacúolos autofágicos. Análises por citometria de fluxo revelaram que a morte parasitária ocorre principalmente por necrose. A combinação da fisalina B, da fisalina F ou do derivado BA5 com o benzonidazol resultou em uma maior atividade anti-*T. cruzi* frente a formas amastigotas quando comparados aos compostos testados de forma isolada. Estes resultados indicam que esteroides, tais como as fisalinas B e F e o derivado BA5, são potenciais candidatos para o tratamento alternativo da doença de Chagas.

Palavras-Chaves: Doença de Chagas, *Trypanosoma cruzi*, esteroides, fisalinas, ácido betulínico.

ABSTRACT

Chagas disease is a zoonosis caused by the hemoflagellate protozoan *Trypanosoma cruzi*, which affects millions of people in Latin America. Disease treatment is based on the use of two drugs, benznidazole and nifurtimox, which present low cure rates in the chronic phase of the disease as well as generating a number of adverse side effects. In this context, the development of new therapies for a better treatment of Chagas disease is necessary. In this study we investigated the anti-*T.cruzi* potential of physalins and betulinic acid, plant-based isolated steroids, in addition to synthetic derivatives from the latter, in *in vitro* assays. Our results demonstrate a high trypanocidal activity of physalins B and F and of the derivative BA5 against trypomastigote forms and on the processes of invasion and development of these on peritoneal macrophages. Electron microscopy revealed that physalin B or BA5 derivative treatment resulted in ultrastructural changes in the plasma membrane, Golgi apparatus, kinetoplast and endoplasmic reticulum of trypomastigotes forms. Additionally, these compounds contributed to the formation of atypical vacuoles in the appearance of myelin figures, which were labeled with MDC to confirm their identity as autophagic vacuoles. Flow cytometry analysis revealed that parasite death occurred mainly by necrosis. When combined with benznidazole, physalin B, physalin F or BA5 derivative, resulted in a higher anti-*T. cruzi* activity against amastigotes when compared to the compounds tested alone. These results indicate that steroids, such as physalins B and F and the derivative BA5, are potential candidates for an alternative treatment of Chagas disease.

Keywords: Chagas disease, *Trypanosoma cruzi*, steroids, physalins, betulinic acid.

LISTA DE FIGURAS

Figura 1. Municípios brasileiros com casos registrados de doença de Chagas aguda no período de 2000 a 2010.

Figura 2 - Rotas de migração da América Latina e estimativa do número total de indivíduos infectados com *T. cruzi* em países não endêmicos.

Figura 3. Ciclo biológico do *Trypanosoma cruzi*.

Figura 4. Estrutura química dos medicamentos disponíveis na clínica. (A) Benzonidazol; (B) Nifurtimox.

Figura 5. Estrutura química das fisalinas B, D, F e G.

Figura 6. Estrutura química do ácido betulínico.

LISTA DE ABREVIACOES

BAA	Acetato do �cido betul�nico
BAME	�ster met�lico do �cido betul�nico
BAMEA	Acetato do �ster met�lico do �cido betul�nico
BOA	�cido betul�nico
DNA	�cido desoxirribonucleico
HIV	Virus da imunodefici�ncia humana
IgG	Imunoglobulina G
MDC	Monodansilcadaverina
MS	Minist�rio da Sa�de
NECT	Terapia combinada com nifurtimox e eflortina
OMS	Organiza�o Mundial da Sa�de
PPM	Partes por milh�o
SSG & PM	Terapia combinada com estibogluconato de s�dio e paromomicina
SVS	Secretaria de Vigil�ncia em Sa�de

SUMÁRIO

1 INTRODUÇÃO GERAL	10
2 OBJETIVOS	12
2.1 GERAL	12
2.2 ESPECÍFICOS	12
3. REVISÃO DE LITERATURA	13
3.1 O <i>Trypanosoma cruzi</i>	13
3.2 CICLO DE VIDA DO <i>Trypanosoma cruzi</i>	14
3.3 A DOENÇA DE CHAGAS	17
3.4 TRATAMENTO	18
3.5 PRODUTOS NATURAIS	20
3.6 AS FISALINAS	21
3.7 O ÁCIDO BETULÍNICO	23
4. CAPÍTULO 1	26
4.1 INTRODUÇÃO	27
4.2 MATERIAIS E MÉTODOS	28
4.3 RESULTADOS	30
4.4 DISCUSSÃO	32
4.5 CONCLUSÃO	36
4.6 REFERÊNCIAS	36
5 CAPÍTULO 2	38
5.1 INTRODUÇÃO	41
5.2 MATERIAIS E MÉTODOS	42
5.3 RESULTADOS	47
5.4 DISCUSSÃO	51
5.5 CONCLUSÃO	53
5.6 REFERÊNCIAS	55
6 DISCUSSÃO GERAL	74
7 CONCLUSÕES/SUMÁRIO DE RESULTADOS	77
8 REFERÊNCIAS	78
9 ANEXOS	90

1 INTRODUÇÃO GERAL

As doenças infecciosas parasitárias afetam milhões de pessoas nas diferentes regiões do planeta e são responsáveis por incapacitar uma fração significativa da população mundial, principalmente em países em desenvolvimento (KETTLER & MARJANOVIC, 2004). Dentre estas doenças se destaca a doença de Chagas (CHAGAS, 1909), uma zoonose causada pelo protozoário hemoflagelado *Trypanosoma cruzi*, que afeta milhões de pessoas na América Latina (PINTO-DIAS, 2006). Estimativas indicam que a infecção acomete cerca de 10 milhões de pessoas na América Latina e é responsável por quatorze mil mortes por ano apenas no Brasil (WHO, 2010; REA *et al.*, 2013).

Uma vez que o indivíduo tenha sido infectado pelo *T. cruzi*, não existe tratamento disponível efetivo para a doença e o desenvolvimento de uma vacina ainda se encontra em estágio experimental (MAYA *et al.*, 2007 GUPTA *et al.*, 2013). As únicas opções de tratamento existentes por mais de 40 anos têm sido os fármacos benzonidazol e nifurtimox. Ambos os quimioterápicos apresentam boas taxas de cura na fase aguda da doença (RASSI *et al.*, 2000), porém são responsáveis por uma série de efeitos colaterais que incluem erupções cutâneas, náuseas, insuficiência renal e hepática e neuropatia periférica (CLAYTON, 2010). Além da toxicidade, já existem relatos de cepas de *T. cruzi* resistentes a estes medicamentos (FILARDY & BRENER, 1987; NEAL & VAN BUEREN, 1988; MURTA *et al.*, 1998). Outra limitação é a fraca ação destes compostos na fase crônica da infecção, que corresponde à forma mais prevalente da doença.

Alternativas promissoras para o benzonidazol e o nifurtimox incluem os inibidores de cruzaina e da biossíntese de ergosterol. Entre os inibidores de cruzaina, o peptídeo K11777 destaca-se pela potente atividade tripanocida. Atualmente, esta molécula encontra-se em estudo clínico de fase I (SAJID *et al.*, 2011). Dentre os inibidores de ergosterol, um exemplo promissor é o posaconazol, com atividade promissora em estudos pré-clínicos e atualmente é o candidato em estudo mais avançado em ensaios clínicos, encontrando-se em estudo clínico de fase II (BUCKNER & URBINA, 2012). Em contraposição, estes compostos possuem um elevado custo de produção, o que pode representar um obstáculo na terapia da doença de Chagas (URBINA, 2010). Considerando-se que o uso terapêutico dos compostos atualmente

disponíveis é limitado, torna-se de grande valia a busca de quimioterápicos alternativos mais eficazes no tratamento da doença de Chagas.

Nesse contexto, a investigação de plantas medicinais e derivados sintéticos originadas de substâncias naturais está entre as estratégias mais utilizadas recentemente no planejamento de agentes antiparasitários (NEWMAN & CRAGG, 2007). Com base em estudos antiparasitários realizados com esteroides extraídos de plantas ou obtidos a partir de precursores vegetais, este trabalho propõe a utilização de esteroides naturais e sintéticos na realização de testes anti- *T. cruzi*, com a finalidade de buscar uma nova alternativa terapêutica no tratamento da doença de Chagas.

2 OBJETIVOS

2.1 OBJETIVO GERAL

Investigar a atividade anti-*T. cruzi* e o mecanismo de ação de esteroides isolados de plantas, fisalinas e ácido betulínico, assim como de derivados sintéticos deste último, em ensaios *in vitro*.

2.2 OBJETIVOS ESPECÍFICOS

- Avaliar o potencial citotóxico dos diferentes esteroides testados;
- Verificar a capacidade destes compostos em inibir a viabilidade de formas tripomastigotas;
- Verificar a capacidade destes compostos em inibir a ação enzimática da cruzaina;
- Determinar as alterações ultraestruturais em tripomastigotas tratados com os compostos mais ativos;
- Determinar o padrão de morte celular em tripomastigotas tratados com os compostos mais ativos;
- Avaliar a capacidade dos compostos em inibir a invasão e o desenvolvimento de formas tripomastigotas em macrófagos peritoneais infectados por *T. cruzi*;
- Avaliar o efeito da combinação dos compostos mais ativos com o benzonidazol no desenvolvimento de formas tripomastigotas em macrófagos peritoneais.

3 REVISÃO DE LITERATURA

3.1 O *Trypanosoma cruzi*

O protozoário flagelado *Trypanosoma cruzi* é o agente causador da doença de Chagas, uma infecção tropical presente principalmente no continente americano. Este parasito pertence à ordem Kinetoplastida e à família Trypanosomatidae, cuja principal característica é a presença de flagelo e cinetoplasto, região da mitocôndria onde se concentra uma grande quantidade de DNA extranuclear (SOUZA, 2002). Estimativas indicam que a infecção acomete cerca de 10 milhões de pessoas na América Latina e é responsável por quatorze mil mortes por ano apenas no Brasil (WHO, 2010; REA *et al.*, 2013).

No Brasil, segundo dados do Ministério da Saúde, no período 2000 a 2010, foram registrados 945 casos da doença de Chagas aguda (**Figura 1**). Estima-se que existem aproximadamente dois milhões de pessoas infectadas no Brasil (SVS/MS, 2010). A doença é transmitida por insetos triatomíneos pertencentes à família Reduviidae, mais especificamente da subfamília Triatominae (COURA *et al.*, 2002), sendo as espécies de maior contribuição na transmissão vetorial o *Triatoma infestans*, *T. dimidiata*, *T. sordida*, *Rhodinus prolixus* e *Panstrongylus megistus* (GARCIA & AZAMBUJA, 1991).

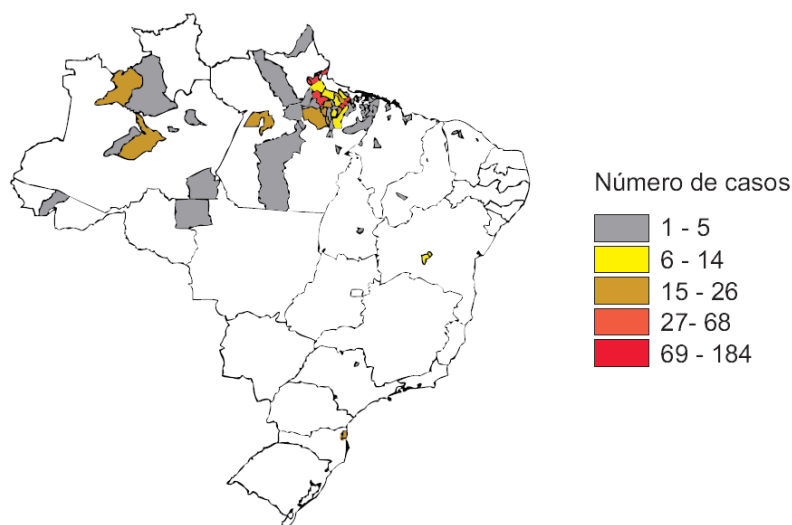


Figura 1 – Municípios brasileiros com casos registrados de doença de Chagas aguda no período de 2000 a 2010. Fonte: SVS/MS.

O aumento dos movimentos migratórios de países endêmicos para países não endêmicos contribuiu para uma mudança no cenário mundial da doença de Chagas. Estima-se que mais de 400.000 indivíduos estejam infectados em países não endêmicos, principalmente nos Estados Unidos e em países da Europa (**Figura 2**) (SCHMUNIS, 2007; COURA & VIÑAS, 2010). Essa nova distribuição reforçar a necessidade de melhorar a vigilância e criar medidas específicas para o combate à doença de Chagas nos países não endêmicos.

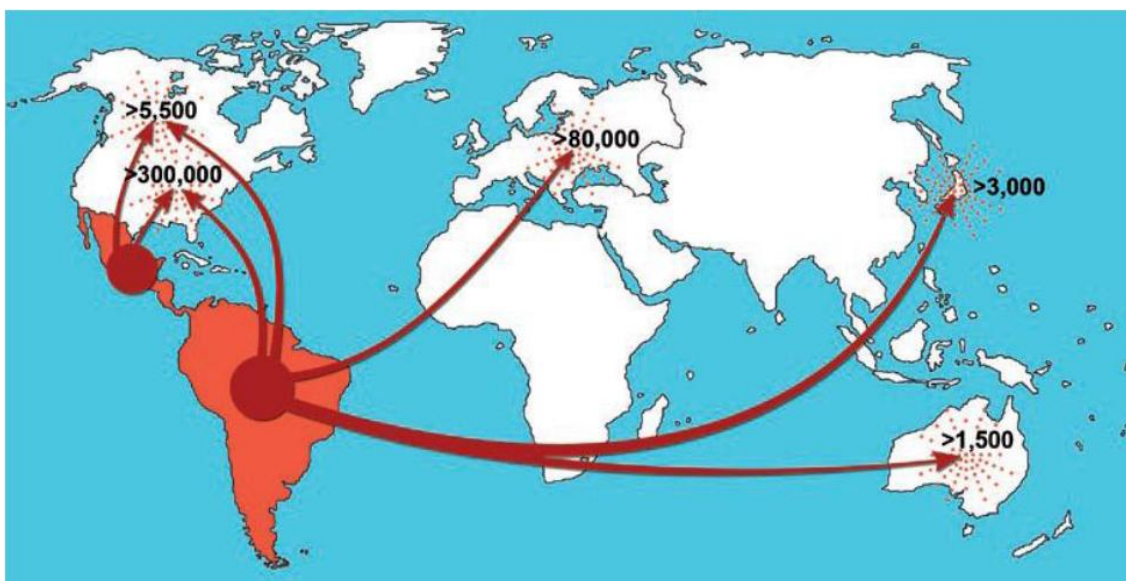


Figura 2 - Rotas de migração da América Latina e estimativa do número total de indivíduos infectados com *T. cruzi* em países não endêmicos. Fonte: COURA & VIÑAS, 2010.

3.2 CICLO DE VIDA DO *Trypanosoma cruzi*

O *T. cruzi* possui um ciclo de vida complexo que compreende diferentes formas morfológicas em hospedeiros vertebrados e invertebrados (COURA *et al.*, 2002). O parasito se apresenta sob três formas: uma forma replicante encontrada no citoplasma das células do hospedeiro vertebrado, conhecida como forma amastigota (do grego, a = desprovido; mastis = chicote, uma alusão ao flagelo); uma forma flagelada, fusiforme, infectiva para vertebrados, incapaz de dividir-se e presente nos hospedeiros vertebrados (tripomastigotas sanguíneos) e nos invertebrados (tripomastigotas metacíclicos); outra forma flagelada que não é infectiva para vertebrados, que replica-se por fissão binária e

está tipicamente presente no intestino médio do hospedeiro invertebrado e é conhecida como forma epimastigota (SOUZA, 2002).

O ciclo de vida se inicia quando um triatomíneo infectado, após a realização do repasto sanguíneo, elimina fezes e urina contendo formas tripomastigotas metacíclicas do parasito, que são capazes de infectar o hospedeiro vertebrado quando entram em contato com mucosas do olho, boca, ferimentos ou quando forem ingeridas (BRENER, 2000). Uma vez dentro do hospedeiro, a interação parasito-hospedeiro ocorre de forma dinâmica, resultante de múltiplos fatores ligados ao *T. cruzi* (cepa, virulência, tamanho do inóculo) e ao homem (sexo, idade, raça) (ANDRADE *et al.*, 1985). Dentro do hospedeiro vertebrado, as formas tripomastigotas podem invadir macrófagos e uma variedade de outras células, podendo residir por algum tempo dentro de fagolisossomos. Quando escapam para o citoplasma, estas se diferenciam para as formas amastigotas e proliferam por divisão binária. Após sucessivas divisões, as formas amastigotas iniciam a sua diferenciação, passando por um período de transição e se diferenciando em formas tripomastigotas sanguíneas. O rompimento da célula hospedeira pode ocorrer antes da total diferenciação de formas amastigotas em formas tripomastigotas, o que gera o aparecimento de diferentes formas no meio externo. No meio extracelular, os tripomastigotas e amastigotas podem atingir outras regiões e infectar novas células (GARCIA & AZAMBUJA, 1991; SOUZA, 2002).

O ciclo de vida se completa quando o sangue contendo formas tripomastigotas sanguíneas de um hospedeiro vertebrado infectado é sugado por um triatomíneo, durante o seu repasto sanguíneo. As formas tripomastigotas sanguíneas se diferenciam em formas epimastigotas na porção média do trato gastrointestinal do inseto e multiplicam-se por fissão binária. Essa forma está adaptada para sobreviver à ação de enzimas presentes no trato gastrointestinal do inseto devido a uma cobertura resistente à ação de proteases e glicosidades, presente na sua superfície (SOUZA, 2002). No intestino posterior, os parasitos sofrem uma diferenciação celular denominada metaciclogênese. Esta envolve mudanças morfológicas e metabólicas que dão origem a formas tripomastigotas metacíclicas, que são as formas liberadas nas excretas dos insetos e capazes de infectar vertebrados (GARCIA & AZAMBUJA, 1991) (**Figura 3**).

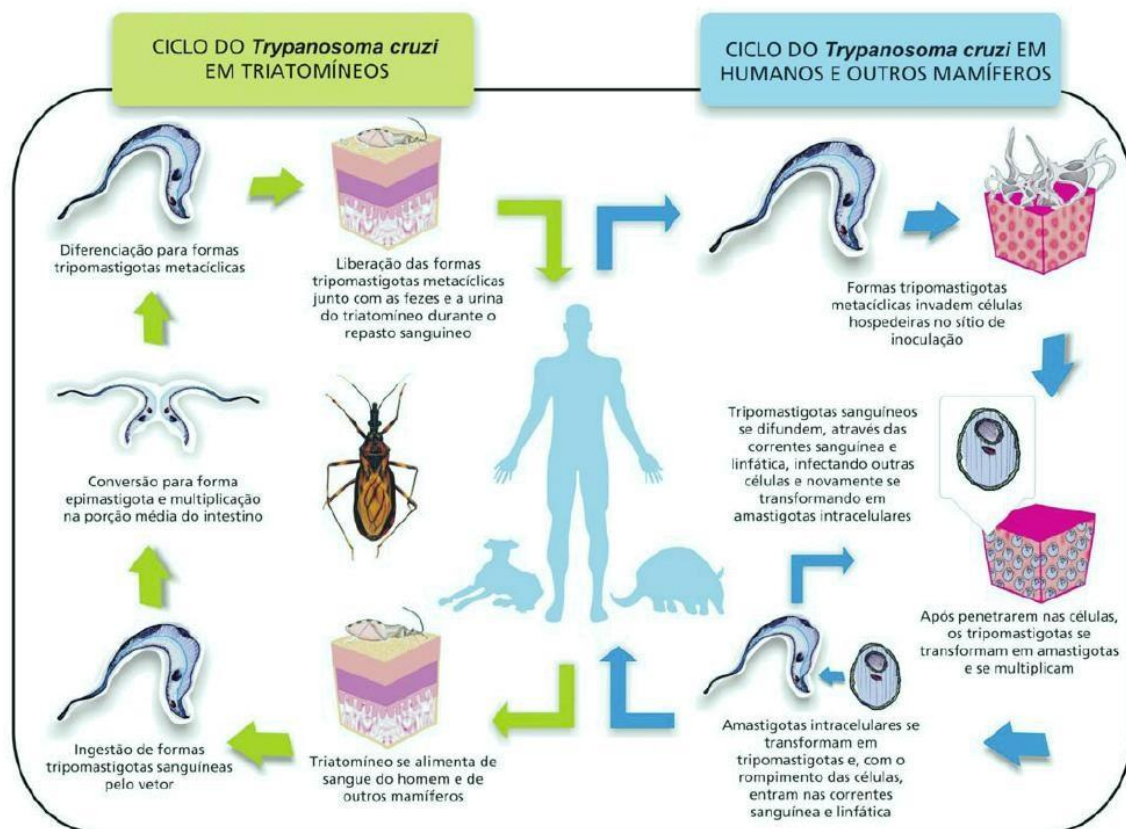


Figura 3 - Ciclo biológico do *Trypanosoma cruzi*. Fonte: Infográfico; Venício Ribeiro, ICICT/Fiocruz.

O parasito pode ainda penetrar no hospedeiro vertebrado por outras vias, tais como: transfusão sanguínea, transplante de órgãos, transmissão congênita ou ingestão acidental de insetos triturados junto a alimentos (contaminação por via oral) (YOSHIDA, 2008).

Casos agudos resultantes da ingestão acidental do parasito têm sido registrados por surtos em diferentes localidades, com maior incidência na região amazônica, onde o consumo de açaí é uma frequente causa de contaminação (MONCAYO & SILVEIRA, 2009). Em 2007, em uma escola de Caracas, Venezuela, 103 crianças foram infectadas com o consumo de suco de goiaba contaminado. Destas, 75 apresentaram sintomatologia para doença de Chagas aguda e uma criança veio a óbito (ALARCÓN DE NOYA *et al.*, 2010). No Brasil, em 2005, 24 casos agudos da doença foram registrados em Santa Catarina, e todos eles foram relacionados com a ingestão de caldo de cana contaminado com o parasito (STEINDEL *et al.*, 2008).

3.3 A DOENÇA DE CHAGAS

A infecção pelo *T. cruzi* inicialmente era restrita a pequenos mamíferos de regiões de matas e campos da América, desde a Patagônia até o sul dos Estados Unidos. Esses animais (tatus, gambás, roedores) conviviam com "barbeiros" silvestres e, entre eles, ainda hoje circula o *T. cruzi* (TARLETON *et al.*, 2007). Com a chegada do homem e os processos de colonização, desequilíbrios ecológicos aconteceram (desmatamentos, queimadas) e os barbeiros invadiram as habitações próximas a ambientes naturais. Como resultado, a infecção chegou ao homem (doença de Chagas) e aos mamíferos domésticos.

A infecção chagásica apresenta duas fases bem distintas: uma fase aguda, correspondente à infecção e disseminação do *T. cruzi* no organismo, e uma fase crônica, caracterizada por duas formas distintas: indeterminada e crônica sintomática. Na maioria dos casos, independente da via de transmissão, a fase aguda da doença é assintomática, provavelmente devido a uma baixa carga parasitária tecidual (RASSI *et al.*, 2010a; KIRCHHOFF, 2011). Contudo, quando a doença se manifesta, o portador apresenta um quadro febril ou outras manifestações clínicas, tais como hepatoesplenomegalia, náuseas, vômitos, diarreia e anorexia. A fase aguda sintomática ocorre principalmente em crianças na primeira década de vida, podendo levar à morte devido a complicações decorrentes de insuficiência cardíaca e processos inflamatórios que envolvem o cérebro (BOAINAIN & RASSI, 1979; RASSI *et al.*, 2010a).

Na grande maioria das vezes, após a fase aguda, a doença de Chagas evolui para fase crônica (RASSI *et al.*, 2010a). A maioria dos indivíduos infectados (cerca de 70%) desenvolve a forma crônica indeterminada da doença, que não apresenta sintomas clínicos. Contudo, cerca de 30% dos indivíduos infectados, após meses ou décadas da infecção evoluem para a fase crônica sintomática: cardíaca, digestiva ou mista. Essa forma da doença é caracterizada pela baixa parasitemia, porém com lesão tecidual e altos índices de anticorpos IgG (ANDRADE *et al.*, 2000).

A forma cardíaca é conhecida por ser a mais grave e frequente manifestação da fase crônica da doença de Chagas. Ela se desenvolve em 20 a 30% dos indivíduos crônicos e é caracterizada por miocardite crônica, insuficiência cardíaca e eventualmente morte súbita, por arritmia cardíaca (RASSI *et al.*, 2000; MARIN-NETO *et al.*, 1999; MARIN-NETO *et al.*, 2010). A forma digestiva, que se desenvolve em 10 a

15% dos indivíduos crônicos, ocorre quase que exclusivamente no sul da bacia amazônica (principalmente na Argentina, Brasil, Chile e Bolívia) e é rara no norte da América do Sul, América Central e México (RASSI *et al.*, 2010a; RASSI *et al.*, 2010b). Essa distribuição geográfica bem definida é provavelmente explicada pelas diferenças existentes entre as cepas do parasito que circulam em cada uma dessas regiões (MILES *et al.*, 2003; CAMPBELL *et al.*, 2004). Esta forma é caracterizada pelo desenvolvimento de disfunções gastrointestinais (principalmente megaesôfago, megacólon ou ambos). Além das duas formas descritas anteriormente, há relatos da existência de uma forma mista, que corresponde à associação entre as formas cardíaca e a digestiva. Em muitos países, o desenvolvimento de megaesôfago geralmente precede o aparecimento de megacólon e/ou da forma cardíaca, contudo a prevalência da forma mista é desconhecida, devido à escassez de estudos apropriados (RASSI *et al.*, 2010a).

3.4 TRATAMENTO

Atualmente, apenas duas drogas estão disponíveis para o tratamento da doença de Chagas, o nitroimidazol benzonidazol e o nitrofurano nifurtimox (**Figura 4**), ambos introduzidos na clínica há mais de 40 anos (COURA, 2003). Estes fármacos atuam através da formação de radicais livres e/ou metabólitos eletrofílicos, que geram danos a proteínas, lipídios e ao DNA do *T. cruzi* (DIAS, 2009). O benzonidazol por apresentar um melhor perfil de eficácia e segurança, quando comparado com o nifurtimox, é utilizado para o tratamento de primeira linha (VIOTTI *et al.*, 2006). Em indivíduos adultos, a dose recomendada de benzonidazol é de 5 mg/Kg por dia, durante um período de 60 dias, enquanto que a dose recomenda de nifurtimox é de 8-10 mg/Kg por dia, durante um período de 60-90 dias (MS, 2005). A intervenção com estes compostos é recomendada em pacientes com a infecção aguda, em crianças, em pessoas recém-infectadas, naqueles com a forma congênita da doença de Chagas e em casos de reagudização devido à imunossupressão (ANDRADE *et al.*, 2011).

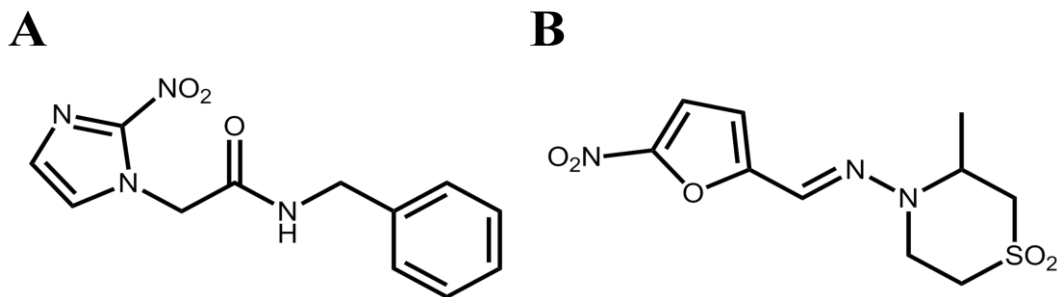


Figura 4. Estrutura química dos medicamentos disponíveis na clínica. (A) Benzonidazol; (B) Nifurtimox.

Ambos os quimioterápicos apresentam boas taxas de cura na fase aguda da doença, sendo capazes de alcançar taxas de cura superiores a 81% (RASSI *et al.*, 2000). Apesar disso, estes são responsáveis por uma série de efeitos colaterais quando administrados por um período prolongado (CASTRO *et al.*, 2006). Este fato é particularmente problemático, visto que um grande número de doses deve ser administrado por um período longo (60 a 90 dias) para que o tratamento obtenha sucesso. Os principais efeitos colaterais causados pela utilização destes medicamentos incluem erupções cutâneas, náuseas, insuficiência renal e hepática e neuropatia periférica (CLAYTON, 2010).

Além da toxicidade, existe uma variação significativa na susceptibilidade de isolados do parasito à ação dessas drogas, algumas cepas naturalmente susceptíveis e resistentes a estes compostos já foram relatadas (FILARDY & BRENER, 1987; NEAL & VAN BUEREN, 1988; MURTA *et al.*, 1998). Outra limitação é a fraca ação destes compostos na fase crônica da infecção. Alguns estudos apontam para um efeito benéfico do benzonidazol, na forma crônica da doença de Chagas. GARCIA e colaboradores (2005) demonstraram uma relação direta entre a diminuição do parasitismo tecidual, diminuição do infiltrado inflamatório e do percentual de área ocupada por tecido fibrótico em animais crônicos tratados com benzonidazol. Recentemente foi iniciado um estudo clínico multicêntrico e duplo cego (BENEFIT – Benzinidazole Evaluation for Interrupting Trypanosomiasis) que visa avaliar o efeito do benzonidazol em 3.000 pacientes (18-75 anos) portadores da fase crônica da doença de Chagas (MARIN-NETO *et al.*, 2008).

Outras alternativas para o tratamento da doença de Chagas incluem inibidores da cruzaina (ou cruzipaína), a principal cisteína protease do parasito, e inibidores da biossíntese de ergosterol. A cruzaina desempenha um papel importante no processo de

internalização do parasito em células de mamíferos (SOUTO-PADRON *et al.*, 1990) e na replicação intracelular do *T. cruzi* (MEIRELLES *et al.*, 1992; MCKERROW *et al.*, 2006). Entre os inibidores de cruzaina, o peptídeo K11777 se destaca pela potente atividade *in vitro* e pelo efeito benéfico sobre camundongos infectados em modelos de infecção aguda e crônica da doença de Chagas. Atualmente, este inibidor se encontra em estudo clínico de fase I (SAJID *et al.*, 2011). Compostos capazes de inibir a síntese de ergosterol também são potenciais candidatos para o tratamento da doença de Chagas. Um exemplo promissor é o posaconazol que atua sobre a enzima C14 α -esterol desmetilase do parasito. Este antifúngico apresentou uma atividade promissora em estudos pré-clínicos e atualmente é o candidato em estudo mais avançado nos ensaios clínicos, encontrando-se em estudo clínico de fase II (BUCKNER & URBINA, 2012). Apesar de promissores, o elevado custo para a produção destes compostos pode representar um obstáculo, tendo em vista que a população chagásica, em sua maioria, possui um baixo poder aquisitivo (URBINA, 2010).

3.5 PRODUTOS NATURAIS

Os produtos naturais são moléculas orgânicas que podem ter origem animal, vegetal ou microbiana. Eles são detentores de uma grande diversidade química e de inúmeras propriedades biológicas. Por milhares de anos, os produtos naturais foram à única fonte de recursos para o tratamento de doenças humanas (YOGEE SWARI & SRIRAM, 2005). Os estudos com produtos naturais possibilitaram a obtenção de inúmeros medicamentos, como por exemplo, a morfina e a aspirina. A morfina, um opióide isolado da planta *Papaver somniferum* consiste em um dos mais potentes analgésicos conhecidos pelo homem e foi essencial na investigação a cerca do funcionamento dos receptores opióides e das vias de endorfinas e encefalinas (IGNELZI & ATKINSON, 1980). A aspirina, um dos medicamentos mais consumido em todo o mundo, tem como princípio ativo o ácido acetilsalicílico obtido a partir do ácido salicílico, substância isolada da *Spiraea ulmaria*, e possui atividade analgésica e antiinflamatória (BOSCH & BANOS, 1998).

Embora os produtos naturais tenham dado uma enorme contribuição para a entrada de novos medicamentos no mercado, em meados do século XX, houve um

aumento gradativo de interesse em produtos sintéticos pela indústria farmacêutica. O interesse em produtos sintéticos aumentou devido aos avanços da química, farmacologia e biologia molecular, que agregados a novos ensaios bioquímicos foram responsáveis pela introdução da triagem de alta-eficiência na década de 90 e pela introdução da química combinatorial (SCHMIDT *et al.*, 2008). Essas mudanças no cenário da indústria farmacêutica diminuíram sensivelmente o interesse em produtos naturais entre 1984 e 2003, que se traduziu no menor volume de investimentos da indústria farmacêutica neste setor (NEWMAN & CRAGG, 2007).

Apesar disso, mais de 60% das novas drogas aprovadas entre os anos de 1981 e 2006 são oriundas direta ou indiretamente de produtos naturais (NEWMAN & CRAGG, 2007). Esse dado, juntamente com os avanços nas técnicas de separação, purificação e identificação de misturas complexas de produtos e a diversidade estrutural presente na natureza, são os responsáveis pela renovação do interesse da indústria farmacêutica nos últimos anos (YOGEE SWARI & SRIRAM, 2005). Desta forma, os produtos naturais permanecem como uma valiosa fonte de busca de novas moléculas para o desenvolvimento de novos medicamentos.

3.6 AS FISALINAS

Physalis angulata L. (Solanaceae) é uma planta herbácea de ciclo anual amplamente difundida nas regiões tropicais e subtropicais dos continentes asiático, africano e sul-americano (TOMASSINI *et al.*, 2000; SILVA & AGRA, 2005; DI STASI & LIMA, 2002). Popularmente é conhecida como mullaca, camapú, bucho de rã e balãozinho (LIN, 1992; CHIANG, 1992). Esta planta pode ser encontrada em todo o território brasileiro e é muito utilizada na medicina popular e na alimentação. Na medicina popular é utilizada com ação anti-inflamatória, antireumática, diurética, sudorífera e para o tratamento da bexiga e do fígado (AGRA, 1980; ALMEIDA, 1993; DUKE & VASQUEZ, 1994). Análises fitoquímicas de extratos da *P. angulata* demonstram a presença de uma variedade de substâncias tais como, flavonoides, alcaloides e uma classe de seco-esteroides, as fisalinas (SOARES *et al.*, 2003; NAGAFUJI *et al.*, 2004).

As fisalinas são vitaesteroides derivados do ergostano com modificações tipo 16-24-ciclo-13-14-seco, de estruturas bastante complexas (TOMASSINI *et al.*, 2000). Estão presentes normalmente a níveis de 30 a 500 partes por milhão (ppm) em raízes, caule e folhas da espécie. Diversos estudos vêm sendo realizados com as fisalinas isoladas da *P. angulata*, comprovando experimentalmente as suas ações biológicas. A atividade antitumoral, bactericida, anti-inflamatória e imunomoduladora já estão descritas na literatura (KAWAI *et al.*, 1991; SILVA *et al.*, 2005; VIERA *et al.*, 2005; MAGALHÃES *et al.*, 2006; SOARES *et al.*, 2006; HELVACI *et al.*, 2010).

Trabalhos recentes também descrevem o potencial antiparasitário dessas moléculas. SÁ e colaboradores (2010) demonstraram o potencial antimalárico das fisalinas B, D, F e G (**Figura 5**). Através de ensaios *in vitro* frente ao *Plasmodium falciparum* foi possível identificar uma potente atividade antimalárica destas fisalinas. SÁ e colaboradores (2010) também demonstraram um efeito benéfico do tratamento de camundongos infectados com *P. berghei* com a fisalina D (50 e 100 mg/Kg), através da redução da parasitemia e o aumento da sobrevida dos animais infectados. A atividade leishmanicida dessas moléculas também já foi comprovada. GUIMARÃES e colaboradores (2009) demonstraram a capacidade das fisalinas B e F em reduzir a proliferação de formas amastigotas em macrófagos infectados com *Leishmania amazonensis* ou *Leishmania major*. Além da potente atividade *in vitro*, os autores também observaram o efeito terapêutico da fisalina F em camundongos infectados com *L. amazonensis*, onde foi possível observar a redução da lesão na derme da orelha dos animais infectados e a redução da carga parasitária em relação aos animais não tratados.

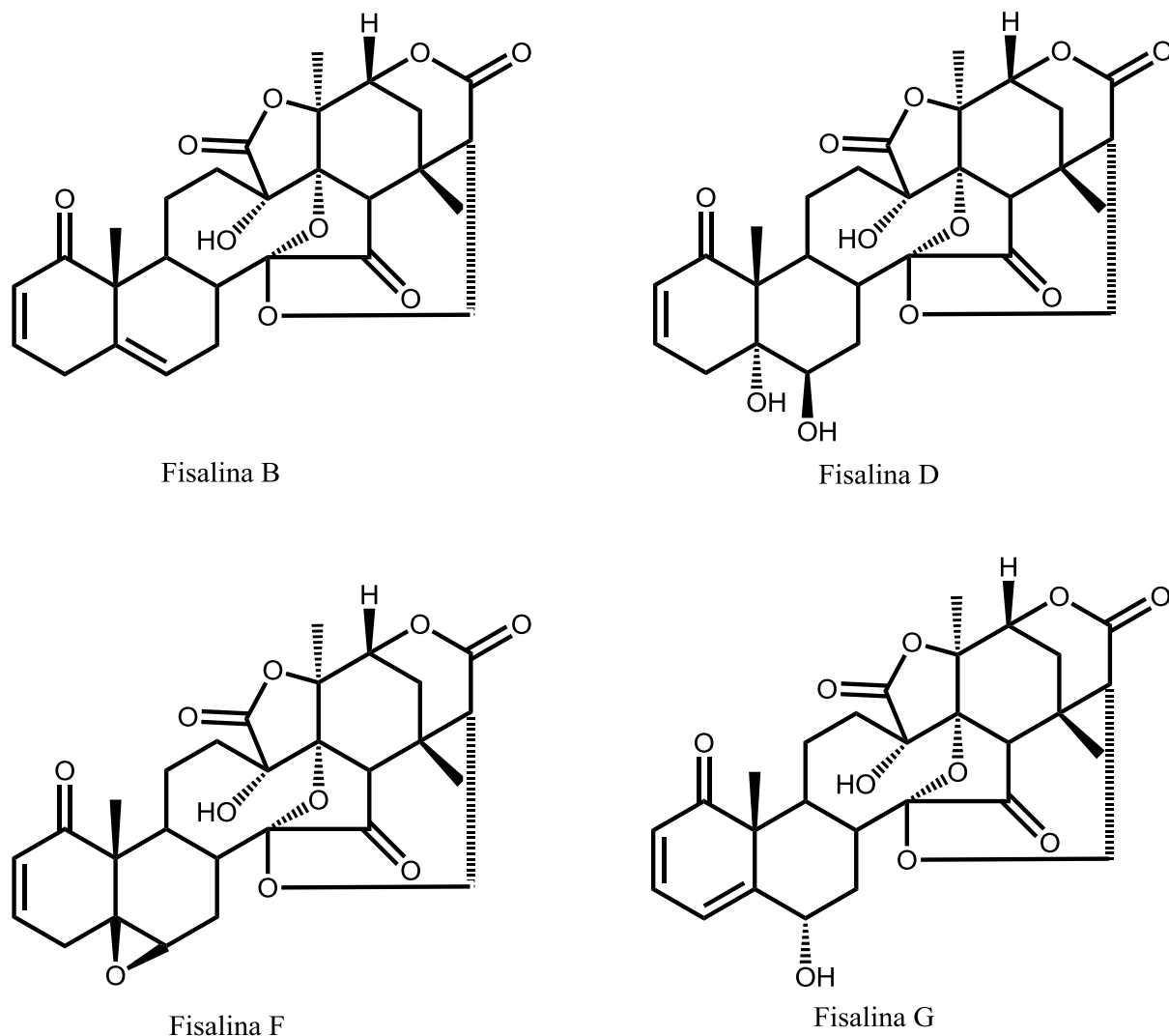


Figura 5. Estrutura química das fisolinas B, D, F e G.

Além da atividade antimalárica e leishmanicida, as fisolinas inibem a proliferação de formas epimastigotas do *T. cruzi* em ensaios *in vitro* e em triatomíneos infectados (CASTRO *et al.*, 2012). Todos esses estudos indicam o potencial antiparasitário destas moléculas.

3.7 O ÁCIDO BETULÍNICO

O ácido betulínico (**Figura 6**) é um triterpeno pentacíclico do tipo lupano amplamente distribuído no reino vegetal. Suas fontes tradicionais são espécies europeias

do gênero *Betula*, que produzem seu álcool precursor, a betulina (KIM *et al.*, 1997; FRIGHETTO *et al.*, 2005) e a casca de inúmeras espécies que ocorrem em regiões tropicais e subtropicais, especialmente as pertencentes ao gênero *Clusia* (MAURYA *et al.*, 1989).

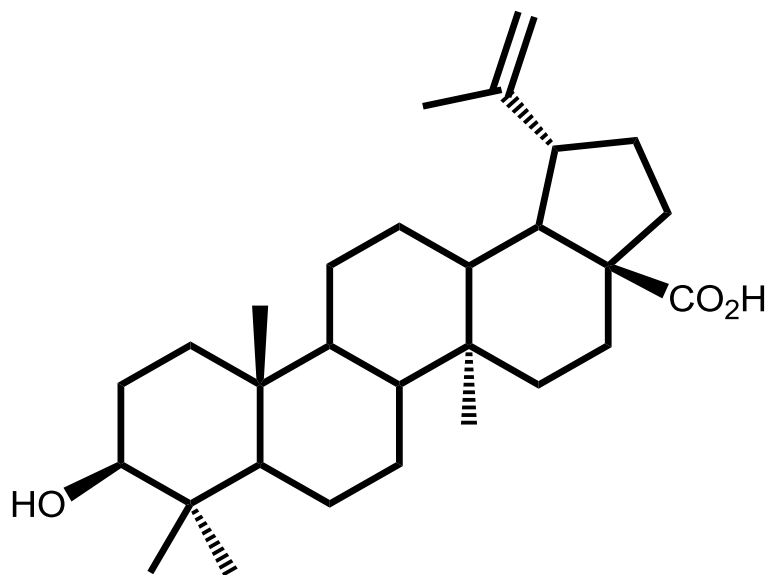


Figura 6. Estrutura química do ácido betulínico.

Sua principal característica é uma potente atividade antitumoral, através da indução de apoptose em células tumorais (FULDA, 2009). Nos últimos anos, a citotoxicidade dessa molécula contra uma variedade de tipos de tumores tem sido extensivamente estudada (PISHA *et al.*, 1995). Inicialmente se acreditava que o ácido betulínico era um inibidor seletivo contra melanomas. Posteriormente a citotoxicidade dessa molécula contra outros tipos de cânceres humanos foi demonstrada (SCHMIDT *et al.*, 1997; FULDA *et al.*, 1999; ZUCO *et al.*, 2002; THURNHER *et al.*, 2003). Em contraste com a potente atividade antitumoral, o ácido betulínico apresenta baixa citotoxicidade contra células não malignas. Além de possuir uma potente atividade antitumoral contra uma variedade de linhagens tumorais *in vitro*, o ácido betulínico suprime o crescimento de tumores em diversos modelos animais, principalmente em modelos de melanomas (PISHA *et al.*, 1995; ZUCO *et al.*, 2002).

Como muitos produtos naturais, o ácido betulínico apresenta uma variedade de atividades biológicas e farmacológicas, além de suas propriedades anticancerígenas. A atividade antioxidante, antimalárica, anti-HIV, analgésica, antiinflamatória e bactericida

já estão descritas na literatura (FUJIOKA *et al.*, 1994; KROGH *et al.*, 1999; CHANDRAMU *et al.*, 2003; YOGEE SWARI & SRIRAM, 2005). Provavelmente a atividade biológica mais importante, depois da citotoxicidade contra células tumorais, é o efeito anti-HIV, através da inibição da replicação viral (FUJOKA *et al.*, 1994).

Além de apresentar inúmeras atividades biológicas e farmacológicas, o ácido betulínico vem sendo utilizado, com sucesso, como protótipo para geração de moléculas mais ativas (YOGEE SWARI & SRIRAM, 2005). Um derivado muito promissor do ácido betulínico é o derivado PA457, que previne a maturação do vírus HIV-1 e a liberação do mesmo por células infectadas (LI *et al.*, 2003). Esta molécula foi bem tolerada quando administrada em dose única em estudos clínicos de fase I e II (SMITH *et al.*, 2007). Atualmente ela se encontra novamente sob investigação em estudos clínicos de fase II (MULLAUER *et al.*, 2010).

CAPÍTULO 1

“PHYSALINS B AND F, SECO-STEROIDS ISOLATED FROM *Physalis angulata* L., STRONGLY INHIBIT PROLIFERATION, ULTRASTRUCTURE AND INFECTIVITY OF *Trypanosoma cruzi*”, PUBLICADO NO PERIÓDICO PARASITOLOGY, NO ANO DE 2013.

O presente trabalho comprova a atividade anti-*T. cruzi* de uma família de compostos naturais isolados, as fisalinas.

Physalins B and F, *seco*-steroids isolated from *Physalis angulata* L., strongly inhibit proliferation, ultrastructure and infectivity of *Trypanosoma cruzi*

CÁSSIO S. MEIRA¹, ELISALVA T. GUIMARÃES^{1,2}, TANIRA M. BASTOS¹, DIOGO R. M. MOREIRA¹, THEREZINHA C. B. TOMASSINI³, IVONE M. RIBEIRO³, RICARDO R. DOS SANTOS⁴ and MILENA B. P. SOARES^{1,4*}

¹Fundação Oswaldo Cruz, Centro de Pesquisas Gonçalo Moniz, Rua Waldemar Falcão, 121, Candeal, Salvador, Bahia, CEP: 40296-710, Brazil

²Departamento de Ciências da Vida, Universidade do Estado da Bahia, Rua Silveira Martins, 2555, Cabula, Salvador, Bahia, CEP: 41150-000, Brazil

³Fundação Oswaldo Cruz, Instituto de Tecnologia em Fármacos (Farmanguinhos), Avenida Comandante Guarany, Jacarepaguá, Rio de Janeiro, RJ, CEP: 22775-903, Brazil

⁴Hospital São Rafael, Centro de Biotecnologia e Terapia Celular, Avenida São Rafael, São Marcos, Salvador, Bahia, CEP: 41253-190, Brazil

(Received 6 April 2013; revised 5 June 2013; accepted 1 July 2013; first published online 4 September 2013)

SUMMARY

We previously observed that physalins have immunomodulatory properties, as well as antileishmanial and antiplasmodial activities. Here, we investigated the anti-*Trypanosoma cruzi* activity of physalins B, D, F and G. We found that physalins B and F were the most potent compounds against trypomastigote and epimastigote forms of *T. cruzi*. Electron microscopy of trypomastigotes incubated with physalin B showed disruption of kinetoplast, alterations in Golgi apparatus and endoplasmic reticulum, followed by the formation of myelin-like figures, which were stained with MDC to confirm their autophagic vacuole identity. Physalin B-mediated alteration in Golgi apparatus was likely due to *T. cruzi* protease perturbation; however physalins did not inhibit activity of the trypanosomal protease cruzain. Flow cytometry examination showed that cell death is mainly caused by necrosis. Treatment with physalins reduced the invasion process, as well as intracellular parasite development in macrophage cell culture, with a potency similar to benznidazole. We observed that a combination of physalins and benznidazole has a greater anti-*T. cruzi* activity than when compounds were used alone. These results indicate that physalins, specifically B and F, are potent and selective trypanocidal agents. They cause structural alterations and induce autophagy, which ultimately lead to parasite cell death by a necrotic process.

Key words: Chagas disease, *Trypanosoma cruzi*, autophagy, *seco*-steroids, physalins.

INTRODUCTION

Chagas disease, caused by the haemoflagellate protozoan *Trypanosoma cruzi*, continues to affect millions of people in Latin America (Pinto-Dias, 2006). Subjects are infected by fecal matter contact of the insect vector (Hemiptera: Reduviidae), but blood transfusion, congenital transmission and ingestion of contaminated food also cause infection (Moncayo and Silveira, 2009). In the human host, infection is characterized by an acute phase followed by a chronic phase, in which cardiac, digestive or neurological disruptions develop (Coura and Castro, 2002).

There is no effective treatment once an individual has been infected with *T. cruzi*, and vaccine development is still in the experimental stage (Maya *et al.* 2007; Gupta *et al.* 2013). Chagas disease treatment is

based on the use of benznidazole, a drug with limited use due to its toxicity and minimal benefits during the chronic phase of infection (Urbina and Docampo, 2003; Moreno *et al.* 2010). Currently, Chagas disease has only two pharmaceutical interventions available in clinical trials. Of these, the most advanced is the antifungal posaconazole, which targets parasite sterol synthesis and is undergoing phase II study (Moton *et al.* 2009; Urbina, 2010). The other is the K11777, a peptide which inhibits protease activity, which is in phase I study (Sajid *et al.* 2011). Therefore, it is clear that more pharmaceutical options must be developed to improve treatment.

Physalis angulata L. (Solanaceae) is an annual herb widely distributed in tropical and subtropical regions. It is rich in steroid compounds, such as physalins and withanolides. Physalins are a group of *seco*-steroids found in stem extracts of many *Physalis* species (Magalhães *et al.* 2006; Damu *et al.* 2007; Jin *et al.* 2012). Because of the chemical similarity with the glucocorticoid class of steroids, physalins are

* Corresponding author. Fundação Oswaldo Cruz, Centro de Pesquisas Gonçalo Moniz. Rua Waldemar Falcão, 121, Candeal, Salvador, Bahia, 40296-710, Brazil. E-mail: milena@bahia.fiocruz.br

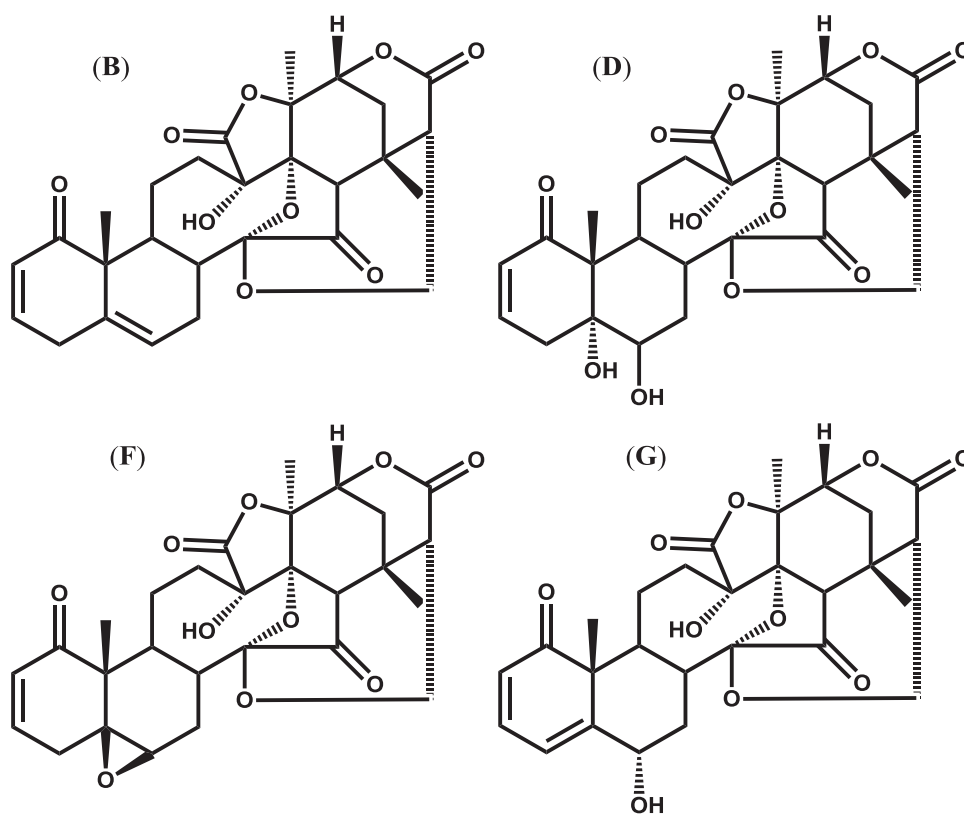


Fig. 1. Structures of physalins B, D, F and G.

well-known anti-inflammatory and immunosuppressant agents (Soares *et al.* 2003, 2006; Jacobo-Herrera *et al.* 2006). These compounds regulate many cellular activities, such as differentiation, proliferation, necrosis and apoptosis, adhesion and migration (Brustolim *et al.* 2010; Wu *et al.* 2012; Reyes-Reyes *et al.* 2013). Based on this, these compounds have been tested for anticancer activity and as inhibitors of pathogenic microbes (Chiang *et al.* 1992; Januário *et al.* 2002; Reyes-Reyes *et al.* 2013). Specifically, we observed that physalins B and F inhibit *Leishmania major* and *Leishmania amazonensis* infection in macrophages and mice (Guimarães *et al.* 2009). We also determined the antimalarial activity of physalins (Sá *et al.* 2011). Interestingly, we found that physalin D reduced blood parasitaemia in *Plasmodium berghei*-infected mice, while physalin F increased parasite load, possibly due to murine immune response interference.

Regarding the anti-*T. cruzi* activity of physalins, it was previously described that they inhibit epimastigote proliferation in axenic media, as well as in *T. cruzi*-infected triatomines (Vieira *et al.* 2008; Castro *et al.* 2009, 2012). The findings suggest physalins are useful compounds for vector-borne transmission control. Here, we report the activity of physalins B, D, F and G (Fig. 1) against bloodstream trypomastigotes, which is the infectious form in humans. After physalin treatment, we examined ultrastructural alteration and parasite death. Next, the activity of physalins B and F to inhibit the parasite

invasion and development in macrophage cell culture was determined.

MATERIALS AND METHODS

Drugs

Physalins B, D, F and G were isolated from *Physalis angulate* L. Plants were collected in Belém do Pará (Brazil) and processed as previously described (Soares *et al.* 2003). Preparations of physalins B, D, F and G (96, 95.6, 97.8 and 95% purity by HPLC, respectively) were dissolved in DMSO and diluted in culture medium for use in the assays. Benznidazole (LAFEPE, Recife, Brazil) was used as a positive control for the anti-*T. cruzi* assays. Amphotericin B (Gibco Laboratories, Gaithersburg, USA) was used as a positive control in the invasion assay. Gentian violet (Synth, São Paulo, Brazil) was used as a reference drug in the cytotoxicity assays.

Animals

Female BALB/c mice (6–8 weeks old) were supplied by the animal breeding facility at Centro de Pesquisa Gonçalo Moniz (Fundação Oswaldo Cruz, Bahia, Brazil) and maintained in sterilized cages under a controlled environment, receiving a rodent balanced diet and water *ad libitum*. All experiments were carried out in accordance with the recommendations of Ethical Issues Guidelines, and were approved by the local Animal Ethics Committee.

Parasite and cell cultures

Trypanosoma cruzi epimastigotes (Y strain) were maintained at 26 °C in LIT medium (Liver Infusion Tryptose) supplemented with 10% fetal bovine serum (FBS; Cultilab, Campinas, Brazil), 1% haemin (Sigma Chemical Co., St. Louis, MO, USA), 1% R9 medium (Sigma), and 50 µg mL⁻¹ of gentamycin (Novafarma, Anápolis, Brazil). Bloodstream trypomastigote forms of *T. cruzi* (Y strain) were obtained from the supernatant of infected LLC-MK2 cells and maintained in RPMI-1640 medium (Sigma Chemical Co., St. Louis, MO, USA) supplemented with 10% FBS and 50 µg mL⁻¹ of gentamycin at 37 °C with 5% CO₂.

Cytotoxicity to host cells

Peritoneal exudate macrophages obtained from BALB/c mice were placed on 96-well plates at a cell density of 5 × 10⁵ cells mL⁻¹ in 200 µL of RPMI-1640 medium (no phenol red) and supplemented with 10% FBS and 50 µg mL⁻¹ of gentamycin and incubated for 24 h at 37 °C and 5% CO₂. Compounds were added in a series of eight concentrations (0.13–200 µM), in triplicate, and incubated for 72 h. 20 µL/well of alamar blue (Invitrogen, Carlsbad, USA) was added to all wells during 10 h. Colorimetric readings were performed at 570 and 600 nm. LC₅₀ values were calculated using data-points gathered from three independent experiments. Gentian violet was used as a positive control, at concentrations ranging from 0.04 to 10 µM.

Antiproliferative activity against epimastigotes

Epimastigotes were counted in a haemocytometer and dispensed into 96-well plates at a cell density of 5 × 10⁶ cells mL⁻¹ in 200 µL of LIT medium. Compounds were tested at eight concentrations, in triplicate. The plate was incubated for 5 days at 26 °C, aliquots of each well were collected and the number of viable parasites was counted in a Neubauer chamber, which was compared with the untreated parasite culture. This experiment was performed three times. Benznidazole was used as a positive control.

Cytotoxicity for trypomastigotes

Trypomastigotes collected from the LLC-MK2 cell supernatant were dispensed into 96-well plates at a cell density of 2 × 10⁶ cells mL⁻¹ in 200 µL of RPMI medium. Compounds were tested at eight concentrations, in triplicate. The plate was incubated for 24 h at 37 °C and 5% CO₂. Aliquots from each well were collected and the number of viable parasites, based on parasite viability, was assessed in a Neubauer chamber and compared with untreated

parasite culture. This experiment was performed three times.

Trypanosoma cruzi infection assay

Peritoneal exudate macrophages were seeded at a cell density of 10⁶ cells mL⁻¹ in a 24-well plate with round coverslips on the bottom. Cells were cultivated in 1 mL of RPMI-1640 medium, supplemented with 10% FBS and incubated for 24 h. Cells were then infected with trypomastigotes at a ratio of 10 parasites per macrophage for 2 h. Free trypomastigotes were removed by successive washes with saline solution. Cultures were incubated in complete medium, in the presence or absence of physalins B, D, F and G (1 µM) or benznidazole (10 µM) for 6 h. After this, the supernatant was removed and fresh medium was added and incubated for 4 days. Cells were fixed in absolute alcohol, stained with haematoxylin and eosin and analysed in an optical microscope (Olympus, Tokyo, Japan). The percentage of infected macrophages and the mean number of amastigotes per 100 macrophages was determined by manual counting.

Trypanosoma cruzi invasion assay

Peritoneal exudate macrophages were cultured at a cell density of 1 × 10⁵ cells mL⁻¹ in a 24-well plate with rounded coverslips on the bottom in 1 mL of RPMI-1640 supplemented with 10% FBS and incubated for 24 h. Cells were then infected with trypomastigotes at a ratio of 100 parasites per macrophage for 2 h, followed by addition of physalin B or F (at 10 µM). Amphotericin B (10 µM) was used as a reference inhibitor. The plate was incubated for 2 h at 37 °C and 5% CO₂, followed by successive washes with saline solution to remove extracellular trypomastigotes. Plate was maintained in RPMI-1640 medium supplemented with 10% FBS at 37 °C for 2 h. Cells were fixed in absolute alcohol, stained with haematoxylin and eosin. The percentage of infected macrophages was determined by manual counting.

Propidium iodide and annexin V staining

Trypomastigotes (1 × 10⁷) in RPMI-1640 medium supplemented with 10% FBS were treated with physalin B (5.0 µM) and incubated for 24 h at 37 °C. Parasites were labelled with propidium iodide (PI) and annexin V using the annexin V-FITC apoptosis detection kit (Sigma Chemical Co, St. Louis, MO, USA) according to the manufacturer's instructions. Acquisition was performed using a BD FACS Calibur flow cytometer (San Jose, CA, USA), and data were analysed in BD CellQuest software (San Jose, CA, USA).

Electron microscopy analysis

Y strain *T. cruzi* trypomastigotes (3×10^7) were treated with physalin B (0.68 or 1.0 μM) and incubated for 24 h at 37 °C. After incubation, parasites were fixed for 1 h at room temperature with 2% formaldehyde and 2.5% glutaraldehyde (Electron Microscopy Sciences, Hatfield, PA, USA) in sodium cacodylate buffer (0.1 M, pH 7.2) for 1 h at room temperature. After fixation, parasites were washed 4 times with sodium cacodylate buffer (0.1 M, pH 7.2), and post-fixed with a 1% solution of osmium tetroxide (Sigma Chemical Co., St. Louis, MO, USA). Cells were subsequently dehydrated in increasing concentrations of acetone (30, 50, 70, 90 and 100%) for 10 min at each step and embedded in Polybed resin (PolyScience family, Warrington, PA, USA). Ultrathin sections were prepared on an ultramicrotome Leica UC7 and sections were collected on 300 mesh copper grids, contrasted with uranyl acetate and lead citrate. Images were collected in a JEOL TEM-1230 transmission electron microscope.

Parasitic vacuole staining

Trypomastigotes (3×10^7) were treated with physalin B (1.0 μM) and incubated for 24 h with 5% CO_2 . After treatment, cells were incubated with 100 μM of monodansylcadaverine (MDC, Sigma Chemical Co., St. Louis, MO, USA) for 20 min in the absence of light. After MDC staining, parasites were washed with PBS twice. The parasites were analysed in a FV1000 confocal microscope (Olympus). As a positive control, parasites were treated with 0.1 $\mu\text{g mL}^{-1}$ of rapamycin (Sigma Chemical Co., St. Louis, MO, USA).

Cruzain inhibition

The recombinant cruzain was expressed and purified according to a previously published protocol (Eakin *et al.* 1993). Protein was activated in acetate buffer (0.1 M; pH 5.5) containing 5.5 mM of DTT (Invitrogen, Carlsbad, USA) and protein concentration was adjusted to a final concentration of 0.1 μM . Protein was aliquoted into a 96-well plate, and compounds (previously dissolved in DMSO) in phosphate buffer (in the presence of 0.01% Triton 100) were added to the respective wells. The plate was incubated for 10 min at 35 °C. After this time, a solution containing protease substrate Z-FR-AMC (Sigma Chemical Co., St. Louis, MO, USA) was added, and following incubation periods 1, 5 or 10 min, the plate was read using the EnVision multilabel reader (PerkinElmer, Shelton, CT, USA). The percentage of cruzain inhibition was calculated using the following equation: $100 - (A1/A \times 100)$, where A1 represents the cruzain RFU in the presence

of the test inhibitor, A refers to the control RFU (cruzain and substrate only). Compound concentration was measured in triplicate. (2*S*,3*S*)-*trans*-epoxysuccinyl-L-leucylamido-3-methylbutane (E-64c) was purchased from Sigma Chemical Co. (catalogue number E0514) and used as a standard cruzain inhibitor.

Statistical analyses

We used a non-linear regression for calculating LC_{50} and IC_{50} values. The selectivity index (SI) was defined as the ratio of LC_{50} by IC_{50} (trypomastigotes). The one-way ANOVA and Bonferroni multiple comparisons were used to determine the statistical significance of the group comparisons in the *in vitro* infection studies and cell invasion study. Results were considered statistically significant when $P < 0.05$. All analyses were performed using Graph Pad Prism version 5.01 (Graph Pad Software, San Diego, CA, USA).

RESULTS

Trypanocidal and cytotoxicity activity

First, we evaluated the trypanocidal activity of physalins B, D, F and G against axenic epimastigotes and bloodstream trypomastigotes from the Y strain of *T. cruzi*. Cytotoxicity was determined in mouse macrophages. Benznidazole and gentian violet were used as trypanocidal and cytotoxic reference drugs, respectively. Activity was described in term of IC_{50} or LC_{50} values (Table 1). Of these, only physalins B and F were able to inhibit epimastigote proliferation, with IC_{50} values of 5.3 ± 1.9 and $5.8 \pm 1.5 \mu\text{M}$, respectively, while benznidazole exhibited an IC_{50} $10.8 \pm 0.9 \mu\text{M}$. All physalins exhibited activity against trypomastigotes. Once again, physalins B and F were the most active, presenting IC_{50} values of 0.68 ± 0.01 and $0.84 \pm 0.04 \mu\text{M}$ respectively, while an IC_{50} of $11.4 \pm 1.8 \mu\text{M}$ was calculated for benznidazole-treated trypomastigotes.

Next, physalin cytotoxicity to host cells (mouse macrophages) was analysed. Compared with gentian violet (LC_{50} $0.48 \pm 0.05 \mu\text{M}$), the cytotoxic reference drug in this assay, physalins demonstrated a lower cytotoxic value. Physalins D and G exhibited cytotoxicity similar to each other and they were less cytotoxic than physalins B and F. Regarding the cellular SI, physalins B and F exhibited a selectivity of 13 and 12 respectively, while physalins D and G were two times less selective.

Investigating the mechanism of action

After confirming that physalins were able to kill parasites, our next step was to understand how they affect parasite cells. In the first set of experiments

Table 1. Cruzain activity, cytotoxicity in macrophages and anti-*Trypanosoma cruzi* activity of purified physalins

Compounds	% cruzain inhibition at 25 μM ^a	Host cells LC ₅₀ \pm s.d. (μM) ^b	Y strain <i>T. cruzi</i> , IC ₅₀ \pm s.d. (μM)		SI ^e
			Epimastigotes ^c	Trypomastigotes ^d	
Physalin B	0	9.4 \pm 0.15	5.3 \pm 1.9	0.68 \pm 0.01	13
Physalin D	5	> 200	NA	37.5 \pm 0.70	5
Physalin F	1	10.1 \pm 0.7	5.8 \pm 1.5	0.84 \pm 0.04	12
Physalin G	0	98.4 \pm 2.4	NA	12.7 \pm 1.7	7
Benznidazole	–	> 200	10.8 \pm 0.9	11.4 \pm 1.8	18
Gentian violet	–	0.48 \pm 0.05	–	–	–
E-64c	100	–	–	–	–

^a Determined after 5 min of incubation with enzyme.

^b Determined in BALB/c macrophages after 72 h of incubation with the compounds.

^c Determined after 5 days of incubation.

^d Determined after 24 h of incubation.

^e SI = selectivity index. NA = no activity.

s.d. = standard deviation. IC₅₀ and LC₅₀ values are means \pm s.d. of two or three independent experiments performed in triplicate.

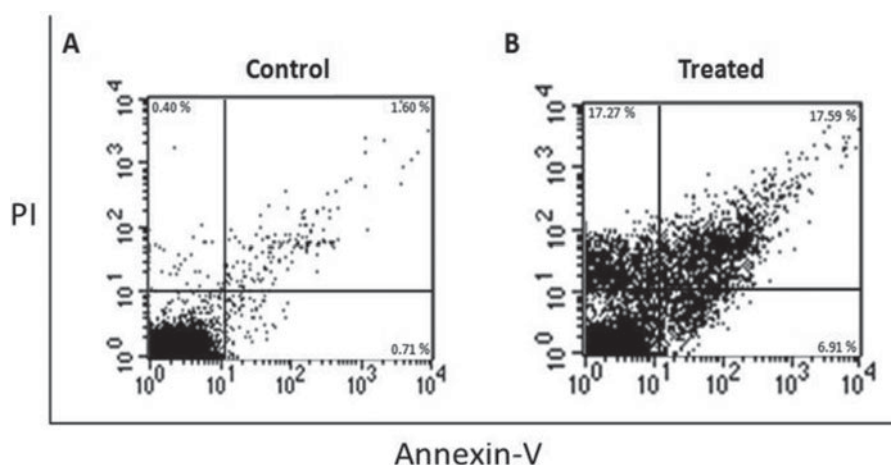


Fig. 2. Physalin B causes parasite cell death by a necrotic process. Flow cytometry examination of annexin V and propidium iodide staining in *Trypanosoma cruzi* trypomastigotes treated with 5 μM of physalin B for 24 h. (A), untreated parasites; (B), physalin B-treated parasites.

investigating the mechanism of action, we treated Y strain trypomastigotes with 5 μM of physalin B, which were incubated for 24 h. Cells were then stained with annexin V and PI and examined by flow cytometry. As shown in Fig. 2, most of the parasite cells treated with physalin B were positively stained for PI when compared with untreated cells. Therefore, physalin-based treatment causes parasite cell death through necrosis induction.

In the second set of experiments, we used electron microscopy to examine the ultrastructural morphology of trypomastigotes treated with physalin B. As we can see in Fig. 3, parasites exhibited kinetoplast enlargement, alterations in the Golgi complex, as well as endoplasmic reticulum morphology. Interestingly, we also observed the presence of myelin-like figures within the cytoplasm. To confirm that these myelin-like figures are parasitic vacuoles, possibly related to autophagy, untreated or

treated trypomastigotes were incubated with monodansylcadaverine (MDC) for 20 min and observed by fluorescence microscopy. In a control experiment, untreated cells presented no detectable MDC staining, while rapamycin-treated cells contained stained cytosolic vacuoles. Following this, we tested physalin B (1.0 μM) which clearly presented stained vacuoles (Fig. 4).

Finally, we tested the ability of physalins to inhibit the activity of recombinant cruzain, the major *T. cruzi* cysteine protease. As Table 1 demonstrates, none of the physalins tested at a concentration of 25 μM exhibited inhibitory properties against cruzain.

Physalins inhibit *T. cruzi* infection in host cells

We tested physalins to inhibit the parasite development in host cells. In this assay, mouse macrophages

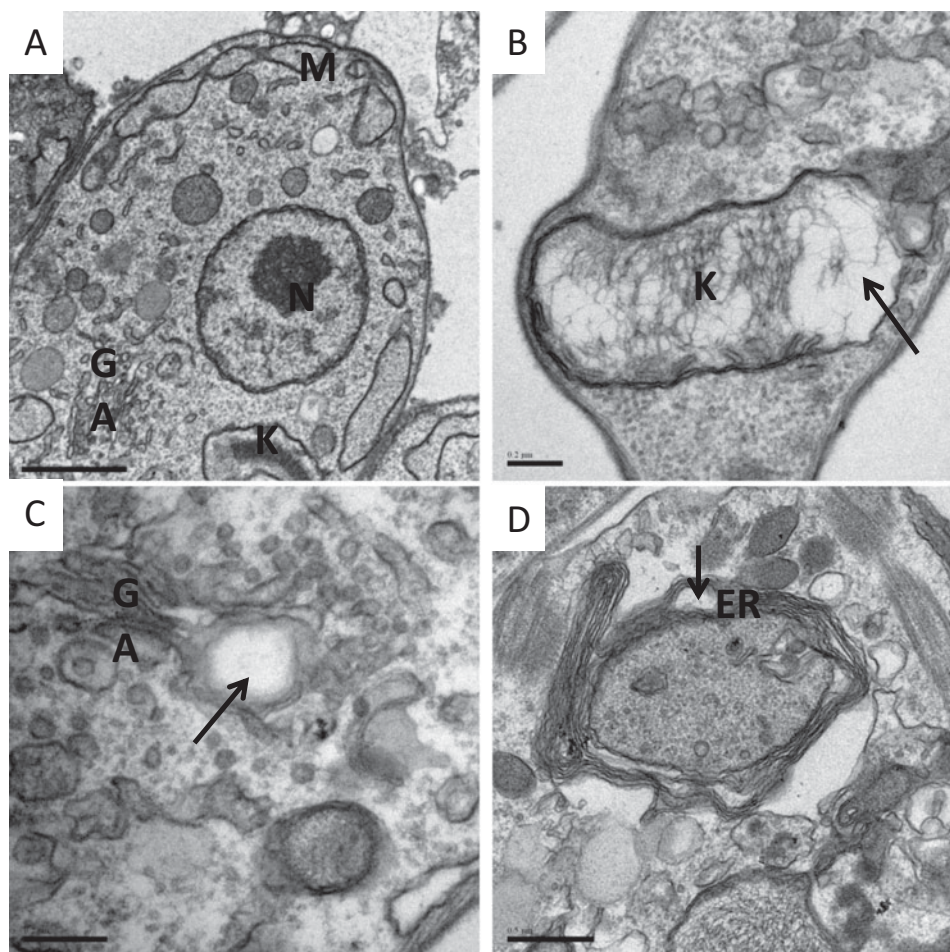


Fig. 3. Physalin B induces significant ultrastructural changes in trypanosomes. (A) shows an image of untreated parasites presenting a typical morphology of the nucleus (N), kinetoplast (K), mitochondria (M) and Golgi apparatus (GA). Treatment for 24 h with physalin B at 0.68 (B and C) or $1.0 \mu\text{M}$ (D) causes kinetoplast enlargement (B), Golgi apparatus disorganization (C) and endoplasmic reticulum disorganization (D). Black arrows indicate changes in organelles. Scale bars: A = $1 \mu\text{m}$; B and C = $0.2 \mu\text{m}$; D = $0.5 \mu\text{m}$.

were infected with Y strain trypanosomes. After infection, the respective physalin ($1.0 \mu\text{M}$) was added to the cell culture. Benznidazole was included in this assay as a positive control. Cells were stained with haematoxylin and eosin and analysed by optical microscopy 4 days post-infection. As shown in Fig. 5, physalins B and F significantly reduced the percentage of infected macrophages and the relative numbers of intracellular parasites when compared with control. Interestingly, activity of physalins B and F was quite similar to that observed in benznidazole. In contrast, physalins D and G did not show significant activity in this assay. When physalins B and F were tested in concentrations above $1.0 \mu\text{M}$, they did not inhibit infection in macrophages, probably due to their immunosuppressive properties (data not shown).

In another experiment, we measure physalins' ability to impair parasite invasion into host cells. In this assay, mouse macrophages were exposed to trypanosomes and at the same time treated with physalins ($10 \mu\text{M}$). After incubating for 2 h, cell

cultures were stained and analysed by optical microscopy. Amphotericin B was used as a positive control. As shown in Fig. 6, physalins B and F significantly inhibited the parasite invasion process in macrophages when compared with untreated cultures. Curiously, while physalins exhibited activity in this assay, equal concentrations of benznidazole did not.

Based on the results described above, a final set of experiments was performed to evaluate the activity in infected macrophages of physalin B or F in combination with benznidazole. As shown in Fig. 7, the combination of physalin and benznidazole reduced the number of infected macrophages as well as the number of amastigotes per macrophage to a greater degree than the respective compound used alone.

DISCUSSION

Pharmacological treatment of Chagas disease has been limited to benznidazole, which has poor efficacy

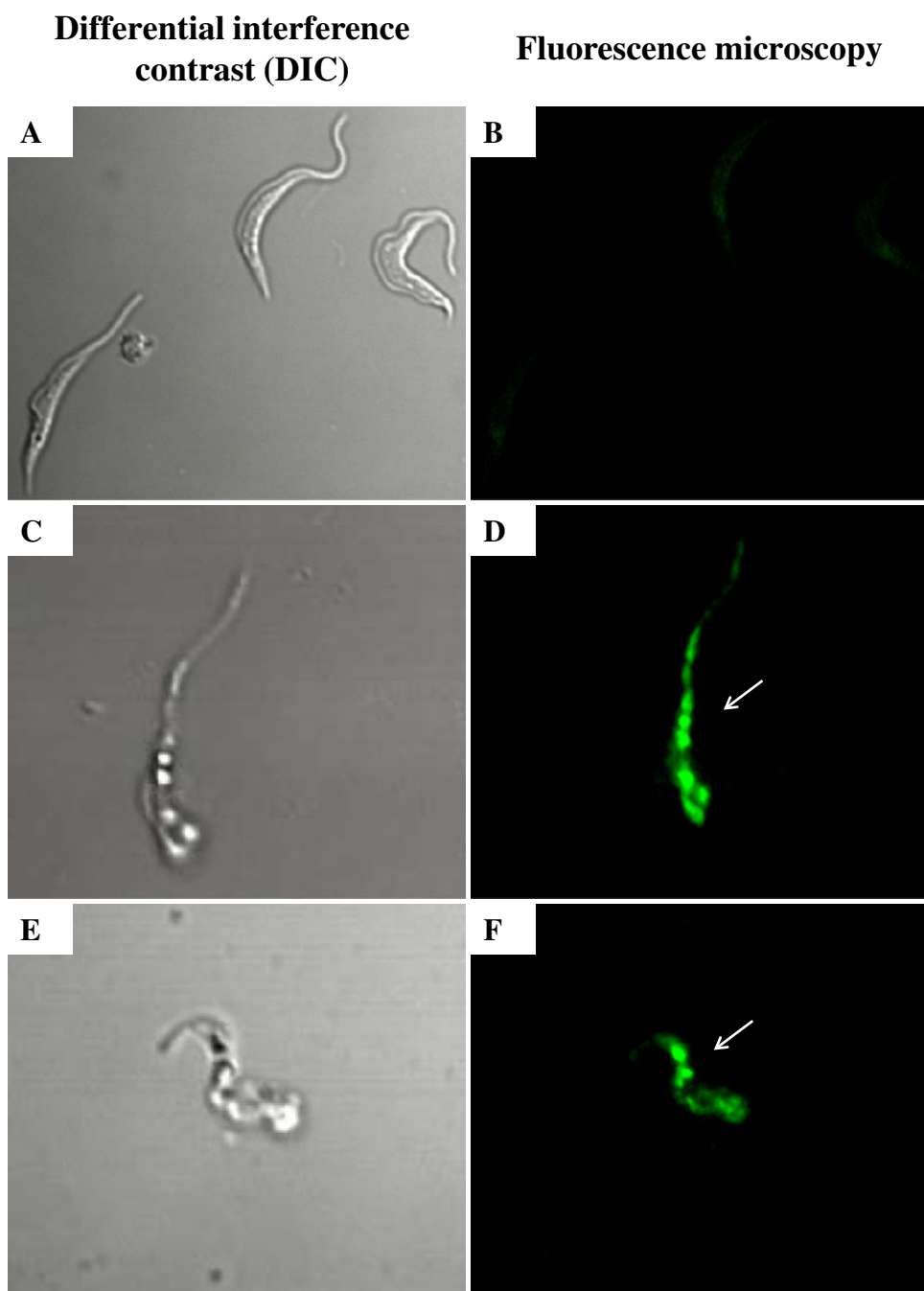


Fig. 4. Physalin B induces the formation of cytosolic vacuoles in *Trypanosoma cruzi*. Trypomastigotes treated with $1.0 \mu\text{M}$ of physalin for 24 h and incubated with MDC for 20 min. Left panels are DIC and right panels are fluorescence microscopy. (A) and (B) show untreated trypomastigotes; (C) and (D) show parasite treated with $0.1 \mu\text{g mL}^{-1}$ of rapamycin (positive control); (E, F) show treated trypomastigotes with physalin B. Arrows indicate the vacuole structures. Images were captured on confocal microscope with a $60\times$ oil-immersion objective at $3\times$ zoom.

and causes drug intolerance, as well as adverse effects in many patients. Emergence of parasite resistance to benznidazole is another subject of concern. A large number of small molecules have been screened as anti-*T. cruzi* agents, however the number is still low when compared with drug discovery efforts for other infectious diseases, such as malaria and AIDS (Goebel *et al.* 2008). Screening of isolated natural compounds is a reliable strategy to identify new anti-*T. cruzi* agents.

The *Physalis* genus is a rich source of unique natural compounds. Of these, the *seco*-steroids physalins are the most investigated in terms of pharmacological property. We previously reported that physalins isolated from *P. angulata* L. are potent immunomodulatory, antileishmanial and antiplasmodial agents. In 2008, Vieira and co-workers reported that physalin F and withaphysalins inhibit proliferation of *T. cruzi* epimastigotes in an axenic medium (Vieira *et al.* 2008). Additionally, Castro and

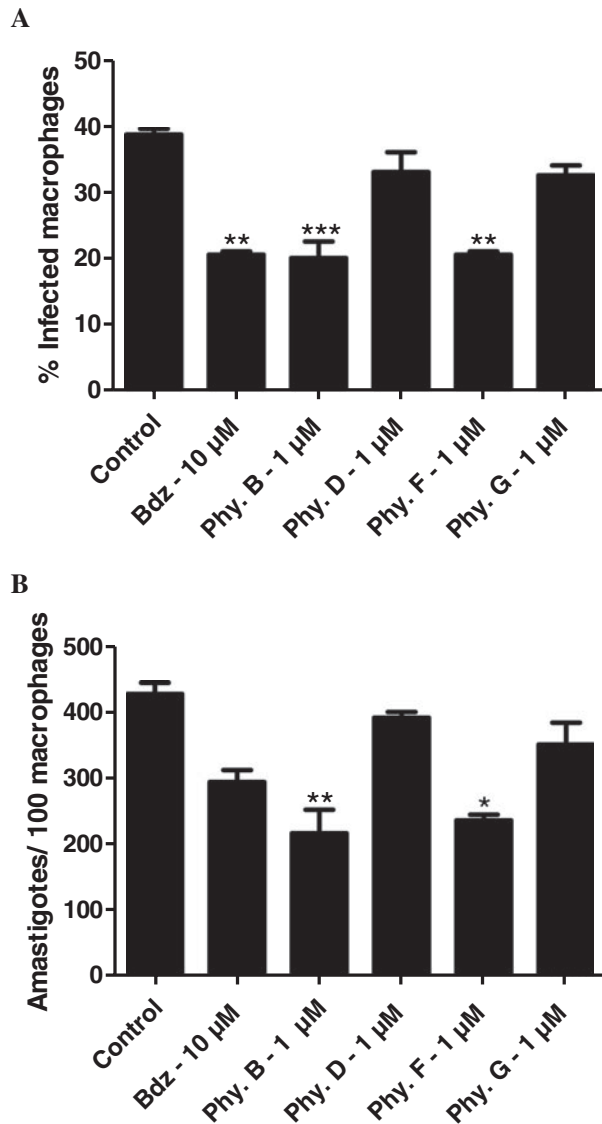


Fig. 5. Physalins B and F inhibit intracellular amastigotes in host cells. Mouse peritoneal macrophages were infected with Y strain trypomastigotes for 2 h and treated with the respective physalin ($1.0 \mu\text{M}$). Infected cells were stained with haematoxylin and eosin and analysed by optical microscopy. (A) shows the percentage of infected macrophages; (B) displays the relative number of amastigotes per 100 macrophages. Bdz = Benznidazole; Phy. = physalin. Values represent the mean \pm S.E.M. in triplicate. * $P < 0.05$; ** $P < 0.01$; *** $P < 0.001$ compared with the control group.

co-workers corroborated these findings, showing that physalin B inhibits *T. cruzi* development in the gut of triatomines (Castro *et al.* 2009, 2012). However, the anti-*T. cruzi* activity of physalins against the infective forms in humans (bloodstream trypomastigotes and amastigotes) have not been described.

In the present study, we determined the anti-*T. cruzi* activity of physalins B, D, F and G purified from *P. angulata*. Only physalin F was previously tested against epimastigotes, therefore we performed an extensive examination of all physalins. As expected,

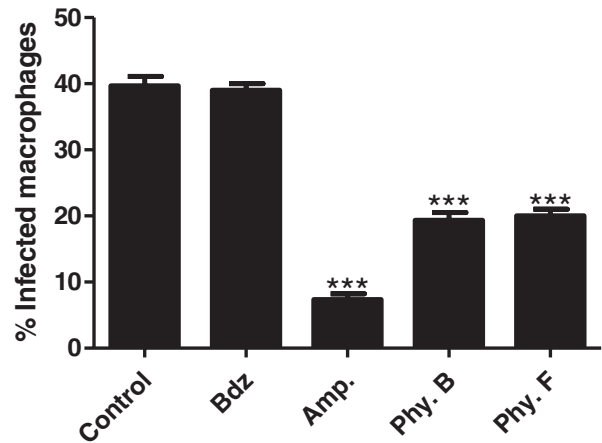


Fig. 6. Physalins B and F reduce the parasite invasion process in host cells. Mouse macrophages were infected with Y strain trypomastigotes and at the same time treated with physalins. The percentage of *T. cruzi*-infected macrophages is shown. Bdz = benznidazole, Amp = amphotericin B. Values represent the mean \pm S.E.M. in triplicate. *** $P < 0.001$ compared with the control group.

we observed that physalins, specifically B and F, are trypanocidal agents. They inhibited epimastigote proliferation, and were toxic against bloodstream trypomastigotes at non-toxic concentrations for mouse macrophages. In addition, they showed a greater potency when compared with benznidazole, the reference anti-*T. cruzi* drug. Regarding the cellular SI, physalins B and F exhibited some selectivity, albeit low for a desirable anti-*T. cruzi* drug candidate.

The chemical difference amongst the four physalins is found in the substituents attached to C5 and C6 in the steroid backbone. Physalins D and G are similar because of the hydroxyl groups present and they did not exhibit trypanocidal activity. In contrast, physalin B and F lack hydroxyl groups in C5 and C6, and demonstrated higher activity, exhibiting a pronounced trypanocidal property. In practice, physalin B and F have equipotent trypanocidal activity.

By using trypomastigotes, we observed that physalins cause parasite cell death through necrotic mechanisms. Also, we saw that physalins alter the morphology of the Golgi complex, kinetoplast and endoplasmic reticulum. In the literature, altered Golgi complex morphology is an indication that *T. cruzi* protease activity was affected (Engel *et al.* 1998). Cruzain is the major cysteine protease present in *T. cruzi* and has been identified as a drug target (Sajid *et al.* 2011). Therefore, we determined the ability of physalins to inhibit the activity of recombinant cruzain; however, physalins did not inhibit it.

Using electron microscopy, formation of myelin-like figures in the parasite treated with physalins was evident. Fluorescence microscopy revealed that parasites treated with physalins were labelled with

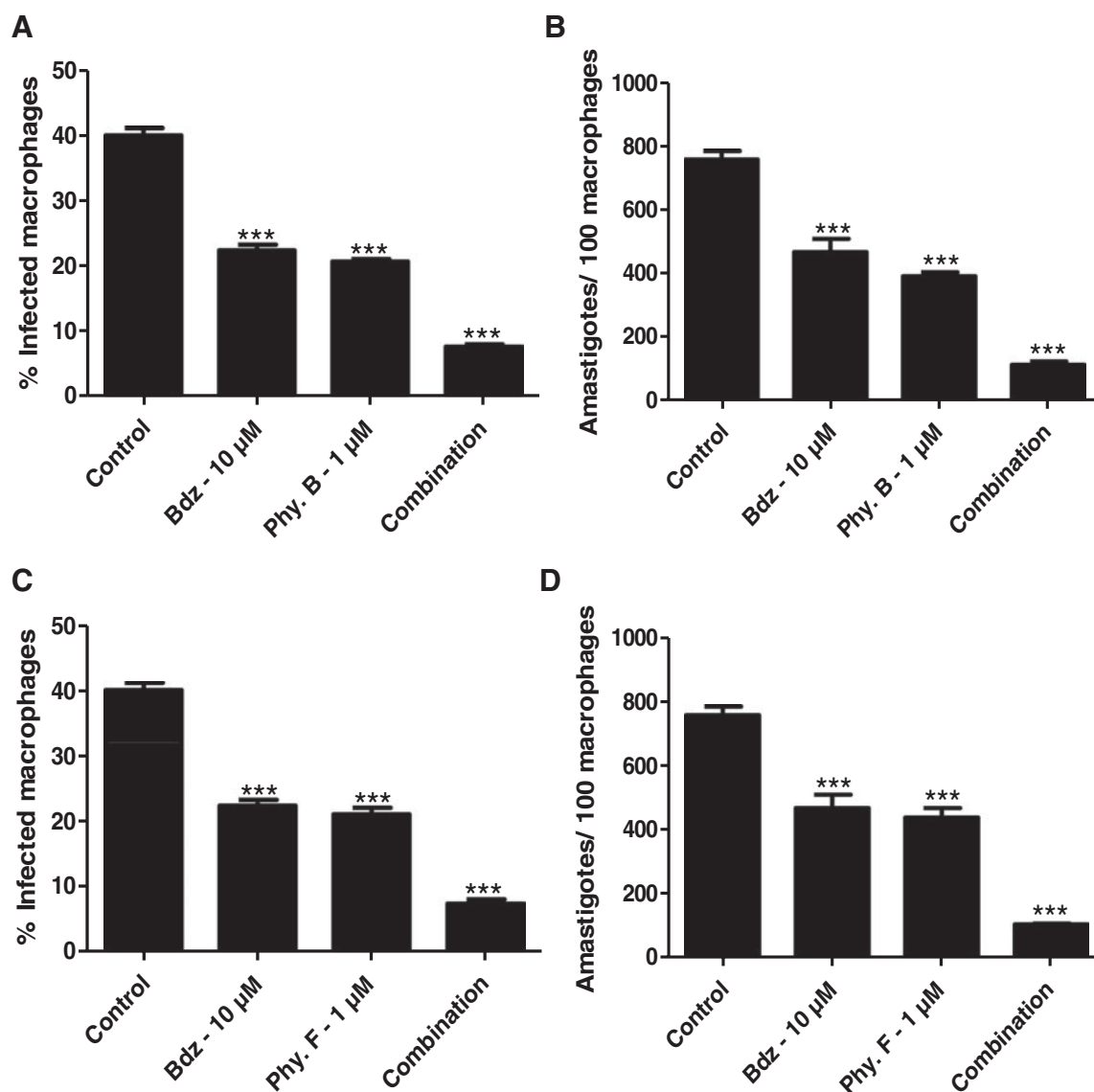


Fig. 7. A combination of physalins and benznidazole is more potent to inhibit amastigotes than compounds when used alone. Mouse peritoneal macrophages were infected with Y strain trypomastigotes for 2 h. Physalins B or F was added alone or in combination with benznidazole. (A) and (B) show the combination of physalins B and benznidazole, while (C) and (D) display the combination of physalins F and benznidazole. Bdz = Benznidazole. Values represent the mean \pm S.E.M. in triplicate. *** $P < 0.001$ compared with the control group.

MDC, a cytosolic vacuole stain (Vanier-Santos and Castro, 2009; Duszenko *et al.* 2011). Therefore, it is possible that the cytosolic vacuoles observed in physalins-treated *T. cruzi* are due to autophagy. In fact, our results are similar to a very recent finding that physalins exert cellular effects by inducing autophagy (He *et al.* 2013a, b).

Most importantly, we analysed physalins effects in the *in vitro* infection. The same order of potency against trypomastigotes was observed when all physalins were tested in *T. cruzi*-infected macrophages. Physalins B and F at $1.0 \mu\text{M}$ were able to reduce intracellular parasite development in macrophages. This was similar to reductions observed in benznidazole-treated infected cells. Physalins B and F are well known for their modulatory property in immune cells (Soares *et al.* 2003, 2006). In fact, we

observed that physalins B or F at concentrations of $5.0 \mu\text{M}$ or higher increased the *T. cruzi* infection in macrophages, probably because they deactivate host macrophages during the infection development.

The parasite invasion process in macrophages takes approximately 2 h, thereby requiring a drug to work quickly (Matsuo *et al.* 2010). In this assay, benznidazole was not active, while amphotericin B was active to stop the parasite invasion. Interestingly, physalins B and F not only reduced parasite burden in infected macrophages, but they also quickly killed trypomastigotes exposed to macrophages, therefore indicating *seco*-steroids stop the parasite invasion process in host cells.

An anti-Chagas disease treatment will likely contain a combination of inhibitors to improve the efficacy of the treatment and avoid parasite resistance.

In recent years, many efforts have been done to identify optimal drug combinations for Chagas disease (Cencig *et al.* 2012; Veiga-Santos *et al.* 2012). In fact, we observed the combination of physalin and benzimidazole has a greater activity to reduce *T. cruzi* infection in macrophages than compounds used alone. The results indicate that the combination of physalin and benzimidazole act in an additive fashion. Altogether, these data argue that the screening for new anti-*T. cruzi* agents based on seco-steroids, specifically those without or with little effects on immune cells, is an attractive line of drug development.

CONCLUSION

Physalins showed potent activity against *T. cruzi* epimastigotes and trypomastigotes. Of these, physalins B and F exhibited the highest potency and selectivity, and similar to the observations on benzimidazole-treated parasites. These compounds achieve trypanocidal activity through autophagy induction, which ultimately results in necrotic parasite death. Regarding the *in vitro* infection, we observed physalins inhibit parasite development, as well as the invasion process in host cells. Moreover, physalins seem suitable for drug combination with other anti-*T. cruzi* agents to control infection.

ACKNOWLEDGEMENTS

M. B. P. S. and R. R. S hold a CNPq fellowship, while D. R. M. M. and C. S. M. thank for FAPESB scholarships.

FINANCIAL SUPPORT

This work received funding by Conselho Nacional de Pesquisas Brasileira (CNPq, grant number 502161/2010-8) and Fundação de Amparo as Pesquisas do Estado da Bahia (FAPESB, grant number 6596).

COMPETING INTERESTS

The authors have declared that no competing interests exist.

REFERENCES

Brustolim, D., Vasconcelos, J. F., Freitas, L. A., Teixeira, M. M., Farias, M. T., Ribeiro, Y. M., Tomassini, T. C. B., Oliveira, G. G., Pontes-de-Carvalho, L. C., Ribeiro-dos-Santos, R. and Soares, M. B. P. (2010). Activity of physalin F in a collagen-induced arthritis model. *Journal of Natural Products* **73**, 1323–13236. doi: 10.1021/np900691w.

Castro, D. P., Figueiredo, M. B., Genta, F. A., Ribeiro, I. M., Tomassini, T. C. B., Azambuja, P. and Garcia, E. S. (2009). Physalin B inhibits *Rhodnius prolixus* hemocyte phagocytosis and microaggregation by the activation of endogenous PAF-acetyl hydrolase activities. *Journal of Insect Physiology* **55**, 532–537. doi: 10.1016/j.jinsphys.2009.01.013.

Castro, D. P., Moraes, C. S., Gonzalez, M. S., Ribeiro, I. M., Tomassini, T. C., Azambuja, P. and Garcia, E. S. (2012). Physalin B inhibits *Trypanosoma cruzi* infection in the gut of *Rhodnius prolixus* by affecting the immune system and microbiota. *Journal of Insect Physiology* **58**, 1620–1625. doi: 10.1016/j.jinsphys.2012.10.001.

Cencig, S., Coltel, N., Truyens, C. and Carlier, Y. (2012). Evaluation of benzimidazole treatment combined with nifurtimox, posaconazole or AmBisome® in mice infected with *Trypanosoma cruzi* strains. *International Journal of Antimicrobial Agents* **40**, 527–532. doi: 10.1016/j.ijantimicag.2012.08.002.

Chiang, H. C., Jaw, S. M. and Chen, P. M. (1992). Inhibitory effects of physalin B and physalin F on various human leukemia cells *in vitro*. *Anticancer Research* **12**, 1155–1162.

Coura, J. R. and De Castro, S. L. (2002). A critical review on Chagas disease chemotherapy. *Memorias Instituto Oswaldo Cruz* **97**, 3–24. doi: 10.1590/S0074-02762002000100001.

Damu, A. G., Kuo, P. C., Su, C. R., Kuo, T. H., Chen, T. H., Bastow, K. F., Lee, K. H. and Wu, T. S. (2007). Isolation, structures, and structure–cytotoxic activity relationships of withanolides and physalins from *Physalis angulata*. *Journal of Natural Products* **70**, 1146–1152. doi: 10.1021/np0701374.

Duszenko, M., Ginger, M. L., Brennand, A., Gualdrón-López, M., Colombo, M. I., Coombs, G. H., Coppens, I., Jayabalasingham, B., Langsley, G., de Castro, S. L., Menna-Barreto, R., Mottram, J. C., Navarro, M., Rigden, D. J., Romano, P. S., Stoka, V., Turk, B. and Michels, P. A. (2011). Autophagy in protists. *Autophagy* **7**, 127–158. doi: 10.4161/auto.7.2.13310.

Eakin, A. E., MacGrath, M. E., McKerrow, J. H., Fletcher, R. J. and Craik, C. S. (1993). Production of crystalizable cruzain, the major cysteine protease from *Trypanosoma cruzi*. *Journal of Biological Chemistry* **268**, 6115–6118.

Engel, J. C., Doyle, P. S., Palmer, J., Hsieh, I., Bainton, D. F. and McKerrow, J. H. (1998). Cysteine protease inhibitors alter Golgi complex ultrastructure and function in *Trypanosoma cruzi*. *Journal of Cell Science* **111**, 597–606.

Goebel, T., Ulmer, D., Projahn, H., Kloeckner, J., Heller, E., Glaser, M., Ponte-Sucré, A., Specht, S., Sarite, S. R., Hoerauf, A., Kaiser, A., Hauber, I., Hauber, J. and Holzgrabe, U. (2008). In search of novel agents for therapy of tropical diseases and human immunodeficiency virus. *Journal of Medicinal Chemistry* **51**, 238–250. doi: 10.1021/jm070763y.

Guimarães, E. T., Lima, M. S., Santos, L. A., Ribeiro, I. M., Tomassini, T. C. B., Ribeiro dos Santos, R., dos Santos, W. L. and Soares, M. B. P. (2009). Activity of physalins purified from *Physalis angulata* *in vitro* and *in vivo* models of cutaneous leishmaniasis. *Journal of Antimicrobial Chemotherapy* **64**, 84–87. doi: 10.1093/jac/dkp170.

Gupta, S., Wan, X., Zago, M. P., Sellers, V. C., Silva, T. S., Assiah, D., Dhiman, M., Nuñez, S., Petersen, J. R., Vázquez-Chagoyán, J. C., Estrada-Franco, J. G. and Garg, N. J. (2013). Antigenicity and diagnostic potential of vaccine candidates in human Chagas disease. *PLOS Neglected Tropical Diseases* **7**, e2018. doi: 10.1371/journal.pntd.0002018.

He, H., Zang, L. H., Feng, Y. S., Wang, J., Liu, W. W., Chen, L. X., Kang, N., Tashiro, S., Onodera, S., Qiu, F. and Ikejima, T. (2013a). Physalin A induces apoptotic cell death and protective autophagy in HT1080 human fibrosarcoma cells. *Journal of Natural Products* **76**, 880–888. doi: 10.1021/np400017k.

He, H., Zang, L. H., Feng, Y. S., Chen, L. X., Kang, N., Tashiro, S. I., Onodera, S., Qiu, F. and Ikejima, T. (2013b). Physalin A induces apoptosis via p53–Noxa-mediated ROS generation, and autophagy plays a protective role against apoptosis through p38–NF-κB survival pathway in A375-S2 cells. *Journal of Ethnopharmacology* **148**, 544–555. doi: 10.1016/j.jep.2013.04.051.

Jacobo-Herrera, N. J., Bremner, P., Marquez, N., Gupta, M. P., Gibbons, S., Muñoz, E. and Heinrich, M. (2006). Physalins from *Witheringia solanaceae* as modulators of the NF-kappaB cascade. *Journal of Natural Products* **69**, 328–331. doi: 10.1021/np050225t.

Januário, A. H., Filho, E. R., Pietro, R. C., Kashima, S., Sato, D. N. and França, S. C. (2002). Antimycobacterial physalins from *Physalis angulata* L. (Solanaceae). *Phytotherapy Research* **16**, 445–448. doi: 10.1002/ptr.939.

Jin, Z., Mashuta, M. S., Stolowich, N. J., Vaisberg, A. J., Stivers, N. S., Bates, P. J., Lewis, W. H. and Hammond, G. B. (2012). Physangulidines A, B, and C: three new antiproliferative withanolides from *Physalis angulata* L. *Organic Letters* **14**, 1230–1233. doi: 10.1021/ol203498a.

Pinto-Dias, J. C. (2006). The treatment of Chagas disease (South American trypanosomiasis). *Annals of Internal Medicine* **144**, 722–774.

Magalhães, H. I., Veras, M. L., Torres, M. R., Alves, A. P., Pessoa, O. D., Silveira, E. R., Costa-Lotuf, L. V., de Moraes, M. O. and Pessoa, C. (2006). *In vitro* and *in vivo* antitumor activity of physalins B and D from *Physalis angulata*. *Journal of Pharmacy and Pharmacology* **58**, 235–241. doi: 10.1211/jpp.58.2.0011.

Maya, J. D., Cassels, B. K., Iturriaga-Vásquez, P., Ferreira, J., Faúndez, M., Galanti, N., Ferreira, A. and Morello, A. (2007). Mode of action of natural and synthetic drugs against *Trypanosoma cruzi* and their

- interaction with the mammalian host. *Comparative Biochemistry and Physiology Part A: Molecular and Integrative Physiology* **146**, 601–620. doi: 10.1016/j.cbpa.2006.03.004.
- Matsuo, A. L., Silva, L. S., Torrecilhas, A. C., Pascoalino, B. S., Ramos, T. C., Rodrigues, E. G., Schenkman, S., Caires, A. C. and Travassos, L. R.** (2010). *In vitro* and *in vivo* trypanocidal effects of the cyclopalladated compound 7a, a drug candidate for treatment of Chagas' disease. *Antimicrobial Agents and Chemotherapy* **54**, 3318–3325. doi: 10.1128/AAC.00323-10.
- Moncayo, A. and Silveira, A. C.** (2009). Current epidemiological trends for Chagas disease in Latin America and future challenges in epidemiology, surveillance and health policy. *Memorias Instituto Oswaldo Cruz* **104**, 17–30. doi: 10.1590/S0074-02762009000900005.
- Moreno, M., D'avoça, D. A., Silva, M. N., Galvão, L. M., Macedo, A. M., Chiari, E., Gontijo, E. D. and Zingales, B.** (2010). *Trypanosoma cruzi* benzimidazole susceptibility *in vitro* does not predict the therapeutic outcome of human Chagas disease. *Memorias Instituto Oswaldo Cruz* **105**, 918–924. doi: 10.1590/S0074-02762010000700014.
- Moton, A., Krishna, G. and Wang, Z.** (2009). Tolerability and safety profile of posaconazole: evaluation of 18 controlled studies in healthy volunteers. *Journal of Clinical Pharmacy and Therapeutics* **34**, 301–311. doi: 10.1111/j.1365-2710.2009.01055.x.
- Reyes-Reyes, E. M., Jin, Z., Vaisberg, A. J., Hammond, G. B. and Bates, P. J.** (2013). Physangulidine A, a withanolide from *Physalis angulata*, perturbs the cell cycle and induces cell death by apoptosis in prostate cancer cells. *Journal of Natural Products* **76**, 2–7. doi: 10.1021/np300457g.
- Sá, M. S., Menezes, M. N., Krettli, A. U., Ribeiro, I. M., Tomassini, T. C. B., Ribeiro dos Santos, R., de Azevedo, W. F., Jr. and Soares, M. B. P.** (2011). Antimalarial activity of physalins B, D, F and G. *Journal of Natural Products* **74**, 2269–2272. doi: 10.1021/np200260f.
- Sajid, M., Robertson, S. A., Brinen, L. S. and McKerrow, J. H.** (2011). Cruzain: the path from target validation to the clinic. *Advances in Experimental Medicine and Biology* **712**, 100–115. doi: 10.1007/978-1-4419-8414-2_7.
- Soares, M. B. P., Bellintani, M. C., Ribeiro, I. M., Tomassini, T. C. B. and Ribeiro dos Santos, R.** (2003). Inhibition of macrophage activation and lipopolysaccharide-induced death by *seco*-steroids purified from *Physalis angulata* L. *European Journal of Pharmacology* **459**, 107–112. doi: 10.1016/S0014-2999(02)02829-7.
- Soares, M. B. P., Brustolin, D., Santos, L. A., Bellintani, M. C., Paiva, F. P., Ribeiro, Y. M., Tomassini, T. C. B. and Ribeiro Dos Santos, R.** (2006). Physalins B, F and G, *seco*-steroids purified from *Physalis angulata* L., inhibit lymphocyte function and allogenic transplant rejection. *International Immunopharmacology* **6**, 408–414. doi: 10.1016/j.intimp.2005.09.007.
- Urbina, J. A.** (2010). New insights in Chagas disease treatment. *Drugs of the Future* **35**, 409–419. doi: 10.1358/dof.2010.035.05.1484391.
- Urbina, J. A. and Docampo, R.** (2003). Specific chemotherapy of Chagas disease: controversies and advances. *Trends in Parasitology* **19**, 495–501. doi: 10.1016/j.pt.2003.09.001.
- Vanier-Santos, M. A. and De Castro, S. L.** (2009). Electron microscopy in antiparasitic chemotherapy: a (close) view to a kill. *Current Drug Targets* **10**, 246–260. doi: 10.2174/138945009787581168.
- Veiga-Santos, P., Barrias, E. S., Santos, J. F. C., de Barros Moreira, T. L., de Carvalho, T. M., Urbina, J. A. and de Souza, W.** (2012). Effects of amiodarone and posaconazole on the growth and ultrastructure of *Trypanosoma cruzi*. *International Journal of Antimicrobial Agents* **40**, 61–71. doi: 10.1016/j.ijantimicag.2012.03.009.
- Vieira, N. C., Espíndola, L. S., Santana, J. M., Veras, M. L., Pessoa, O. D., Pinheiro, S. M., de Araújo, R. M., Lima, M. A. and Silveira, E. R.** (2008). Trypanocidal activity of a new pterocarpan and other secondary metabolites of plants from Northeastern Brazil flora. *Bioorganic Medicinal Chemistry* **16**, 1676–1682. doi: 10.1016/j.bmc.2007.11.027.
- Wu, S. Y., Leu, Y. L. and Chang, Y. L.** (2012). Physalin F induces cell apoptosis in human renal carcinoma cells by targeting NF-kappaB and generating reactive oxygen species. *PLoS ONE* **7**, e40727. doi: 10.1371/journal.pone.0040727.

CAPÍTULO 2

“ANTIPARASITIC EVALUATION OF TRITERPENOIDS RELATED TO BETULINIC ACID REVEALS POTENT AND SELECTIVE ANTI-*Trypanosoma cruzi* INHIBITORS “, EM FASE DE SUBMISSÃO.

O presente trabalho comprova a atividade anti-*T. cruzi* de uma série de triterpenos e demonstra o potencial do ácido betulínico como protótipo para geração de derivados mais potentes e seletivos.

**Antiparasitic evaluation of triterpenoids related to betulinic acid
reveals potent and selective anti-*Trypanosoma cruzi* inhibitors**

Cássio Santana Meira¹, Taís Soares Macedo¹, José Maria Barbosa-Filho²,
Celso Amorim Camara³, Tania Maria Sarmento da Silva³, Adriana
Lanfredi-Rangel¹, Elisalva Teixeira Guimarães^{1,4}, Diogo Rodrigo de
Magalhães Moreira^{1,5}, Milena Botelho Pereira Soares^{1,5*}

¹ Centro de Pesquisas Gonçalo Moniz, Fundação Oswaldo Cruz, Salvador, BA, Brazil.

² Laboratório de Tecnologia Farmacêutica, Universidade Federal da Paraíba, João Pessoa, PB, Brazil.

³ Departamento de Química, Universidade Federal Rural de Pernambuco, Recife, PE, Brazil.

⁴ Universidade do Estado da Bahia, Departamento de Ciências da Vida, Salvador, BA, Brazil.

⁵ Hospital São Rafael, Centro de Biotecnologia e Terapia Celular, Salvador, BA, Brazil.

*Corresponding author: Milena Botelho Pereira Soares. Centro de Pesquisas Gonçalo Moniz, Fundação Oswaldo Cruz. Rua Waldemar Falcão, 121, Candeal, Salvador, Bahia, Brazil. Postal code: 40296-710. Phone: (+55)7131762260 ; fax: (+55)7131762272. Email address: milena@bahia.fiocruz.br

Abstract

We previously observed that betulinic acid and its ester derivatives have antiplasmodial activity. Here, we investigated the anti-*T. cruzi* and antiplasmodial activities of betulinic acid and its semi-synthetic derivatives. We found that betulinic acid is a broad, potent and selective anti-*T. cruzi* compound and this was enhanced by semi-synthetic derivatives BA5 and BA8. Electron microscopy of trypomastigotes incubated with BA5 showed membrane blebbing, flagella retraction, the formation of numerous atypical vacuoles within the cytoplasm as well as Golgi cisternae dilatation. In addition, flow cytometry examination showed that parasite death is mainly caused by necrosis. Treatment with the most potent derivatives reduced the invasion process, as well as intracellular parasite development in macrophage host cells, with a potency and selectivity similar to that observed in benznidazole-treated cells. Finally, we observed that combination of compound BA5 and benznidazole have a greater anti-*T. cruzi* activity than when compounds were used alone. In contrast with the potent anti-*T. cruzi* activity, these compounds exhibited low antimalarial activity when compared to mefloquine. Overall, these results indicate that betulinic acid and specifically its derivative BA5, are potent and selective antiparasitic agents with strong anti-*T. cruzi* activity.

Keywords: Chagas disease, *Trypanosoma cruzi*, *Plasmodium falciparum*, triterpenoids, betulinic acid.

Introduction

Chagas disease and malaria are caused by protozoan parasites and constitute serious public health problems worldwide with few successful treatment options. It is estimated that Chagas disease affects about 8–10 million people with 100 million at risk of acquiring the disease (WHO, 2010). Also known as American Trypanosomiasis, it is caused by the flagellate protozoan *Trypanosoma cruzi* and considered one of the most important protozoan diseases that occurs in Latin America. Pharmacotherapy is based on two drugs, the nitroheterocyclic compound (nifurtimox) and a nitroimidazole (benznidazole). However, both drugs are effective only in the acute phase and in the short-term chronic phase of infection. Furthermore, accompanying these limitations are the severe side effects associated with treatment (Viotti *et al.*, 2009; Sánchez-Sancho *et al.*, 2010). This scenario emphasizes a need to develop safer and more effective drugs.

Severe malaria, caused by *Plasmodium falciparum*, kills nearly a million children each year in Africa alone. This infectious disease consists in one of the world's largest public health problems (Miller *et al.*, 2013). Malaria treatment has been based on a narrow variety of drugs, with current pharmacologic intervention relying heavily on artemisinin based combination therapies. Moreover, the increase in drug-resistant parasites has been reported. These challenges, combined with the insecticide-resistant vectors and the lack of a vaccine makes the research and development of new antimalarial agents a matter of great relevance to public health (Murray *et al.*, 2012).

Natural products play an important role in drug discovery and development. Specifically, terpenoids are well-known anti-infective agents endowed with a broad range of activity (Evers *et al.*, 1996; Hashimoto *et al.*, 1997). This is exemplified by betulinic acid, a lupane-type pentacyclic triterpenoid with strong anti-HIV activity that has advanced in clinical trials (Baglin *et al.*, 2003). Based on these interesting aspects, a

number of triterpenoids, both naturally-occurring and semi-synthetic, have been investigated as antiparasitic agents (Yogeeswari & Sriram, 2005). More specific in the case of betulinic acid, it not only has antiviral activity but also a broad spectrum antiprotozoal activity against the erythrocytic stage of chloroquine-resistant *P. falciparum* strain, as well as antileishmania activity (Magaraci *et al.*, 2003; Hoet *et al.*, 2007; Chen *et al.*, 2010; Innocente *et al.*, 2012). In view of these findings, betulinic acid is considered a prototype for the design and synthesis of antiprotozoal agents. In recent years, chemical modifications of the carboxyl group have suggested that this part of the molecule can produce derivatives with enhanced antiprotozoal activity when compared to betulinic acid (Gros *et al.*, 2006; Da Silva *et al.*, 2013). Based on these facts, we investigated the *in vitro* activity of betulinic acid and related triterpenoids (lupeol, solasodine, hecogenin acetate and diosgenin acetate), as well as a number of semi-synthetic betulinic acid derivatives against Y strain trypomastigotes of *Trypanosoma cruzi*, as well as against W2 strain of *Plasmodium falciparum*.

Materials and Methods

Chemistry

Betulinic acid (BA) was extracted from the bark of *Ziziphus joazeiro* Mart. (Rhamnaceae) by using a previously described method (Barbosa-Filho *et al.*, 1985). Lupeol was isolated from the stem bark of *Diploptropis ferruginea* Benth. (Fabaceae) (Almeida *et al.*, 2005). Solasodine was extracted from the fruits of *Solanum paludosum* Moric. (Solanaceae) (Barbosa-Filho *et al.*, 1991). Diosgenin acetate was extracted from *Dioscorea cayenensis* Lam. (Dioscoreaceae) (Barbosa-Filho *et al.*, 1981). Hecogenin acetate was purchased from Sigma-Aldrich (Saint Louis, MO, USA). The betulinic acid

acetate (BAA), betulonic acid (BOA), betulinic acid methyl ester (BAME) and betulinic acid methyl ester acetate (BAMEA) were prepared as previously described in literature (Kim *et al.*, 2001; Urban *et al.*, 2005; Uzenkova *et al.*, 2005). Semi-synthetic compounds (BA1 to BA8) were prepared from betulinic acid using protocols described in the literature (Da Silva *et al.*, 2013). Prior to pharmacological evaluation, all compound structures and purity were determined by NMR, IR, MS and elemental analysis. The structure of betulinic acid and other compounds used in this study are shown in **Figures 1** and **2**.

Cytotoxicity to mammalian cells

Peritoneal exudate macrophages obtained from BALB/c mice were placed into 96-well plates at a cell density 1×10^5 cells/well in RPMI-1640 medium without phenol red (Sigma) supplemented with 10% of fetal bovine serum (FBS; Cultilab, Campinas, Brazil), and 50 $\mu\text{g/mL}$ of gentamycin (Novafarma, Anápolis, Brazil) and incubated for 24 h at 37°C and 5% CO_2 . After that time, each compound was added in triplicate at eight concentrations ranging from 0.04 to 100 μM and incubated for 72 h. Twenty μL /well of AlamarBlue (Invitrogen, Carlsbad, CA, USA) was added to the plates during 10 h. Colorimetric readings were performed at 570 and 600 nm. LC_{50} values were calculated using data-points gathered from three independent experiments. Gentian Violet (Synth, São Paulo, Brazil) was used as a cytotoxicity control, at concentrations ranging from 0.04 to 10 μM . This experiment was repeated three times.

Antimalarial activity

W2 strain *P. falciparum* (chloroquine-resistant) was maintained in a continuous culture of human erythrocytes (blood group O^+) using the RPMI 1640 medium

supplemented with 10% of human plasma. Parasites grown at 1 – 2% parasitemia and 2.5% hematocrit were distributed into 96-well culture plates and incubated with the compounds at five different concentrations, ranging from 0.12 to 10 μM diluted in culture medium (RPMI 1640) in the absence of hypoxanthine. After 24 h, 0.5 μCi of [^3H]-hypoxanthine was added, the plate were incubated again and parasites were harvested using a cell harvester to quantify the [^3H]-hypoxanthine incorporation in a β -radiation counter. Mefloquine (Farmaguinhos, Rio de Janeiro, Brazil) was used as standard drug.

Cytotoxicity for trypomastigotes

Bloodstream trypomastigotes forms of *T. cruzi* (Y strain) were obtained from supernatants of LLC-MK2 cells previously infected and maintained in RPMI-1640 medium supplemented with 10 % FBS, and 50 $\mu\text{g/mL}$ gentamycin at 37 °C and 5% CO_2 . Parasites (4×10^5 cells/well) were dispensed into 96-well plates and the test inhibitors were added at eight concentrations ranging from 0.04 to 100 μM in triplicate and the plate was incubated for 24 h at 37° C and 5% of CO_2 . Aliquots of each well were collected and the number of viable parasites was assessed in a Neubauer chamber and compared to untreated cultures. Benznidazole (LAFEPE, Recife, Brazil) was used as positive control anti-*T. cruzi* in the studies. This experiment was performed three times.

In vitro *T. cruzi* infection assay

Peritoneal exudate macrophages were plated at a cell density of 2×10^5 cells/well in 24 well-plates with sterile coverslips on the bottom in RPMI supplemented with 10% FBS and incubated for 24 h. Cells were then infected with trypomastigotes at a ratio of

10 parasites per macrophage for 2 h. Free trypomastigotes were removed by successive washes using saline solution. Cultures were incubated in complete medium alone or with the compounds under investigation in different concentrations for 6 h. The medium was replaced with fresh medium and the plate was incubated for 4 days. Cells were fixed in absolute alcohol and the percentage of infected macrophages and the mean number of amastigotes/100 macrophages was determined by manual counting after hematoxylin and eosin staining in an optical microscope (Olympus, Tokyo, Japan). The percentage of infected macrophages and the relative number of amastigotes per macrophage was determined by counting 100 cells per slide. This experiment was performed three times.

Invasion assay

Peritoneal macrophages (10^5 cells) were plated onto sterile coverslips in 24-well plates and kept for 24 h. The plate was washed with saline solution and trypomastigotes were then added at a cell density of 1×10^7 parasites/well along with the addition of BA5, or BA6 or BA8 (50 μ M). The plate was incubated for 2 h at 37° C and 5% CO₂, followed by successive washes with saline solution to remove extracellular trypomastigotes. Plates were maintained in RPMI medium supplemented with 10% FBS at 37° C for 2 h. Infected macrophages were examined for the presence of amastigotes by optical microscopy using a standard hematoxylin and eosin staining. Amphotericin B (Gibco Laboratories, Gaithersburg, MD, USA) was used as a positive control in this assay.

Ultrastructural studies

Trypomastigotes at a cell density of 1×10^7 cells/mL in 24 well-plates were treated with test inhibitor BA5 (2 or 4 μ M) or not for 24 h. Parasites were then fixed with 2% formaldehyde and 2.5% glutaraldehyde (Electron Microscopy Sciences, Hatfield, PA, USA) in sodium cacodylate buffer (0.1 M, pH 7.2) for 1 h at room temperature. After fixation, parasites were washed 3 times with sodium cacodylate buffer (0.1 M, pH 7.2), and post-fixed with a 1.0 % solution of osmium tetroxide containing 0.8% potassium ferrocyanide (Sigma) for 1 h. Cells were subsequently dehydrated in increasing concentrations of acetone (30, 50, 70, 90 and 100%) for 10 min at each step and embedded in Polybed resin (PolyScience family, Warrington, PA, USA). Ultrathin sections on copper grids were contrasted with uranyl acetate and lead citrate and observed under a ZEISS 109 transmission electron microscope. For scanning electron microscopy, trypomastigotes treated with or without BA 505 (2 or 4 μ M) and fixed in the same conditions were washed in 0.1 M cacodylate buffer, and allowed to adhere in coverslips pre-coated with poly-L-lysine (Sigma). Cells were then post-fixed with a solution of osmium tetroxide containing 0.8% of potassium ferrocyanide for 30 min and dehydrated in crescent concentrations of ethanol (30, 50, 70, 90 and 100%). The samples were dried until the critical point, metallized with gold and analyzed in a JEOL JSM-6390LV scanning electron microscope.

Propidium iodide and annexin V staining

Trypomastigotes 1×10^7 /mL in 24 well-plates were treated with 5 or 10 μ M of BA5 in RPMI supplemented with FBS at 37°C for 24 or 72 h and labeled for propidium iodide (PI) and annexin V using the annexin V-FITC apoptosis detection kit (Sigma), according to the manufacturer's instructions. Acquisition and analyses was performed using a FACS Calibur flow cytometer (Becton Dickinson, CA, USA), with FlowJo

software (Tree Star, OR, USA). A total of 10,000 events were acquired in the region previously established as that corresponding to trypomastigotes forms of *T. cruzi*.

Statistical analyses

To determine the lethal concentration 50% of BALB/c mice macrophages (LC₅₀) and the inhibitory concentration 50% (IC₅₀) of the trypomastigotes and amastigotes forms of *T. cruzi*, we used nonlinear regression. The one-way ANOVA followed by Bonferroni's multiple comparison test was used to determine the statistical significance of the group comparisons in the in vitro infection studies and cell invasion study. Results were considered statistically significant when $P < 0.05$. All analyzes were performed using Graph Pad Prism version 5.01 (Graph Pad Software, San Diego, CA, USA).

Results

Isolation and semi-synthesis

Figure 1 shows the exact chemical structure of naturally-occurring triterpenoids and ester semi-synthetic derivatives, while **Figure 2** shows the new semi-synthetic derivatives. The new semi-synthetic derivatives were prepared by amide bond formation using betulinic acid as starting compound. This enabled the synthesis of eight derivatives which contain a 6-member heterocyclic ring attached at C28 position.

Antiparasitic activity and cytotoxicity against mammalian cells

Once the compounds had been chemically characterized, we focused on evaluating their biological activity. First, we evaluated the antiparasitic activity of the natural products and the semi-synthetic derivatives against W2 strain of *Plasmodium*

falciparum and Y strain trypomastigotes of *Trypanosoma cruzi*. As shown in **Table 1**, only five compounds, including betulinic acid, exhibited antiplasmodial activity. The betulinic acid showed an IC_{50} value of 9.9 μM whereas the derivatives BA4, BA5, BA6 and BA8 showed IC_{50} values lower than 3 μM . Despite presenting a high activity than betulinic acid, the semi-synthetic derivatives were less potent than mefloquine, which showed IC_{50} value of 0.04 μM . Regarding to the trypanocidal activity against the trypomastigote form of *T. cruzi*, apart from synthetic compounds BA1, BA2 and the natural products hecogenin acetate and diosgenin acetate, all compounds showed trypanocidal activity. In this assay, the betulinic acid showed an IC_{50} value of 19.5 μM , a weak activity when compared with the semi-synthetic derivatives BA4, BA5, BA6 and BA8 that demonstrated IC_{50} values of 10.2 μM , 1.8 μM , 5.4 μM and 5 μM , respectively. In addition to the increased potency when compared to betulinic acid, derivatives demonstrated IC_{50} values smaller than the value of the reference drug (benznidazole = 11.4 μM).

Next, compounds cytotoxicity to mouse macrophages was analyzed. As shown in **Table 1**, the compounds were several times less cytotoxic in comparison to gentian violet (LC_{50} = 0.48 μM), the reference drug in this assay. On the other hand, the betulinic acid showed a weak selectivity against *P. falciparum* and no selectivity against trypomastigotes forms of *T. cruzi*. Already the semi-synthetic derivatives BA4, BA5, BA6 and BA8 showed a greater selectivity against the parasites. For example, the derivative BA8 was 50 times more cytotoxic against *P. falciparum* than peritoneal macrophages.

Investigating the mechanism of action

After confirming that compounds were able to kill parasites, our next step was to understand how they affect parasite cells through assays with trypomastigotes forms of *T. cruzi*, after determining that the trypanocidal activity of the compounds was better than the antimalarial activity. For this purpose we used scanning electron microscopy (SEM) and transmission electron microscopy (TEM) to examine the ultrastructural morphology of trypomastigotes (Y strain) treated with the most potent derivative BA5 for 24 h. As we can see in **Figure 3** untreated trypomastigotes showed the typical elongated shape of the parasite without visible alterations in the plasma membrane or in cell volume (**Fig. 3A**). On the other hand, trypomastigotes treated with the semi-synthetic derivative BA5 (2 or 4 μM) showed flagella retraction (**Fig. 3B**), some loss of plasma membrane integrity and body deformation (**Fig. 3C**). Furthermore, thin sections of untreated trypomastigotes observed by TEM revealed normal appearance of organelles, intact plasma membrane and parasite cytoplasm without alterations (**Fig. 4A**). However, treatment with BA5 (2 or 4 μM) caused plasma membrane alterations (**Fig. 4B**), the formation of numerous atypical vacuoles within the cytoplasm (**Fig. 4C**), dilatation of some Golgi cisternae (**Fig. 4D**) and profiles of endoplasmic reticulum involving organelles as nucleus accompanied by the formation of autophagosomes (**Fig. 4E and 4F**).

Finally, to understand the mechanism by which compound BA5, the most potent semi-synthetic derivative causes parasite death, a double staining with annexin V and propidium iodide was performed for flow cytometry analysis. After 24 h of incubation, parasites treated with BA5 at 5 μM and 10 μM presented 6.79 % and 24.08 % of cells PI positive, respectively. This increase in PI positive parasites was also observed after 72 h of treatment. As shown in **Figure 5**, following 72 h of incubation, parasites treated with BA5 at 5 μM and 10 μM presented 48.6 % and 92.1 % of cells positive for PI

stained, respectively. These results indicate that the BA5 derivative induces a necrotic process in trypomastigotes of *T. cruzi*.

In vitro infection studies

Since the semi-synthetic BA4, BA5, BA6 and BA8 derivatives showed a higher activity against extracellular forms of *T. cruzi* and low cytotoxicity to mammalian cells, we investigated the ability of these semi-synthetic derivatives to inhibit the development of parasites in host cells. For this purpose, macrophages previously infected with Y strain trypomastigotes were treated with 50 μ M of the compounds. Cells were stained with hematoxylin and eosin and observed by optical microscopy in order to evaluate the ability of drugs on reduce the percentage of infected macrophages and the relative number of amastigotes per 100 cells. Benznidazole was used as a positive control. As shown in **Figure 6**, the treatment with the semi-synthetic compounds significantly decreased the percentage of infected macrophages ($P < 0.001$) and the relative number of amastigotes per 100 macrophages ($P < 0.001$) when compared with untreated cultures. When tested at different concentrations, it was possible to calculate the IC_{50} value of the derivatives against intracellular amastigotes. As shown in **Table 2**, the derivatives presented a similar activity when compared to that observed in benznidazole.

We also evaluate the effect of the most potent derivatives on the invasion process. In this assay, mouse macrophages were exposed to trypomastigotes and at the same time treated with the semi-synthetic BA5, BA6 and BA8 derivatives (50 μ M) for 2 h. After this time, the cells were washed with saline solution to remove extracellular parasites and incubated for 2 additional hours. Cells were stained with hematoxylin and eosin and analyzed by optical microscopy. Amphotericin B was used as a positive

control for this experiment. As shown in **Figure 7**, the derivatives significantly inhibited the parasite invasion in comparison to untreated cells ($P < 0.001$), but not as efficiently as the positive control amphotericin B, although they were more effective than benznidazole, that show a weak activity on this assay.

Finally, we performed a final set of experiments to evaluate the effect of the combination of the most potent semi-synthetic derivative (BA5) with benznidazole in parasite development in host cells. As shown in **Figure 8A and 8B**, the combination of BA5 and benznidazole at low concentrations reduced the number of infected macrophages as well as the number of amastigotes per 100 macrophages to a greater degree than the respective compound used alone. The combination showed an even more advantageous effect at higher concentrations. As shown in **Figure 8C and 8D**, the combination of BA5 (50 μM) with benznidazole (50 μM) practically eradicated the infection in macrophages, which was not observed when compounds were tested alone. More importantly, this was achieved without affecting host cell viability (data not shown).

Discussion

An effective antiprotozoal treatment continues to be necessary due to acquired resistance of *P. falciparum* to aminoquinoline and artemisinin regimes and the lack of existing anti-Chagas disease drugs (Baird *et al.*, 2005; Muñoz *et al.*, 2011). Screening of isolated natural and semi-synthetic compounds is a reliable strategy to identify new antiprotozoal agents (Newman & Cragg, 2007). Terpenoids are a rich source of antiparasitic compounds (Jimenez-Ortiz *et al.*, 2005; Da Silva *et al.*, 2013; Sülsen *et al.*, 2013). Of these, triterpenoids, such as betulinic acid, are some of the most investigated in terms of potency and selectivity. In the present study, we investigated the anti-*T.*

cruzi and anti-*P. falciparum* activity of natural triterpenoids related to betulinic acid and its ester and amide semi-synthetic derivatives containing substituents attached in the lupane backbone.

Here, we observed that most of the triterpenoids, specially the semi-synthetic derivatives, are selective anti-*T. cruzi* agents. The incorporation of an ester showed a weak contribution to enhance the trypanocidal activity against trypomastigotes. Similar results were found previously with epimastigotes forms (Domínguez-Carmona *et al.*, 2010). On the other hand the incorporation of an amide on C-28 enhanced the anti-*T. cruzi* activity. This led to the identification of compound BA5, which exhibited a potency superior to benznidazole, the current standard drug. We also observed a substantial enhancement of antimalarial activity for semi-synthetic derivatives in comparison to betulinic acid, however these compounds were less potent than mefloquine. To date, there exist a number of reports in the literature describing the chemical modifications of betulinic acid at C-28 position to produce semi-synthetic derivatives with enhanced antimalarial, anti-tumor and anti-viral activities (Jeong *et al.*, 1999; Baltina *et al.*, 2003; Sá *et al.*, 2009; Domínguez-Carmona *et al.*, 2010). This is the first report, regarding the contribution of the incorporation of amides on C-28 as drug design strategy to enhance the antiprotozoal activity.

An examination of parasite morphology revealed that compound BA5 is parasiticidal, by altering parasite ultrastructure. It induced flagella retraction, loss of plasma membrane integrity and notable cell body deformation. Interestingly, the treatment with BA5 also led to the formation of numerous and atypical vacuoles within the cytoplasm, as well as the dilatation of Golgi cisternae. Lack of membrane integrity and cytoplasmic vacuolization are often associated to necrotic parasitic death (Rodriguez *et al.*, 2006; Zong and Thompson, 2006). Through flow cytometry assays,

we confirmed the parasitic death by necrosis. In addition, we observed that the treatment produced endoplasmatic reticulum profiles involving organelles as nucleus accompanied by the formation of autophagosomes, typical features of autophagy (Tsujimoto & Shimizu, 2005; Fernandes *et al.*, 2012).

Most importantly, the semi-synthetic derivatives were able to prevent the parasite development and invasion into host cells, with potency similar to benznidazole. As a limitation, these compounds didn't eliminate intracellular amastigotes even in the highest concentration tested. However, the derivative BA5 exhibited enhanced antitrypanosomal activity when used in combination to benznidazole, which is capable of substantially eradicating the infection at the highest concentration tested. These results encourage further investigations, since the combination of drugs is becoming increasingly attractive to combat parasitic diseases (Musa *et al.*, 2012; Alirol *et al.*, 2013; Diniz *et al.*, 2013).

Altogether, these findings reinforce that terpenoids are active antimalarial and antitrypanosomal agents and at the same time do not cause host cell toxicity. Therefore, the screening for structurally-related BA5 derivatives for anti-*T. cruzi* treatment is an attractive line of drug development.

Conclusion

Chagas disease and malaria are life-threatening infections. *P. falciparum* is susceptible to betulinic acid, making this class of compounds appealing for drug development. Here, we have reported the synthesis and antiparasitic evaluation of betulinic acid and its new semi-synthetic derivatives. By varying substituents attached to the amide group, we could find substituents that retain, enhance or greatly increase the antiprotozoal activity, in comparison to betulinic acid. Specifically, we identified the betulinic acid derivative BA5 as a broad, potent and selective anti-*T. cruzi* agents,

which destroy parasite cells by necrotic death and acts additively in combination to benznidazole.

References

Alirol E, Schrumpf D, Amici Heradi J, Riedel A, de Patoul C, Quere M, Chappuis F. Nifurtimox-eflornithine combination therapy for second-stage gambiense human African trypanosomiasis: Médecins Sans Frontières experience in the Democratic Republic of the Congo. *Clin Infect Dis*. 2013; 56(2): 195-203.

Almeida JRGS, José Maria Barbosa-Filho JM, Cabral AGS, Agra MF, Da Cunha EVL, Da Silva MS, Nascimento SC, Braz-Filho R. Diploflavone, a new flavonoid from *Diploptropis ferruginea* Benth. (Fabaceae). *J Braz Chem Soc*. 2005; 16(5): doi:0.1590/S0103-50532005000800027.

Baglin I, Mitaine-Offer AC, Nour M, Tan K, Cavé C, Lacaille-Dubois MA. A review of natural and modified betulinic, ursolic and echinocystic acid derivatives as potential antitumor and anti-HIV agents. *Mini Rev Med Chem*. 2003; 3(6): 525-539.

Baird JK. Effectiveness of antimalarial drugs. 2005; 352(15): 1565-1577.

Baltina LA, Flekhter OB, Nigmatullina LR, Boreko EI, Pavlova NI, Nikolaeva SN, Savinova OV, Tolstikov GA. Lupane triterpenes and derivatives with antiviral activity. *Bioorg Med Chem Lett*. 2003; 13(20): 3549-3552.

Barbosa-Filho JM, Medeiros DF, Bhattacharyya J. Estudos em Dioscoreaceas Brasileiras. Parte II: Isolamento e identificação de diosgenina e yamogenina e outros esteroides nas raízes de *Dioscorea cayenensis* L. var. *rotundata* Lam. *Ciencia Cultura Saúde*. 1981; 3(2):35-37.

Barbosa-Filho JM, Trigueiro JA, Cheriyan UO, Bhattacharyya J. Constituents of the stem-bark of *Ziziphus joazeiro*. *J Nat Prod*. 1985; 48(1): 152-152.

Barbosa-Filho JM, Agra MF, Oliveira RAG, Paulo MQ, Troling G, Cunha EVL, Ataíde JR, Bhattacharyya J. Chemical and pharmacological investigation of *Solanum* species of Brazil - a search for solasodine and other potentially useful therapeutic agents. *Mem Inst Oswaldo Cruz*. 1991; 86: 189-191.

Chen Y, Li S, Sun F, Han H, Zhang X, Fan Y, Tai G, Zhou Y. In vivo antimalarial activities of glycoalkaloids isolated from Solanaceae plants. *Pharm Biol*. 2010; 48(9): 1018-1024.

Da Silva GN, Maria NR, Schuck DC, Cruz LN, de Moraes MS, Nakabashi M, Graebin C, Gosmann G, Garcia CR, Gnoatto SC. Two series of new semisynthetic triterpene derivatives: differences in anti-malarial activity, cytotoxicity and mechanism of action. *Malar J*. 2013. 12(89): doi: 10.1186/1475-2875-12-89.

Diniz Lde F, Urbina JA, de Andrade IM, Mazzeti AL, Martins TA, Caldas IS, Talvani A, Ribeiro I, Bahia MT. Benznidazole and posaconazole in experimental Chagas disease: positive interaction in concomitant and sequential treatments. *Plos Negl Trop Dis*. 2013; 7(8): e2367.

Domínguez-Carmona DB, Escalante-Erosa F, García-Sosa K, Ruiz-Pinell G, Gutierrez-Yapu D, Chan-Bacab MJ, Giménez-Turba A, Peña-Rodríguez LM.. Antiprotozoal activity of betulinic acid derivatives. *Phytomedicine*. 2010;17(5): 379-382.

Evers M, Poujade C, Soler F, Ribeill Y, James C, Lelièvre Y, Gueguen JC, Reisdorf D, Morize I, Pauwels R, De Clercq E, Hénin Y, Bousseau A, Mayaux JF, Le Pecq JB, Dereu N. Betulinic acid derivatives: a new class of specific inhibitors of human immunodeficiency virus type 1 entry. *J Med Chem.* 1996; 39(5): 1056-1068.

Fernandes MC, Da Silva EN, Pinto AV, De Castro SL, Menna-Barreto RF. A novel triazolic naphthofuranquinone induces autophagy in reservosomes and impairment of mitosis in *Trypanosoma cruzi*. *Parasitology.* 2012; 139(1): 26-36.

Gros L, Lorente SO, Jimenez CJ, Yardley V, Rattray L, Wharton H, Little S, Croft SL, Ruiz-Perez LM, Gonzalez-Pacanowska D, Gilbert IH Evaluation of azasterols as anti-parasitics. *J Med Chem.* 2006; 49(20): 6094-6103.

Hashimoto F, Kashiwada Y, Cosentino LM, Chen CH, Garrett PE, Lee KH. Anti-AIDS agents--XXVII. Synthesis and anti-HIV activity of betulinic acid and dihydrobetulinic acid derivatives. *Bioorg Med Chem.* 1997; 5(12): 2133-2143.

Hoet S, Pieters L, Muccioli GG, Habib-Jiwan JL, Opperdoes FR, Quetin-Leclercq J. Antitrypanosomal activity of triterpenoids and sterols from the leaves of *Strychnos spinosa* and related compounds. *J Nat Prod.* 2007; 70(8):1360-1363.

Innocente AM, Silva GN, Cruz LN, Moraes MS, Nakabashi M, Sonnet P, Gosmann G, Garcia CR, Gnoatto SC. Synthesis and antiplasmodial activity of betulinic acid and ursolic acid analogues. *Molecules.* 2012; 17(10): 12003-12014.

Jeong HJ, Chai HB, Park SY, Kim DS. Preparation of amino acid conjugates of betulinic acid with activity against human melalona. *Bioorg Med Chem Lett*. 1999; 9(8): 1201-1204.

Jimenez-Ortiz V, Brengio SD, Giordano O, Tonn C, Sanchez M, Burgos MH, Sosa MA. The trypanocidal effect of sesquiterpene lactones helenalin and mexicanin on cultured epimastigotes. *J Parasitol*. 2005; 91(1): 170–174.

Kim JY, Koo HM, Kim DSHL. Development of C-20 modified betulinic acid derivatives as antitumor agents. *Bioorg Med Chem Lett*. 2001; 11(17):2405–2408.

Magaraci F, Jimenez CJ, Rodrigues C, Rodrigues JC, Braga MV, Yardley V, de Luca-Fradley K, Croft SL, de Souza W, Ruiz-Perez LM, Urbina J, Gonzalez Pacanowska D, Gilbert IH. Azasterols as inhibitors of sterol 24-methyltransferase in leishmania species and *Trypanosoma cruzi*. *J Med Chem*. 2003; 46(22): 4714-4727.

Miller LH, Ackerman HC, Su XZ, Wellems TE. Malaria biology and disease pathogenesis: insights for new treatments. *Nat Med*. 2013;19(2):156-67.

Muñoz MJ, Murcia L, Segovia M. The urgent need to develop new drugs and tools for the treatment of Chagas disease. *Expert Rev Anti Infect Ther*. 2011; 9(1): 5-7.

Murray CJL, Rosenfeld LC, Lim SS, Andrews KG, Foreman KJ, Haring D, Fullman N, Naghavi M, Lozano R, Lopez AD. Global malaria mortality between 1980 and 2010: a systematic analysis. *Lancet*. 2012; 379(9814):413–431.

Musa A, Khalil E, Hailu A, Olobo J, Balasegaram M, Omollo R, Edwards T, Rashid J, Mbui J, Musa B, Abuzaid AA, Ahmed O, Fadlalla A, El-Hassan A, Mueller M, Mucee G, Njoroge S, Manduku V, Mutuma G, Apadet L, Lodenyo H, Mutea D, Kirigi G, Yifru S, Mengistu G, Hurissa Z, Hailu W, Weldegebreal T, Tafes H, Mekonnen Y, Makonnen E, Ndegwa S, Sagaki P, Kimutai R, Kesusu J, Owiti R, Ellis S, Wasunna M. Sodium stibogluconate (SSG) & paromomycin combination compared to SSG for visceral leishmaniasis in East Africa: a randomized controlled trial. *pLoS Negl Trop Dis*. 2012; 6(6): e.1674.

Newman DJ, Cragg GM. Natural products as sources of new drugs over the last 25 years. *J Nat Prod*. 2007; 70: 461-477.

Rodrigues JC, Seabra SH, De Souza W. Apoptosis-like death in parasitic protozoa. *Braz. J Morphol Sci*. 2006; 23(2): 87-98.

Sá MS, Costa JF, Krettli AU, Zalis MG, Maia GL, Sette IM, Câmara C de A, Filho JM, Giuliatti-Harley AM, Ribeiro Dos Santos R, Soares MB. Antimalarial activity of betulinic acid and derivatives in vitro against *Plasmodium falciparum* and in vivo in *P. berghei*-infected mice. *Parasitol Res*. 2009; 105(1): 275-279.

Sánchez-Sancho F, Campillo NE, Páez JA. Chagas disease: progress and new perspectives. *Curr Med Chem*. 2010;17(5):423-52.

Sülsen VP, Cazorla SI, Frank FM, Laurella LC, Muschietti LV, Catalán CA, Martino VS, Malchiodi EL. Natural terpenoids from *Ambrosia* species are active in vitro and in vivo against human pathogenic trypanosomatids. 2013; 7(10): e2494.

Tsujimoto Y, Shimizu S. Another way to die: Autophagic programmed cell death. *Cell Death Differ*. 2005; 12: 1528-1534.

Urban M, Sarek J, Tislerova I, Dzubak P, Hajduch M. Influence of esterification and modification of A-ring in a group of lupane acids on their cytotoxicity. *Bioorg Med Chem*. 2005; 13(19):5527–5535.

Uzenkova NV, Petrenko NI, Shakirov MM, Shul'ts EE, Tolstikov GA. Synthesis of 30-amino derivatives of lupane triterpenoids. *Chem Nat Compounds*. 1005; 41:692–700.

Viotti R, Vigliano C, Lococo B, Alvarez MG, Petti M, Bertocchi G, Armenti A. Side effects of benznidazole as treatment in chronic Chagas disease: fears and realities. *Expert Rev Anti Infect Ther* (2009); 7(2):157-163.

World Health Organization First WHO Report on Neglected Tropical Diseases: Working to Overcome the Global Impact of Neglected Tropical Diseases World Health Organization, Geneva (2010), pp. 1–172.

Yogeeswari P, Sriram D. Betulinic acid and its derivatives: a review on their biological properties. *Curr Med Chem*. 2005; 12(6): 657-666.

Zong WX, Thompson CB. Necrotic death as a cell fate. *GenesDev.* 2006; 20(1):1-15.

Legends to figures

Figure 1: Naturally-occurring terpenoids and ester semi-synthetic derivatives.

Figure 2. New semi-synthetic betulinic acid derivatives.

Figure 3. Scanning electron microscopy of trypomastigotes of *T. cruzi* treated with BA5 (2 or 4 μM) for 24 h. (A) Control parasites showing the elongated body and intact plasma membrane; (B) trypomastigote treated with BA5 (2 μM) showing alterations in cell shape and flagella retraction; (C) trypomastigotes treated with BA5 (4 μM) showing loss of plasma membrane integrity and body deformation. White arrows indicate the alterations reported. Scale bars = 2 μm .

Figure 4. Transmission electron microscopy of trypomastigotes of *T. cruzi* treated with BA5 (2 or 4 μM) for 24 h. (A) Control parasites, presenting a typical morphology of the nucleus (N), kinetoplast (K) and mitochondria (M); (B-D) trypomastigotes treated with BA5 (2 μM) showing membrane blebbing (B), the formation of numerous and atypical vacuoles within the cytoplasm (C) and dilatation of some Golgi cisternae (D); (E and F) trypomastigotes treated with BA5 (4 μM) showing profiles of endoplasmic reticulum involving organelles accompanied by the formation of autophagosomes. Black arrows indicate changes in the organelles. Scale bars: A, E and F = 0.5 μm ; B-D = 0.2 μm .

Figure 5. Flow cytometry analysis of trypomastigotes treated with BA5 and incubated with propidium iodide (PI) and annexin V. (A) Untreated trypomastigotes after 24 h of incubation; (B and C) trypomastigotes treated with 5 μM and 10 μM of BA5 respectively by 24 h; (D) untreated trypomastigotes after 72 h of incubation; (E and F) trypomastigotes treated with 5 μM or 10 μM of BA5, respectively, for 72 h.

Figure 6. The betulinic acid derivatives inhibit the growth of intracellular amastigotes of *T. cruzi*. Mouse peritoneal macrophages were infected with Y strain trypomastigotes for 2 h and treated with betulinic acid derivatives (50 μ M) or benznidazole (50 μ M), a standard drug. Infected cells were stained with hematoxylin and eosin and analyzed by optical microscopy. The percentage of infected macrophages (A) and the relative number of amastigotes in 100 macrophages (B) are higher in untreated infected controls than in cultures treated with 50 μ M of the test-inhibitors BA4, BA5, BA6 and BA8. Bdz is benznidazole. Values represent the mean \pm SEM of triplicate.***, $P < 0.001$ **, $P < 0.01$ compared with the untreated group.

Figure 7. The betulinic acid derivatives impair *T. cruzi* trypomastigote invasion in macrophages. Mouse macrophages were simultaneously infected with 10^7 Y strain trypomastigotes and treated with 50 μ M of the test-inhibitor for 2 h. The percentage of infected macrophages is higher in untreated infected cells than in cells treated with 50 μ M of test-inhibitors BA5, BA6 or BA8. Bdz is benznidazole and AmpB is amphotericin B. ***, $P < 0.001$.

Figure 8. A simultaneous treatment with BA5 and benznidazole shows a high eradication rate of the infection in vitro. A combined therapy with both compounds increased the inhibition of the infection with no cytotoxicity effects on macrophages. (A and B) treatment with the IC_{50} values of the drugs and the combination of the IC_{50} values. (C and D) treatment with 50 μ M of the drugs and the combination of 50 μ M of each compound. Bdz is benznidazole. Comb. is combination. ***, $P < 0.001$.

Figure 1

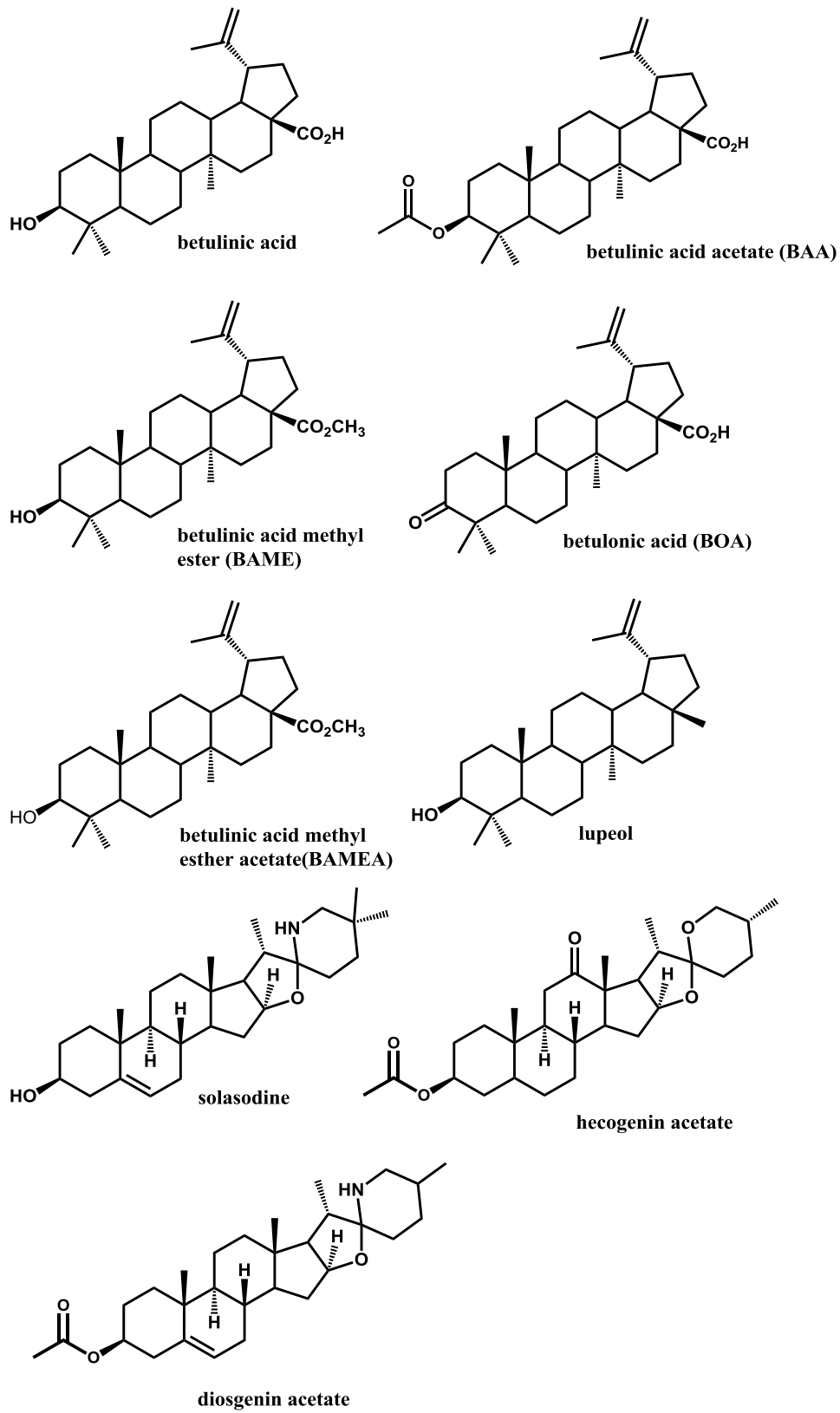


Figure 2

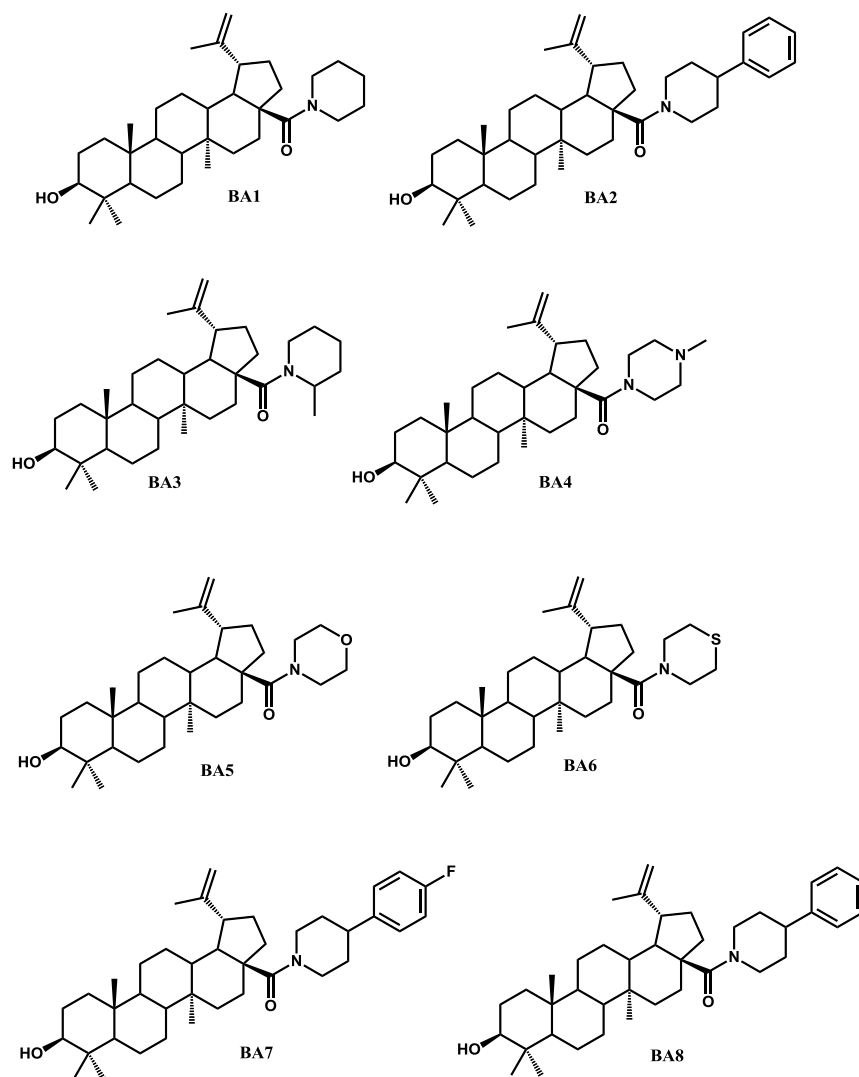


Figure 3

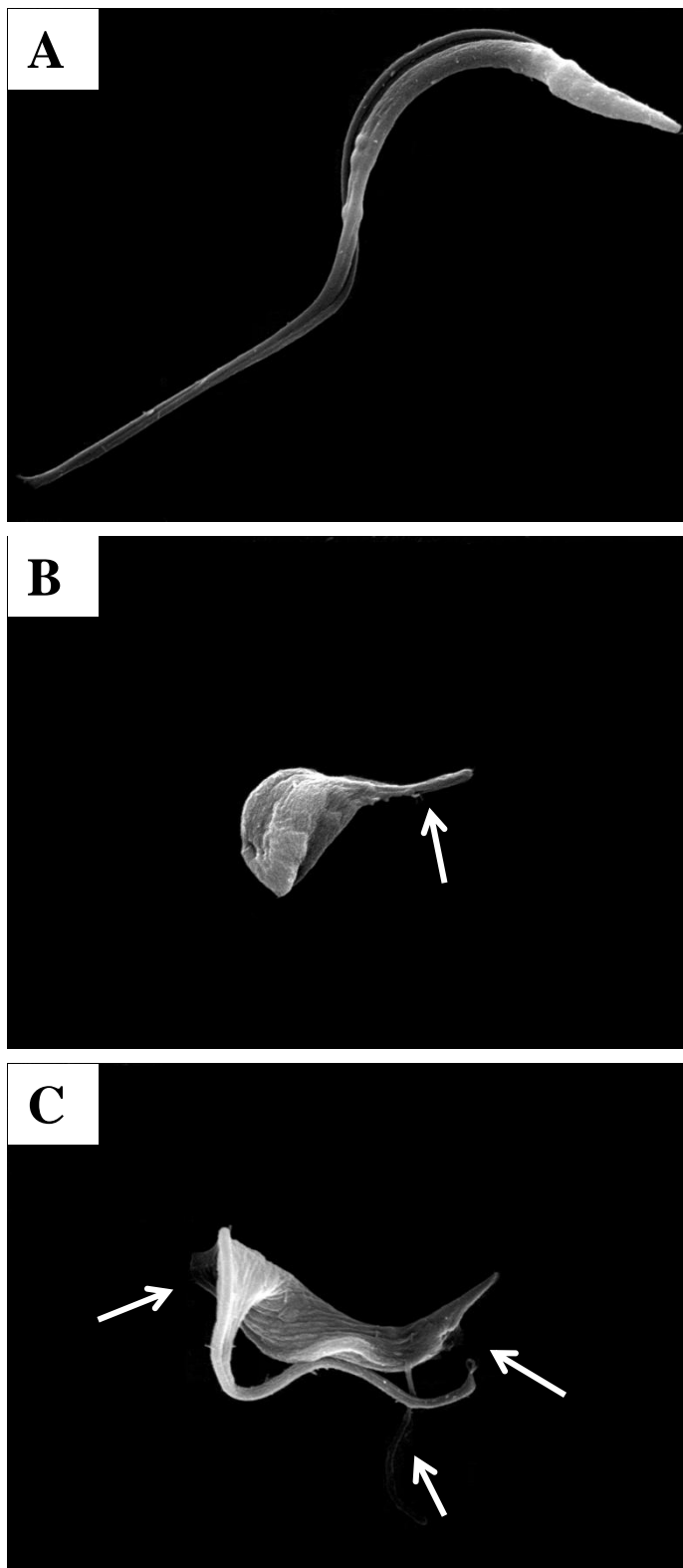


Figure 4

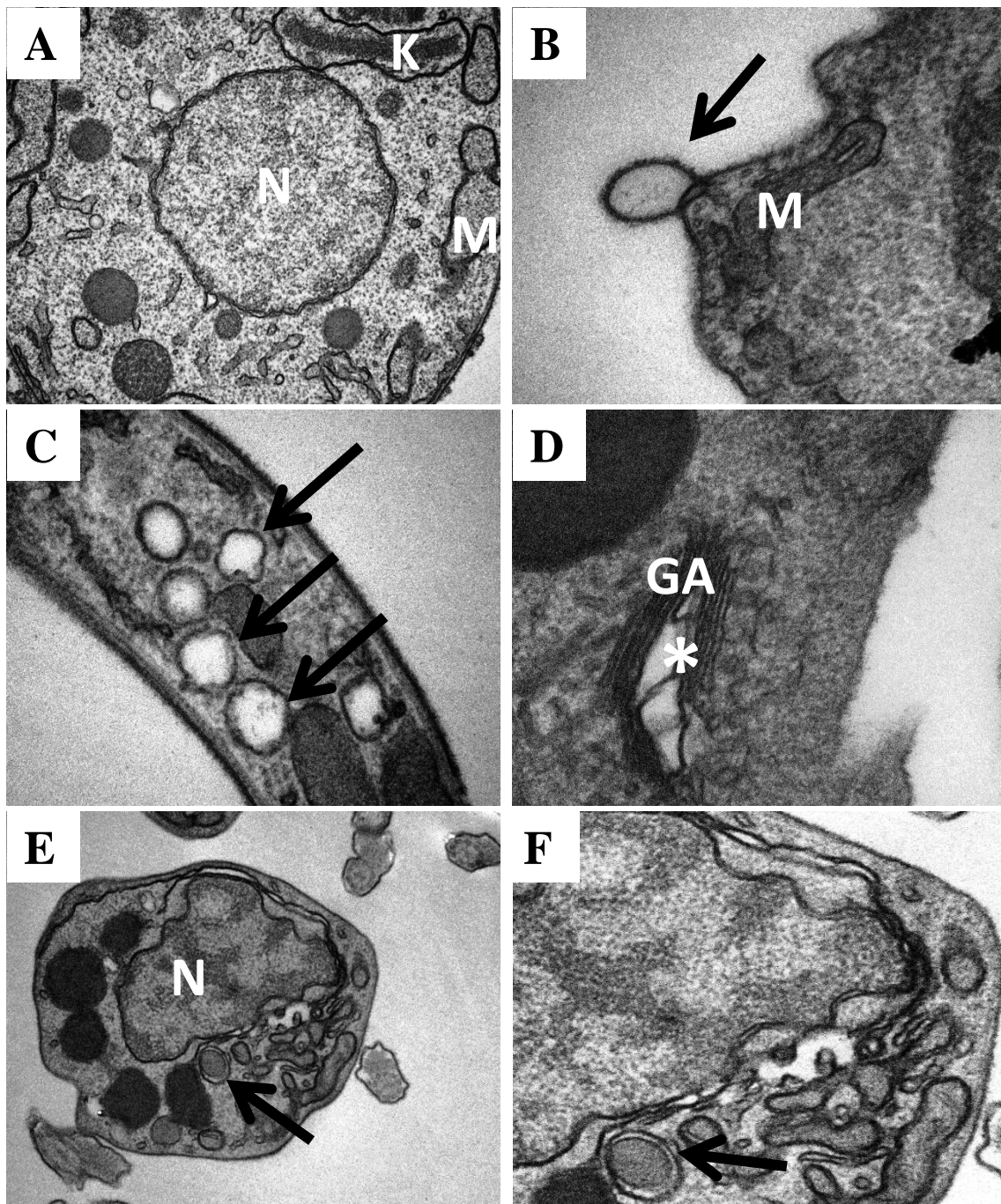


Figure 5

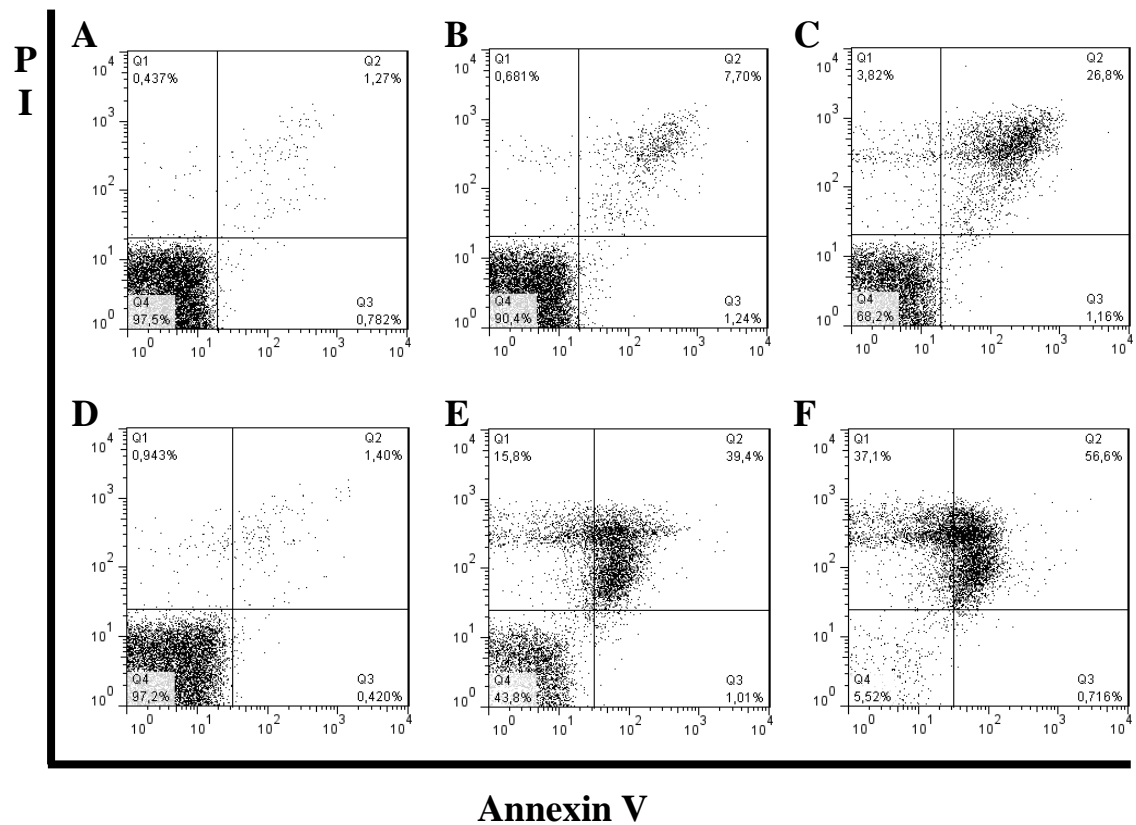


Figure 6

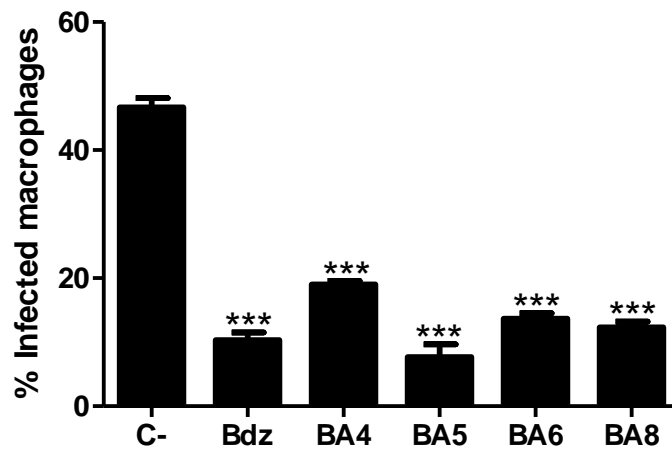
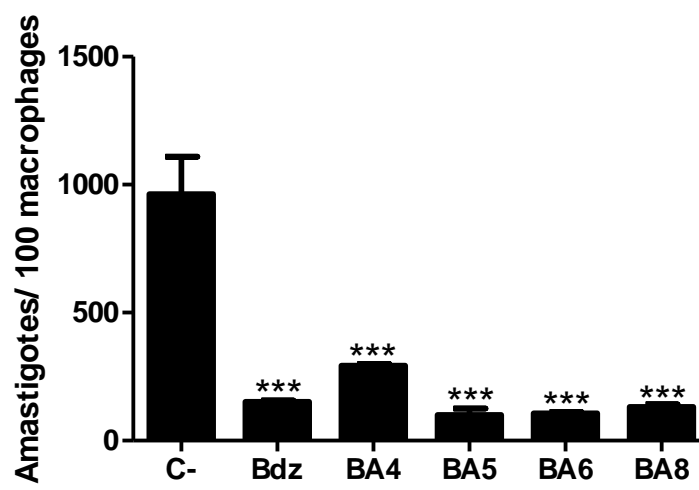
A**B**

Figure 7

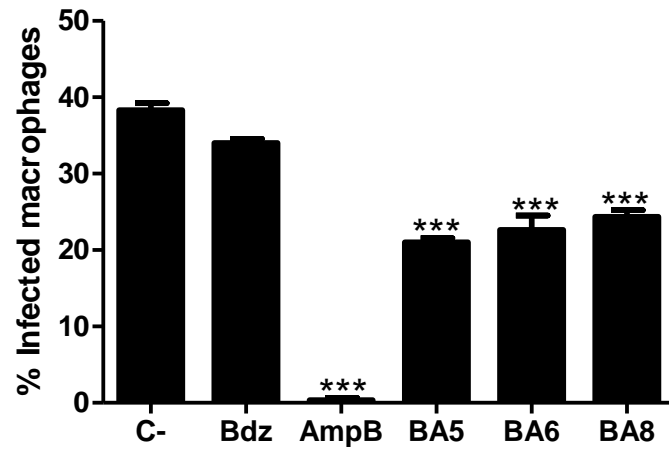


Figure 8

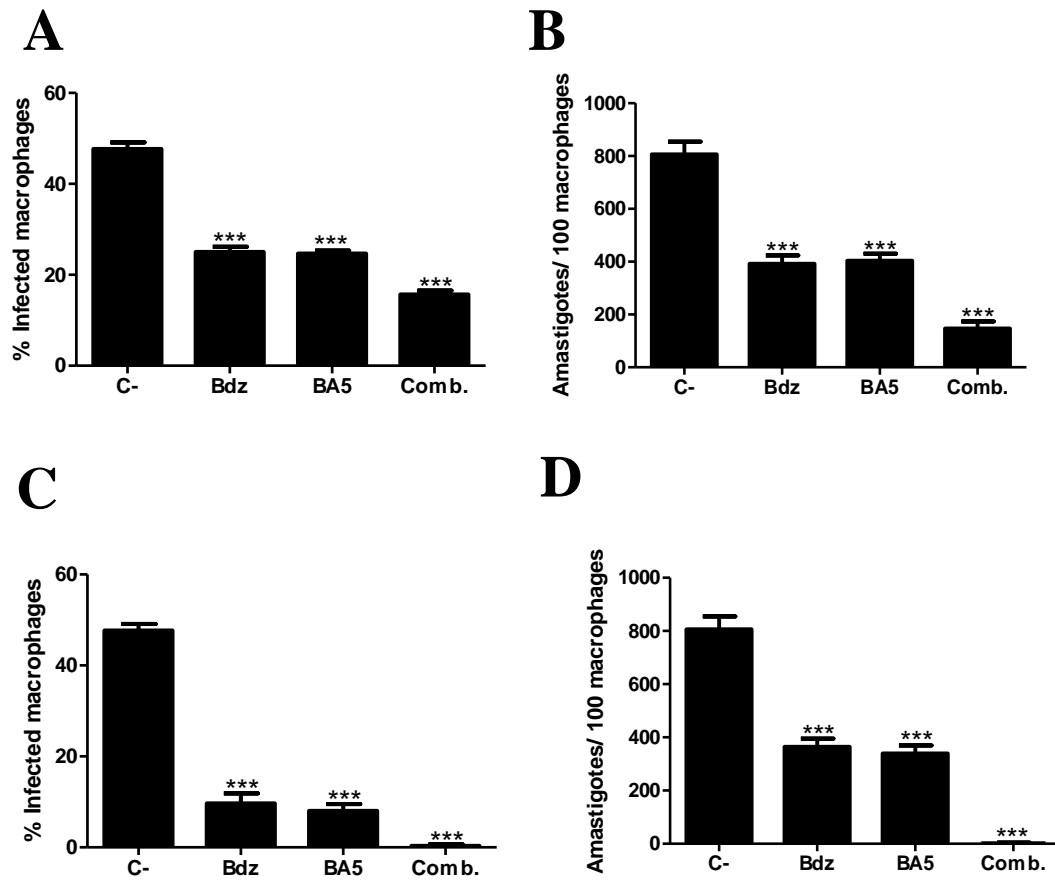


Table 1. Cytotoxicity against macrophages, antimalarial and anti-*Trypanosoma cruzi* activity of betulinic acid and derivatives

Compound	LC₅₀ (μM)	IC₅₀ Pla. (μM)	IC₅₀ Try. (μM)
BA	18.8 (± 0.07)	9.9 (± 0.52)*	19.5 (± 0.95)
BAA	40 (± 0.86)	6 (± 0.06)*	18.6 (± 0.45)
BAME	39.6 (± 0.87)	51.6 (± 10.8)*	26.5 (± 2.1)
BOA	69.2 (± 0.60)	10 (± 1.3)*	86.2 (± 1.9)
BAMEA	26.3 (± 1.1)	45.8 (± 36.3)*	71.4 (± 2.8)
BA1	>100	>10	>100
BA2	>100	>10	>100
BA3	>100	>10	13.7 (± 2.3)
BA4	39.7 (± 0.5)	2.2 (± 1.2)	10.2 (± 1.04)
BA5	31.1 (± 1.2)	2.5 (± 0.84)	1.8 (± 0.04)
BA6	28.7 (± 1.1)	2.7 (± 0.83)	5.4 (± 1.3)
BA7	>100	>10	55 (± 0.58)
BA8	53.5 (± 0.40)	1.6 (± 0.06)	5 (± 0.50)
Lupeol	>100	>10	70 (± 2.1)
Solasodine	75.1 (± 1.2)	>10	79.5 (± 0.50)
Hecogenin	>100	>10	>100
Diosgenin acetate	>100	>10	>100
Gentian Violet	0.48 (± 0.04)	-	-
Mefloquine	-	0.04 (± 0.01)	-
Benznidazole	-	-	11.4 (±1.4)

IC₅₀ = inhibitory concentration 50 %; LC₅₀ = lethal concentration 50 %. ND= Not determined. Values are means ± SD of three independent experiments performed in triplicate. * values extracted from Sá *et al.*, 2009.

Table 2. Activity against intracellular forms.

Compound	IC₅₀ Ama. (μM)
BA4	18.9 (± 1.2)
BA5	10.6 (± 0.79)
BA6	12.4 (±1.7)
BA8	13.2 (± 1.6)
Bdz	13.5 (± 1.3)

Values are expressed as the mean ± SD of three independent experiments.

6 DISCUSSÃO GERAL

Apesar dos avanços significativos na profilaxia da doença de Chagas gerados pelo controle da transmissão natural, aumento do controle na triagem em bancos de sangue e sobre casos de transmissão congênita, a doença de Chagas ainda representa um grave problema de saúde pública, principalmente na América Latina (BRENER, 2000; MATSUO *et al.*, 2010). O tratamento farmacológico desta enfermidade é limitado a duas drogas: o benzonidazol e o nifurtimox. Como já foi citado anteriormente, estes medicamentos possuem boas taxas de cura na fase aguda da doença, porém não são tidos como drogas ideais pois tem baixa eficácia na fase crônica da doença, apresentam diversos efeitos colaterais e já existem relatos de cepas resistentes a esses medicamentos (FILARDY & BRENER, 1987; NEAL & VAN BUEREN, 1988; MURTA *et al.*, 1998). Devido a essas limitações, o surgimento de novos medicamentos que exerçam uma menor toxicidade sobre o hospedeiro e possuam uma maior eficácia quando comparados com os fármacos que já são utilizados na clínica torna-se necessário. Nesse contexto, o presente trabalho visou avaliar a atividade anti-*T. cruzi* de esteroides naturais e derivados sintéticos dos mesmos.

Os resultados do presente trabalho demonstram a atividade tripanocida das fisalinas B, D, F e G. Dentre elas, as fisalinas B e F exibiram os melhores perfis. Apesar da similaridade química, as fisalinas D e G apresentaram uma atividade tripanocida inferior às fisalinas B e F, sugerindo que as pequenas diferenças entre as fisalinas proporcionam atividade citotóxica e tripanocida variadas. Entre as fisalinas, a principal diferença química encontra-se nos substituintes ligados a C-5 e C-6 do esqueleto esteroide. As fisalinas D e G são semelhantes por causa dos grupos hidroxilas presentes e ambas apresentam uma moderada atividade tripanocida. Em contraste, nas fisalinas B e F faltam os grupos hidroxilas em C-5 e C-6 e ambas apresentam uma potente atividade tripanocida. Essas diferenças estruturais parecem contribuir também para atividade antimalárica *in vitro* e leishmanicida acentuada das fisalinas B e F em relação às fisalinas D e G (SÁ *et al.*, 2011; GUIMARÃES *et al.*, 2010).

Foi observado também que o ácido betulínico apresentou uma ação anti-*T. cruzi* moderada. Apesar da similaridade química dos esteroides naturais testados, estes apresentaram uma fraca atividade anti-*T. cruzi* ou ausência da mesma nos ensaios

biológicos. Este dado evidencia que a atividade tripanocida é dependente da estrutura química do esteroide e não uma característica geral da classe.

Entre os derivados sintéticos do ácido betulínico, as modificações presentes nos esteroides BAA, BAME, BOA e BAMEA não otimizaram a atividade anti-*T. cruzi*. Estes derivados possuem modificações nos substituintes do C-3 ou C-28 do ácido betulínico. Os resultados demonstram que estas modificações diminuíram a toxicidade para células de mamíferos, porém também diminuíram a atividade anti-*T. cruzi* contra formas tripomastigotas, com exceção do BAA, que é a forma oxidada do ácido betulínico. Estudos prévios demonstram a atividade anti-*T. cruzi* do ácido betulínico sobre a proliferação de formas epimastigotas da cepa Tulahuen e uma diminuição da atividade nos derivados: BAA, BAME e BOA (DOMÍNGUEZ-CARMONA *et al.*, 2010). Apesar da fraca ação dos derivados sobre o *T. cruzi*, as modificações presentes nestas moléculas parecem contribuir para o aumento da atividade leishmanicida e antimalárica, em especial a modificação presente no acetato do ácido betulínico (DOMÍNGUEZ-CARMONA *et al.*, 2010).

Por outro lado, os derivados BA1 à BA8, que possuem um grupo amida na posição C-28, apresentaram em sua maioria uma atividade tripanocida potente. A exceção a esta regra foi a atividade dos derivados BA1, BA2 e BA7. Diversos trabalhos relatam modificações estruturais nos substituintes C-3, C-20 e C-28 do ácido betulínico (KIM *et al.*, 1998). As modificações no C-20 mostraram pouca contribuição em estudos com linhagens de células tumorais (KIM *et al.*, 2001). Entretanto, as modificações no C-3 ou C-28 parecem promissoras (MULLAUER *et al.*, 2010). Modificações realizadas no C-28 já contribuíram para a otimização da atividade anti-HIV, antitumoral, anti-influenza A e anti-herpes (SUN *et al.*, 1998; JEONG *et al.*, 1999; BALTIMA *et al.*, 2003; PAVLOVA *et al.*, 2003). Neste trabalho foi possível observar a contribuição da inserção de amins no C-28 para um aumento da atividade anti-*T. cruzi*.

Através da utilização de formas tripomastigotas observamos que os esteroides mais ativos causam a morte parasitária através da indução de um processo necrótico, evidenciando uma perda da permeabilidade da membrana plasmática do parasito (VANIER-SANTOS & DE CASTRO, 2009; VEIGA-SANTOS *et al.*, 2013). Foi possível identificar também diversas alterações na ultraestrutura induzidas pelo tratamento com os esteroides mais ativos, em especial alterações no complexo de Golgi e o aparecimento de estruturas membranosas concêntricas. Na literatura, alteração na morfologia do complexo de Golgi é um indicativo de que proteases do *T. cruzi* podem

estar sendo afetadas (ENGEL *et al.*, 1998). A cruzaina é a principal cisteína protease do *T. cruzi* e um dos principais alvos moleculares utilizados para o desenvolvimento de drogas (SAJID *et al.*, 2011). Assim, determinou-se a capacidade dos esteroides em inibir a ação catalítica da cruzaina. No entanto, os esteroides testados não foram capazes de inibi-la (dados não mostrados).

O aumento da vacuolização citoplasmática e a presença de estruturas membranosas concêntricas são características típicas de autofagia (TSUJIMOTO & SHIMIZU, 2005; FERNANDES *et al.*, 2012). Através de microscopia de fluorescência com parasitos tratados com o esteroide mais potente (a fisalina B), foi possível detectar uma marcação positiva para monodansilcadaverina (MDC), um composto lisossomotrópico fluorescente utilizado para identificação da proteína cadaverina, presente em vesículas autofágicas (VANIER-SANTOS & DE CASTRO, 2009; DUSZENKO *et al.*, 2011). Esses resultados são similares a achados recentes que demonstram que as fisalinas exercem efeitos celulares através da indução de autofagia (HE *et al.*, 2013a; HE *et al.*, 2013b).

Nos últimos anos, a combinação de fármacos com diferentes mecanismos de ação tem sido muito utilizada para melhorar a eficácia terapêutica, diminuir a toxicidade acumulativa de medicamentos e evitar o desenvolvimento de resistência quimioterápica pelo parasito (COURA, 2007). A terapia combinada com nifurtimox e eflortina (NECT) para o tratamento de indivíduos portadores da fase avançada da tripanossomíase africana e a terapia combinada com estibogluconato de sódio e paromomicina (SSG & PM) para leishmaniose visceral na África são exemplos concretos da importância que a combinação de fármacos pode ter no combate a doenças parasitárias (MELAKU *et al.*, 2007; PRIOTTO *et al.*, 2009; MUSA *et al.*, 2012; ALIROL *et al.*, 2013). Nesse contexto, muitos esforços têm sido feitos para identificar combinações de medicamentos ideais para a doença de Chagas (CENCIG *et al.*, 2012; DINIZ *et al.*, 2013). No presente trabalho observamos que a combinação da fisalina B ou fisalina F ou do derivado BA5 com o benzonidazol proporcionou uma redução no desenvolvimento de tripomastigotas em macrófagos superior à ação dos compostos testados de forma isolada. Os resultados indicam um efeito aditivo da combinação entre os esteróides e o benzonidazol. No seu conjunto, estes dados sugerem que a busca de novos agentes anti-*T. cruzi* com base em esteroides é uma linha atraente para o desenvolvimento de drogas.

7 CONCLUSÕES/SUMÁRIO DE RESULTADOS

- Os esteroides testados apresentaram baixa citotoxicidade para células de mamíferos;
- Os esteroides testados apresentaram potente atividade contra formas tripomastigotas de *T. cruzi*, em especial, as fisalinas B e F e o derivado BA5;
- Os esteroides não foram capazes de inibir a ação enzimática da cruzaina;
- Foi observada uma série de alterações na ultraestrutura de formas tripomastigotas tratados com os esteroides mais ativos, como dilatação do complexo de Golgi, formação de perfis de retículo endoplasmático envolvendo diversas organelas e o aparecimento de figuras mielínicas, que tiveram sua identidade como vacúolos autofágicos confirmada pela marcação com MDC;
- O tratamento de formas tripomastigotas com os esteroides mais potentes induz a morte parasitária principalmente por necrose;
- Os esteroides foram capazes de reduzir o número de macrófagos infectados e amastigotas por macrófago;
- A combinação da fisalina B ou fisalina F ou do derivado BA5 com o benzonidazol apresentou melhores taxas de inibição do que os compostos testados de forma isolada, sem afetar as células hospedeiras.

8 REFERENCIAS

AGRA, M. F. Contribuição ao estudo de plantas medicinais da Paraíba. Fortaleza: VI Simpósio de plantas medicinais do Brasil. Resumos, p. 64-66, 1980.

ALARCÓN DE NOYA, B. *et al.* Large urban outbreak of orally acquired acute Chagas disease at a school in Caracas, Venezuela. **J Infect Dis.** v. 201, n. 9, p. 1308-1315, 2010.

ALIROL, E. *et al.* Nifurtimox-eflornithine combination therapy for second-stage gambiense human African trypanosomiasis: Médecins Sans Frontières experience in the Democratic Republic of the Congo. **Clin Infect Dis.** v. 56, p. 195-203, 2013.

ALMEIDA, E. R. Plantas medicinais brasileiras: Conhecimentos populares e científicos. 1 ed. São Paulo: Hermus, 1993.

ANDRADE, S. G. Morphological and behavioral characterization of *Trypanosoma cruzi* strains. **Rev Soc Bras Med Trop.** v. 18, p. 29-46, 1985.

ANDRADE, J. P. *et al.* Latin American Guidelines for the diagnosis and treatment of Chagas heart disease: executive summary. **Arq Bras Cardiol.** v. 96, p. 434-442, 2011.

ANDRADE, Z. Patologia da doença de Chagas. In: Brener, Z., Andrade, Z., Barral-Netto, M. (Eds.), *Trypanosoma cruzi e Doença de Chagas*, 2 ed. Rio de Janeiro: Guanabara Koogan, p. 201–230, 2000.

BALTINA, L. A. *et al.* Lupane triterpenes and derivatives with antiviral activity. **Bioorg Med Chem Lett.** v. 13, p. 3549-3552, 2003.

BRENER, Z.; ANDRADE, Z. A.; BARRAL-NETO, M. *Trypanosoma cruzi e a doença de Chagas*. 2 ed. Rio de Janeiro: Guanabara Koogan. p. 152-174, 2000.

BOIAIANAN, E.; RASSI, A. Terapêutica etiológica da doença de Chagas. **Arq Bras Cardiol.** v. 32, p. 251-254, 1979.

BOSCH, F.; BANOS, J. E. Acetylsalicylic acid and its derivatives: history of discovery. **AINE**, v. 2, p. 108-117, 1998.

BUCKNER, F. S.; URBINA, J. A. Recent Developments in Sterol 14-demethylase inhibitors for Chagas disease. **Int J Parasitol Drugs Drug Resist.** v. 2, p. 236-242, 2012.

CAMPBELL, D. A.; WESTENBERGER, S. J.; STURM, N. R. The determinants of Chagas disease: connecting parasite and host genetics. **Curr Mol Med.** v. 4, p. 549-562, 2004.

CASTRO, D. P. *et al.* Physalin B inhibits *Trypanosoma cruzi* infection in the gut of *Rhodnius prolixus* by affecting the immune system and microbiota. **J Insect Physiol.** v. 58, p. 1620-1625, 2012.

CASTRO, J. A.; DE MECCA, M. M.; BATERL, L. C. Toxic side effects of drugs used to treat Chagas' disease (American trypanosomiasis). **Human Exp Toxicol.** v. 25, p. 471-479, 2006.

CENCIG, S. *et al.* Evaluation of benznidazole treatment combined with nifurtimox, posaconazole or AmBisome® in mice infected with *Trypanosoma cruzi* strains. **Int J Antimicrob Agents.** v. 40, p. 527-532, 2012.

CHAGAS, C. Nova tripanozomíaze humana: estudos sobre a morfologia e o ciclo evolutivo do *Schizotrypanum cruzi* n. gen., n. sp., agente etiológico de nova entidade mórbida do homem. **Mem Inst Oswaldo Cruz.** v. 1, p. 159-219, 1909.

CLAYTON, J. Chagas disease: pushing through the pipeline. **Nature.** v. 465, suppl. S12-S15, 2010.

CHANDRAMU, C. *et al.* Isolation, characterization and biological activity of betulinic acid and ursolic acid from *Vitex negundo* L. **Phytother Res.** v. 17, p. 127-134, 2003.

CHIANG, H. C. *et al.* Antitumor agent, physalin F from *Physalis angulata* L. **Anticancer Res.** v. 12, p. 837-844, 1993.

COURA, J. R. *et al.* Emerging Chagas disease in Amazonian Brazil. **Trends Parasitol.** v. 18, p. 171-176, 2002.

COURA, J. R. Tripanosomose, doença de Chagas. **Cienc. Cult.** v. 55, p. 30-33, 2003.

COURA, J. R. Chagas disease: what is known and what is needed – A background article. **Mem Inst Oswaldo Cruz.** v. 102, suppl. 1, p. 113-122, 2007.

COURA, J. R.; VIÑAS, P. A. Chagas disease: a new worldwide challenge. **Nature.** v. 465, suppl. S6-S7, 2010.

DIAS, L. C. *et al.* Quimioterapia da doença de Chagas: estado da arte e perspectivas no desenvolvimento de novos fármacos. **Quim Nova.** v. 32, p. 2444-2457, 2009.

DINIZ, L. F. *et al.* Benznidazole and posaconazole in experimental Chagas disease: positive interaction in concomitant and sequential treatments. **Plos Negl Trop Dis.** v. 7, e2367, 2013.

DI STASI, L. C.; HIRUMA-LIMA, C. A.. **Plantas medicinais na Amazônia e na Mata Atlântica.** 2 ed. São Paulo: UNESP, 2002.

DOMÍNGUEZ-CARMONA, D. B. *et al.* Antiprotozoal activity of betulinic acid derivatives. **Phytomedicine.** v. 17, p. 379-382, 2010.

DUKE, J. A., VASQUEZ, R. Amazonian Ethnobotanical Dictionary. Boca Raton, Florida: CRC Press Inc., 1994.

DUSZENKO, M. *et al.* Autophagy in protists. **Autophagy.** v. 7, p. 127-158, 2011.

ENGEL, J. C. *et al.* Cysteine protease inhibitors cure an experimental *Trypanosoma cruzi* infection. **J Exp Med.** v. 188, p. 725-734, 1998.

FERNANDES, M. C. *et al.* A novel triazolic naphthofuranquinone induces autophagy in reservosomes and impairment of mitosis in *Trypanosoma cruzi*. **Parasitology.** v. 139, p. 26-36, 2012.

FILARDY, L. S.; BRENER, Z. Susceptibility and natural resistance of *Trypanosoma cruzi* strains to drugs used clinically in Chagas disease. **Trans R Soc Trop Med Hyg.** v. 81, p. 755-759, 1987.

FRIGHETTO, N. *et al.* Purification of betulinic acid from *Eugenia florida* (Myrtaceae) by high-speed counter-current chromatography. **Phytochem Anal.** v. 16, p. 411-414, 2005.

FUJIOKA, T. *et al.* Anti-AIDS agents, 11. Betulinic acid and platanic acid as anti-HIV principles from *Syzygium claviflorum*, and the anti-HIV activity of structurally related triterpenoids. **J Nat Prod.** v. 57, p. 243-247, 1994.

FULDA, S. *et al.* A new chemotherapeutic agent in the treatment of neuroectodermal tumors. **Klin Padiatr.** v. 211, p. 319-322, 1999.

FULDA, S. Betulinic acid: A natural product with anticancer activity. **Mol Nutr Food Res.** v. 53, p. 140-146, 2009.

GARCIA, E. S.; AZAMBUJA, P. Development and interactions of *Trypanosoma cruzi* within the insect vector. **Parasitol Today.** v. 7, p. 240-244, 1991.

GARCIA, S. *et al.* Treatment with benznidazole during the chronic phase of experimental chagas' disease decreases cardiac alterations. **Antimicrob Agents Chemother.** v. 49, p. 1-7, 2005.

GUIMARÃES, E. T. *et al.* Activity of physalins purified from *Physalis angulata* *in vitro* and *in vivo* models of cutaneous leishmaniasis. **J Antimicrob Chemother.** v. 64, p. 84-87, 2009.

GUIMARÃES, E. T. *et al.* Effects of seco-steroids purified from *Physalis angulata* L., Solanaceae, on the viability of *Leishmania* sp. **Rev Bras Farmacogn.** v. 20, p. 945-949, 2010.

GUPTA, S. *et al.* Antigenicity and diagnostic potential of vaccine candidates in human Chagas disease. **Plos Negl Trop Dis.** doi: 10.1371/journal.pntd.0002018, 2013.

HE, H. *et al.* Physalin A induces apoptotic cell death and protective autophagy in HT1080 human fibrosarcoma cells. **J Nat Prod.** v. 76, p. 880-888, 2013a.

HE, H. *et al.* Physalin A induces apoptosis via p53-Noxa-mediated ROS generation, and autophagy play a protective role against apoptosis through p38-NF- κ B survival pathway in A375-S2 cells. **J Ethnopharmacol.** v. 148, p. 544-555, 2013b.

HELVACI, S. *et al.* Antimicrobial activity of the extracts and physalin D from *Physalis alkekengi* and evaluation of antioxidant potential of physalin D. **Pharma Biol.** v. 48, p. 142-150, 2010.

IGNELZI, R. J.; ATKINSON, J. H. Pain and its modulation. Part 2. Efferent mechanisms. **Neurosurg.** v. 6, p. 584 –590, 1980.

JEONG, H. J. *et al.* Preparation of amino acid conjugates of betulinic acid with activity against human melanoma. **Bioorg Med Chem Lett.** v. 9, 1201-1204, 1999.

KAWAI, M. *et al.* Benzilic acid rearrangement-type reaction of physalis to neophysalins. Structural revision of one of the dehydration products of physalin A. **Tetrahedon.** v. 47, p. 2103-2110, 1991.

KIM, D. S. H. L. *et al.* A concise semi-synthetic approach to betulinic acid from betulin. **Synth Commun.** v. 27, p. 1607-1612, 1997.

KIM, D. S. *et al.* Synthesis of betulinic acid derivatives with activity against human melanoma. **Bioorg Med Chem Lett.** v. 8, p. 1707-1712, 1998.

KIM, J. Y. *et al.* Development of C-20 modified betulinic acid derivatives as antitumor agents. **Bioorg Med Chem Lett.** v. 11, p. 2405-2408, 2001.

KIRCHHOFF, L. V. Epidemiology of American trypanosomiasis (Chagas disease). **Adv Parasitol.** v. 75, p. 1-18, 2011.

KETTLER, H. E.; MARJANOVIC, S. Engaging biotechnology companies in the development of innovative solutions for diseases of poverty. **Nat Rev.** v. 3, p. 171 -176, 2004.

KROGH, R. *et al.* Isolation and identification of compounds with antinociceptive action from *Ipomea pes-caprae* (L.) R. Br. **Pharmazie.** v. 54, p. 464-466, 1999.

LI, F. *et al.* PA-457: a potent HIV inhibitor that disrupts core condensation by targeting a late step in Gag processing. **Proc Natl Acad Sci USA.** v. 100, p. 13555-13560, 2003.

LIN, Y.S. *et al.* Immunomodulatory activity of various fractions derived from *Physalis angulata* L. extract. **Am J Chin Med.** v. 20, p. 233–243,1992.

MAGALHÃES, H. I. *et al.* *In vitro* and *in vivo* antitumor activity of physalin B and D from *Physalis angulata*. **J Pharma and Pharmacol.** v. 58, p. 235-241, 2006.

MARIN-NETO, J. A.; SIMÕES, M. V.; SARABANDA, A. V. Chagas heart disease. **Arq Bras Cardiol.** v. 72, p. 247-280, 1999.

MARIN-NETO, J. A. The BENEFTI trial: testing the hypothesis that trypanocidal therapy is beneficial for patients with chronic Chagas heart disease. **Mem Inst Oswaldo Cruz.** v. 104, p. 319-324, 2008.

MARIN-NETO, J. A. *et al.* Chagas heart disease. In: Yusuf S, Cairns JA, Camm AJ, Fallen EL, Gersh BJ, eds. Evidence-based cardiology, 3rd edn. London: BMJ Books, p. 823-841, 2010.

MATSUO, A. L. *et al.* In vitro and in vivo trypanocidal effects of the cyclopalladated compound 7a, a drug candidate for treatment of Chagas' disease. **Antimicrob Agents Chemother.** v. 54, p. 3318-3325, 2010.

MAURYA, S. K. *et al.* Content of betulin and betulinic acid, antitumor agents of *Zizyphus* species. **Fitoterapia.** v. 60, p. 468-469, 1989.

MAYA, J. D. *et al.* Mode of action of natural and synthetic drugs against *Trypanosoma cruzi* and their interaction with the mammalian host. **Comp Biochem Physiol A Mol and Integr Physiol.** v. 146, p. 601-620, 2007.

MCKERROW, J. *et al.* Proteases in parasitic diseases. **Annu Rev Pathol.** v. 1, p. 497-536, 2006.

MEIRELLES, M. *et al.* Inhibitors of the major cysteinyl proteinase (GP57/51) impair host cell invasion and arrest the intracellular development of *Trypanosoma cruzi* *in vitro*. **Mol Biochem Parasitol.** v. 52, p. 175-184, 1992.

MELAKU, Y. *et al.* Treatment of kala-azar in southern Sudan using a 17-day regimen of sodium stibogluconate combined with paromomycin: a retrospective comparison with 30-days sodium stibogluconate monotherapy. **Am J Trop Med Hyg.** v. 77, p. 89-94, 2007.

MILES, M. A.; FELICIANGELI, M. D.; DE ARIAS, A. R. American trypanosomiasis (Chagas's disease) and the role of molecular epidemiology in guiding control strategies. **B M J.** v. 326, p. 1444-1448, 2003.

MINISTÉRIO DA SAÚDE DO BRASIL. Brazilian Consensus on Chagas disease. **Rev Soc Bras Med Trop.** v. 38, p. 7-29, 2005.

MONNCAYO, A.; SILVEIRA, A. C. Current epidemiological trends for Chagas disease in Latin America and future challenges in epidemiology, surveillance and health policy. **Mem. Inst. Oswaldo Cruz.** v. 104, Suppl. I, p. 17-30, 2009.

MULLAUER, F. B. *et al.* Betulinic acid, a natural compound with potent anticancer effects. **Anti-Cancer Drug.** v. 21, p. 215-227, 2010.

MURTA, S. M. *et al.* Molecular characterization of susceptible and naturally resistant strains of *Trypanosoma cruzi* to benznidazole and nifurtimox. **Mol Biochem Parasitol.** v. 93, p. 203-214, 1998.

MUSA, A. *et al.* Sodium stibogluconate (SSG) & paromomycin combination compared to SSG for visceral leishmaniasis in East Africa: a randomized controlled trial. **plos Negl Trop Dis.** v. 6 – e.1674, 2012.

NAGAFUJI, S. *et al.* Trypanocidal constituents in plants 4. Withanolides from aerial parts of *Physalis angulata*. **Bio Pharm Bull.** v. 27, p. 193-197, 2004.

NEAL, R. A.; VAN BUEREN, J. Comparative studies of drug susceptibility of five strains of *Trypanosoma cruzi* *in vivo* and *in vitro*. **Trans R Soc Trop Med Hyg.** v. 82, p. 709-714, 1988.

NEWMAN, D. J.; CRAGG, G. M. Natural products as sources of new drugs over the last 25 years. **J Nat Prod.** v. 70, p. 461-477, 2007.

PAVLOVA, N. I. *et al.* Antiviral activity of betulin, betulinic and betulonic acids against some enveloped and non-enveloped viruses. **Fitoterapia.** v. 74, p. 489-492, 2003.

PINTO-DIAS, J. C. The treatment of Chagas disease (South American trypanosomiasis). **Ann of Intern Med.** v. 144, p. 722-774, 2006.

PISHA, E. *et al.* Discovery of betulinic acid as a selective inhibitor of human melanoma that functions by induction of apoptosis. **Nat Med.** v. 1, p. 1046-1051, 1995.

PRIOTTO, G. *et al.* Nifurtimox-eflornithine combination therapy for second-stage African *Trypanosoma brucei gambiense* trypanosomiasis: a multicentre, randomized, phase III, non-inferiority trial. **Lancet.** v. 4, p. 56-64, 2009.

RASSI, A. Jr.; RASSI, A.; LITTLE, W. C. Chagas heart disease. **Clin Cardiol.** v. 23, p. 883-889, 2000.

RASSI, A. Jr.; RASSI, A.; MARIN-NETO, J. A. Chagas disease. **Lancet.** v. 375, p. 1388-1402, 2010a.

RASSI, A. Jr.; RASSI, A.; MARIN-NETO, J. A. Antitrypanosomal agents: treatment or threat ? **Lancet.** v. 376, p. 768-769, 2010b.

REA, A. *et al.* Soulmamarin isolated from *Calophyllum brasiliense* (Clusiaceae) induces plasma membrane permeabilization of *Trypanosoma cruzi* and mitochondrial dysfunction. **Plos Negl Trop Dis.** v. 7, p. e2556, 2013.

SÁ, M. S. *et al.* Antimalarial activity of physalins B, D, F and G. **J Nat Prod.** v. 74, p. 2269-2272, 2011.

SAJID, M. *et al.* Cruzain: the path from target validation to the clinic. **Adv Exp Med Biol.** v. 712, p. 100-115, 2011.

SCHMIDT, B. *et al.* A natural history of botanical therapeutics. **Metabolism.** v. 57, suppl. S3-S9, 2008.

SCHMIDT, M. L. *et al.* Betulinic acid induces apoptosis in human neuroblastoma cell lines. **Eur J Cancer.** v. 33, p. 2007-2010 1997.

SCHMUNIS, G. A. Epidemiology of Chagas disease in non endemic countries: the role of international migration. **Mem Inst Oswaldo Cruz.** v. 102, suppl. 1, p. 75-86, 2007.

SECRETARIA DE VIGILÂNCIA EM SAÚDE, MINISTÉRIO DA SAÚDE. Boletim eletrônico epidemiológico: Situação epidemiológica das zoonoses de interesse para a saúde pública. v. 2, p. 10-11, 2010.

SILVA, K. N.; AGRA, M. F. Estudo farmacobotânico comparativo entre *Nicandra physalodes* e *Physalis angulata* (Solanaceae). **Rev Bras Farmacogn.**, João Pessoa, v. 15, p. 344-351, 2005.

SILVA, M. T. G.; *et al.* Studies on antimicrobial activity, *in vitro*, of *Physalis angulata* L. (Solanaceae) fraction and physalin B bringing out the importance of assay determination. **Mem Inst Oswaldo Cruz**, Rio de Janeiro, v. 100, p. 779-782, 2005.

SIMÕES, C. M. O. *et al.* Farmacognosia: da planta ao medicamento UFRGS e UFSC, 5º edição, 2003.

SMITH, P. F. *et al.* Phase I and II study of the safety, virologic effect and pharmacokinetics/pharmacodynamics of single-dose 3-O-(3',3'-dimethylsuccinyl) betulonic acid (bevirimat) against human immunodeficiency virus infection. **Antimicrob Agents Chemother.** v. 51, p. 3574-3581, 2007.

SOARES, M. B. P. *et al.* Inhibition of macrophage activation and lipopolysaccharide-induced death by seco-steroids purified from *Physalis angulata* L. **Eur J Pharmacol.** v. 459, p. 107-112, 2003.

SOARES, M. B. P. *et al.* Physalins B, F and G, seco-steroids purified from *Physalis angulata* L., inhibit lymphocyte function and allogeneic transplant rejection. **Int. Immunopharmacol.**, [S.l.], v. 6, p. 408-414, 2006.

SOUTO-PADRON, T. *et al.* Cysteine proteinase in *Trypanosoma cruzi*: immunocytochemical localization and involvement in parasite-host cell interaction. **J Cell Sci.** v. 96, p. 485-490, 1990.

SOUZA, W. Special organelles of some pathogenic protozoa. **Parasitol Res.** v. 88, p. 1013-1025, 2002.

STEELE, J. C. *et al.* In vitro and in vivo evaluation of betulinic acid as an antimalarial. **Pytother Res.** v. 13, p. 115-119, 1999.

STEINDEL, M. *et al.* Characterization of *Trypanosoma cruzi* isolated from humans, vectors, and animal reservoirs following an outbreak of acute human Chagas disease in Santa Catarina. Brazil. **Diagn. Microbiol. Infect. Dis.** v. 60, p. 25-32, 2008.

SUN, I. C. *et al.* Anti-AIDS agents. 34. Sythesis and structure-activity relationships of betulin derivatives as anti-HIV agents. **J Med Chem.** v. 41, p. 4648-4657, 1998.

TARLETON, R. L. *et al.* The challegens of Chagas disease-grim outlook or glimmer of hope. **Plos Med.** v. 12, p. 201-210, 2007.

THURNHER, D. *et al.* Betulinic acid: A new cytotoxic compound against malignant head and neck cancer cells. **Head Neck.** v. 25, p. 732-740, 2003.

TOMASSINI, T. C. B. *et al.* Gênero *Physalis* – Uma Revisão Sobre Vitaesteróides. **Quím Nova.** v. 23, p. 47-57, 2000.

TSUJIMOTO, Y.; SHIMIZU, S. Another way to die: Autophagic programmed cell death. **Cell Death Differ.** v. 12, p. 1528-1534, 2005.

URBINA, J. A. Specific chemotherapy of Chagas disease: relevance, current limitations and new approaches. **Acta Trop.** v. 115, p. 55-68, 2010.

VEIGA-SANTOS, P. *et al.* The natural compounds piperovatine and piperlonguminine induce autophagic cell death on *Trypanosoma cruzi*. **Acta Trop.** v. 125, p. 349-356, 2013.

VANNIER-SANTOS, M. A.; DE CASTRO, S. L. Electron microscopy in antiparasitic chemotherapy: A (close) view to a kill. **Curr Drug Targets.** v. 10, p. 246-260, 2009.

VIEIRA, A.T. et al. Mechanisms of the anti-inflammatory effects of the natural secosteroids physalins in a model of intestinal ischaemia and reperfusion injury. **Br J Pharmacol.** v. 146, p. 244-251, 2005.

VIOTTI, R. *et al.* Long-term cardiac outcomes of treating chronic Chagas disease with benznidazole versus no treatment: a nonrandomized trial. **Ann Intern Med.** v. 144, p.724-734, 2006.

YOGEE SWARI, P.; SRIRAM, D. Betulinic acid and its derivatives: A review on their biological properties. **Curr Med Chem.** v. 12, p. 657-666, 2005.

YOSHIDA, N. *Trypanosoma cruzi* infection by oral route: how the interplay between parasite and host components modulates infectivity. **Parasitol Int.** v. 57, p. 105-109, 2008.

ZUCO, V. Selective cytotoxicity of betulinic acid on tumor cell lines, but not on normal cells. **Cancer Lett.** v. 175, p. 17-25, 2002.

ANEXO 1

Dos Santos Filho JM, Moreira DR, de Simone CA, Ferreira RS, McKerrow JH, **Meira CS**, Guimarães ET, Soares MB. Optimization of anti-*Trypanosoma cruzi* oxadiazoles leads to identification of compounds with efficacy in infected mice. **Bioorganic & Medicinal Chemistry**. v. 20, p. 6423-6433, 2012.



Optimization of anti-*Trypanosoma cruzi* oxadiazoles leads to identification of compounds with efficacy in infected mice

José Maurício dos Santos Filho^{a,*}, Diogo Rodrigo M. Moreira^{b,e}, Carlos Alberto de Simone^c,
Rafaela Salgado Ferreira^{d,†}, James H. McKerrow^d, Cássio Santana Meira^e,
Elisalva Teixeira Guimarães^{e,f}, Milena Botelho Pereira Soares^{e,g}

^a Departamento de Engenharia Química, Centro de Tecnologia e Geociências, Universidade Federal de Pernambuco, CEP 50740-521, Recife, PE, Brazil

^b Departamento de Ciências Farmacêuticas, Centro de Ciências da Saúde, Universidade Federal de Pernambuco, 50740-520, Recife, PE, Brazil

^c Departamento de Física e Informática, Instituto de Física, Universidade de São Paulo, CEP 13560-970, São Carlos, SP, Brazil

^d Sandler Center for Drug Discovery in Parasitic Diseases, University of California, San Francisco, CA 94158, USA

^e Centro de Pesquisas Gonçalo Moniz, Fundação Oswaldo Cruz, CEP 40296-750, Salvador, BA, Brazil

^f Departamento de Ciências da Vida, Universidade Estadual da Bahia, CEP 41150-000, Salvador, BA, Brazil

^g Centro de Biotecnologia e Terapia celular, Hospital São Rafael, CEP 41253-190, Salvador, BA, Brazil

ARTICLE INFO

Article history:

Received 6 July 2012

Revised 16 August 2012

Accepted 23 August 2012

Available online 31 August 2012

Keywords:

Chagas disease

Trypanosoma cruzi

Cruzain

Oxadiazoles

Hydrazones

Bioisosterism

ABSTRACT

We recently showed that oxadiazoles have anti-*Trypanosoma cruzi* activity at micromolar concentrations. These compounds are easy to synthesize and show a number of clear and interpretable structure–activity relationships (SAR), features that make them attractive to pursue potency enhancement. We present here the structural design, synthesis, and anti-*T. cruzi* evaluation of new oxadiazoles denoted **5a–h** and **6a–h**. The design of these compounds was based on a previous model of computational docking of oxadiazoles on the *T. cruzi* protease cruzain. We tested the ability of these compounds to inhibit catalytic activity of cruzain, but we found no correlation between the enzyme inhibition and the antiparasitic activity of the compounds. However, we found reliable SAR data when we tested these compounds against the whole parasite. While none of these oxadiazoles showed toxicity for mammalian cells, oxadiazoles **6c** (fluorine), **6d** (chlorine), and **6e** (bromine) reduced epimastigote proliferation and were cidal for trypomastigotes of *T. cruzi* Y strain. Oxadiazoles **6c** and **6d** have IC₅₀ of 9.5 ± 2.8 and 3.5 ± 1.8 μM for trypomastigotes, while Benznidazole, which is the currently used drug for Chagas disease treatment, showed an IC₅₀ of 11.3 ± 2.8 μM. Compounds **6c** and **6d** impair trypomastigote development and invasion in macrophages, and also induce ultrastructural alterations in trypomastigotes. Finally, compound **6d** given orally at 50 mg/kg substantially reduces the parasitemia in *T. cruzi*-infected BALB/c mice. Our drug design resulted in potency enhancement of oxadiazoles as anti-Chagas disease agents, and culminated with the identification of oxadiazole **6d**, a trypanosomicidal compound in an animal model of infection.

© 2012 Elsevier Ltd. All rights reserved.

1. Introduction

It is estimated that 10% of the whole Latin America population is suffering from American trypanosomiasis or Chagas disease, caused by the intracellular protozoan *Trypanosoma cruzi*.^{1,2} This situation is alarming because there are no vaccines available and the current treatment, which is only based on benznidazole (Bdz), suffers limitations of efficacy and toxicity.^{3,4}

The *T. cruzi* cysteine-protease cruzain is an important drug target because it is expressed in all stages of the parasite life cycle and play key roles as a virulence factor.^{5–8} An important proof-concept

of cruzain as a drug target is that its inhibitors efficiently eradicate parasites in host-cells and substantially reduce parasitemia in different animal models of infection.^{9,10} The current status of cruzain inhibitor research is quite promising because some of these lead compounds are nonpeptidic and quite similar to drug-like compounds, a step that is important for successful drug development.^{10–12} Therefore, the identification or structural optimization of cruzain inhibitors is a promising avenue for Chagas disease chemotherapy.

There is a substantial number of papers reporting oxadiazoles as anti-parasitics. Oxadiazoles are frequently explored as bioisosters of ester and amide functionalities. From this point of view, oxadiazoles are considered potential cysteine protease inhibitors because they are similar to peptide bonds.^{13–15} There are reports showing that oxadiazoles are potent inhibitors versus cruzain of *T. cruzi* and the cathepsin-L-like cysteine protease of *Leishmania*

* Corresponding author. Tel.: +55 81 21267288; fax: + 55 81 21267278.

E-mail address: mauricio_santosfilho@yahoo.com.br (J.M. dos Santos Filho).

† Present address: Departamento de Bioquímica e Imunologia, Universidade Federal de Minas Gerais, Belo Horizonte, MG, Brazil.

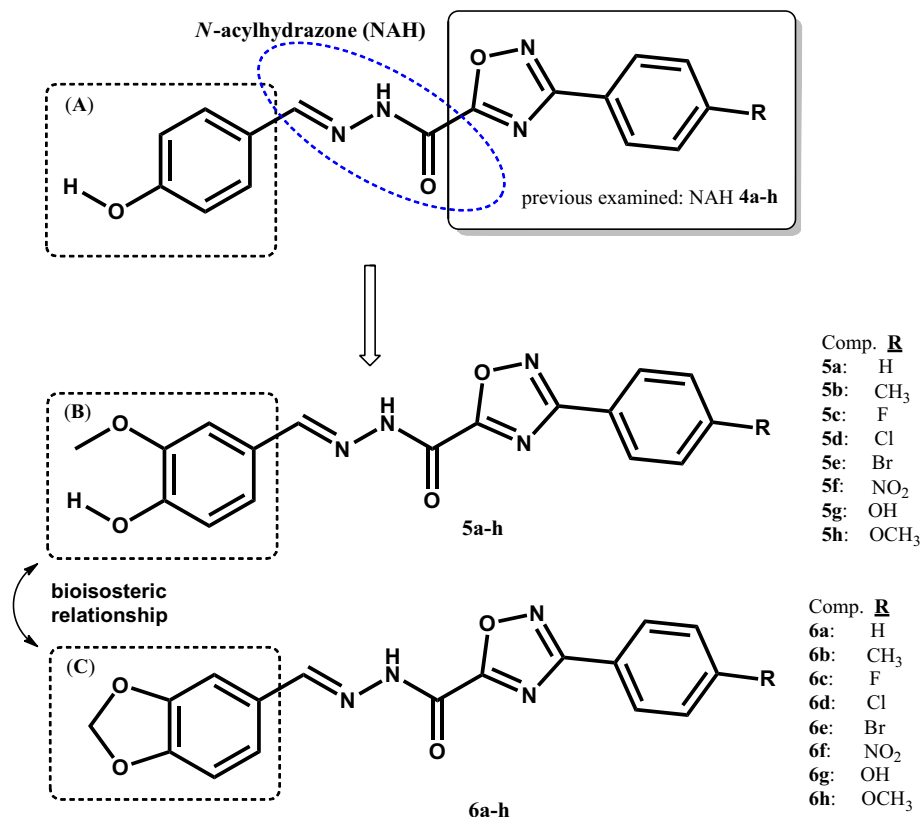


Figure 1. Structural design of oxadiazoles **5a-h** and **6a-h** as trypanocidal compounds.

mexicana.^{16–20} In light of these findings, we found reasonable to explore oxadiazoles as anti-*T. cruzi* agents. In 2009, we reported a congener series of *N*-acylhydrazone 1,2,4-oxadiazoles, denoted **4a-h**, exhibiting toxicity for trypomastigotes of *T. cruzi* Y strain.²¹ The oxadiazoles **4a-h** showed minimal toxicity for mouse splenocytes and a clear set of structure–activity relationships. A computational model of docking suggested oxadiazoles **4a-h** might be cruzain ligands. This model also suggested that the 4-hydroxyphenyl group near to the *N*-acylhydrazone is probably oriented in a region of cruzain structure which is also the binding site for highly-potent cruzain inhibitors.¹² Based on this binding model, we thought that structural modifications on 4-hydroxyphenyl might lead to potency enhancement (Fig. 1).

The functional activity of oxadiazole **4a-h** as trypanosomicidal compounds led us to explore potency enhancement by molecular modification. For this study, we synthesized oxadiazoles **5a-h** and **6a-h**, composed of the 3-aryl-1,2,4-oxadiazole-5-carbohydrazides of the previously identified anti-*T. cruzi* oxadiazoles **4a-h** with a replacement of 4-hydroxyphenyl group by 4-hydroxy-3-methoxyphenyl for **5a-h** and 1,3-benzodioxole for **6a-h**. These chemical replacements were selected due to the analogy between these chemical groups (Fig. 1).^{22–24} Enhancement of anti-*T. cruzi* activity in parasite cells was indeed achieved for oxadiazoles **6a-h**, furthermore these oxadiazoles impaired trypomastigote development and invasion into host-cells, and mice orally treated with oxadiazole **6d** had a substantial reduction of parasitemia.

2. Results and discussion

2.1. Chemistry

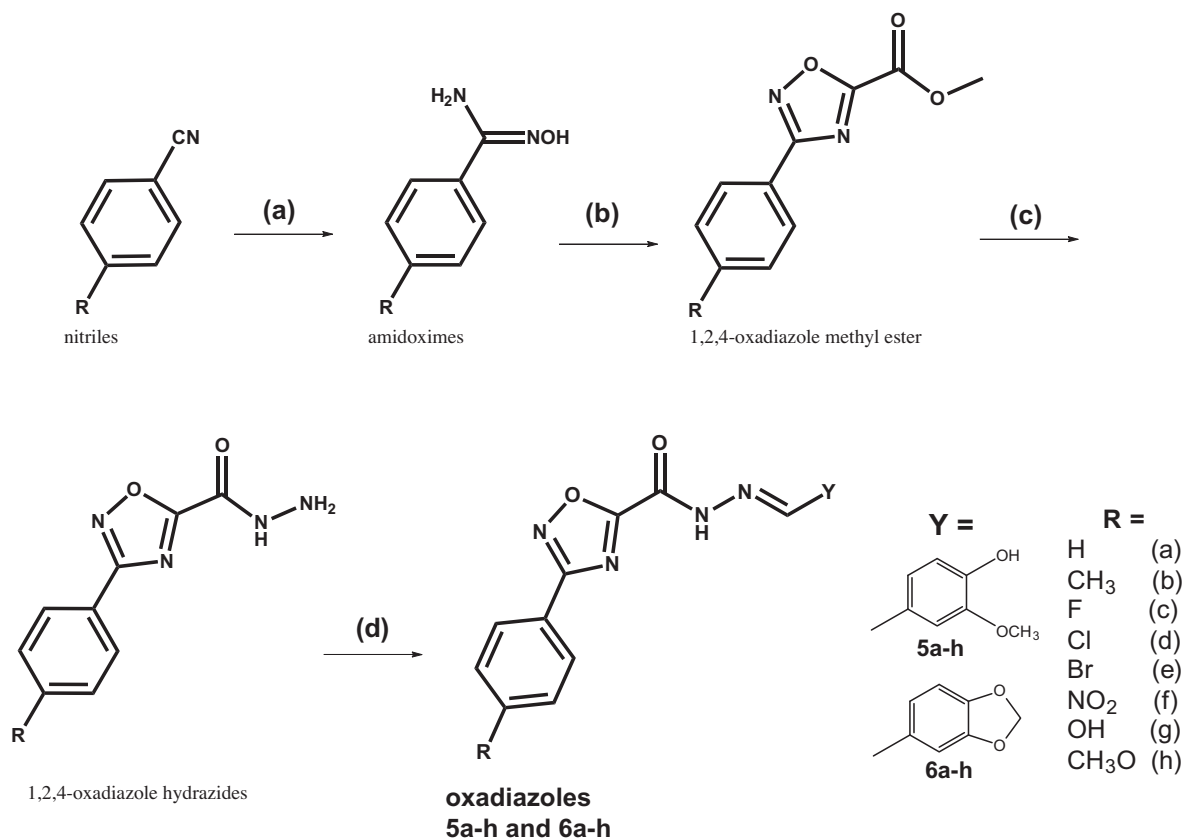
The synthesis of compounds **5a-h** and **6a-h** is depicted in Scheme 1 and is based on a method previously described by our

group.²⁵ This starts with 4-substituted aryl amidoximes, which are freshly prepared from commercially available nitriles; then they react with methyloxalyl chloride yielding the 1,2,4-oxadiazolic compounds in good yields. Further conversion of 1,2,4-oxadiazole methylesters into 1,2,4-oxadiazole hydrazides is achieved with quantitative yields by reacting them with hydrazine hydrate at 0 °C during 2 h.

These hydrazides, which are key intermediates in our research to investigate the pharmacological properties of 1,2,4-oxadiazoles,²⁶ are of easy synthesis and produces the final compounds, *N*-acylhydrazones **5a-h** and **6a-h**. To establish a SAR between our previously studied oxadiazoles (compounds **4a-h**) and oxadiazoles **5a-h** and **6a-h** described here, we used the same substituents in both cases (R = H, CH₃, F, Cl, Br, OCH₃, OH, NO₂). The σ_p -Hammett values for these substituents range from –0.37 for OH to 0.78 for NO₂, and therefore the electronic contribution of the *para*-substituent on the phenyl group varies significantly and allows us to investigate the importance of each substituent. The physical and spectroscopic data for the compounds **5a-h** are described here (experimental materials), while the spectral characterization for **6a-h** has been previously described.²⁶

N-Acylhydrazones can yield a mixture of *Z*- and *E*-isomers,²⁴ but the ¹H NMR analysis revealed that the *E*-isomers predominated (>98%). The mild conditions we used for preparing *N*-acylhydrazones **5a-h** and **6a-h** (short reaction time and room temperature) explain the predominance of the *E*-isomer in the crude products. The X-ray analysis of **6f** crystal obtained by crystallization from a dimethylformamide solution exclusively produced the *E*-diastereomer (Fig. 2), confirming the ¹H NMR data.

Quantum chemistry calculations (ab initio) suggested a planar and *E*-geometry for compounds **6a-h** and showed that two stable conformers of this geometry are possible, differing only by 2.74 kcal/mol.²⁶ The conformer of lowest energy is synperiplanar,



Scheme 1. Reagents and conditions: (a) $\text{NH}_2\text{OH}\cdot\text{HCl}$, Na_2CO_3 , $\text{H}_2\text{O}/\text{MeOH}$, reflux, 4 h; (b) $\text{ClOCCO}_2\text{CH}_3$, dry THF, reflux, 4.5 h; (c) NH_2NH_2 55%, EtOH, 0 °C, 2 h; (d) EtOH, H_2SO_4 (cat.), aromatic aldehyde, room temperature, 10 min.

with the carbonyl oxygen and the iminic hydrogen *syn* to each other. The higher stability of this conformer is because of a non-classical hydrogen bond between $\text{C}=\text{O}$ and $\text{CH}=\text{N}$, like a five-member ring. The antiperiplanar conformer has the carbonyl oxygen and the iminic hydrogen in opposite sides (*anti*), and therefore an intramolecular interaction is not possible. The conformations we predicted by quantum chemistry and the observed one by X-ray are different. The antiperiplanar conformer observed in the crystalline structure can be explained. By X-ray diffraction, the crystal structure of compound **6f** presents one molecule of DMF in the asymmetric unit. The position of the DMF molecule allows its oxygen atom to interact with two hydrogen atoms of the NAH from the imine group ($\text{CH}=\text{N}$) and the amide group ($\text{N}-\text{H}$) and it provides stability for an antiperiplanar conformer.

2.2. Pharmacology

Once the compounds had been chemically characterized, we focused on evaluating their biological activity. All compounds were evaluated against *T. cruzi*. We first assayed the cell viability of mouse splenocytes treated with oxadiazoles **5a-h** and **6a-h**. Given that the compounds showed no toxicity in this assay, having an LC_{50} higher than 100 $\mu\text{g}/\text{mL}$, they were evaluated against epimastigotes (axenic culture) and bloodstream trypomastigotes of Y strain *T. cruzi*, using benznidazole (Bdz) as a control drug. The compounds that showed IC_{50} values comparable to Bdz were further selected for in vitro and in vivo assays. The ability of these compounds to inhibit the activity of cruzain was also performed in parallel to the parasite cell assays. All compounds were initially tested at 100 μM . For active compounds, a dose–response curve was determined and the IC_{50} calculated. Table 1 summarizes the cruzain and anti-*T. cruzi* activities for oxadiazoles **5a-h** and **6a-h**.

None of the oxadiazoles **5a-h** showed anti-*T. cruzi* activity. This was an unexpected finding because compounds **5a-h** only differ from our early examined oxadiazoles (**4a-h**)²¹ by the introduction of a 3-methoxy group. But we found potent trypanosomicidal activities for oxadiazoles **6a-h**. We first noted that the halogenated oxadiazoles **6c**, **6d**, and **6e** were able to inhibit *T. cruzi*, with IC_{50} values quite similar to Bdz (Table 1). For example, oxadiazoles **6c** (fluorine) and **6d** (chlorine) have IC_{50} of 9.5 ± 2.8 and 3.5 ± 1.8 μM for Y strain trypomastigotes, quite similar to Benznidazole (IC_{50} of 11.3 ± 2.8 μM) respectively. Neither oxadiazoles **6c**, **6d**, and **6e** nor benznidazole affected the cell viability of mouse splenocytes up to 100 $\mu\text{g}/\text{mL}$, while these compounds clearly affect parasite proliferation (epimastigotes) and motility (trypomastigotes). The absence of toxicity for mouse splenocytes shows that the cell effects of oxadiazoles and Bdz are specific for *T. cruzi*.

After confirming that the oxadiazoles were able to kill *T. cruzi* parasites, our next step was to understand how these compounds affect the infection of host cells by trypomastigotes.^{27,28} We tested oxadiazoles **6c**, **6d**, and **6e** in an in vitro model of parasite infection in macrophages. Macrophages were infected with Y strain trypomastigotes and then treated with compounds at 10 $\mu\text{g}/\text{mL}$, including Bdz. Cells were analyzed by light microscopy and the percentage of infected macrophages and the number of amastigotes were determined and compared to untreated infected cells (negative control) and cells treated with benznidazole (positive control).

In untreated-infected macrophages (negative control), the percentage of infected cells is high (Figs. 3 and S1, Supplementary data). As a result, trypomastigotes complete the intracellular cycle into amastigotes, resulting in an average of almost 800 amastigotes per 100 host-cells (Fig. 3).²⁹ When 10 $\mu\text{g}/\text{mL}$ of oxadiazoles **6c** and **6d** are added, the percentage of infected macrophages is significantly reduced when compared to untreated cells. Oxadiazole **6e**,

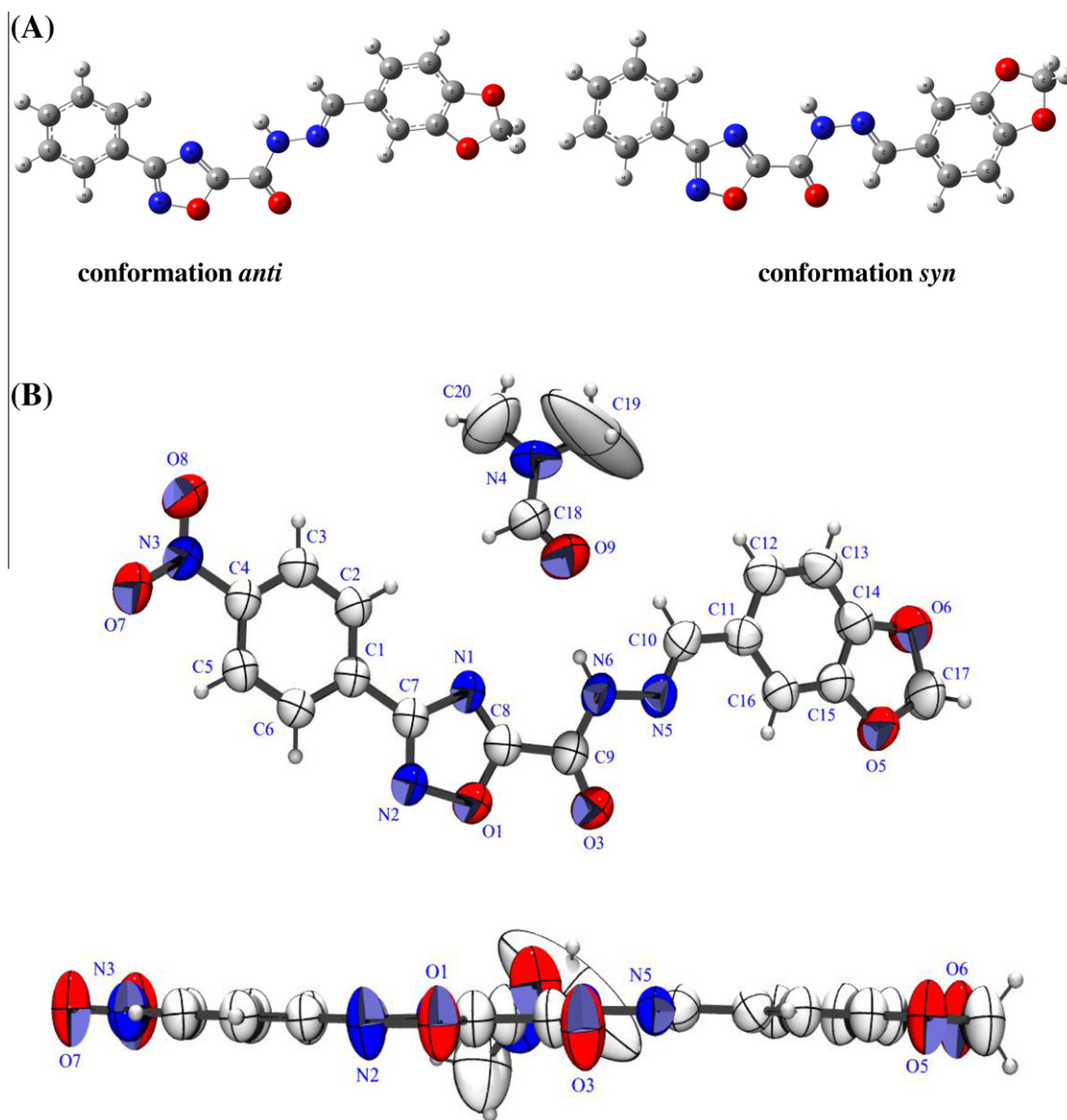


Figure 2. (A) General representation of the *syn* and *anti* conformers for oxadiazoles **6a–h**. (B) Top: structure of **6f** determined by X-ray analysis (ORTEP-3 view, displacement ellipsoids are drawn at a 50% level), highlighting the *E*-geometry and the *anti* arrangement. The bottom highlights that the molecule is entirely planar.

a bromine analog that was cidal for trypanomastigotes (Table 1), had no activity in these assays. When 10 $\mu\text{g}/\text{mL}$ of oxadiazoles **6c** or **6d** are added at the moment of infection, the number of infected cells is lower than untreated-infected macrophages (Fig. S2 Supplementary data). This suggests that oxadiazoles **6c** and **6d** impair trypanomastigote invasion into host-cells. The oxadiazoles **6c** and **6d** arrested trypanomastigote development and invasion of macrophages. Therefore, potency enhancement of anti-*T. cruzi* activity was achieved for oxadiazoles **6a–h** when compared to our previously studied oxadiazoles **4a–h**.²¹

We also investigated the ability of these compounds to inhibit the recombinant cysteine protease of *T. cruzi*, cruzain.¹⁸ As seen in Table 1, oxadiazoles **5d**, **5e** and **6e** showed high-affinity for cruzain (IC_{50} from 40 to 200 nM). Cruzain inhibition by these three oxadiazoles was higher when they were pre-incubated with the enzyme, consistent with a covalent-mechanism of inhibition. *N*-Acyhydrazones such as compounds **5d** and **5e** may undergo Michael-addition reactions, yielding covalent adducts with cruzain.³⁰ Other oxadiazoles of the series **5a–h** and **6a–h** did not show significant cruzain inhibition at 100 μM , so no SAR could be drawn. The cruzain inhibition observed for oxadiazoles **5d**, **5e** and **6e** was not

due to nonspecific binding. The assay was repeated in the absence and the presence of 0.1% Triton X-100.¹⁸ The level of cruzain inhibition did not vary among these conditions, suggesting that enzyme inhibition is not due to compound aggregation. Since there is no reliable correlation between cruzain inhibition and trypanosomicidal properties, the trypanosomicidal effects of oxadiazoles are only in part due to cruzain inhibition, other targets and biochemical pathways must be involved.

To further investigate the mechanism of action of oxadiazoles **6c** and **6d**, ultrastructural alterations in bloodstream trypanomastigotes were analyzed. Electron micrographs are shown in Figure 4. In comparison to untreated parasites, trypanomastigotes incubated with **6c** and **6d** had membrane protrusions in about 80% of cells. Oxadiazoles **6c** and **6d** caused mitochondria degeneration, Golgi apparatus and endoplasmic reticulum disorganization, followed by kinetoplast enlargement. When infected macrophages were treated with 3.5 μM of oxadiazole **6d**, we could observe that oxadiazole **6d** targets mitochondria, causing fragmentation as well as the formation of atypical vacuoles which contain mitochondrial components (Fig. 5). High-affinity cruzain inhibitors, such as peptide K777, are believed to induce structural alterations in Golgi

Table 1
Cruzain and anti-*T. cruzi* activities

Compound	R	% Cruzain inhibition 100 μM^a	Y strain <i>T. cruzi</i> IC ₅₀ μM (\pm SD)		Mouse splenocytes LC ₅₀ ^d ($\mu\text{g}/\text{mL}$)
			Trypomastigotes ^b	Epimastigotes ^c	
5a	H	47	ND	ND	>100
5b	CH ₃	14	ND	ND	>100
5c	F	63	ND	ND	>100
5d	Cl	92 (0.04)	ND	ND	>100
5e	Br	100 (0.2)	ND	ND	>100
5f	NO ₂	47	ND	ND	>100
5g	OH	25	ND	ND	>100
5h	CH ₃ O	35	ND	ND	>100
6a	H	32	ND	ND	>100
6b	CH ₃	49	ND	ND	>100
6c	F	34	9.5 (\pm 2.8)	12.2 (\pm 7.6)	>100
6d	Cl	42	3.5 (\pm 1.8)	7.5 (\pm 4.8)	>100
6e	Br	95 (0.03)	13.4 (\pm 1.8)	14.0 (\pm 5.4)	>100
6f	NO ₂	NT	ND	ND	>100
6g	OH	17	ND	ND	>100
6h	CH ₃ O	44	ND	ND	>100
Bdz ^e	—	—	11.3 (\pm 1.8)	7.5 (\pm 2.1)	—
GV ^e	—	—	—	—	0.11

^a Cruzain inhibition after a 10 min pre-incubation with the inhibitor. The results represent the average of duplicates. Values in parenthesis represent IC₅₀ values in μM , which were determined based on at least 9 compound concentrations in duplicate.

^b Determined after 24 h of incubation of trypomastigotes with the compounds. Values were calculated from five concentrations using data obtained from at least two independent experiments (SD given in parenthesis).

^c Determined after 5 days of incubation of epimastigotes with the compounds. IC₅₀ was calculated from five concentrations using data obtained from at least two independent experiments (SD given in parenthesis).

^d Toxicity for splenocytes of BALB/c mouse after 24 h of incubation in the presence of the compounds.

^e Bdz = Benznidazole; GV = Gentian Violet. Nd., not determined, due to the lack of activity in the tested concentration. SD = standard deviation.

apparatus, endoplasmic reticulum, and to alter protein trafficking into lysosomes/reservosomes.³¹ Alterations of mitochondria and kinetoplast are not observed for well-known cruzain inhibitors.^{31,32} These information differed from those observed here for oxadiazoles **6c** and **6d**. What we observed is that oxadiazoles substantially alter the mitochondrial morphology, therefore proteins involved in parasite metabolism and bioenergetics might be the molecular targets for oxadiazoles. Instead of attempting to identify these target proteins, we decided to evaluate whether these compounds reduce blood parasitemia in *T. cruzi*-infected mice.

To determine the maximum tolerated dose (MTD), single oral treatment of oxadiazole **6d** to uninfected BALB/c mice ($n = 3/\text{group}$) at doses of 25, 50, and 100 mg/kg was performed. Mice treated with **6d** appeared normal and no mortality was observed. We also measured serum biochemical components in uninfected mice treated with **6d** (Table S1). In comparison to untreated and uninfected mice, treatment with **6d** did not systematically change serum components, suggesting the toxicity of these oxadiazoles is not a major concern. Based on this, oxadiazoles **6c** and **6d** were administered at dose of 50 mg/kg to infected mice.

BALB/c mice were infected with Y strain trypomastigotes³³ and treated or not with **6c**, **6d**, and Bdz. In untreated, infected mice, blood parasitemia was observed after day 8 of parasite inoculation and peaked on day 10 (Fig. 6). Benznidazole (Bdz) gi-

ven orally at 100 mg/kg once a day for 5 days (starting from day 5 after infection) almost eradicated blood parasitemia. Compound **6d** substantially reduced blood parasitemia ($p < 0.001$) compared to untreated infected mice. Compound **6c** did not reduce parasitemia as much as compound **6d**, as expected based on its lower potency. Compound **6e** was not tested due to low solubility.

N-Acylylhydrazones are known for their in vitro trypanosomicidal and cruzain inhibition effects.^{34–37} However, very few *N*-acylylhydrazones that are effective in reducing in vivo infection have been identified.³⁸ One method for increasing the efficacy of anti-*T. cruzi* *N*-acylylhydrazones is through the combination with oxadiazole chemistry.^{19–21} From our past studies, we discovered that *N*-acylylhydrazones derived from 1,2,4-oxadiazole chemistry were less potent trypanosomicidal agents than benznidazole, but at least they were more selective for parasite than to mammalian cells.²¹ Here, our main aim was to improve the cidal potency by molecular modification. We knew from past SAR model that the *N*-acylylhydrazone motif is more suitable and tolerates molecular modification. In view of this, we planned compounds **5a–h** and **6a–h**. This structural design was successful and led us to identify the anti-*T. cruzi* oxadiazole denoted **6d**.

We believe that compound **6d** merits further chemical optimization because: (a) it has a selectivity window of at least 50 (host cell

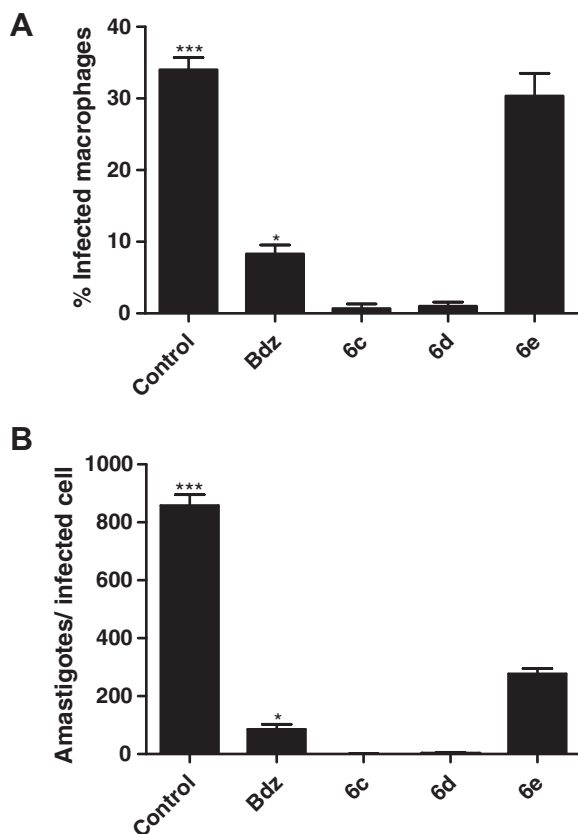


Figure 3. Oxadiazoles impair *T. cruzi* trypomastigote development in macrophages. The percentage of infected macrophages (A) and the mean number of amastigotes/infected cell (B) are higher in untreated infected controls than in cultures treated with 10 $\mu\text{g}/\text{mL}$ of test-inhibitors **6c** or **6d**. Bdz is benznidazole. Experiment done in triplicate. Standard deviations are shown as error bars. ***, $p < 0.001$; *, $p < 0.05$.

toxicity $\text{LC}_{50}/T. cruzi \text{IC}_{50}$); (b) it is efficient and well-tolerated in oral treatment; (c) at a dose of 50 mg/kg (140 $\mu\text{mol}/\text{kg}$) parasitemia was reduced in vivo; (d) **6d** is a low-molecular weight, achiral, and nonpeptidic compound. These functional properties and chemical features are desirable for a Chagas disease drug candidate.³⁹

3. Conclusions

From our past studies, oxadiazoles were less potent cidal than benznidazole, but they were more selective for parasite versus mammalian cells. Here, our effort was to improve their cidal potency by molecular modification of substituents. To this end, trypanosomicidal properties as well cruzain inhibition of 3-aryl-1,2,4-oxadiazole-5-carbohydrazides containing a 4-hydroxy-3-methoxyphenyl **5a–h** or 1,3-benzodioxole **6a–h** were determined. Oxadiazole **6d**, which features a 1,3-benzodioxole group near to the *N*-acylhydrazone was identified as the most potent and selective trypanosomicidal compound among them, and endowed with efficacy in reducing blood parasitemia in a mouse model of acute infection. The efficacy observed for oxadiazole **6d** in in vitro and in vivo models of infection argues favorably for oxadiazoles as antiparasitic agents and therefore the synthetic redesign of variant forms of oxadiazole **6d** is worthy.

4. Experimental section

4.1. Chemistry

Melting points were determined on a Gallenkamp capillary apparatus and are uncorrected. Infrared spectra were determined

using KBr discs on a Perkin–Elmer Paragon 500 FT-IR spectrometer. ^1H NMR spectra were determined on a Bruker DPX-200 spectrometer, with chemical shifts δ reported in ppm unities relative to the internal standard TMS, using $\text{DMSO}-d_6$ as solvent. Mass spectral were determined by using a Finnigan mass spectrometers model MAT 8200 for low resolution mass spectrometry (MS) and the MAT 95 for high resolution mass spectrometry (HRMS). Values for HRMS lie within the permitted limit intervals with resolution of 10,000. The reactions were monitored by thin layer chromatography (TLC), performed on plates prepared with a 0.2 mm thick silica gel 60 (PF-254 with gypsum, Merck). The developed chromatograms were visualized under ultraviolet light at 254–265 nm. For column chromatography, silica gel 60 (230–400 mesh, Merck) was used. All common laboratory chemicals were purchased from commercial sources and used without previous purification. Crystallographic data for compound **6f** can be obtained free of charge at the Cambridge Crystallographic Data Centre (CCDC, deposit number 870707, www.ccdc.cam.ac.uk/data_request/cif).

4.1.1. General procedure for preparation of compounds **5a–h**

To a stirred suspension of 0.01 mol of appropriate hydrazide in 5 mL of ethanol, 3–4 drops of concentrated sulfuric acid were added, changing the mixture to a clear solution. Then, vanillin (0.01 mol) previously dissolved in 5 mL of ethanol was added to the mixture at room temperature. After few seconds, a colored solid precipitated and the mixture was stirred for 10 min before the addition of 10 mL of water. After vacuum filtration, the solid was washed with cold water/ethanol 1:1 and then with cold water. Recrystallization from dioxane/water mixture afforded the crystalline solids. Yields, melting points, spectroscopic and spectrometric data are listed below for each compound.

4.1.1.1. 3-Phenyl-*N'*-[(4-hydroxy-3-methoxyphenyl)methylene]-1,2,4-oxadiazole-5-carbohydrazide (5a**).** Yield: 91%; Mp 216 °C (from dioxane/ H_2O); IR (KBr, cm^{-1}): $\nu = 3494$ (br O–H), 3448 (N–H, acyl hydrazone), 3190 (C–H, imine), 1674 (C=O), 1594 (C=N, imine), 1516 (C=N, heterocyclic). ^1H NMR (200 MHz, $\text{DMSO}-d_6$) δ : 12.6 (s, 1H, CONH), 9.71 (s, 1H, OH), 8.48 (s, 1H, N=CH), 8.09–8.06 (m, 2H, ortho to oxadiazole ArH), 7.63–7.59 (m, 3H, meta/para to oxadiazole ArH), 7.31 (s, 1H, 2 to hydrazone ArH), 7.11 (d, 1H, $^3J = 8.3$ Hz, 6 to hydrazone ArH), 6.84 (d, 1H, $^3J = 7.8$ Hz, 5 to hydrazone ArH), 3.82 (s, 3H, OCH_3). MS (m/z): 338 (M^+ , 100), 192 (M-phenyloxadiazole, 14), 164 (192-CO, 6), 149 (192-HNCO, 43), 136 (164- N_2 , 70). HRMS for $\text{C}_{17}\text{H}_{14}\text{N}_4\text{O}_4$ calcd (found): 338.10151 (338.10238).

4.1.1.2. 3-(4-Methylphenyl)-*N'*-[(4-hydroxy-3-methoxyphenyl)methylene]-1,2,4-oxadiazole-5-carbohydrazide (5b**).** Yield: 92%; Mp 213 °C (from dioxane/ H_2O); IR (KBr, cm^{-1}): $\nu = 3479$ (br O–H; N–H, acyl hydrazone), 3181 (C–H, imine), 1702 (C=O), 1607 (C=N, imine), 1515 (C=N, heterocyclic). ^1H NMR (200 MHz, $\text{DMSO}-d_6$) δ : 12.6 (s, 1H, CONH), 9.70 (s, 1H, OH), 8.47 (s, 1H, N=CH), 7.97 (d, 2H, $^3J = 8.1$ Hz, ortho to oxadiazole ArH), 7.41 (d, 2H, $^3J = 8.1$ Hz, meta to oxadiazole ArH), 7.31 (d, 1H, $^4J = 1.7$ Hz, 2 to hydrazone ArH), 7.10 (dd, 1H, $^4J = 1.7$ Hz, $^3J = 8.4$ Hz, 6 to hydrazone ArH), 6.84 (d, 1H, $^3J = 8.4$ Hz, 5 to hydrazone ArH), 3.82 (s, 3H, OCH_3), 2.38 (s, 3H, CH_3). MS (m/z): 352 (M^+ , 100), 192 (M-phenyloxadiazole, 14), 164 (192-CO, 3), 149 (192-HNCO, 60), 136 (164- N_2 , 78). HRMS for $\text{C}_{18}\text{H}_{16}\text{N}_4\text{O}_4$ calcd (found): 352.11716 (352.11712).

4.1.1.3. 3-(4-Fluorophenyl)-*N'*-[(4-hydroxy-3-methoxyphenyl)methylene]-1,2,4-oxadiazole-5-carbohydrazide (5c**).** Yield: 90%; Mp 216 °C (from dioxane/ H_2O); IR (KBr, cm^{-1}): $\nu = 3486$ (br O–H), 3446 (N–H, acyl hydrazone), 3197 (C–H, imine), 1677

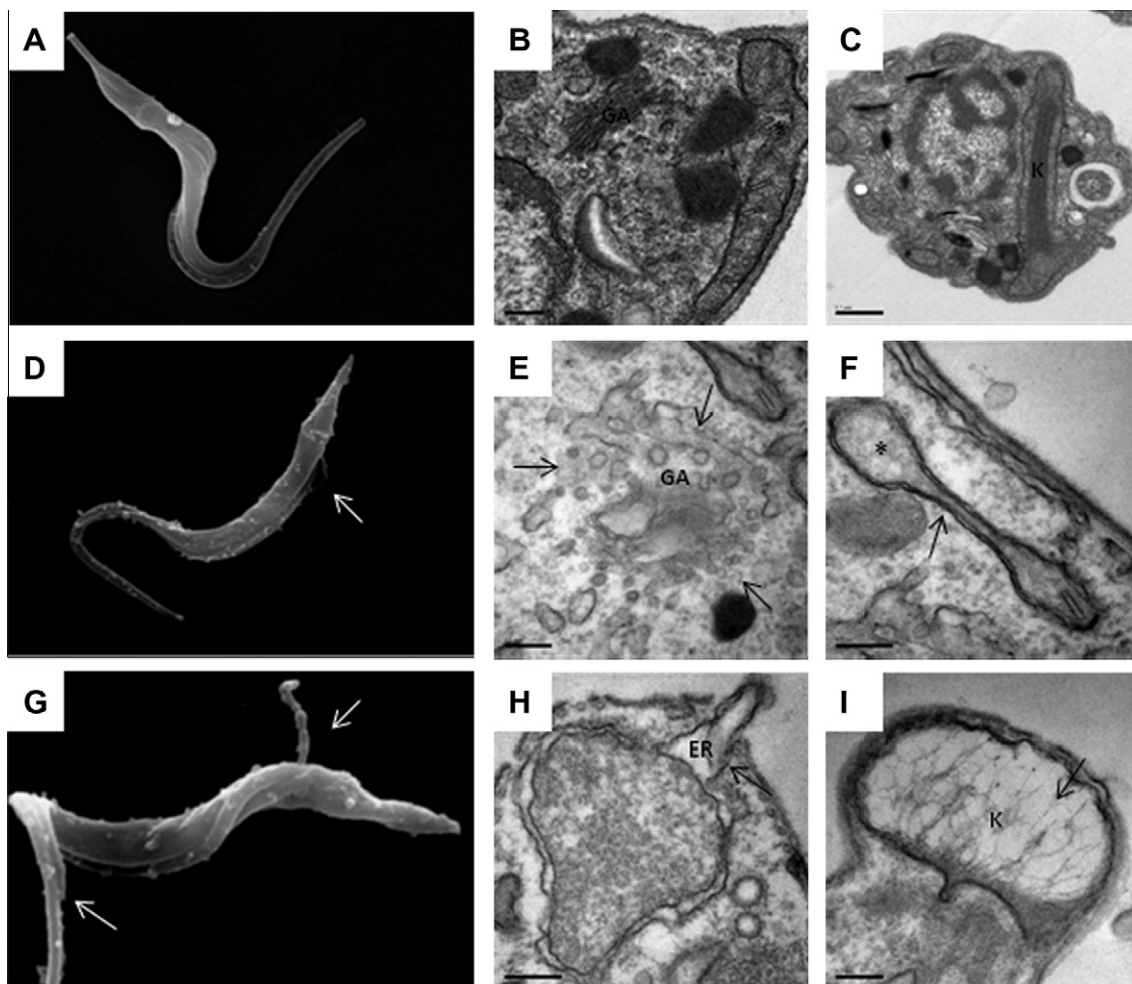


Figure 4. Oxadiazoles induce ultrastructural changes in bloodstream trypomastigotes. Using SEM, we observed plasma membrane protrusions (arrows) in cells treated with compounds **6c** (30 μ M; D) or **6d** (10 μ M; G); untreated cells (A). Using TEM, untreated trypomastigotes highlighting Golgi apparatus and mitochondria (B) and kinetoplast (C). In cells treated with **6c** (9.5 μ M, E, F) or **6d** (3.5 μ M, H, I), we observed alterations in Golgi apparatus (E), mitochondria (F), membranes of endoplasmic reticulum (H), and kinetoplast (I). GA = Golgi apparatus; * = Mitochondria; ER = endoplasmic reticulum; K = kinetoplast.

(C=O), 1592 (C=N, imine), 1516 (C=N, heterocyclic). ^1H NMR (200 MHz, DMSO- d_6) δ : 12.6 (s, 1H, CONH), 9.70 (s, 1H, OH), 8.47 (s, 1H, N=CH), 8.13 (dd, 2H, $^4J_{F-H} = 5.2$ Hz, $^3J = 8.8$ Hz, ortho to oxadiazole ArH), 7.46 (t, 2H, $J = 8.8$ Hz, meta to oxadiazole ArH), 7.3 (d, 1H, $^4J = 1.3$ Hz, 2 to hydrazone ArH), 7.11 (dd, 1H, $^4J = 1.3$ Hz, $^3J = 8.2$ Hz, 6 to hydrazone ArH), 6.84 (d, 1H, $^3J = 7.9$ Hz, 5 to hydrazone ArH), 3.82 (s, 3H, OCH₃). MS (m/z , %): 356 (M^+ , 100), 192 (M-phenyloxadiazole, 14), 164 (192-CO, 6), 149 (192-HNCO, 68), 136 (164-N₂, 72). HRMS Calcd for C₁₇H₁₃N₄O₄F calcd (found): 356.09208 (356.09178).

4.1.1.4. 3-(4-Chlorophenyl)-N'-[(4-hydroxy-3-methoxyphenyl)methylene]-1,2,4-oxadiazole-5-carbohydrazide (5d). Yield: 88%; Mp 219 °C (from dioxane/H₂O); IR (KBr, cm⁻¹): $\nu = 3501$ (br O-H), 3446 (N-H, acyl hydrazone), 3223 (C-H, imine), 1678 (C=O), 1591 (C=N, imine), 1517 (C=N, heterocyclic). ^1H NMR (200 MHz, DMSO- d_6) δ : 12.6 (s, 1H, CONH), 9.71 (s, 1H, OH), 8.47 (s, 1H, N=CH), 8.09 (d, 2H, $^3J = 8.5$ Hz, ortho to oxadiazole ArH), 7.69 (d, 2H, $J = 8.1$ Hz, meta to oxadiazole ArH), 7.30 (d, 1H, $^4J = 1.3$ Hz, 2 to hydrazone ArH), 7.11 (dd, 1H, $^4J = 1.3$ Hz, $^3J = 9.8$ Hz, 6 to hydrazone ArH), 6.84 (d, 1H, $^3J = 8.1$ Hz, 5 to hydrazone ArH), 3.82 (s, 3H, OCH₃). MS (m/z , %): 372/375 (M^+ , 100/34), 192 (M-phenyloxadiazole, 21), 164 (192-CO, 7), 149 (192-HNCO, 97), 136 (164-N₂, 98). HRMS for C₁₇H₁₃N₄O₄Cl calcd (found): 372.06253 (372.06334).

4.1.1.5. 3-(4-Bromophenyl)-N'-[(4-hydroxy-3-methoxyphenyl)methylene]-1,2,4-oxadiazole-5-carbohydrazide (5e). Yield: 88%; Mp 212 °C (from dioxane/H₂O); IR (KBr, cm⁻¹): $\nu = 3329$ (br O-H), 3217 (N-H, acyl hydrazone), 3190 (C-H, imine), 1674 (C=O), 1583 (C=N, imine), 1516 (C=N, heterocyclic). ^1H NMR (200 MHz, DMSO- d_6) δ : 12.7 (s, 1H, CONH), 9.70 (s, 1H, OH), 8.47 (s, 1H, N=CH), 8.02 (d, 2H, $^3J = 8.5$ Hz, ortho to oxadiazole ArH), 7.83 (d, 2H, $J = 8.5$ Hz, meta to oxadiazole ArH), 7.30 (d, 1H, $^4J = 1.3$ Hz, 2 to hydrazone ArH), 7.11 (dd, 1H, $^4J = 1.3$ Hz, $^3J = 8.2$ Hz, 6 to hydrazone ArH), 6.84 (d, 1H, $^3J = 7.8$ Hz, 5 to hydrazone ArH), 3.82 (s, 3H, OCH₃). MS (m/z , %): 416/418 (M^+ , 59/59), 192 (M-phenyloxadiazole, 21), 164 (192-CO, 7), 149 (192-HNCO, 100), 136 (164-N₂, 97). HRMS for C₁₇H₁₃N₄O₄Br calcd (found): 416.01202 (416.01187).

4.1.1.6. 3-(4-Nitrophenyl)-N'-[(4-hydroxy-3-methoxyphenyl)methylene]-1,2,4-oxadiazole-5-carbohydrazide (5f). Yield: 91%; Mp 383 °C (from dioxane/H₂O); IR (KBr, cm⁻¹): $\nu = 3490$ (br O-H), 3280 (N-H, acyl hydrazone), 1697 (C=O), 1596 (C=N, imine), 1513 (C=N, heterocyclic). ^1H NMR (200 MHz, DMSO- d_6) δ : 12.8 (s, 1H, CONH), 9.70 (s, 1H, OH), 8.48 (s, 1H, N=CH), 8.46 (d, 2H, $^3J = 9.3$ Hz, meta to oxadiazole ArH), 8.34 (d, 2H, $^3J = 8.8$ Hz, ortho to oxadiazole ArH), 7.31 (d, 1H, $^4J = 1.3$ Hz, 2 to hydrazone ArH), 7.12 (dd, 1H, $^4J = 1.3$ Hz, $^3J = 8.3$ Hz, 6 to hydrazone ArH), 6.85 (d, 1H, $^3J = 8.3$ Hz, 5 to hydrazone ArH), 3.82 (s,

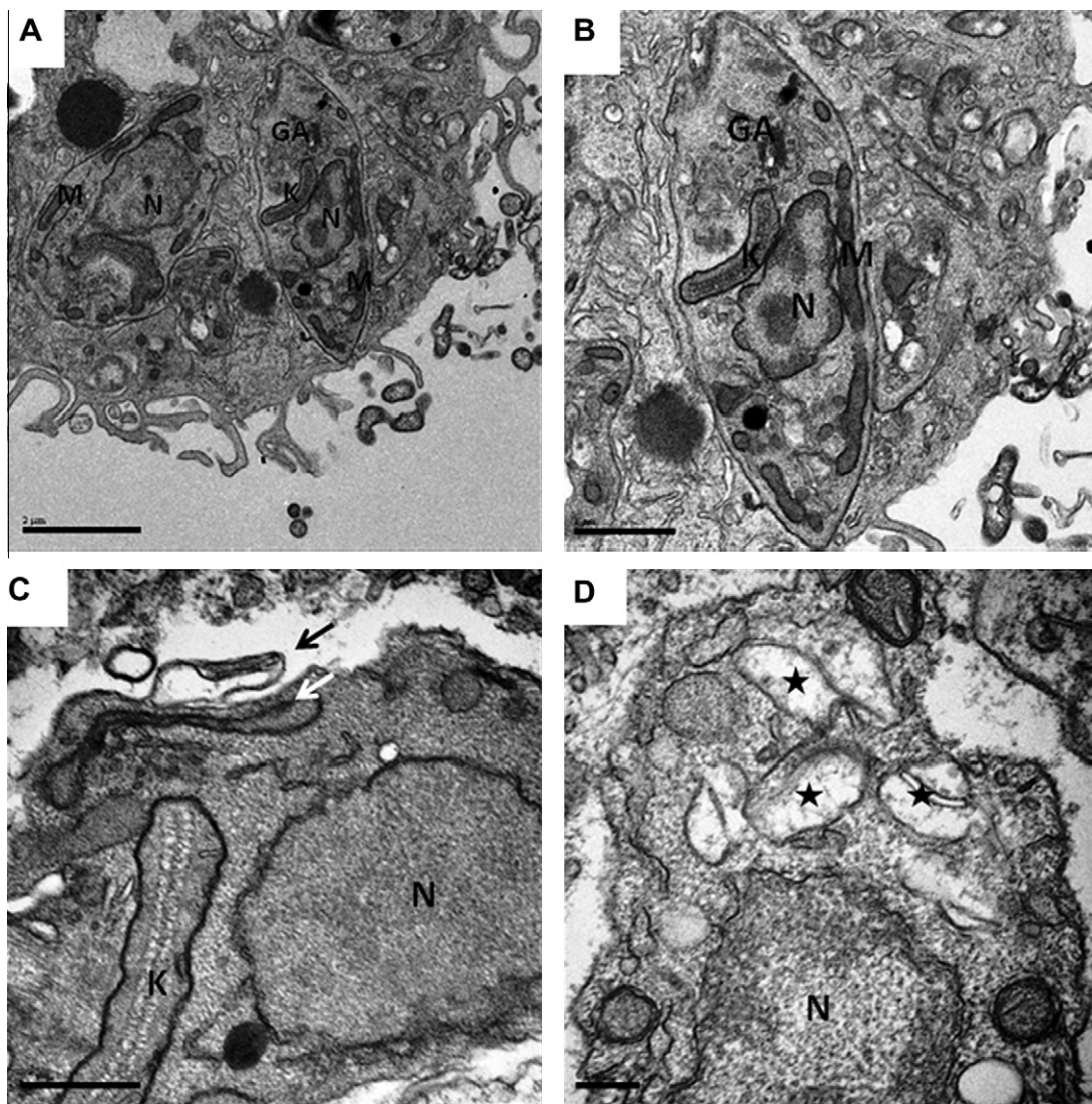


Figure 5. Oxadiazole **6d** induces structural changes in intracellular amastigotes. (A and B) TEM of untreated cells highlighting nucleus (N) and Golgi apparatus (GA). (C and D) in cells treated with 3.25 μM of **6d** we observed alterations in membrane (black arrow), degradation of mitochondria (white arrow) as well atypical mitochondrial vacuoles (black stars). Scale of 2.0 (A), 1.0 (B), 0.5 (C), and 0.2 μm (D).

3H, OCH₃). MS (*m/z*,%): 383 (M⁺, 100), 192 (M-phenyloxadiazole, 18), 164 (192-CO, 6), 149 (192-HNCO, 73), 136 (164-N₂, 62). HRMS for C₁₇H₁₃N₅O₆ calcd (found): 383.08658 (383.08753).

4.1.1.7. 3-(4-Hydroxyphenyl)-N-[(4-hydroxy-3-methoxyphenyl)methylene]-1,2,4-oxadiazole-5-carbohydrazide (5g).

Yield: 99%; Mp 264 °C (from dioxane/H₂O); IR (KBr, cm⁻¹): ν = 3518, 3499 (O-H), 3293 (N-H, acyl hydrazone), 1693 (C=O), 1596 (C=N, imine), 1512 (C=N, heterocyclic). ¹H NMR (200 MHz, DMSO-*d*₆) δ : 12.6 (s, 1H, CONH), 10.2 (s, 1H, para to oxadiazole OH), 9.69 (s, 1H, OH), 8.46 (s, 1H, N=CH), 7.91 (d, 2H, ³J = 8.8 Hz, ortho to oxadiazole ArH), 7.30 (d, 1H, ⁴J = 1.3 Hz, 2 to hydrazone ArH), 7.11 (dd, 1H, ⁴J = 1.5 Hz, ³J = 8.2 Hz, 6 to hydrazone ArH), 6.94 (d, 2H, ³J = 8.8 Hz, meta to oxadiazole ArH), 6.84 (d, 1H, ³J = 8.2 Hz, 5 to hydrazone ArH), 3.82 (s, 3H, OCH₃). MS (*m/z*,%): 354 (M⁺, 100), 192 (M-phenyloxadiazole, 8), 164 (192-CO, 3), 149 (192-HNCO, 32), 136 (164-N₂, 42). HRMS for C₁₇H₁₄N₄O₅ calcd (found): 354.09642 (354.09733).

4.1.1.8. 3-(4-Methoxyphenyl)-N-[(4-hydroxy-3-methoxyphenyl)methylene]-1,2,4-oxadiazole-5-carbohydrazide (5h).

Yield: 97%; Mp 221 °C (from dioxane/H₂O); IR (KBr, cm⁻¹): ν = 3500–

3000 (br O-H), 3415 (N-H, acyl hydrazone), 1677 (C=O), 1597 (C=N, imine), 1512 (C=N, heterocyclic). ¹H NMR (200 MHz, DMSO-*d*₆) δ : 12.6 (s, 1H, CONH), 9.70 (s, 1H, OH), 8.47 (s, 1H, N=CH), 8.02 (d, 2H, ³J = 8.9 Hz, ortho to oxadiazole ArH), 7.31 (d, 1H, ⁴J = 1.3 Hz, 2 to hydrazone ArH), 7.15 (d, 2H, ³J = 8.6 Hz, meta to oxadiazole ArH), 7.11 (dd, 1H, ⁴J = 1.3 Hz, ³J = 8.3 Hz, 6 to hydrazone ArH), 6.84 (d, 1H, ³J = 8.3 Hz, 5 to hydrazone ArH), 3.84 (s, 3H, para to oxadiazole OCH₃), 3.82 (s, 3H, OCH₃). MS (*m/z*,%): 368 (M⁺, 100), 192 (M-phenyloxadiazole, 10), 164 (192-CO, 4), 149 (192-HNCO, 35), 136 (164-N₂, 42). HRMS for C₁₈H₁₆N₄O₅ calcd (found): 368.11207 (368.11232).

4.2. Animals

Female BALB/c mice (6–8 weeks old) were supplied by the animal breeding facility at Centro de Pesquisas Gonçalo Moniz (Fundação Oswaldo Cruz, Bahia, Brazil) and maintained in sterilized cages under a controlled environment, receiving a balanced diet for rodents and water ad libitum. All experiments were carried out in accordance with the recommendations of Ethical Issues Guidelines, and were approved by the local Animal Ethics Committee.

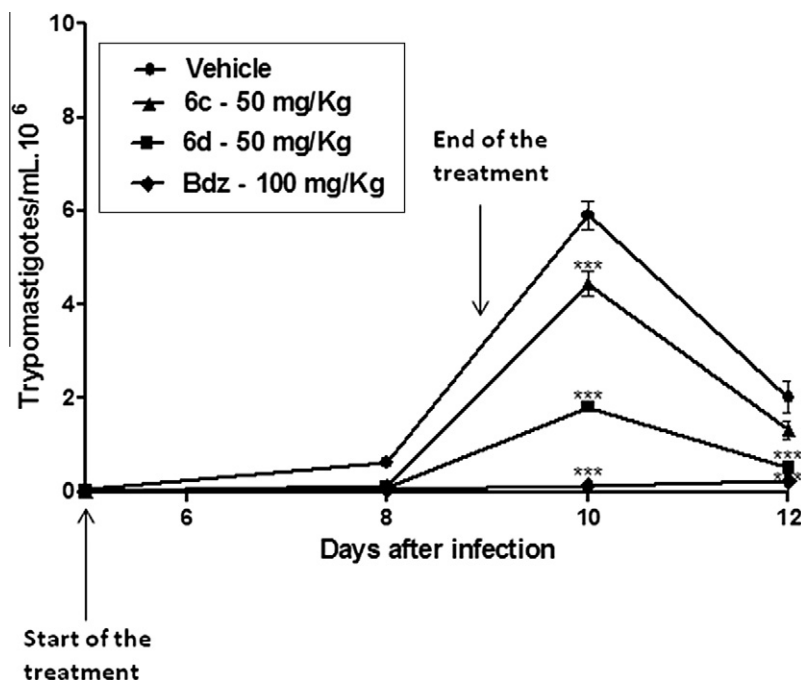


Figure 6. Oxadiazole **6d** substantially reduces parasitemia in mice. Female BALB/c mice were infected with 10^4 Y strain trypomastigotes. Five days after infection, mice were treated orally with compounds **6c** and **6d** in one daily dose of 50 mg/kg or Benznidazole (Bdz, at 100 mg/kg), during five consecutive days. Parasitemia was monitored by counting the number of trypomastigotes in fresh blood samples. Values represent the mean \pm SEM of six mice per group. Two independent experiments, data are from one experiment. ***, $p < 0.001$ compared to untreated-infected group (vehicle).

4.3. Parasites

Epimastigotes of *T. cruzi* (Y strain) were maintained at 26 °C in LIT medium (Liver Infusion Tryptose) supplemented with 10% fetal bovine serum (FBS) (Cultilab, Campinas, SP, Brazil), 1% hemin (Sigma Co, St. Louis, MO, USA), 1% R9 medium (Sigma Co), and 50 μ g/mL gentamycin (Novafarma, Anápolis, GO, Brazil). Bloodstream trypomastigotes forms of *T. cruzi* were obtained from supernatants of LLC-MK₂ cells previously infected and maintained in RPMI-1640 medium (Sigma Co.) supplemented with 10% FBS, and 50 μ g/mL gentamycin at 37 °C and 5% CO₂.

4.4. Cruzain inhibition

Cruzain activity was measured by monitoring the cleavage of the fluorogenic substrate Z-Phe-Arg-aminomethylcoumarin (Z-FR-AMC), as previously described.¹⁸ All assays were performed in 96-well plate format, in a final volume of 200 μ L, in sodium acetate 0.1 M (pH 5.5), in the presence of 5 mM dithiothreitol (DTT) and 0.01% Triton X-100, except for evaluation of detergent-sensitivity, when inhibition was also evaluated in 0% and 0.1% Triton for comparison. The enzyme was present at the final concentration of 0.4 nM and the substrate at 2.5 μ M ($K_m = 2 \mu$ M). All assays were performed in duplicate and followed for 5 min, and cruzain activity was calculated based on initial rates of substrate cleavage compared to a DMSO control. All compounds were dissolved in DMSO. The initial screen was performed at 100 μ M of each compound. Compounds were first evaluated for time-dependence by comparing percentages of enzyme inhibition by a compound with or without pre-incubation with enzyme for 10 min. During the pre-incubation step, cruzain and compound concentrations were 10-fold higher than in the final assay. Since compounds were observed to be time-dependent, consistently with a covalent mode of inhibition, all subsequent assays were performed with a 10 min pre-incubation. Compounds which inhibited over 50% of cruzain activity at 100 μ M had their IC₅₀ determined and were further evalu-

ated for detergent-sensitivity. Dose–response curves were determined based on at least nine compounds concentrations, varying from 100 μ M to 0.1 nM in fourfold dilutions. Data was analyzed with Prism 4 (GraphPad) employing non-linear regression.

4.5. Cytotoxicity to mouse splenocytes

Splenocytes obtained from BALB/c mice were placed into 96-well plates at a cell density of 5×10^6 cells/well in RPMI-1640 medium supplemented with 10% of FBS and 50 μ g mL⁻¹ of gentamycin. Each test inhibitor was used in five concentrations (1.23, 3.70, 11.11, 33.33, and 100 μ g mL⁻¹) in triplicate. To each well, an aliquot of test inhibitor suspended in DMSO was added. Controls included wells only containing either solvent (untreated cells) or gentian violet (positive control). The plate was incubated for 24 h at 37 °C and 5% CO₂. After incubation, 1.0 μ Ci of ³H-thymidine (Perkin Elmer, Waltham, USA) was added to each well, and the plate was returned to the incubator. The plate was then transferred to a beta-radiation counter (Multilabel Reader, Finland), and the percent of ³H-thymidine was determined. Cell viability was measured as the percent of ³H-thymidine incorporation for treated-cells in comparison to untreated cells. LD₅₀ values were calculated using data-points gathered from two independent experiments.

4.6. Antiproliferative activity for epimastigotes

Epimastigotes were counted in a hemocytometer and then dispensed into 96-well plates at a cell density of 10^6 cells/well. Test inhibitors, dissolved in DMSO, were diluted into five different concentrations (1.23, 3.70, 11.11, 33.33, and 100 μ g/mL) and added to the respective wells in triplicate. The plate was incubated for 5 days at 26 °C, and aliquots of each well were collected and the number of viable parasites were counted in a Neubauer chamber, and compared to untreated parasite culture. IC₅₀ calculation was carried out using non-linear regression on Prism 4.0 GraphPad

software. This experiment was done in triplicate, and benznidazole (LAFEPE, Pernambuco, Brazil) was used as the reference inhibitor.

4.7. Cytotoxicity for trypomastigotes

Trypomastigotes collected from the supernatants of LLC-MK₂ cells were dispensed into 96-well plates at a cell density of 4×10^5 cells/well. Test inhibitors, dissolved in DMSO, were diluted into five different concentrations and added into their respective wells, and the plate was incubated for 24 h at 37 °C and 5% of CO₂. Aliquots of each well were collected and the number of viable parasites, based on parasite motility, was assessed in a Neubauer chamber. The percentage of inhibition was calculated in relation to untreated cultures. IC₅₀ calculation was also carried out using a non-linear regression with Prism 4.0 GraphPad software. This experiment was repeated once, and benznidazole was used as the positive control.

4.8. Trypomastigote development

Peritoneal exudate macrophages were seeded at a cell density of 2×10^5 cells/well in a 24 well-plate with rounded coverslips on the bottom in RPMI supplemented with 10% FBS and incubated for 24 h. Cells were then infected with trypomastigotes at a ratio of 10 parasites per macrophage for 2 h. Free trypomastigotes were removed by successive washes using saline solution. Each test inhibitor was dissolved in DMSO at 10 µg/mL and incubated for 6 h. The medium was replaced by a fresh medium and the plate was incubated for 4 days. Cells were fixed in methanol and the percentage of infected macrophages and the mean number of amastigotes/infected macrophages was determined by manual counting after Giemsa staining in an optical microscope (Olympus, Tokyo, Japan). The percentage of infected macrophages and the number of amastigotes per macrophage was determined by counting 100 cells per slide.

4.9. Trypomastigote invasion

Peritoneal macrophages (10^5 cells) were plated onto 13-mm glass coverslips in 24-well plate and kept for 24 h. The plate was washed with saline solution and then trypomastigotes were added at a cell density of 1.25×10^7 along with the addition of test inhibitor (stock solution at 10 µg/mL). The plate was incubated for 2 h at 37 °C and 5% CO₂, followed by five washes with saline solution to remove extracellular trypomastigotes. Plates were maintained in RPMI medium supplemented with 10% FBS at 37 °C for 2 h. Infected cells were examined for the presence of amastigotes by optical microscopy using a standard Giemsa staining.

4.10. Ultrastructural studies

Trypomastigotes at a cell density of 3×10^7 were treated with test inhibitors **6c** (9.5 µM) and **6d** (3.5 µM) for 24 h. Parasites were then fixed with 2% formaldehyde and 2.5% glutaraldehyde (Electron Microscopy Sciences, PA, USA) in sodium cacodylate buffer (0.1 M, pH 7.2) for 1 h at room temperature. After fixation, parasites were washed three times with sodium cacodylate buffer (0.1 M, pH 7.2), and post-fixed with a 1.0% solution of osmium tetroxide (Sigma Chemical Co., MO, USA) for 1 h. Cells were subsequently dehydrated in increasing concentrations of acetone (30%, 50%, 70%, 90% and 100%) for 10 min at each step and embedded in resin Polybed (PolyScience family, Warrington, PA, USA). Ultrathin sections were prepared on an ultramicrotome Leica UC7 and sections were collected on copper grids of 300 meshes, contrasted with uranyl acetate and lead citrate and ob-

served under a JEOL TEM-1230 transmission electron microscope. For scanning electron microscopy, trypomastigotes treated with **6c** (30 µM) or **6d** (10 µM) and fixed in the same conditions were washed in 0.1 M cacodylate buffer, and allowed to adhere in coverslips pre-coated with poly-L-lysine (Sigma Co.). After adherence, cells were post-fixed with a solution of osmium tetroxide containing 0.8–1% of potassium ferrocyanide for 30 min. Cells were subsequently dehydrated in the presence of increasing concentrations of ethanol (30%, 50%, 70%, 90%, and 100%) during 15 min each step, and then subjected to the critical point, metallized with gold and analyzed in a JEOL JSM-6390LV scanning electron microscope. The same procedure was performed for TEM in infected macrophages treated with compound **6d**.

4.11. Toxicity in mice

Female BALB/c mice (6–8 weeks old; $n = 3$ /group) were orally treated with oxadiazole **6d** at doses of 100, 50 and 25 mg/kg. Animals were monitored for signs of general toxicity, including behavior and feeding, until 24 h after treatment. Heparinized blood samples were collected after 24 h of treatment, centrifuged for 3 min. to separate out from cells and then serum components were analyzed using Analyst[®] (Hemagen, Columbia, USA) platform system.

4.12. Infection in mice

Female BALB/c mice (6–8 weeks old) were infected with bloodstream trypomastigotes by intraperitoneal inoculation of 10^4 parasites in 100 µL of saline solution and then mice were divided in groups (six animals per group). After the day 5 of infection, treatment with 50 mg/kg weight of drugs **6c** and **6d** was given orally for five consecutive days. For the control group, Benznidazole was given orally at dose of 100 mg/kg weight. Animal infection was monitored daily by counting the number of motile parasites in 5 µL of fresh blood sample drawn from the lateral tail veins as recommended by standard protocols.³³

4.13. Statistical analyses

To determine the statistical significance of each group in the in vitro/in vivo experiments, the one-way ANOVA test and the Bonferroni for multiple comparisons were used. A p value <0.05 was considered of statistical significance. The data are representative of at least two or three experiments ran in triplicate.

Acknowledgements

J.M.S.F. thanks Universität Bremen for recording NMR, MS, and HRMS. C.A.S. and M.B.P.S. thank CNPq for the fellowship, while D.R.M.M. thanks FAPESB for a scholarship. C.A.S. is also thankful to the Instituto de Física de São Carlos (University of Sao Paulo, Brazil) for allowing the use of KappaCCD diffractometer. This work received funding by Universidade Federal de Pernambuco (UFPE), Conselho Nacional de Pesquisas Brasileira (CNPq, grant 478454/2010-4), and Fundação de Amparo as Pesquisas do Estado da Bahia (FAPESB, grant 6596).

Supplementary data

Supplementary data associated with this article can be found, in the online version, at <http://dx.doi.org/10.1016/j.bmc.2012.08.047>. These data include MOL files and InChiKeys of the most important compounds described in this article.

References and notes

1. Coura, J. R.; de Castro, S. L. *Mem. Inst. Oswaldo Cruz* **2002**, *97*, 3.
2. Dias, J. C. *Mem. Inst. Oswaldo Cruz* **2009**, *104*, 41.
3. Urbina, J. A. *Acta Tropica* **2010**, *115*, 55.
4. Olivieri, B. P.; Molina, J. T.; de Castro, S. L.; Pereira, M. C.; Calvet, C. M.; Urbina, J. A.; Araújo-Jorge, T. C. *Int. J. Antimicrob. Agents* **2010**, *36*, 79.
5. McKerrow, J. H.; Sun, E.; Rosenthal, P. J.; Bouvier, J. *Annu. Rev. Microbiol.* **1993**, *47*, 821.
6. Brinen, L. S.; Hansell, E.; Cheng, J.; Roush, W. R.; McKerrow, J. H.; Fletterick, R. J. *Structure* **2000**, *8*, 831.
7. Doyle, P. S.; Zhou, Y. M.; Hsieh, I.; Greenbaum, D. C.; McKerrow, J. H.; Engel, J. C. *Plos Pathog.* **2011**, *7*, e1002139.
8. Kerr, I. D.; Lee, J. H.; Farady, C. J.; Marion, R.; Rickert, M.; Sajid, M.; Pandey, K. C.; Caffrey, C. R.; Legac, J.; Hansell, E.; McKerrow, J. H.; Craik, C. S.; Rosenthal, P. J.; Brinen, L. S. *J. Biol. Chem.* **2009**, *284*, 25697.
9. Engel, J. C.; Doyle, P. S.; McKerrow, J. H. *J. Exp. Med.* **1998**, *188*, 725.
10. Barr, S. C.; Warner, K. L.; Kornreic, B. G.; Piscitelli, J.; Wolfe, A.; Benet, L.; McKerrow, J. H. *Antimicrob. Agents Chemother.* **2005**, *49*, 5160.
11. Brak, K.; Doyle, P. S.; McKerrow, J. H.; Ellman, J. A. *J. Am. Chem. Soc.* **2008**, *130*, 6404.
12. Brak, K.; Kerr, I. D.; Barrett, K. T.; Fuchi, N.; Debnath, M.; Ang, K.; Engel, J. C.; McKerrow, J. H.; Doyle, P. S.; Brinen, L. S.; Ellman, J. A. *J. Med. Chem.* **2010**, *53*, 1763.
13. Boström, J.; Hogner, A.; Llinas, A.; Wellner, E.; Plowright, A. T. *J. Med. Chem.* **2012**, *55*, 1817.
14. Warmus, J. S.; Flamme, C.; Zhang, L. Y.; Barrett, S.; Bridges, A.; Chen, H.; Gowan, R.; Kaufman, M.; Sebolt-Leopold, J.; Leopold, W.; Merriman, R.; Ohren, J.; Pavlovsky, A.; Przybranowski, S.; Tecle, H.; Valik, H.; Whitehead, C.; Zhang, E. *Bioorg. Med. Chem. Lett.* **2008**, *18*, 6171.
15. Cottrell, D. M.; Capers, J.; Salem, M. M.; DeLuca-Fradley, K.; Croft, S. L.; Werbovetz, K. A. *Bioorg. Med. Chem.* **2004**, *12*, 2815.
16. Cerecetto, H.; Maio, R. D.; González, M.; Risso, M.; Saenz, P.; Seoane, G.; Denicola, A.; Peluffo, G.; Quijano, C.; Olea-Azar, C. *J. Med. Chem.* **1999**, *42*, 1945.
17. Steert, K.; Berg, M.; Mottram, J. C.; Westrop, G. D.; Coombs, G. H.; Cos, P.; Maes, L.; Joossens, J.; Van der Veken, P.; Haemers, A.; Augustyns, K. *ChemMedChem* **2010**, *5*, 1734.
18. Ferreira, R. F.; Bryant, C.; Ang, K. K. H.; McKerrow, J. H.; Shoichet, B. K.; Renslo, A. R. *J. Med. Chem.* **2009**, *52*, 5005.
19. Ishii, M.; Jorge, S. D.; de Oliveira, A. A.; Palace-Berl, F.; Sonehara, I. Y.; Pasqualoto, K. F.; Tavares, L. C. *Bioorg. Med. Chem.* **2011**, *19*, 6292.
20. Dürüst, Y.; Karakus, H.; Kaiser, M.; Tasdemir, D. *Eur. J. Med. Chem.* **2012**, *48*, 296.
21. Dos Santos Filho, J. M.; Leite, A. C. L.; de Oliveira, B. G.; Moreira, D. R. M.; Lima, M. S.; Soares, M. B. P.; Leite, L. F. C. *Bioorg. Med. Chem.* **2009**, *17*, 6682.
22. Fraga, C. A. M.; Barreiro, E. J. *Curr. Med. Chem.* **2005**, *12*, 23.
23. Lima, P. C.; Lima, L. M.; da Silva, K. C. M.; Léda, P. H.; de Miranda, A. L.; Fraga, C. A. M.; Barreiro, E. J. *Eur. J. Med. Chem.* **2000**, *35*, 187.
24. Fraga, C. A. M.; Barreiro, E. J. *Curr. Med. Chem.* **2006**, *13*, 167.
25. Dos Santos Filho, J. M.; Lima, J. G.; Leite, L. F. C. C. *J. Heterocycl. Chem.* **2009**, *46*, 722.
26. Dos Santos Filho, J. M.; Lima, J. G.; Leite, L. F. C. C.; Silva, J. P.; Pitta, I. R. *Heterocycl. Commun.* **2005**, *11*, 29.
27. Maldonado, C. R.; Marin, C.; Olmo, F.; Huertas, O.; Quirós, M.; Sánchez-Moreno, M.; Rosales, M. J.; Salas, J. M. *J. Med. Chem.* **2010**, *53*, 6964.
28. Soares, M. B. P.; Silva, C. V.; Bastos, T. M.; Guimarães, E. T.; Figueira, C. P.; Smirlis, D.; Azevedo-Jr, W. F. *Acta Tropica* **2012**, *112*, 224.
29. Matsuo, A. L.; Silva, L. S.; Torrecilhas, A. C.; Pascoalino, B. S.; Ramos, T. C.; Rodrigues, E. G.; Schenkman, S.; Caires, A. C.; Travassos, L. R. *Antimicrob. Agents Chemother.* **2010**, *54*, 3318.
30. Ifa, D. R.; Rodrigues, C. R.; Alencastro, R. B.; Barreiro, E. J. *Mol. Struct.* **2000**, *505*, 11.
31. Engel, J. C.; Doyle, P. S.; Palmer, J.; Hsieh, I.; Bainton, D. F.; McKerrow, J. H. *J. Cell Sci.* **1998**, *111*, 597.
32. Vannier-Santos, M. A.; de Castro, S. L. *Curr. Drug Targets* **2009**, *10*, 246.
33. Romanha, A. J.; Castro, S. L.; Soeiro, M. N.; Lannes-Vieira, J.; Ribeiro, I.; Talvani, A.; Bourdin, B.; Blum, B.; Olivieri, B.; Zani, C.; Spadafora, C.; Chiari, E.; Chatelain, E.; Chaves, G.; Calzada, J. E.; Bustamante, J. M.; Freitas-Jr, L. H.; Romero, L. I.; Bahia, M. T.; Lotrowska, M.; Soares, M.; Andrade, S. G.; Armstrong, T.; Degrave, W.; Andrade, Z. A. *Mem. Inst. Oswaldo Cruz* **2010**, *105*, 233.
34. Bettiol, E.; Samanovic, M.; Murkin, A. S.; Raper, J.; Buckner, F.; Rodriguez, A. *Plos Negl. Trop. Dis.* **2009**, *3*, e384.
35. Caffrey, C. R.; Schanz, M.; Nkemngu, N. J.; Brush, M.; Hansell, E.; Cohen, F. E.; Flaherty, T. M.; McKerrow, J. H.; Steverding, D. *Int. J. Antimicrob. Agents* **2002**, *19*, 227.
36. Carvalho, S. A.; Lopes, F. A.; Salomão, K.; Romeiro, N. C.; Wardell, S. M.; de Castro, S. L.; da Silva, E. F.; Fraga, C. A. M. *Bioorg. Med. Chem.* **2008**, *16*, 413.
37. Carvalho, S. A.; Feitosa, L. O.; Soares, M.; Costa, T. E.; Henriques, M. G.; Salomão, K.; de Castro, S. L.; Kaiser, M.; Brun, R.; Wardell, J. L.; Wardell, S. M.; Trossini, G. H.; Andricopulo, A. D.; da Silva, E. F.; Fraga, C. A. M. *Eur. J. Med. Chem.* **2012**, *54*, 512.
38. Salomão, K.; de Souza, E. M.; Carvalho, S. A.; da Silva, E. F.; Fraga, C. A. M.; Barbosa, H. S.; de Castro, S. L. *Antimicrob. Agents Chemother.* **2010**, *54*, 2023.
39. Moreira, D. R. M.; Leite, A. C. L.; Santos, R. R.; Soares, M. B. P. *Curr. Drug Targets* **2009**, *10*, 212.

ANEXO 2

Moreira DR, Costa SP, Hernandez MZ, Rabello MM, DE Oliveira Filho GB, De Melo CM, Da Rocha LF, De Simone CA, Ferreira RS, Fradico JR, **Meira CS**, Guimarães ET, Srivastava RM, Pereira VR, Soares MB, Leite AC. Structural investigation of anti-Trypanosoma cruzi 2-iminothiazolidin-4-ones allows the identification of agents with efficacy in infected mice. **Journal of Medicinal Chemistry**. v. 55, p. 10918-10936, 2012.

Structural Investigation of Anti-*Trypanosoma cruzi* 2-Iminothiazolidin-4-ones Allows the Identification of Agents with Efficacy in Infected Mice

Diogo Rodrigo Magalhaes Moreira,^{*,†,‡} Salvana Priscylla Manso Costa,[‡] Marcelo Zaldini Hernandes,[‡] Marcelo Montenegro Rabello,[‡] Gevanio Bezerra de Oliveira Filho,[‡] Cristiane Moutinho Lagos de Melo,[§] Lucas Ferreira da Rocha,[§] Carlos Alberto de Simone,^{||} Rafaela Salgado Ferreira,⁺ Jordana Rodrigues Barbosa Fradico,⁺ Cássio Santana Meira,[⊥] Elisalva Teixeira Guimarães,^{⊥,#} Rajendra Mohan Srivastava,[†] Valéria Rêgo Alves Pereira,[§] Milena Botelho Pereira Soares,^{⊥,♦} and Ana Cristina Lima Leite[‡]

[†]Departamento de Química Fundamental, Centro de Ciências Exatas and da Natureza, Universidade Federal de Pernambuco, 50670-901, Recife, PE, Brazil

[‡]Departamento de Ciências Farmacêuticas, Centro de Ciências da Saúde, Universidade Federal de Pernambuco, 50740-520, Recife, PE, Brazil

[§]Centro de Pesquisas Aggeu Magalhaes, Fundação Oswaldo Cruz, CEP, 50670-420, Salvador-PE, Brazil

^{||}Departamento de Física and Informática, Instituto de Física, Universidade de São Paulo, CEP 13560-970, São Carlos, SP, Brazil

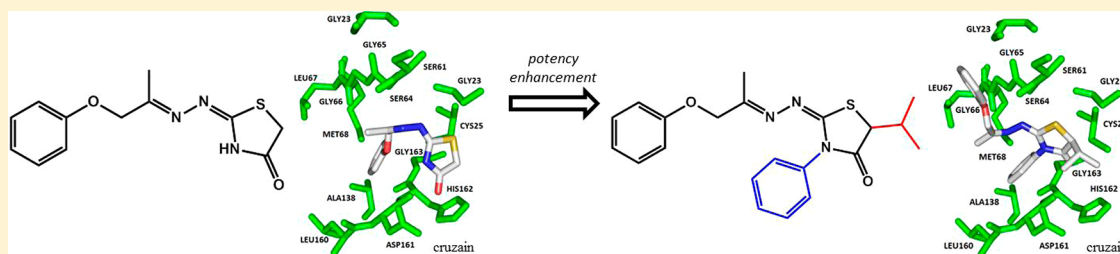
⁺Departamento de Bioquímica and Imunologia, Universidade Federal de Minas Gerais, CEP 31270-901, Belo Horizonte, MG, Brazil

[#]Departamento de Ciências da Vida, Universidade Estadual da Bahia, CEP 41150-000, Salvador, BA, Brazil

[⊥]Centro de Pesquisas Gonçalo Moniz, Fundação Oswaldo Cruz, CEP 40296-710, Salvador, BA, Brazil

[♦]Centro de Biotecnologia and Terapia Celular, Hospital São Rafael, CEP 41253-190, Salvador, BA, Brazil

S Supporting Information



ABSTRACT: We modified the thiazolidinic ring at positions N3, C4, and C5, yielding compounds 6–24. Compounds with a phenyl at position N3, 15–19, 22–24, exhibited better inhibitory properties for cruzain and against the parasite than 2-iminothiazolidin-4-one 5. We were able to identify one high-efficacy trypanocidal compound, 2-minothiazolidin-4-one 18, which inhibited the activity of cruzain and the proliferation of epimastigotes and was cidal for trypomastigotes but was not toxic for splenocytes. Having located some of the structural determinants of the trypanocidal properties, we subsequently wished to determine if the exchange of the thiazolidine for a thiazole ring leaves the functional properties unaffected. We therefore tested thiazoles 26–45 and observed that they did not inhibit cruzain, but they exhibited trypanocidal effects. Parasite development was severely impaired when treated with 18, thus reinforcing the notion that this class of heterocycles can lead to useful cidal agents for Chagas disease.

INTRODUCTION

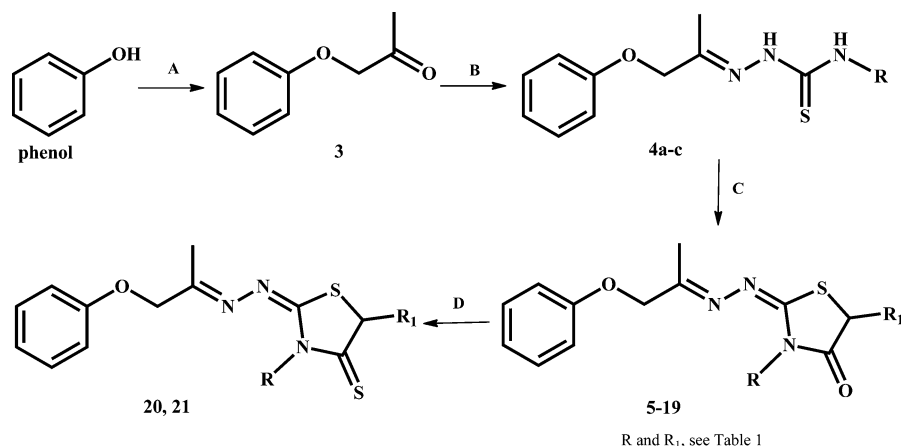
The World Health Organization estimates that 5–10% of Latin America's population is afflicted by Chagas disease, which is caused by the protozoan *Trypanosoma cruzi*.¹ Current treatment is solely based on benznidazole (Bdz), a nitroimidazole compound. Bdz is cidal for bloodstream trypomastigotes and thus efficient in eliminating parasite in circulation during the initial stages of infection (acute and asymptomatic chronic).^{2,3} The efficacy of Bdz for patients with Chagas-related cardiomyopathy is still unknown,

although a clinical trial (BENEFIT) aiming to investigate this is expected to be concluded in 2013.^{4,5} However, many patients experience drug intolerance and adverse effects for Bdz.⁶ Thus, there is a need to look for other drugs to treat Chagas disease.

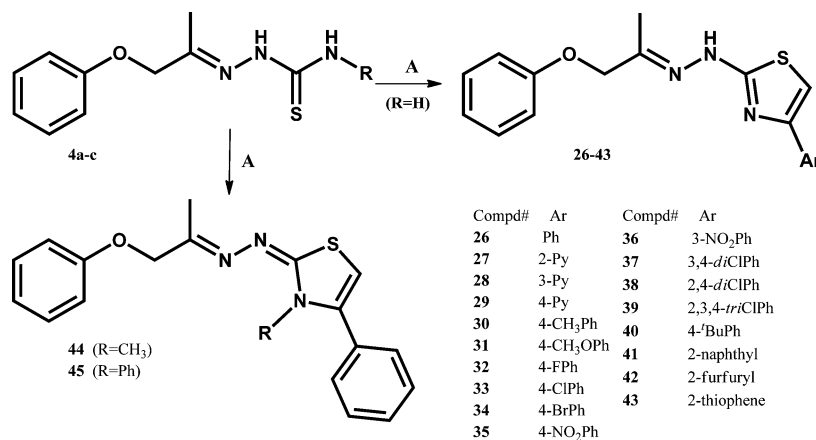
A useful strategy for anti-*T. cruzi* drug design is to inhibit the cysteine protease cruzain. Most of the functional properties of

Received: July 25, 2012

Published: November 20, 2012

Scheme 1. Synthetic Procedures for 2-Iminothiazolidin-4-ones 5-19 and 2-Iminothiazolidin-4-thiones 20, 21^a

^aReagents and conditions: (A) 2-chloroacetone, K₂CO₃, butanone, ultrasound bath, rt, 2 h, yield of 68% (B) thiosemicarbazides, EtOH, AcOH, ultrasound bath, rt, 30 min, yields of 65–82%; (C) ethyl 2-bromoacetate or ethyl 2-substituted-2-bromoacetates; NaOAc, EtOH, reflux, overnight, yields of 38–84%; (D) Lawesson's reagent, 1,4-dioxane/toluene, reflux, 20 h, yields of 54% (20) and 60% (21).

Scheme 2. General Synthetic Procedures for 2-Imino-1,3-thiazoles 26–45^a

^aReagents and conditions: (A) substituted 2-bromoacetophenones, 2-propanol, ultrasound irradiation, rt, 30–60 min, yields of 48–85%.

were prepared by reacting the respective thiosemicarbazones 4a–c with commercially available ethyl 2-bromoacetate or preparing the desired 2-substituted-2-bromoacetates. These reactions were carried out in the presence of an excess of anhydrous NaOAc under reflux, affording compounds 5–19 in acceptable yields (38–84%). For the conversion of 2-iminothiazolidin-4-ones 7 and 19 into 2-iminothiazolidin-4-thiones 20 and 21, we used Lawesson's reagent as the thionation reagent (yields of 54% and 60%, respectively) (Scheme 1). 2-Imino-1,3-thiazoles 26–45 were prepared via a Hantzsch synthesis between thiosemicarbazones 4a–c and substituted 2-bromoacetophenones (Scheme 2). These reactions proceed well upon refluxing with ethanol (1–3 h), but we adapted them under ultrasound conditions²⁹ using propanol as a solvent³⁰ and observed excellent yields in general (48–85%) and shorter times (30 min in most cases).

We attempted to define the relative configuration of the iminic bond. Chemical shifts in the methyl and methylene of the aryloxypropylimine group were diagnostically useful for identifying an *E*-isomer (for details, see the Experimental Section). Moreover, we succeeded in crystallizing the 2-iminothiazolidin-4-one 12 and the thiosemicarbazones 4a and 4c suitable for X-ray analysis. High-performance chromatography revealed a

mixture of isomers (9.5/0.5) for thiosemicarbazones 4a and 4c, and the major isomer has an *E*-geometry. On the other hand, chromatographic analysis in practice revealed only one major isomer for compounds 5–24 and 26–45. 2-Iminothiazolidin-4-one 12 has an *E*-geometry (Figure 2). It is therefore highly probable that all 2-iminothiazolidin-4-ones 5–24 as well as 2-imino-1,3-thiazoles 26–45 have the same *E*-geometry. For compounds 5–9, an important structural assignment is the location of an iminic bond in C2. X-ray analysis and quantum chemistry calculations for other 2-iminothiazolidin-4-ones structurally related to compounds 5–9 had suggested that the iminic bond is exocyclic in relation to heterocyclic ring (Figure S1, Supporting Information). It would, therefore, seem fair to suggest that the structures proposed for 5–9 are the correct ones.

Structure–Activity Relationships (SAR). We first assayed the viability of BALB/c mouse splenocytes treated with 2-iminothiazolidin-4-ones 5–19 and 22–24, 2-iminothiazolidin-4-thiones 20 and 21, or 2-imino-1,3-thiazoles 26–45. Once the toxicity to mammalian cells had been determined, we focused on evaluating their effects in *T. cruzi* in vitro assays. We tested against epimastigotes (axenic culture) and bloodstream trypomastigotes of the Y strain (Tables 1, 2, and 4). Compounds that showed IC₅₀ values comparable to benznidazole (Bdz) or

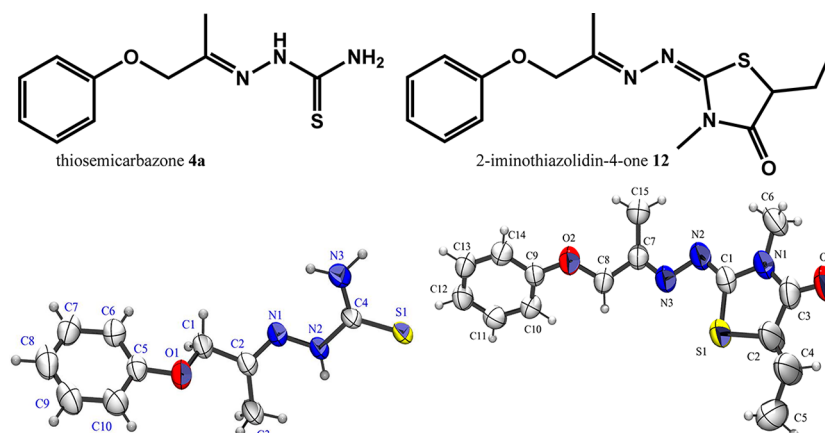
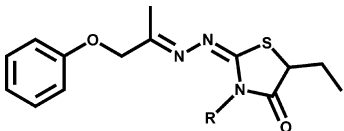


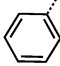
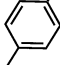
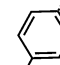
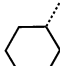
Figure 2. Structures of compounds 4a and 12 determined by X-ray analysis. Anisotropic thermal ellipsoids are drawn at a 50% level. For details, see the Experimental Section and Supporting Information.

Table 1. Anti-*T. cruzi* Activities of 2-Iminothiazolidin-4-ones 5-19 and 2-Iminothiazolidin-4-thiones 20, 21

Cpd	R ₁	Y strain <i>T. cruzi</i> IC ₅₀ (μM)		toxicity to splenocytes μg/mL (μM) ^[c]
		trypomastigotes ^[a]	epimastigotes ^[b]	
5	H	19.0	23.2	>100 (380)
6	CH ₃	ND	ND	>100
7	C ₂ H ₅	ND	ND	>100
8	CH(CH ₃) ₂	16.8	12.2	>100
9	Ph	18.7	34.8	25
10	H	ND	ND	>100
11	CH ₃	ND	ND	25
12	C ₂ H ₅	ND	ND	>100
13	CH(CH ₃) ₂	10.7	14.0	>100 (313)
14	Ph	18.0	12.0	>100 (283)
15	H	18.0	25.8	>100
16	CH ₃	29.0	31.8	100
17	C ₂ H ₅	5.8	11.1	100 (272)
18	CH(CH ₃) ₂	6.1	4.9	>100 (262)
19	Ph	11.1	15.6	>100 (240)
20	Ph/Ph	11.2	4.2	100 (231)
21	H / C ₂ H ₅	31.5	26.1	25 (81)
Bdz	-	6.2	6.6	25 (96)
Nfx	-	2.7	1.9	1.0
SAP	-	-	-	<1.0

^aDetermined 24 h after incubation of trypomastigotes with the compounds. ^bDetermined 11 days after incubation of epimastigotes with the compounds. IC₅₀ was calculated from at least five concentrations using concentrations in triplicate (SD ± 10%). ^cHighest nontoxic concentration for mouse splenocytes after 24 h of incubation in the presence of the compounds. Bdz: benznidazole; Nfx: nifurtimox; Sap: saponin.

Table 2. Modification of the 2-Iminothiazolidin-4-one 17 toward Compounds 22–24^a


Cpd	R	Y strain <i>T. cruzi</i> IC ₅₀ (μM)		toxicity to splenocytes μg/mL (μM) ^[c]
		Trypomastigotes ^[a]	epimastigotes ^[b]	
17		5.8	11.1	100 (272)
22		19.9	15.0	100 (262)
23		9.0	6.8	100 (251)
24		ND ^[d]	ND	>100 (268)

^aSee footnote in Table 1. ND, not determined.

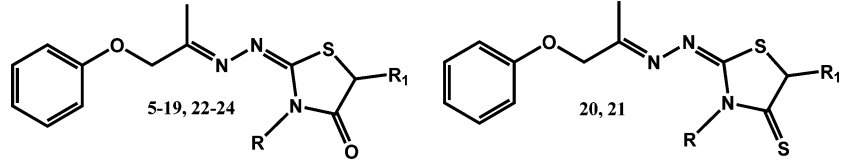
nifurtimox (Nfx) were further selected for assays of in vitro infection of host cells. The inhibitory activity against cruzain was measured based on the cleavage of the substrate Z-FR-AMC.³¹ Compounds were first tested at 20 or 100 μM, and a dose–response curve was determined and the IC₅₀ calculated for the

most active compounds. We also evaluated the compounds against the mammalian proteases cathepsins L and S (Tables 3 and 4).

Of all the tested compounds, 2-iminothiazolidin-4-one 18 possessed the highest overall trypanocidal potency, with IC₅₀ values of 6.1 and 4.9 μM for bloodstream trypomastigotes and axenic epimastigotes of the Y strain, respectively (Table 1). It also had trypanocidal properties comparable to those of BdZ. However, 2-iminothiazolidin-4-one 18 does not affect the cell viability of mouse splenocytes even at concentrations of up to 100 μg/mL (262 μM).

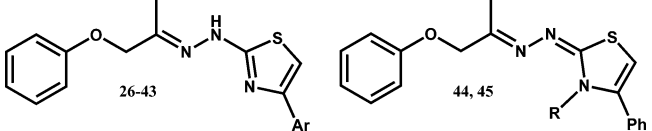
The SAR study which led to the identification of 2-iminothiazolidin-4-one 18 began with two kinds of modifications of the thiazolidinic ring: (a) variation of the substituents at C5; (b) replacement of NH with *N*-methyl and *N*-phenyl. These modifications yielded 2-iminothiazolidin-4-ones 5–19. For cruzain inhibition, we observed that modifications at N3 affect cruzain inhibition more than those at C5. For example, most compounds with a free NH (5–9) or an *N*-methyl (10–14) did not inhibit cruzain, while compounds with an *N*-phenyl (15–19) did (Table 3). For *T. cruzi*, we observed somewhat similar behavior, except for compounds 5, 8, and 13 which displayed good trypanocidal properties. In general, *N*-phenyl compounds 15–19 were potent trypanocidal agents.

We observed interesting SAR when different substituents were attached at C5 in 2-iminothiazolidin-4-ones 15–19. Inserting a methyl (16), ethyl (17), or isopropyl (18) at position C5 did not increase the affinity for cruzain when compared to the nonsubstituted 2-iminothiazolidin-4-one 15; all of them had

Table 3. Protease Inhibition


compd	<i>T. cruzi</i> cruzain ^a		cathepsin L (% inhibition at 100 μM) ^b	IC ₅₀ μM (SD)	
	% inhibition at 20 μM	IC ₅₀ , μM		cathepsin L	cathepsin S
5	0 ± 2		1 ± 1.5	>100	>100
6	3		0		NT
7	5		5		ND
8	60.8	18.9 ± 0.9	11 ± 2		ND
9	63 ± 2	ND ^d	NT		NT
10	0		NT		NT
11	0		NT		NT
12	50	31.9 ± 1.0	6	>100	>100
13	81	8.0 ± 0.1	0 ± 2	>100	>100
14	27 ± 4	ND ^d	NT		NT
15	66	10.2 ± 0.5	0	>100	>100
16	50	10.8 ± 1.0	0		NT
17	66 (64) ^c	9.5 ± 0.07	4 ± 1	>100	>100
18	78 (81) ^c	6.6 ± 0.05	10 ± 4	>100	>100
19	43 ± 2	ND ^d	15 ± 2		NT
20	72 ± 5.0 (79) ^c	7.0 ± 0.4	89 ± 5	10.8 ± 0.7	NT
21	48 ± 1.0	18.7 ± 2.0	81 ± 6	13.8 ± 2.0	NT
22	65	11.8 ± 0.5	NT		NT
23	71	8.7 ± 0.1	NT		NT
24	10 ± 2		NT		NT

^aAfter 10 min of preincubation with the inhibitor before adding the fluorescent cruzain substrate Z-FR-AMC. ^bAfter 45 min of incubation before adding the fluorescent cathepsin substrate Z-FR-pNA. Percentage of inhibition is the average of triplicate runs determined in one experiment. IC₅₀ was calculated from at least seven concentrations. ^cIn parentheses, experiments using 0.01% of Triton X-100 in the reaction buffer. ^dNot determined because of the low solubility in 0.1 M sodium acetate pH 5.5. NT is not tested.

Table 4. Cruzain and Anti-*T. cruzi* Activities of 2-Imino-1,3-thiazoles 26–45


compd	Ar/R	% of cruzain inhibition at 20 μM ^a	Y strain <i>T. cruzi</i> , IC ₅₀ (μM)		toxicity splenocytes $\mu\text{g/mL}$ (μM) ^d
			trypomastigotes ^b	epimastigotes ^c	
26	Ph	no inhib	19.6	ND	50 (154)
27	2-Py	no inhib	34.8	11.8	100 (308)
28	3-Py	no inhib	12.3	20.5	100 (308)
29	4-Py	13.3 \pm 3.8 ^e	3.9	4.0	100 (308)
30	4-CH ₃ Ph	no inhib	49.7	67.0	100 (296)
31	4-CH ₃ OPh	no inhib	17.8	14.9	100 (283)
32	4-FPh	no inhib	11.5	41.3	>100 (293)
33	4-ClPh	13 \pm 6	ND	57.1	100 (280)
34	4-BrPh	25 \pm 1	ND	49.8	100 (249)
35	4-NO ₂ Ph	no inhib	5.7	1.9	100 (271)
36	3-NO ₂ Ph	no inhib	3.8	4.0	100 (271)
37	3,4-diClPh	20 \pm 6	17.0	19.0	25 (63.9)
38	2,4-diClPh	40 \pm 6	17.0	42.2	<1 (2.8)
39	2,3,4-triClPh	no inhib	ND	ND	>1 (2.3)
40	4- ^t BuPh	no inhib	ND	ND	50 (131)
41	β Naph	no inhib	36.4	83.0	>100 (268)
42	2-furfuryl	4.7 \pm 3.2 ^e	17.7	26.6	>100 (319)
43	2-thiophene	30 \pm 6 ^e	37.6	16.6	50 (128)
44	CH ₃	no inhib	174.7	25.6	10 (29.5)
45	Ph	no inhib	61.1	2.6	>100 (250)

^aAfter 10 min of preincubation with the inhibitor before adding the fluorescent protease substrate Z-FR-AMC. ^bDetermined 24 h after incubation of trypomastigotes with the compounds. ^cDetermined 11 days after incubation of epimastigotes with the compounds. IC₅₀ was calculated from at least five concentrations using concentrations in triplicate (SD \pm 10%). ^dHighest nontoxic concentration for mouse splenocytes after 24 h of incubation in the presence of the compounds. ^eCompounds tested at 100 μM . no inhib mean no cruzain inhibition was observed.

the same range of IC₅₀s. However, varying substituents at C5 resulted in different trypanocidal compounds. For example, ethyl (17), and isopropyl (18) compounds were 4-times more potent than compound 15. 2-Iminothiazolidin-4-ones 17 and 18 have an IC₅₀ of 5.8 and 6.1 μM for trypomastigotes, which is equal in potency to BdZ (IC₅₀ of 6.1 μM) and roughly half as potent as Nfx (IC₅₀ of 2.7 μM). Of the five *N*-phenyl 2-iminothiazolidin-4-ones 15–19, only the compound which has a phenyl at C5 (19) showed low inhibitory properties for cruzain but exhibited trypanocidal effects.

Given these promising results, we next wanted to determine whether the conversion of 2-iminothiazolidin-4-ones into 2-iminothiazolidin-4-thiones leads to enhanced potency. We selected 2-iminothiazolidin-4-ones 12 (inactive as trypanocidal and cruzain inhibitor) and 19 (a potent trypanocidal and weak inhibitor of cruzain) to convert into their respective thione variants (Tables 1 and 3). The data revealed that attaching a thionyl at C4 improves cruzain affinity. 2-Iminothiazolidin-4-one 12 did not inhibit cruzain at 20 μM , while 2-iminothiazolidin-4-thione 21 had an IC₅₀ of 18.7 \pm 2.0 μM . This was even more pronounced when we compared 2-iminothiazolidin-4-thione 20 with 2-iminothiazolidin-4-one 19. Compound 20 exhibited an IC₅₀ of 7.0 \pm 0.4 μM for cruzain, while compound 19 had an IC₅₀ > 20 μM . In relation to *T. cruzi*, 21 showed low trypanocidal activity while its counterpart 12 was inactive and compounds 19 and 20 were almost equipotent. In general, replacing a carbonyl with thiocarbonyl enhances the inhibitory properties of 2-iminothiazolidin-4-ones against cruzain, but it does not

necessarily lead to a significant enhancement of potency against the parasite.

Of the compounds described in Table 1, the phenyl group in N3 was identified as the best substituent for conferring anti-*T. cruzi* and cruzain inhibition properties, along with an ethyl or isopropyl attached to C5. We aimed to enhance potency by preparing 17 analogues. To this end, we attached other substituents to N3. We succeeded in preparing 2-iminothiazolidin-4-ones 22, 23, and 24 (Table 2). Replacing an *N*-phenyl (17) with *N*-cyclohexyl (24) was deleterious for cruzain affinity and for anti-*T. cruzi* activity, while replacing it with *N*-tolyl (22) or *N*-(4-methoxyphenyl) (23) retains cruzain affinity. Similar to *N*-phenyl 17, variants 22 and 23 were toxic for trypomastigotes.

The inhibitory property of 2-iminothiazolidin-4-ones 5–24 for cruzain is centered on the key role of the thiazolidinic ring. We decided to explore the thiazolidine–thiazole isosterism. To this end, a congener series of 2-imino-1,3-thiazoles 26–45 was prepared, covering a variety of substitutions at position C4. However, none of the thiazoles inhibited cruzain activity (Table 4). 2-Iminothiazolidin-4-ones and 2-imino-1,3-thiazoles can be viewed as potential bioisosteric heterocycles,²⁸ but this did not prove to be the case, at least not in terms of cruzain inhibition. We first thought the lack of cruzain inhibition for thiazoles 26–45 was merely due to the presence of an aromatic ring at C4. However 2-iminothiazolidin-4-ones 9 and 19 bear a phenyl group at C5, and they still have some activity against cruzain (Figure 3). It seems that the cruzain binding site requires stereo- and electronic-specificity. Nonetheless, 2-imino-1,3-thiazoles 26–45 have a broad range of trypanocidal properties.

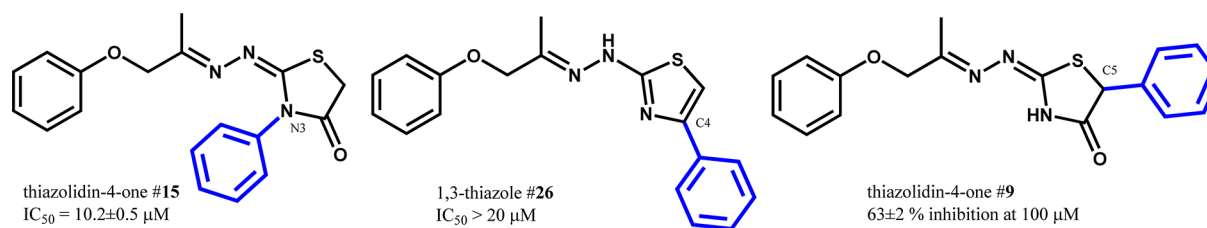


Figure 3. Structure–activity relationships of 2-iminothiazolidin-4-ones versus 2-imino-1,3-thiazoles. Biochemical data for cruzain.

Of all the tested compounds, 2-imino-1,3-thiazoles **29** and **36** possessed the highest overall trypanocidal potency. Compounds **29** and **36** had trypanocidal activity comparable to that of Bdz, with IC₅₀ values of 3.9 and 3.8 μM for bloodstream Y strain trypomastigotes, respectively. 2-Imino-1,3-thiazole **29** was identified when the phenyl ring at C4 was replaced with a pyridine ring. Replacing phenyl (**26**) with a pyridine ring (compounds **27–29**) changes the magnitude of trypanocidal properties for Y strain trypomastigotes. A 2-pyridine ring (**27**) was less potent than a phenyl (**26**), but a 3-pyridine (**27**) and a 4-pyridine (**29**) increased the trypanocidal property without affecting mouse splenocytes. While appending a pyridine ring at C4 is beneficial, this is not the case when a 2-furfuryl (**42**) or a 2-thiophene (**43**) ring is attached.

We also analyzed the effect of para substitution on the phenyl ring. A 4-tolyl (**30**) is two times less cidal for trypomastigotes than phenyl (**26**), while a 4-methoxyphenyl (**31**) has the same potency as phenyl (**26**). When halogens were attached to the phenyl ring, a pronounced substituent effect was observed.³² 4-Fluorophenyl (**32**) is twice as toxic for trypomastigotes as phenyl thiazole (**26**) but still less potent than Bdz or Nfx. However, the same trypanocidal property was not observed when other halogen atoms were attached, such as 4-chloro (**33**), 4-bromo (**34**), or dichloro (**37–39**), all of them having poor trypanocidal properties. Dichloro (compounds **37** and **38**) and trichloro (**39**) thiazoles were also toxic to mouse splenocytes. However, inserting a nitro group at the para position (**35**) and ortho position (**36**) produced the most potent anti-*T. cruzi* thiazoles. For example, 4-nitrophenyl thiazole **35** inhibited the proliferation of epimastigotes (IC₅₀ of 1.9 μM) and is toxic for trypomastigotes (IC₅₀ of 5.7 μM) without affecting the cell viability of mouse splenocytes, i.e., nontoxic at 100 μg/mL (271 μM).

Finally, we prepared and tested 2-imino-1,3-thiazoles containing a methyl (**44**) or phenyl (**45**) located at N3. In comparison to nonsubstituted 2-imino-1,3-thiazole **26**, which has IC₅₀ = 19.6 μM for trypomastigotes, thiazoles **44** and **45** exhibited an IC₅₀ of 174.7 and 61.1 μM, respectively. This suggests that a NH is important for maintaining trypanocidal properties.

To sum up the SAR for 2-imino-1,3-thiazoles **26–45**, optimal trypanocidal thiazoles resulted when electron-withdrawing groups such as 4-fluoro, 3-nitro, and 4-nitro were attached to the phenyl ring at C4. Chloro, bromo, and dichloro proved to be detrimental. Electron-releasing groups such as methyl, methoxy, and *tert*-butyl are of little or no benefit when compared to nonsubstituted thiazole **26**. Exchanging phenyl (**26**) with a naphthyl group (**41**) is not good, **41** being half as potent as **26**.

Once we determined that *N*-phenyl 2-iminothiazolidin-4-ones **15–19**, **22–24** as well as 2-iminothiazolidin-4-thiones **20**, **21** inhibited the catalytic activity of cruzain to some degree, we wondered whether this inhibitory property was only for cruzain and not for other cysteine proteases. To this end, we assayed these compounds for inhibition of cathepsins L and S. At 100 μM, none the *N*-phenyl 2-iminothiazolidin-4-ones **15–19** and **22–24** inhibited cathepsins, while the 2-iminothiazolidin-4-thiones

20 and **21** inhibited cathepsins. As we can infer from Table 3, some of the *N*-phenyl 2-iminothiazolidin-4-ones, such as **17** and **18**, were at least 10 times more selective for cruzain than for cathepsins.

A referee suggested that the weak to moderate potency of 2-iminothiazolidin-4-ones in inhibiting cruzain may be caused by a nonspecific reactivity toward enzymatic nucleophiles or compound aggregation involving nonspecific attachment to the enzyme surface. The *N*-phenyl 2-iminothiazolidin-4-ones **15–19**, **22–24** do not possess general inhibitory properties for cysteine proteases; they only display inhibitory properties for cruzain. Therefore, a nonspecific reactivity toward enzymatic nucleophiles is not the case for these compounds. The same cannot be said for 2-iminothiazolidin-4-thiones **20** and **21**, which inhibit both cruzain and cathepsin without selectivity. But to ascertain that *N*-phenyl 2-iminothiazolidin-4-ones **15–19** and **22–24** do inhibit cruzain without compound aggregation, we needed to repeat some reactions by adding 0.01% of detergent.³¹ As shown in Table 3, cruzain inhibition by compounds **17**, **18**, or **20** was not altered once the detergent (Triton X-100) was added, reinforcing the notion that cruzain inhibition by 2-iminothiazolidin-4-ones is specific.

We also wanted to gain information about the cruzain inhibition in the parasite cells. However, there is no cruzain gene knockout *T. cruzi* cell culture, and the existing cruzain-deficient cell line is also resistant to cruzain inhibitors. To overcome this limitation, we decided to treat the parasite with the *N*-phenyl 2-iminothiazolidin-4-one **18** and examine the ultrastructural alterations as well as the protease activity.

Bloodstream trypomastigotes as well as infected macrophages were treated with 3.9 μM **18** and examined with transmission electron microscopy (TEM) and scanning electron microscopy (SEM). This compound caused severe ultrastructural alterations in the parasite (for complete details, see the Figures S2 and S3 in Supporting Information). In particular, we saw an atypical morphology in the Golgi complex, such as dilation of cisternae and atypical vacuoles, which are characteristic alterations caused by cruzain inhibitors.³³

Besides the evidence collected with electron microscopy, we also gained information by performing zymography assays with epimastigotes. Epimastigotes were treated with the 2-iminothiazolidin-4-ones **18** and incubated for 48 h. The SDS-page gel containing 0.1% gelatin was loaded per slot with 20 μg of parasite protein. As seen in Figure S4 (Supporting Information), the nontreated epimastigote extract displayed proteolytic activity for gelatin, while the cells treated with the cruzain inhibitor E-64 or a protease inhibitor cocktail did not. The treatment of epimastigotes with the 2-iminothiazolidin-4-ones **18** reduces the proteolytic activity in a concentration-dependent manner.

Putative Binding Model. The cruzain inhibition of compounds **5–24** indicates that a hydrophobic substituent at C5, such as ethyl (**17**) and isopropyl (**8**, **13**, **18**), renders excellent cruzain inhibitors, better than if a phenyl is attached at

C5 (9, 19). These findings are consistent with another report showing that the attachment of a hydrophilic substituent at C5 in 2-iminothiazolidin-4-ones, such as *N*-methylacetamide and esters, does not enhance the inhibitory properties of 2-iminothiazolidin-4-ones with regard to cruzain.³⁴ In the case of position N3, a phenyl group is well tolerated, but a methyl (10, 11) and cyclohexyl (24) are not so well tolerated. To clarify these relationships, these compounds were investigated using molecular docking with cruzain.

The binding mode for these ligands was determined as the highest (most positive) score among the possible solutions for each ligand, generated according to the Goldscore Fitness Function. Figure 4 shows the superimposition of the best docking

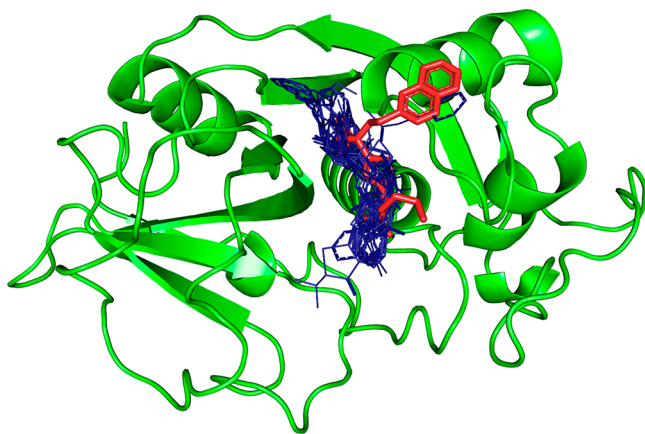


Figure 4. Superimposition of the docking solutions (blue lines) for compounds that have IC_{50} for cruzain: 8R, 8S, 12R, 12S, 13R, 13S, 15, 16R, 16S, 17R, 17S, 18R, 18S, 20R, 20S, 21R, 21S, 22R, 22S, 23R, 23S, and the crystallographic structure of the “KB2” (54) cocrystallized ligand (red-stick). Figure generated with Pymol.⁴⁹

solutions for compounds that have IC_{50} values experimentally determined for cruzain, which are: 8R, 8S, 12R, 12S, 13R, 13S, 15, 16R, 16S, 17R, 17S, 18R, 18S, 20R, 20S, 21R, 21S, 22R, 22S, 23R, 23S, and the crystallographic structure of the “KB2” (triazole 54) cocrystallized ligand. To compare in silico versus in vitro cruzain data, IC_{50} values were first converted into pIC_{50} values (equals $-\log IC_{50}$ for cruzain inhibition, at molar concentration).

Figure 5 shows the association observed between the in silico docking scores and the pIC_{50} data, which indicates that the most potent compounds, or the compounds with the highest values

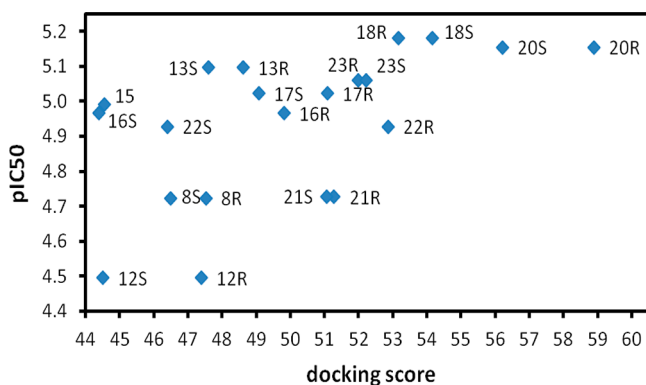


Figure 5. Trend observed between the in vitro (pIC_{50} for cruzain inhibition) and in silico (docking score) results. The S and the R symbols stand for the respective enantiomer.

for pIC_{50} , are usually those with the higher docking scores, demonstrating that the molecules with more stable or positive docking scores (i.e., greater in silico affinity for cruzain) are also the most potent cruzain inhibitors (i.e., greater in vitro pIC_{50} values).

To identify the molecular reasons for the two extremes of potency (highest and lowest in vitro results, 18S and 12R, respectively), we performed a detailed analysis of the intermolecular interactions. The enantiomer with higher in silico affinity was selected in each case. The differences between these two molecules are as follows: (i) the presence of a phenyl ring linked to the N3 nitrogen atom of the thiazolidinic ring in molecule 18S, instead of a methyl group in molecule 12R; (ii) an isopropyl group at position C5 of the thiazolidinic ring for molecule 18S, rather than an ethyl group for 12R. It seems that the additional hydrophobicity of the phenyl and isopropyl groups in 2-iminothiazolidin-4-one 18S provides a greater contact surface for interactions with cruzain hydrophobic residues, as shown in Figures 6 and 7.

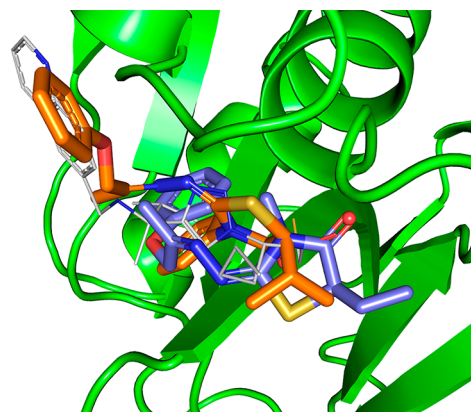


Figure 6. Superimposition of the docking solutions for compounds 12R (blue stick) and 18S (orange stick) and the crystallographic structure of the “KB2” (54) cocrystallized ligand (gray line).

The difference between the binding modes of these molecules is shown in detail in Figure 7 and Table 5. The hydrophobic residues are highlighted in green, those that participate in the hydrogen bond are highlighted in cyan, and $\pi-\pi$ stacking interactions are highlighted in orange. The benzene ring linked to the N3 nitrogen atom is capable of forming a $\pi-\pi$ interaction with the HIS162 amino acid residue, which may be a key interaction for positioning the phenoxy group close to SER61, SER64, GLY65, GLY66, and LEU67 residues, providing greater stability for the complex by way of hydrophobic contact and one hydrogen bond, highlighted in Figure 7B. These differences ensured that the docking solution for molecule 18S was the only one in the series of compounds that came closer to the crystal position of the “KB2” ligand, as shown in Figures 4 and 6.

In Vitro and in Vivo Infection. Given the selectivity of these compounds against extracellular forms of *T. cruzi*, we next examined the activity for the intracellular parasite. To this end, we assayed an in vitro model of parasite development using mouse macrophages infected with Y strain trypomastigotes. Four days postinfection, untreated control had 35–40% of macrophages infected and a high mean number of intracellular amastigotes. In this assay, 10 μ M Bdz reduces roughly half of infected cells as well the number of intracellular amastigotes, indicating a severe impairment of parasite development. Once we had this assay validated, we first tested the three most potent

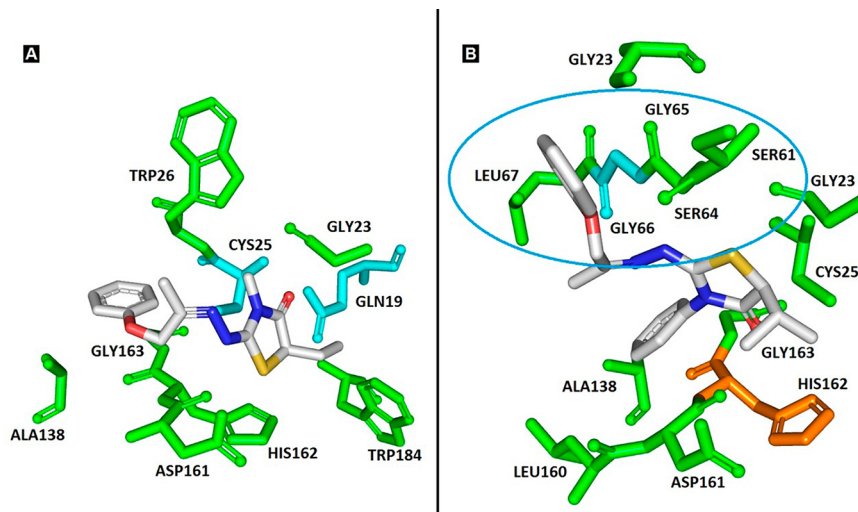


Figure 7. Detailed view of the docking solutions for (A) compound **12R** and (B) compound **18S**. Hydrophobic interactions (green), hydrogen bonds (cyan), and the π - π interactions (orange). The highlighted residues (blue circle) interacting with molecule **18S** are involved with the additional intermolecular interactions responsible for the greater affinity of this inhibitor, as shown in Table 5.

Table 5. Molecular Interaction of Cruzain with Molecules 12R and 18S^a

cruzain residues	molecules	
	12R	18S
GLN19	3.0	
GLY23	HC	HC
CYS25	2.5	HC
TRP26	HC	
SER61		HC
SER64		HC
GLY65		HC
GLY66		2.9
LEU67		HC
ALA138	HC	HC
LEU160		HC
ASP161	HC	HC
HIS162	HC	PI
GLY163	HC	HC
TRP184	HC	

^aHC means hydrophobic contacts, PI means π - π stacking, and the numbers are the hydrogen bond distances in angstroms.

cruzain inhibitors, 2-iminothiazolidin-4-ones **16**, **17**, and **18** as well as the 2-imino-1,3-thiazoles **29** and **35**.

At a concentration of 10 μ M, we observed that 2-iminothiazolidin-4-one **18** was able to reduce the number of infected cells with efficacy more pronounced than that seen with Bdz-treated cells. 2-Iminothiazolidin-4-ones **16** and **17** were less potent than Bdz. 2-Imino-1,3-thiazole **29**, which was a trypanocidal compound for bloodstream parasites, had no significant activity in reducing the infection in macrophages. Yet 4-nitro derivative **35** inhibited the in vitro infection similarly to Bdz (Table S1, Supporting Information).

We next examined the 2-iminothiazolidin-4-ones **5** and **18** at a concentration of 50 μ M. As seen in Figure 8A and B, compound **18** as well as Bdz substantially reduces the intracellular parasites in most of the microscopy fields ($P < 0.001$). We determined the IC_{50} values of these compounds to reduce the percentage of infected macrophages (Table 6), and we found that 2-iminothiazolidin-4-one **18** has an IC_{50} of $10.1 \pm 0.09 \mu$ M, almost identical to that of Bdz

(IC_{50} of $13.9 \pm 0.39 \mu$ M). 2-Iminothiazolidin-4-one **5**, which had an IC_{50} of 19.0 μ M for bloodstream parasites but did not inhibit cruzain, showed an IC_{50} of $19.5 \pm 1.1 \mu$ M to reduce the percentage of infected macrophages.

Table 1 shows that in concentrations up to 100 μ g/mL (262 μ M), the 2-iminothiazolidin-4-one **18** does not affect cell viability of mouse splenocytes. We next wanted to determine the IC_{50} value. Strikingly, compound **18** does not affect either cell viability or proliferation (under mitogen challenge) of splenocytes (IC_{50} values $>262 \mu$ M), in contrast to an IC_{50} of $10.1 \pm 0.09 \mu$ M for intracellular *T. cruzi* (Table 6). The selectivity index (SI) value can be estimated to be over 25. For comparison, compound **5**, our simplest 2-iminothiazolidin-4-one variant, has an SI of 10.

On the one hand, we have potency enhancement from 2-iminothiazolidin-4-one **5** to **18** (Table 6). On the other hand, we have observed that even at a concentration of 50 μ M, 2-iminothiazolidin-4-one **18** does not eradicate the infection in a culture of macrophages. The same is observed under treatment with Bdz. As seen in Figure 8C, we only approached eradication of the in vitro intracellular parasite under the simultaneous treatment of Bdz and **18**.

Chemically inhibiting parasite invasion is a desirable functional property for any Chagas disease drug candidate. For that reason, we assayed an invasion experiment with Y strain trypomastigotes in mouse macrophages.³⁵ After 60 min of parasite exposure, about 35% of macrophages are infected (untreated control). Bdz did not impair parasite viability in the invasion assay, even at 50 μ M; so we decided to use amphotericin B (AmpB) as a reference drug. At 50 μ M, AmpB was quite efficient in inhibiting parasite invasion into macrophages. Our best cruzain and *T. cruzi* inhibitor, *N*-phenyl 2-iminothiazolidin-4-one **18**, also decreased parasite invasion ($P < 0.01$) albeit less than AmpB did. 2-Iminothiazolidin-4-one **5** only attenuated the invasion ($P < 0.05$), and thiazole **29** did not have any significant effect in this assay (Figure 8D).

Finally, we evaluated the in vivo efficacy of *N*-phenyl 2-iminothiazolidin-4-one **18** to reduce blood parasitemia (acute phase). Starting on day 5 postinfection (dpi), compound **18** was orally administered once a day at 250 μ mol/kg for 5 consecutive days in BALB/c mice infected with 10^4 Y strain trypomastigotes. Controls included untreated and Bdz-treated infected mice.

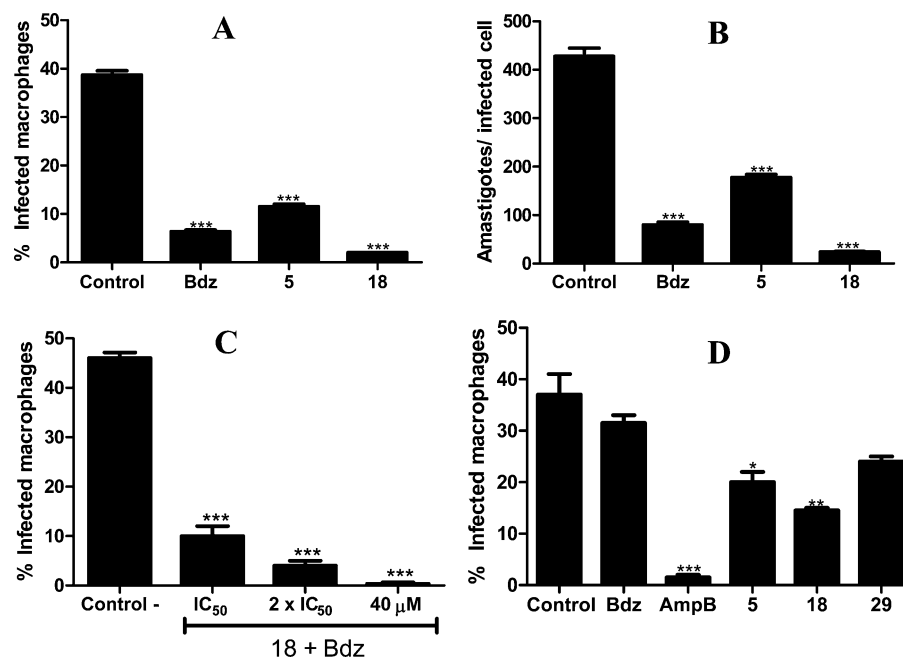


Figure 8. 2-Iminothiazolidin-4-one 18 severely impairs intracellular parasite development. The infection ratio (A) and the mean number of intracellular amastigotes per host cell (B) are higher in untreated controls than in cultures treated with test inhibitors 5, 18, or Bdz. Macrophages were infected with Y strain trypomastigotes for 2 h, and test inhibitors were then added at 50 μM . Cell cultures were incubated for 4 days. Significance: ***, $P < 0.001$; *, $P < 0.01$. (C) Combined treatment of 2-iminothiazolidin-4-one 18 (40 μM) and Bdz (40 μM) approaches an eradication of in vitro infection. Macrophages were infected with Y strain trypomastigotes for 2 h, and the combination of drugs was simultaneously added. Cell cultures were incubated for 4 days. Significance: ***, $P < 0.001$. (D) 2-Iminothiazolidin-4-one 18 attenuates parasite invasion in host cells, while Bdz does not. Y strain trypomastigotes and each test inhibitor (at 50 μM) were simultaneously added to the cell culture of macrophages and incubated for 2 h. ***, $P < 0.001$; **, $P < 0.01$; *, $P < 0.05$. All test inhibitors were tested in triplicate concentrations, and two independent experiments were carried out. Standard deviations are shown as error bars. Bdz is benznidazole; AmpB is amphotericin B.

Table 6. Comparison of the Pharmacological Properties between the 2-Iminothiazolidin-4-ones 5 and 18

compd	IC_{50} ($\pm\text{SD}$), μM				
	intracellular parasite ^a	toxicity for splenocytes ^b	antiproliferative for splenocytes ^c	index (SI) ^d	% parasitemia reduction in mice ^e
5	19.5 \pm 1.1	>200	98 \pm 10	10	—
18	10.1 \pm 0.09	>262	>262	25	89.6
controls	13.9 \pm 0.39 (benznidazole)	1.7 \pm 0.002 (saponin)	0.01 $\mu\text{g}/\text{mL}$ (cyclosporine A)	—	>99 (benznidazole)

^aDetermined 4 days after incubation of infected macrophages. IC_{50} values calculated in regard to the percent of treated infected cells in comparison to untreated infected cells. ^bDetermined 24 h after incubation of mouse splenocytes. Cell viability measured using the incorporation of tritiated thymidine. ^cSplenocyte proliferation was induced by concanavalin A. The effect on the proliferation was determined 72 h after incubation of mouse splenocytes using the AlamarBlue. SD is the standard deviation. ^dCellular selective index was estimated using the ratio (IC_{50} for splenocytes)/(IC_{50} for amastigotes). ^eCalculated as [(average vehicle group – average treated group)/average vehicle group] \times 100%. Values of blood parasitemia were taken from day 5 of treatment.

The course of infection was monitored by counting blood parasites in a hemocytometer, and animal survival was followed for one month.³⁶ As seen in Figure 9 and Table 6, compound 18 was efficient in reducing 89.6% of blood parasitemia ($P < 0.001$ of significance) when compared to untreated control. Bdz was even more effective than 18, nearly eradicating blood parasites (>99% of parasitemia reduction). No signs of toxicity or body weight loss were observed in mice of the treatment groups.

DISCUSSION

Thiosemicarbazones are known for their powerful in vitro trypanocidal and cruzain inhibition effects.^{13–17} However, currently, very few thiosemicarbazones that are effective in reducing in vivo *T. cruzi* infection have been described.³⁷ One method for increasing the efficacy of anti-*T. cruzi* thiosemicarbazones is through complexation with transition metals.^{38–40} Another possibility is the chemical modification of thiosemicarbazones by

synthetic redesign. We found that 2-iminothiazolidin-4-ones are structural analogues of thiosemicarbazones and endowed with in vitro trypanocidal properties. In previous studies, we discovered that 2-iminothiazolidin-4-ones were less potent trypanocidal agents than thiosemicarbazones, but at least 2-iminothiazolidin-4-ones were more selective for parasite than for mammalian cells.^{25–27} Here, our principal aim was to improve the cidal potency by molecular modification. We knew from past studies that the thiazolidinidic ring is more important for trypanocidal activity than the hydrazone and aryl groups. We chose the aryloxypropylimine group as a common core for designing compounds 5–45 because of the remarkable functional property of the drug candidate aryloxymethyl ketone triazole 54.²³ We next wanted to identify the main structural determinants for trypanocidal and cruzain inhibition in this class of 2-iminothiazolidin-4-ones. Here, we have identified most of them after screening the 2-iminothiazolidin-4-ones 5–24 and comparing them with 2-imino-1,3-thiazoles 26–45.

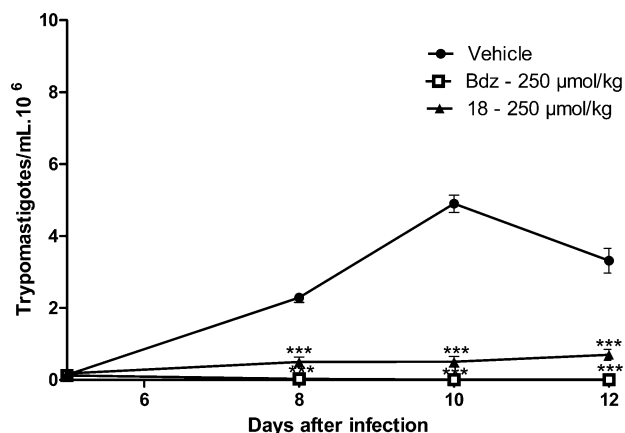


Figure 9. 2-Iminothiazolidin-4-one **18** substantially reduces the parasitemia in mice. Female BALB/c mice were infected with 10^4 Y strain trypomastigotes. Five days postinfection (dpi) mice were orally treated once a day with compound **18** or benznidazole (Bdz) at a dose of $250 \mu\text{mol/kg}$ during five consecutive days. Parasitemia was monitored by counting the number of trypomastigotes in fresh blood samples. Values represent the mean \pm SEM of six mice per group. Two independent experiments; data are representative from one experiment. Significance (***, $P < 0.0001$) compared to untreated infected group (vehicle).

We first observed that, with few exceptions, most of the nonsubstituted 2-iminothiazolidin-4-ones **5–9** or those containing a methyl at N3 **10–14** are inactive or poor cruzain inhibitors, and there was no reliable relationship between trypanocidal effects and chemical structure. In contrast, 2-iminothiazolidin-4-ones containing a phenyl group at N3 (**15–19**, **22–24**) inhibit cruzain and share trypanocidal properties. They are effective against the parasite but with the notable advantage that they do not affect either the viability or the proliferation of host cells.

With regard to the mechanism of action, we cannot confirm whether the anti-*T. cruzi* property is entirely due to the inhibition of cruzain alone. We argue that the trypanocidal properties of compounds **15–24** are, to some degree, a result of cruzain inhibition. This statement is based on the ability of 2-iminothiazolidin-4-ones to inhibit the catalytic activity of recombinant cruzain (competition experiments), to alter the morphology of the Golgi complex (electron microscopy), and to impair the proteolytic activity in the whole parasite (zymography assays with epimastigotes).

The model of docking for 2-iminothiazolidin-4-one **18** with cruzain shows that the phenyl ring linked to the N3 nitrogen is capable of forming a π - π interaction with the HIS162 amino acid. This interaction would seem to be the reason for the phenoxy group being located at a position which allows important hydrophobic contacts and hydrogen bond interactions, giving greater stability to the complex. The same is not predicted for 2-iminothiazolidin-4-one containing a methyl at N3, such as compound **12**. This model is consistent with recombinant cruzain inhibition and also provides an explanation for why the attachment of the phenyl on the heterocyclic ring is important for cruzain inhibition, in addition to explaining the importance of an alkyl group, such as ethyl and isopropyl, at position C5.

Despite the structural analogy, the functional properties of 2-iminothiazolidin-4-ones **5–24** and 2-imino-1,3-thiazoles **26–45** are distinguishable. 2-Iminothiazolidin-4-ones inhibited the catalytic activity of cruzain while none of the tested thiazoles did. Therefore, they do not behave as antiparasitic bioisosteres.

Our findings corroborate a very recent work describing that 2-imino-1,3-thiazoles are trypanocidal agents by altering the ergosterol biosynthesis instead of inhibiting the catalytic activity of cruzain.⁴¹ In agreement with this, we also found 2-imino-1,3-thiazoles are trypanocidal agents, and a few of them were equipotent to Bdz, such as thiazoles **29**, **35**, and **36**. There was a clear trend toward trypanocidal potency as polar substituents on the phenyl at C4 are attached to 2-imino-1,3-thiazoles. This led to some of the most potent thiazole variants examined, such as compounds **29** (4-pyridine), **32** (4-fluor), **35** (4-nitro), and **36** (3-nitro). This contrasts with the incorporation of an alkyl (**30**, **31**, **40**) or naphthyl (**41**) group, which, in the same position, decreased the cidal effects of the thiazole.

The selectivity of 2-iminothiazolidin-4-ones seems to be more consistent than that of 2-imino-1,3-thiazoles, because some thiazole variants were toxic to mouse splenocytes. Moreover, the mechanism through which thiazoles arrest parasite growth remains unknown. In view of these findings, we decided to search for more information on the trypanocidal effects of 2-iminothiazolidin-4-ones. We selected 2-iminothiazolidin-4-one **18**, the most potent cruzain inhibitor among the examined compounds. With regard to the functional activity of **18**, it inhibits the catalytic activity of cruzain but not that of cathepsins L and S, clearly arrests parasite growth (epimastigotes) and motility (trypomastigotes), impairs intracellular trypomastigote development into amastigotes, and attenuates trypomastigote invasion of macrophages. Using electron microscopy, we observed that 2-iminothiazolidin-4-one **18** alters the parasite morphology, in particular, altering the structure of the Golgi complex in a way very similar to that for other cruzain inhibitors. Moreover, 2-iminothiazolidin-4-one **18** reduces the protease activity in epimastigotes; both experiments suggest that cruzain is involved with the trypanocidal activity of 2-iminothiazolidin-4-one **18**. Finally, the antiparasitic effect of compound **18** was reinforced by its efficacy in reducing blood parasitemia in *T. cruzi*-infected mice.

One potential downside to **18** is that it does not eradicate parasitemia in mice (acute infection), a desirable property already demonstrated for other Chagas disease drug candidates.^{23,42–44} However, the design of anti-*T. cruzi* 2-iminothiazolidin-4-one **18** is a remarkable achievement for our program, especially because it worked orally. Synthetic redesign of the aryloxypropylimine group is one possible way to optimize the efficacy of compound **18**.

CONCLUSIONS

A detailed SAR study of anti-*T. cruzi* 2-iminothiazolidin-4-ones was conducted. It included molecular modifications on the thiazolidinic ring, as well isosteric exchanges of the carbonyl carbon and of the heterocycle itself. We observed a remarkable improvement in trypanocidal properties and cruzain inhibition only when positions N3 and C5 in the thiazolidinic ring were simultaneously substituted. This led to the identification of potent *N*-phenyl 2-iminothiazolidin-4-ones **15–19**, **22–24**. Replacement of the carbonyl with thiocarbonyl (**20**, **21**) did not produce a clear enhancement in potency, and exchanging the thiazolidinic for a thiazole ring **26–45** was deleterious for cruzain affinity, although some thiazoles did exhibit trypanocidal properties. Of compounds **15–24**, we found consistent trypanocidal effects for **18**, thereby corroborating the notion that this class of heterocycles can lead to useful cidal agents for Chagas disease treatment.

EXPERIMENTAL SECTION

Equipment and Reagents. All reagents were used as purchased from commercial sources (Sigma-Aldrich, Acros Organics, Vetec, or Fluka). Moisture-sensitive reactions were carried out under a nitrogen atmosphere. Progress of the reactions was followed by thin-layer chromatography (silica gel 60 F₂₅₄ in aluminum foil). Purity of the target compounds was confirmed by combustion analysis (for C, H, N, S) performed by a Carlo-Erba instrument (model EA 1110). Chemical identity was confirmed with NMR and IR spectroscopy and accurate mass. IR was determined in KBr pellets. For NMR, we used a Varian UnityPlus 400 MHz (400 MHz for ¹H and 100 MHz for ¹³C) and Bruker AMX-300 MHz (300 MHz for ¹H and 75.5 MHz for ¹³C) instruments. DMSO-*d*₆, acetone-*d*₆, CDCl₃, and D₂O were purchased from CIL or Sigma-Aldrich. Chemical shifts are reported in ppm, and multiplicities are given as s (singlet), d (doublet), t (triplet), q (quartet), m (multiplet), and dd (doublet), and coupling constants (*J*) in hertz. NH signals were localized in each spectrum after the addition of a few drops of D₂O. Structural assignments were corroborated by DEPT, HMBC and HSBC experiments. Mass spectrometry experiments were performed on a Q-TOF spectrometer (nanoUPLC-Xevo G2 Tof, Waters) or LC-IT-TOF (Shimadzu). When otherwise specified, ESI was carried out in the positive ion mode. Typical conditions were capillary voltage of 3 kV, cone voltage of 30 V, and a peak scan between 50 and 1000 *m/z*. To determine the molecular structure of thiosemicarbazones **4a** and **4c** as well as 2-iminothiazolidin-4-one **12**, a crystal of the corresponding compound was mounted on a Enraf-Nonius Kappa diffractometer equipped with a CCD detector (95 mm camera on κ -goniostat), and reflections were measured using monochromatic Mo K α radiation (0.71073 Å) at room temperature.

General Procedure for the Synthesis of 2-Iminothiazolidin-4-ones 5–19 and 22–24. Example for compound 5: Thiosemicarbazone **4a** (1.12 g, 5 mmol), anhydrous sodium acetate (1.2 g, 15 mmol), and 100 mL of ethanol were added to a 250 mL round-bottom flask under magnetic stirring and slightly warmed for 10–15 min. Then ethyl 2-bromoacetate (1.6 g, 10 mmol) was added, and the colorless reaction was refluxed for 18 h. After cooling back to rt, the precipitate was filtered off and the solvent was evaporated to half of its volume and then cooled to 0 °C. A white solid was obtained, filtered in a Büchner funnel with a sintered disc filter, washed with cold water, and then dried over SiO₂. Products were purified by column chromatography or recrystallization using the solvent system detailed below for each compound. Purity of compounds were >95% as determined by combustion analysis.

2-((1-Phenoxypropan-2-ylidene)hydrazono)thiazolidin-4-one (5). After elution with hexane/toluene (1:1), colorless crystals were obtained, yield = 0.7 g, 53%. Mp (°C): 130–131. IR (KBr): 3196 (N–H), 3006 (C–H), 1734 (C=O), 1649 and 1595 (C=N) cm⁻¹. ¹H NMR (300 MHz, DMSO-*d*₆): δ 1.98 (s, 3H, CH₃), 3.83 (s, 2H, S–CH₂), 4.66 (s, 2H, CH₂), 6.92–6.99 (m, 3H, Ar), 7.28 (t, 2H, Ar), 11.90 (s, 1H, NH). ¹³C NMR (75.5 MHz, DMSO-*d*₆): δ 14.8 (CH₃), 32.8 (CH₂, heterocycle), 70.9 (CH₂), 114.5 (CH, Ar), 120.9 (CH, Ar), 129.5 (CH, Ar), 158.1 (C=N), 161.9 (C–O, Ar), 164.1 (S–C=N), 173.9 (C=O). HRMS (ESI): 286.0599 [M + Na]⁺. Anal. Calcd for C₁₂H₁₃N₃O₂S: C, 54.74; H, 4.98; N, 15.96; S, 12.18. Found: C, 54.42; H, 5.02; S, 11.91; N, 15.78.

2-((1-Phenoxypropan-2-ylidene)hydrazono)-5-methylthiazolidin-4-one (6). After elution with hexane/ethyl acetate (3:1), yellowish crystals were obtained, yield = 0.11 g, 33%. Mp (°C): 117–120. IR (KBr): 3195 (N–H), 1710 (C=O), 1640 and 1602 (C=N) cm⁻¹. ¹H NMR (300 MHz, DMSO-*d*₆): δ 1.46 (d, 3H, J 7.8 Hz, CH₃), 2.02 (s, 3H, CH₃), 4.11 (t, 1H, J 7.8 Hz, CH), 4.66 (s, 2H, CH₂), 6.93–6.99 (m, 3H, Ar), 7.28 (t, 2H, Ar), 11.79 (s, 1H, NH). ¹³C NMR (75.5 MHz, DMSO-*d*₆): δ 14.5 (CH₃), 18.6 (CH₃), 41.7 (CH), 70.9 (CH₂), 114.6 (CH, Ar), 120.8 (CH, Ar), 129.3 (CH, Ar), 158.0 (C=N), 161.8 (C–O, Ar), 161.9 (S–C=N), 176.5 (C=O). HRMS (ESI): 278.0995 [M + H]⁺. Anal. Calcd for C₁₃H₁₅N₃SO₂: C, 56.30; H, 5.45; N, 15.15; S, 11.56. Found: C, 56.16; H, 5.38; S, 11.21; N, 15.09.

2-((1-Phenoxypropan-2-ylidene)hydrazono)-5-ethylthiazolidin-4-one (7). After elution with hexane/toluene (2:1), yellowish crystals were obtained, yield = 0.15 g, 51%. Mp (°C): 133. IR (KBr): 1715 (C=O), 1614 and 1596 (C=N) cm⁻¹. ¹H NMR (400 MHz, DMSO-*d*₆): δ 0.94

(t, J 7.2 Hz, 3H, CH₃), 1.73–1.81 (m, 1H, J 7.2 and 4.4 Hz, CH₂), 1.92–1.98 (m, 1H, J 7.2 and 4.4 Hz, CH₂), 2.02 (s, 3H, CH₃), 4.12–4.15 (q, 1H, J 7.6 and 4.4 Hz, CH asymmetric), 4.67 (s, 2H, CH₂), 6.92–7.00 (m, 3H, Ar), 7.28 (t, 2H, Ar), 11.94 (broad s, 1H, NH). ¹³C NMR (100 MHz, DMSO-*d*₆): 10.1 (CH₃), 14.5 (CH₃), 25.4 (CH₂), 48.8 (CH), 70.9 (CH₂), 114.6 (CH, Ar), 120.8 (CH, Ar), 129.3 (CH, Ar), 158.1 (C=N), 161.9 (C–O, Ar), 162.1 (S–C=N), 175.6 (C=O). Anal. Calcd for C₁₄H₁₇N₃SO₂: C, 57.71; H, 5.88; N, 14.42; S, 11.00; found: C, 57.64; H, 5.69; N, 14.25; S, 10.89.

2-((1-Phenoxypropan-2-ylidene)hydrazono)-5-isopropylthiazolidin-4-one (8). Crystallization from cyclohexane afforded colorless crystals, yield = 0.14 g, 38%. Mp (°C): 139. IR (KBr): 2967 (C–H), 1725 (C=O), 1640 and 1580 (C=N) cm⁻¹. ¹H NMR (400 MHz, DMSO-*d*₆): δ 0.86 (d, 3H, J 4.0 Hz, CH₃), 0.96 (d, 3H, J 4.0 Hz, CH₃), 1.97 and 2.01 (two s, 3H, CH₃), 2.35 (broad s, 1H, CH), 4.25 (s, 1H, CH), 4.61 and 4.67 (two s, 2H, CH₂), 6.98 (t, 3H, Ar), 7.28 (d, 2H, Ar), 11.86 (s, 1H, NH). ¹³C NMR (100 MHz, DMSO-*d*₆): 14.7 (CH₃), 16.2 (CH₃), 20.2 (CH₃), 29.8 (CH), 54.4 (CH), 70.9 (CH₂), 114.7 (CH, Ar), 120.9 (CH, Ar), 129.4 (Ar), 158.1 (C=N), 162.1 (C), 175.2 (C=O). HRMS (ESI): 306.1265 [M + H]⁺. Anal. Calcd for C₁₅H₁₉N₃SO₂: C, 58.99; H, 6.27; N, 13.76; S, 10.50; found: C, 59.53; H, 6.21; S, 8.69; N, 13.38.

2-((1-Phenoxypropan-2-ylidene)hydrazono)-5-phenylthiazolidin-4-one (9). Crystallization from toluene afforded colorless crystals, yield = 0.14 g, 41%. Mp (°C): 150. IR (KBr): 3391 (N–H), 1709 (C=O), 1640 and 1599 (C=N) cm⁻¹. ¹H NMR (400 MHz, acetone-*d*₆): δ 1.92 and 2.06 (s, 3H, CH₃), 3.58 (br s, NH+HDO), 4.67 and 5.01 (s, 2H, CH₂), 5.34 (s, 1H, CH), 6.90–7.01 (m, 3H, Ar), 7.27 (br s, 7H, Ar). ¹³C NMR and DEPT (100 MHz, acetone-*d*₆): 14.8 and 26.3 (CH₃), 51.4 (CH), 65.1 and 71.0 (CH₂), 114.2 (CH, Ar), 114.2 (CH, Ar), 120.9 (CH, Ar), 128.3 (CH, Ar), 128.7 (CH, Ar), 129.4 (CH, Ar), 130.4 (CH, Ar), 137.4 (C–N, Ar), 157.0 and 157.1 (C=N), 161.2 and 162.8 (C–O, Ar), 164.4 (S–C=N), 176.1 (C=O). HRMS (ESI): 340.1129 [M + H]⁺. Anal. Calcd for C₁₈H₁₇SO₂N₃: C, 63.70; H, 5.05; N, 12.38; S, 9.45; found: C, 64.01; N, 12.60; H, 5.60; S, 8.73.

2-((1-Phenoxypropan-2-ylidene)hydrazono)-3-methylthiazolidin-4-one (10). Crystallization from cyclohexane afforded colorless crystals, yield = 0.15 g, 54%. Mp (°C): 112. IR (KBr): 1721 (C=O), 1636 and 1580 (C=N) cm⁻¹. ¹H NMR (400 MHz, DMSO-*d*₆): δ 2.06 (s, 3H, CH₃), 3.13 (s, 3H, N–CH₃), 3.87 (s, 2H, CH₂), 4.70 and 5.02 (two s, 2H, CH₂–O), 6.94–7.00 (m, 3H, Ar), 7.27–7.30 (m, 2H, Ar). ¹³C NMR (100 MHz, DMSO-*d*₆): 14.4 and 19.4 (CH₃), 29.2 (N–CH₃), 31.9 (CH₂), 64.9 and 70.8 (CH₂), 114.2 (CH, Ar), 114.7 (CH, Ar), 120.9 (CH, Ar), 129.4 (CH, Ar), 158.0 (C=N), 163.1 (C), 172.0 (C=O). HRMS (ESI): 278.0995 [M + H]⁺. Anal. Calcd for C₁₃H₁₅N₃SO₂: C, 56.30; H, 5.45; N, 15.15; S, 11.56; found: C, 56.54; H, 5.40; S, 9.89; N, 14.91.

2-((1-Phenoxypropan-2-ylidene)hydrazono)-3,5-dimethylthiazolidin-4-one (11). Crystallization from toluene afforded colorless crystals, yield = 0.18 g, 60%. Mp (°C): 67. IR (KBr): 1720 (C=O), 1632 (C=N), 1581 (C=N) cm⁻¹. ¹H NMR (300 MHz, DMSO-*d*₆): δ 1.48 (d, 3H, J 7.2 Hz, CH₃), 2.06 (s, 3H, CH₃), 3.14 (s, 3H, N–CH₃), 4.16–4.23 (q, 1H, J 7.2 Hz, CH), 4.69 (s, 2H, CH₂), 6.92–7.00 (m, 3H, Ar), 7.26–7.31 (m, 2H, Ar). ¹³C NMR (75.5 MHz, DMSO-*d*₆): 14.6 (CH₃), 18.7 (CH₃), 29.4 (N–CH₃), 41.2 (CH), 70.8 (CH₂), 114.7 (CH, Ar), 120.9 (CH, Ar), 129.4 (CH, Ar), 158.1 (C=N), 161.9 (C–O, Ar), 163.3 (S–C=N), 175.1 (C=O). HRMS (ESI): 292.1134 [M + H]⁺. Anal. Calcd for C₁₄H₁₇N₃SO₂: C, 57.71; H, 5.88; N, 14.42; S, 11.00; found: C, 57.70; H, 5.91; N, 14.38; S, 11.10.

2-((1-Phenoxypropan-2-ylidene)hydrazono)-3-methyl-5-ethylthiazolidin-4-one (12). Crude was washed with ethyl ether, affording colorless crystals, yield = 0.26 g, 76%. Mp (°C): 129. IR (KBr): 1718 (C=O), 1636 and 1582 (C=N) cm⁻¹. ¹H NMR (300 MHz, DMSO-*d*₆): δ 0.92 (t, 3H, J 7.5 Hz, CH₃), 1.74–1.82 (m, 1H, CH₂), 1.95–1.98 (m, 1H, CH₂), 2.06 (s, 3H, N–CH₃), 3.18 (s, 3H, N–CH₃), 4.21–4.25 (q, 1H, J 4.2 and 7.8 Hz, CH), 4.70 (s, 2H, CH₂), 6.93–7.01 (m, 3H, Ar), 7.26–7.32 (m, 2H, Ar). ¹³C NMR (75.5 MHz, DMSO-*d*₆): 10.3 (CH₃), 14.6 (CH₃), 25.5 (CH₂), 29.3 (N–CH₃), 48.2 (CH), 70.8 (CH₂), 114.7 (CH, Ar), 120.9 (CH, Ar), 129.5 (CH, Ar), 158.0 (C=N), 161.9 (C–O, Ar), 163.4 (S–C=N), 174.2 (C=O). HRMS (ESI): 306.1283

[M + H]⁺. Anal. Calcd for C₁₅H₁₉N₃O₂S: C, 58.99; N, 13.76; H, 6.27; S, 10.50; found: C, 59.15; H, 6.09; N, 13.32; S, 9.43.

2-((1-Phenoxypropan-2-ylidene)hydrazono)-3-methyl-5-isopropylthiazolidin-4-one (**13**). Crystallization from cyclohexane afforded colorless crystals, yield = 0.25 g, 70%. Mp (°C): 138. IR (KBr): 1717 (C=O), 1634 and 1581 (C=N) cm⁻¹. ¹H NMR (300 MHz, DMSO-*d*₆): δ 0.80 (d, 3H, *J* 6.6 Hz, CH₃), 0.97 (d, 3H, *J* 6.9 Hz, CH₃), 2.07 (s, 3H, CH₂), 2.39–2.42 (m, 1H, CH), 3.151 and 3.34 (s, 3H, N–CH₃), 4.31 (d, 1H, *J* 3.9 Hz, CH), 4.70 (s, 2H, CH₂), 6.92–7.00 (m, 3H, Ar), 7.26–7.31 (m, 3H, Ar). ¹³C NMR (75.5 MHz, DMSO-*d*₆): 14.5 (CH₃), 16.4 (CH₃), 20.2 (CH₃), 30.4 (CH), 31.3 (CH₃–N), 53.7 (CH), 70.8 (CH₂), 114.7 (CH, Ar), 120.9 (CH, Ar), 129.4 (CH, Ar), 158.1 (C=N), 161.9 (C–O, Ar), 163.5 (S–C=N), 173.7 (C=O). HRMS (ESI): 320.0915 [M + H]⁺. Anal. Calcd for C₁₆H₂₁N₃SO₂: C, 60.16; H, 6.63; N, 13.16; S, 10.04; found: C, 60.40; H, 6.14; N, 13.11; S, 9.66.

2-((1-Phenoxypropan-2-ylidene)hydrazono)-3-methyl-5-phenylthiazolidin-4-one (**14**). Crystallization from toluene afforded colorless crystals, yield = 0.25 g, 70%. Mp (°C): 157. IR (KBr): 1716 (C=O), 1628 and 1589 (C=N) cm⁻¹. ¹H NMR (300 MHz, DMSO-*d*₆): 1.98 and 2.12 (s, 3H, CH₃), 3.23 and 3.36 (s, 3H, N–CH₃), 4.71 (s, 2H, CH₂), 5.49 (s, 1H, CH), 6.94–7.00 (m, 3H, Ar), 7.25–7.30 (m, 3H, Ar), 7.37 (br s, 4H, Ar). ¹³C NMR (75.5 MHz, DMSO-*d*₆): 14.7 (CH₃), 26.3 and 29.8 (N–CH₃), 50.0 (CH), 70.7 (CH₂), 114.7 (CH, Ar), 120.9 (CH, Ar), 128.3 (CH, Ar), 128.5 (CH, Ar), 128.8 (CH, Ar), 129.4 (CH, Ar), 136.5 (C–N, Ar), 158.0 (C=N), 161.5 (C–O, Ar), 163.8 (S–C=N), 172.9 (C=O). HRMS (ESI): 354.0728 [M + H]⁺. Anal. Calcd for C₁₉H₁₉SO₂N₃: C, 64.57; H, 5.42; N, 11.89; S, 9.07; found: C, 64.41; N, 12.01; H, 5.39; S, 9.13.

2-((1-Phenoxypropan-2-ylidene)hydrazono)-3-phenylthiazolidin-4-one (**15**). Crystallization from toluene afforded colorless crystals, yield = 0.25 g, 70%. Mp (°C): 139. IR (KBr): 1716 (C=O), 1628 and 1589 (C=N) cm⁻¹. ¹H NMR (300 MHz, DMSO-*d*₆): 1.98 and 2.12 (s, 3H, CH₃), 3.23 and 3.36 (s, 3H, N–CH₃), 4.71 (s, 2H, CH₂), 5.49 (s, 1H, CH), 6.94–7.00 (m, 3H, Ar), 7.25–7.30 (m, 3H, Ar), 7.37 (broad s, 4H, Ar). ¹³C NMR (75.5 MHz, DMSO-*d*₆): 14.7 (CH₃), 26.3 and 29.8 (N–CH₃), 50.0 (CH), 70.7 (CH₂), 114.7 (CH, Ar), 120.9 (CH, Ar), 128.3 (CH, Ar), 128.5 (CH, Ar), 128.8 (CH, Ar), 129.4 (CH, Ar), 136.5 (C–N, Ar), 158.0 (C=N), 161.5 (C–O, Ar), 163.8 (S–C=N), 172.9 (C=O). HRMS (ESI): 354.0728 [M + H]⁺. Anal. Calcd for C₁₈H₁₇SO₂N₃: C, 63.70; H, 5.05; N, 12.38; S, 9.45; found: C, 63.65; N, 12.28; H, 5.13; S, 10.31.

2-((1-Phenoxypropan-2-ylidene)hydrazono)-3-phenyl-5-methylthiazolidin-4-one (**16**). Crystallization from toluene afforded yellowish crystals, yield = 0.3 g, 84%. Mp (°C): 138. IR (KBr): 1722 (C=O), 1631 and 1577 (C=N) cm⁻¹. ¹H NMR (400 MHz, DMSO-*d*₆): 1.61 (d, 3H, *J* 7.2 Hz, CH₃), 1.80 and 1.97 (s, 3H, CH₃), 4.40 (q, 1H, *J* 7.2 Hz, CH), 4.67 (s, 2H, CH₂), 6.73 (d, 2H, *J* 8.0 Hz, Ar), 6.93 (m, 1H, Ar), 7.23 (t, 2H, *J* 7.9 Hz, Ar), 7.38–7.51 (m, 5H, Ar). ¹³C NMR (100 MHz, DMSO-*d*₆): 18.8 and 19.4 (CH₃), 26.2 (CH₃), 41.2 (CH), 64.5 (CH₂), 114.0 (CH, Ar), 121.0 (CH, Ar), 127.9 (CH, Ar), 128.4 (CH, Ar), 128.7 (CH, Ar), 129.6 (CH, Ar), 135.0 (C–N, Ar), 157.6 (C=N), 160.9 (C–O, Ar), 164.4 (S–C=N), 174.6 (C=O). HRMS (ESI): 354.1264 [M + H]⁺. Anal. Calcd for C₁₉H₁₉SO₂N₃: C, 64.57; H, 5.42; N, 11.89; S, 9.07; found: C, 64.50; H, 5.39; S, 10.89; N, 11.80.

2-((1-Phenoxypropan-2-ylidene)hydrazono)-3-phenyl-5-ethylthiazolidin-4-one (**17**). Crystallization from cyclohexane/toluene (1:1) afforded colorless crystals, yield = 0.26 g, 70%. Mp (°C): 118. IR (KBr): 1722 (C=O), 1634 and 1576 (C=N) cm⁻¹. ¹H NMR (400 MHz, DMSO-*d*₆): 1.01 (t, *J* 7.2 Hz, 3H, CH₃), 1.81 (s, 3H, CH₃), 1.89–1.98 (m, 1H, CH₂), 2.03–2.09 (m, 1H, CH₂), 4.38–4.41 (q, 1H, *J* 7.2 and 4.4 Hz, CH), 4.66 (s, 2H, CH₂), 6.92–6.98 (m, 3H, Ar), 7.26–7.30 (m, 2H, Ar), 7.34 and 7.36 (two s, 2H, Ar), 7.41–7.44 (m, 1H, Ar), 7.48–7.51 (m, 2H, Ar). ¹³C NMR (100 MHz, DMSO-*d*₆): 10.1 (CH₃), 14.6 (CH₃), 25.7 (CH₂), 48.1 (CH), 70.6 (CH₂), 114.7 (CH, Ar), 120.9 (CH, Ar), 127.9 (CH, Ar), 128.5 (CH, Ar), 128.8 (CH, Ar), 129.4 (CH, Ar), 134.9 (C–N, Ar), 158.0 (C=N), 161.5 (C–O, Ar), 163.6 (S–C=N), 173.8 (C=O). HRMS (ESI): 368.1422 [M + H]⁺. Anal. Calcd for C₂₀H₂₁SO₂N₃: C, 65.37; H, 5.76; N, 11.44; S, 8.73; found: C, 65.31; H, 5.64; S, 8.07; N, 11.27.

2-((1-Phenoxypropan-2-ylidene)hydrazono)-3-phenyl-5-isopropylthiazolidin-4-one (**18**). Crude was washed with ethyl ether, affording colorless crystals, yield = 0.3 g, 78%. Mp (°C): 128–130. IR (KBr): 1724 (C=O), 1632 and 1579 (C=N) cm⁻¹. ¹H NMR (400 MHz, DMSO-*d*₆): 1.01 (d, 3H, *J* 4.0 Hz, CH₃), 1.08 (d, 3H, *J* 4.0 Hz, CH₃), 1.86 (s, 3H, CH₃), 2.51 (t, 1H, *J* 4.0 and 3.4 Hz, CH), 4.52 (m, 1H, *J* 3.4 Hz, CH), 4.72 (s, 2H, CH₂), 6.97–7.03 (m, 3H, Ar), 7.31–7.38 (m, 4H, Ar), 7.46–7.56 (m, 3H, Ar). ¹³C NMR (100 MHz, DMSO-*d*₆): 14.6 (CH₃), 16.4 (CH₃), 20.1 (CH₃), 30.4 (CH), 53.6 (CH), 70.6 (CH₂), 114.7 (CH, Ar), 120.9 (CH, Ar), 127.8 (CH, Ar), 128.5 (CH, Ar), 128.9 (CH, Ar), 129.4 (CH, Ar), 134.8 (C–N, Ar), 158.0 (C=N), 161.4 (C–O, Ar), 163.8 (S–C=N), 173.4 (C=O). HRMS (ESI): 382.1580 [M + H]⁺. Anal. Calcd for C₂₁H₂₃SO₂N₃: C, 66.12; H, 6.08; N, 11.01; S, 8.41; found: C, 66.48; H, 5.70; S, 6.73; N, 10.81.

2-((1-Phenoxypropan-2-ylidene)hydrazono)-3,5-diphenylthiazolidin-4-one (**19**). Crystallization from cyclohexane afforded colorless crystals, yield = 0.32 g, 74%. Mp (°C): 159. IR (KBr): 1715 (C=O), 1628 and 1590 (C=N) cm⁻¹. ¹H NMR (400 MHz, acetone-*d*₆): 1.01 (d, 3H, *J* 4.0 Hz, CH₃), 1.08 (d, 3H, *J* 4.0 Hz, CH₃), 1.86 (s, 3H, CH₃), 2.51 (t, 1H, *J* 4.0 and 3.4 Hz, CH), 4.52 (m, 1H, *J* 3.4 Hz, CH), 4.72 (s, 2H, CH₂), 6.97–7.03 (m, 3H, Ar), 7.31–7.38 (m, 4H, Ar), 7.46–7.56 (m, 3H, Ar). ¹³C NMR (100 MHz, acetone-*d*₆): 14.6 (CH₃), 16.4 (CH₃), 20.1 (CH₃), 30.4 (CH), 53.6 (CH), 70.6 (CH₂), 114.7 (CH, Ar), 120.9 (CH, Ar), 127.8 (CH, Ar), 128.5 (CH, Ar), 128.9 (CH, Ar), 129.4 (CH, Ar), 134.8 (C–N, Ar), 158.0 (C=N), 161.4 (C–O, Ar), 163.8 (S–C=N), 173.4 (C=O). HRMS (ESI): 416.1433 [M + H]⁺. Anal. Calcd for C₂₄H₂₁SO₂N₃: C, 69.37; H, 5.09; N, 10.11; S, 7.72; found: C, 69.35; H, 5.00; S, 8.01; N, 10.21.

Synthesis of 2-Iminothiazolidine-4-thiones 20 and 21. Example for Compound 21: A solution of 2-iminothiazolidin-4-one **9** (0.34 g, 1.5 mmol) in anhydrous 1,4-dioxane/toluene (1:1, 50 mL) was added to a 100 mL round-bottom flask under magnetic stirring in N₂ and slightly warmed. Then Lawesson's reagent (1.0 g, 2.6 mmol) was added in portions, and the brownish mixture was kept under stirring and heating overnight. After cooling back to rt, the solvent was evaporated to half volume. Water was added and extracted with ethyl ether and then brine. The organic layers were then combined and dried with MgSO₄, and solvent was removed under reduced pressure and then dried over SiO₂. The compound was isolated after column chromatography.

2-((1-Phenoxypropan-2-ylidene)hydrazono)-3,5-diphenylthiazolidin-4-one (**20**). After elution with hexane/ethyl acetate (7:3) to a short silica gel column, yellowish crystals were obtained, yield = 0.2 g, 54%. Mp (°C): 131. IR (KBr): 1620 and 1596 (C=N) cm⁻¹. ¹H NMR (400 MHz, acetone-*d*₆): 1.90 (s, 3H, CH₃), 4.69 (s, 2H, CH₂), 5.40 (s, 1H, CH), 6.91–7.03 (m, 3H, Ar), 7.24–7.30 (m, 2H, Ar), 7.35–7.40 (m, 3H, Ar), 7.42–7.7.56 (m, 6H, Ar). ¹³C NMR (100 MHz, acetone-*d*₆): 27.5 (CH₃), 56.1 (CH), 72.0 (CH₂), 115.2 (CH, Ar), 115.7 (CH, Ar), 121.9 (CH, Ar), 129.01 (CH, Ar), 129.32 (CH, Ar), 129.38 (CH, Ar), 129.72 (CH, Ar), 129.84 (CH, Ar), 130.4 (CH, Ar), 136.6 (C–N, Ar), 138.0 (C–N, Ar), 159.6 (C=N), 162.4 (C–O, Ar), 168.0 (S–C=N), 189.1 (C=S). Anal. Calcd for C₂₄H₂₁S₂O₃N₃: C, 66.79; H, 4.90; N, 9.74; S, 14.86; found: C, 66.81; H, 5.00; S, 15.11; N, 14.01.

2-((1-Phenoxypropan-2-ylidene)hydrazono)-5-ethylthiazolidin-4-thione (**21**). After elution with hexane/ethyl acetate (7:3), yellowish crystals were obtained, yield = 0.28 g, 60%. Mp (°C): 111. IR (KBr): 1620 and 1590 (C=N) cm⁻¹. ¹H NMR (300 MHz, DMSO-*d*₆): 0.92 (t, 3H, *J* 7.5 Hz, CH₃), 1.74–1.82 (m, 1H, CH₂), 1.95–1.98 (m, 1H, CH₂), 2.06 (s, 3H, CH₃), 4.20–4.24 (q, 1H, *J* 4.2 and 7.8 Hz, CH), 4.70 (s, 2H, CH₂), 6.93–7.00 (m, 3H, Ar), 7.26–7.32 (m, 2H, Ar). ¹³C NMR (75.5 MHz, DMSO-*d*₆): 10.3 (CH₃), 14.6 (CH₃), 25.5 (CH₂), 49.0 (CH), 70.8 (CH₂), 114.7 (CH, Ar), 121.0 (CH, Ar), 129.5 (CH, Ar), 158.0 (C=N), 161.9 (C–O, Ar), 163.4 (S–C=N), 188.9 (C=S). Anal. Calcd for C₁₄H₁₇S₂O₃N₃: C, 54.69; H, 5.57; N, 13.67; S, 20.86; found: C, 54.71; H, 5.60; S, 19.99; N, 14.05.

2-((1-Phenoxypropan-2-ylidene)hydrazono)-3-(4-tolyl)-5-ethylthiazolidin-4-one (**22**). Crystallization from cyclohexane/toluene (1:1) afforded colorless crystals, yield = 0.26 g, 68%. Mp (°C): 140. IR (KBr): 1722 (C=O), 1634 and 1575 (C=N) cm⁻¹. ¹H NMR (400 MHz, DMSO-*d*₆): 1.01 (t, *J* 7.2 Hz, 3H, CH₃), 1.81 (s, 3H, CH₃), 1.89–1.98 (m, 1H, CH₂), 2.03–2.09 (m, 1H, CH₂), 2.67 (s, 3H, CH₃) 4.38–4.40

(q, 1H, *J* 7.2 and 4.5 Hz, CH), 4.66 (s, 2H, CH₂), 6.92–6.98 (m, 3H, Ar), 7.20–7.27 (m, 2H, Ar), 7.29 (d, 2H, Ar), 7.60 (d, 2H, Ar). ¹³C NMR (100 MHz, DMSO-*d*₆): 10.1 (CH₃), 14.6 (CH₃), 23.5 (CH₃), 25.7 (CH₂), 48.1 (CH), 70.6 (CH₂), 114.7 (CH, Ar), 120.9 (CH, Ar), 127.9 (CH, Ar), 128.5 (CH, Ar), 129.4 (CH, Ar), 134.9 (C–N, Ar), 158.0 (C=N), 161.5 (C–O, Ar), 163.6 (S–C=N), 174.1 (C=O). Anal. Calcd for C₂₁H₂₃SO₂N₃: C, 66.12; H, 6.08; N, 11.01; S, 8.41; found: C, 66.10; H, 6.01; S, 9.10; N, 11.11.

2-((1-Phenoxypropan-2-ylidene)hydrazono)-3-(4-anisyl)-5-ethylthiazolidin-4-one (23). Crystallization from toluene afforded colorless crystals, yield = 0.28 g, 70%. Mp (°C): 162. IR (KBr): 1722 (C=O), 1630 and 1576 (C=N) cm⁻¹. ¹H NMR (400 MHz, DMSO-*d*₆): 1.00 (t, *J* 7.2 Hz, 3H, CH₃), 1.81 (s, 3H, CH₃), 1.89–1.98 (m, 1H, CH₂), 2.02–2.08 (m, 1H, CH₂), 3.82 (s, 3H, OCH₃) 4.38–4.40 (q, 1H, *J* 7.2 and 5 Hz, CH), 4.66 (s, 2H, CH₂), 6.92–6.98 (m, 3H, Ar), 7.20–7.27 (m, 2H, Ar), 7.29 (d, 2H, *J* 9.1 Hz, Ar), 7.69 (d, 2H, *J* 9.1 Hz, Ar). ¹³C NMR (100 MHz, DMSO-*d*₆): 11.0 (CH₃), 14.6 (CH₃), 25.7 (CH₂), 48.1 (CH), 54.0 (CH₃), 63.5 and 70.6 (CH₂), 114.7 (CH, Ar), 120.9 (CH, Ar), 127.9 (CH, Ar), 128.5 (CH, Ar), 129.4 (CH, Ar), 134.9 (C–N, Ar), 155 (C–O, Ar) 157.0 (C=N), 161.5 (C–O, Ar), 163.6 (S–C=N), 174.1 (C=O). Anal. Calcd for C₂₁H₂₃SO₃N₃: C, 63.45; H, 5.83; N, 10.57; S, 8.07; found: C, 63.44; H, 5.91; S, 8.99; N, 10.42.

2-((1-Phenoxypropan-2-ylidene)hydrazono)-3-(cyclohexyl)-5-ethylthiazolidin-4-one (24). Crystallization from cyclohexane afforded colorless crystals, yield = 0.26 g, 71%. Mp (°C): 139–141. IR (KBr): 1728 (C=O), 1630 and 1576 (C=N) cm⁻¹. ¹H NMR (400 MHz, DMSO-*d*₆): 1.00 (t, *J* 7.2 Hz, 3H, CH₃), 1.81 (s, 3H, CH₃), 1.89–1.98 (m, 1H, CH₂), 2.02–2.08 (m, 1H, CH₂), 3.82 (s, 3H, OCH₃) 4.38–4.40 (q, 1H, *J* 7.2 and 5 Hz, CH), 4.66 (s, 2H, CH₂), 6.92–6.98 (m, 3H, Ar), 7.20–7.27 (m, 2H, Ar), 7.29 (d, 2H, *J* 9.1 Hz, Ar), 7.69 (d, 2H, *J* 9.1 Hz, Ar). HRMS (ESI): 374.1919 [M + H]⁺. Anal. Calcd for C₂₀H₂₇SO₂N₃: C, 64.31; H, 7.29; N, 11.25; S, 8.58; found: C, 64.31; H, 7.21; N, 11.39; S, 9.00.

General Procedure for the Synthesis of 2-Imino-1,3-thiazoles 26–45. Example for Compound 26: Thiosemicarbazone **4a** (0.24 g, 1 mmol) dissolved in 2-propanol (5 mL) was transferred to a boiling tube and placed in an ultrasound bath (40 MHz, 180 V). Then 2-bromoacetophenone (0.21 g, 1.1 mmol) was added to the mixture and allowed to react until the consumption of the starting materials (30–45 min). The reaction was cooled, and the colorful precipitate was separated in a Büchner funnel with a sintered disc filter, washed with cold propanol followed by cold water, and then dried over SiO₂ in a glass desiccator under vacuum. Pure products were obtained after recrystallization using the solvent system detailed below for each compound.

2-((1-Phenoxypropan-2-ylidene)hydrazinyl)-4-phenyl-1,3-thiazole (26). Crystallization from methanol afforded pinkish crystals, yield = 0.25 g, 77%. Mp (°C): 157. IR (KBr): 1618 (C=N), cm⁻¹. ¹H NMR (400 MHz, DMSO-*d*₆): 2.03 (s, 3H, CH₃), 4.63 (s, 2H, CH₂), 6.07 (broad s, 1H, N–H), 6.93–7.01 (m, 3H, 2H Ar and 1H thiazole), 7.27–7.42 (m, 6H, Ar), 7.83–7.86 (m, 2H, Ar). ¹³C NMR and DEPT (100 MHz, DMSO-*d*₆): 14.7 (CH₃), 71.8 (CH₂), 104.5 (CH, thiazole), 115.2 (CH, Ar), 121.4 (CH, Ar), 126.0 (CH, Ar), 128.0 (CH, Ar), 128.2 (CH, Ar), 128.7 (CH, Ar), 129.4 (CH, Ar), 129.9 (Ar), 134.7 (Ar), 148.1 (C=CH, thiazole), 158.1 (C–O), 169.9 (S–C=N). HRMS (ESI): 324.1171 [M + H]⁺. Anal. Calcd for C₁₈H₁₇SON₃: C, 66.85; H, 5.30; N, 12.99; S, 9.91; found: C, 66.52; H, 5.40; N, 13.00; S, 9.71.

2-((1-Phenoxypropan-2-ylidene)hydrazinyl)-4-(2-pyridinyl)-1,3-thiazole (27). Crystallization from methanol afforded greenish crystals, yield = 0.24 g, 74%. Mp (°C): 136. IR (KBr): 3364 (N–H), 1620 and 1582 (C=N) cm⁻¹. ¹H NMR (400 MHz, DMSO-*d*₆): 2.05 (s, 3H, CH₃), 4.65 (s, 2H, CH₂), 5.5–6.5 (broad s, 1H, NH), 6.92–7.02 (m, 3H, Ar), 7.27–7.31 (m, 2H, Ar), 7.82 (t, 1H, *J* 8.0 and 9.6 Hz, Ar), 8.14 (s, 1H, CH thiazole), 8.35 (d, 1H, *J* 10 Hz, Ar), 8.46 (t, 1H, *J* 10 Hz, Ar), 8.75 (d, 1H, *J* 8 and 9.6 Hz, Ar). ¹³C NMR and DEPT (100 MHz, DMSO-*d*₆): 13.0 and 14.6 (CH₃), 69.71 and 71.4 (CH₂), 114.4 (CH, thiazole), 114.8 (CH, Ar), 121.0 (CH, Ar), 123.1 (CH, Ar), 124.7 (CH, Ar), 129.5 (CH, Ar), 143.3 (CH, Ar), 143.6 (CH, Ar), 144.8 (CH, Ar), 146.4 (Ar), 149.2 (C=CH, thiazole), 158.0 (C=N), 158.7 (C–O, Ar), 170.0 and 170.6 (S–C=N). HRMS (ESI): 325.1123 [M + H]⁺.

2-((1-Phenoxypropan-2-ylidene)hydrazinyl)-4-(3-pyridinyl)-1,3-thiazole (28). Crystallization from methanol afforded greenish crystals, yield = 0.2 g, 61%. Mp (°C): 136. IR (KBr): 1621 and 1586 (C=N) cm⁻¹. ¹H NMR (400 MHz, DMSO-*d*₆): 2.05 (s, 3H, CH₃), 4.64 (s, 2H, CH₂), 5.5–6.5 (broad s, 1H, NH), 6.92–7.02 (m, 3H, Ar), 7.27–7.30 (m, 2H, Ar), 7.82 (t, 1H, *J* 10 Hz, Ar), 8.14 (s, 1H, CH of thiazole), 8.40 (d, 2H, *J* 10 Hz, Ar), 8.46 (t, 1H, *J* 10 Hz, Ar), 8.81 (s, 1H, Ar). ¹³C NMR (100 MHz, DMSO-*d*₆): 14.1 (CH₃), 69.71 and 71.4 (CH₂), 114.4 (CH, thiazole), 114.7 (CH, Ar), 120.9 (CH, Ar), 125.5 (CH, Ar), 129.1 (CH, Ar), 129.4 (CH, Ar), 131.2 (Ar), 137.0 (Ar), 148.2, 149.1 (C=N), 158.0 (C–O, Ar), 169.4 (S–C=N).

2-((1-Phenoxypropan-2-ylidene)hydrazinyl)-4-(4-pyridinyl)-1,3-thiazole (29). Crystallization from methanol afforded greenish crystals, yield = 0.23 g, 70%. Mp (°C): 140. IR (KBr): 3339 (N–H), 1617 and 1567 (C=N) cm⁻¹. ¹H NMR (400 MHz, DMSO-*d*₆): 2.03 (s, 3H, CH₃), 4.63 (s, 2H, CH₂), 6.94–7.00 (m, 3H, Ar), 7.28 (broad s, 2H, Ar), 7.28 (d, *J* 9 Hz, 2H, Ar), 7.70 (d, *J* 9 Hz, 2H, Ar), 11.28 (broad s, 1H, NH). ¹³C NMR and DEPT (100 MHz, DMSO-*d*₆): 14.3 (CH₃), 71.2 (CH₂), 114.4 (CH, thiazole), 114.7 (CH, Ar), 120.9 (CH, Ar), 125.5 (CH, Ar), 129.1 (CH, Ar), 129.4 (CH, Ar), 131.2 (Ar), 137.0 (Ar), 148.2, 149.1 (C=N), 158.0 (C–O, Ar), 169.4 (S–C=N).

2-((1-Phenoxypropan-2-ylidene)hydrazinyl)-4-(4-tolyl)-1,3-thiazole (30). Crystallization from methanol afforded yellowish crystals, yield = 0.2 g, 60%. Mp (°C): 160. IR (KBr): 1618 (C=N) cm⁻¹. ¹H NMR (400 MHz, DMSO-*d*₆): 2.03 (s, 3H, CH₃), 2.32 (s, 3H, CH₃), 4.63 (s, 2H, CH₂), 6.17 (broad s, 1H, N–H), 6.92–7.00 (m, 3H, Ar), 7.20–7.30 (m, 5H, 4H of Ar and 1H of thiazole), 7.71–7.74 (m, 2H, Ar). ¹³C NMR (100 MHz, DMSO-*d*₆): 14.8 (CH₃), 21.2 (CH₃), 71.6 (CH₂), 103.6 (CH, thiazole), 115.2 (CH, Ar), 121.4 (CH, Ar), 126.0 (CH, Ar), 128.0 (CH, Ar), 128.2 (CH, Ar), 129.3 (CH, Ar), 129.6 (CH, Ar), 129.9 (CH, Ar), 130.1 (Ar), 137.5 (Ar), 158.5 (C–O, Ar), 169.9 (S–C=N). HRMS (ESI): 338.1327 [M + H]⁺. Anal. Calcd for C₁₉H₁₉SON₃: C, 67.63; H, 5.68; N, 12.45; S, 9.50; found: C, 67.60; H, 5.64; N, 12.23; S, 9.40.

2-((1-Phenoxypropan-2-ylidene)hydrazinyl)-4-(4-anisyl)-1,3-thiazole (31). Crystallization from ethanol afforded pale greenish crystals, yield = 0.25 g, 70%. Mp (°C): 168. IR (KBr): 1613 and 1601 (C=N) cm⁻¹. ¹H NMR (300 MHz, DMSO-*d*₆): 1.99 and 2.04 (s, 3H, CH₃), 3.76 (s, 3H, OCH₃), 4.64 and 4.90 (s, 2H, CH₂), 6.91–7.01 (m, 5H, Ar), 7.17 (s, 1H, CH of thiazole), 7.24–7.32 (d, 2H, *J* 2.5 Hz, Ar), 7.72–7.81 (d, 2H, *J* 2.5 Hz, Ar), 10.55 (broad s, 1H, N–H). ¹³C NMR and DEPT (75.5 MHz, DMSO-*d*₆): 14.6 (CH₃), 55.2 (OCH₃), 71.1 (CH₂), 102.3 (CH, thiazole), 114.1 (CH, Ar), 113.7 (CH, Ar), 114.8 (CH, Ar), 121.0 (CH, Ar), 125.8 (CH, Ar), 127.1 (CH, Ar), 129.3 (CH, Ar), 129.6 (CH, Ar), 146.8 (CH=C), 149.6 (C=N), 158.1 (C–O, Ar), 159.2 (C–O, Ar), 169.5 (S–C=N). HRMS (ESI): 354.1282 [M + H]⁺. Anal. Calcd for C₁₉H₁₉SO₂N₃: C, 64.57; H, 5.42; N, 11.89; S, 9.07; found: C, 64.60; H, 5.35; N, 11.80; S, 8.91.

2-((1-Phenoxypropan-2-ylidene)hydrazinyl)-4-(4-fluorophenyl)-1,3-thiazole (32). Off-white crystals, yield = 0.29 g, 85%. Mp (°C): 157. IR (KBr): 1619 and 1608 (C=N) cm⁻¹. ¹H NMR (300 MHz, DMSO-*d*₆): 1.98 and 2.03 (s, 3H, CH₃), 4.59 and 4.62 (s, 2H, CH₂), 6.89–6.97 (m, 3H, Ar), 7.20–7.30 (m, 5H, 4H of Ar and 1CH of thiazole), 7.82–7.87 (m, 2H, Ar), 10.53 (broad s, 1H, N–H). After addition of D₂O, the signal at δ 10.53 ppm decreased. ¹³C NMR (75.5 MHz, DMSO-*d*₆): 14.7 (CH₃), 71.2 (CH₂), 104.3 (CH, thiazole), 114.5 (CH, Ar), 114.8 (CH, Ar), 115.2 (CH, Ar), 121.1 (CH, Ar), 127.8 (CH, Ar), 127.9 (CH, Ar), 129.6 (CH, Ar), 129.8 (C–F), 130.0 (C–F), 146.7 (Ar), 146.9 (CH=C), 148.5 (C=N), 158.1 (C–O), 169.4 and 169.7 (S–C=N). HRMS (ESI): 342.1099 [M + H]⁺. Anal. Calcd for C₁₈H₁₆SOFN₃: C, 63.32; H, 4.72; N, 12.31; S, 9.39; found: C, 63.40; H, 4.69; N, 12.30; S, 9.22.

2-((1-Phenoxypropan-2-ylidene)hydrazinyl)-4-(4-chlorophenyl)-1,3-thiazole (33). Crystallization from ethanol afforded reddish crystals, yield = 0.26 g, 72%. Mp (°C): 164–165. IR (KBr): 1620 and 1586 (C=N) cm⁻¹. ¹H NMR (300 MHz, DMSO-*d*₆): 2.09 (s, 3H, CH₃), 4.63 and 4.90 (s, 2H, CH₂), 6.90–7.00 (m, 3H, Ar), 7.25–7.46 (m, 5H, 4H of Ar and 1CH of thiazole), 7.80–7.85 (d, 2H, *J* 7.8 Hz, Ar), 10.61 (broad s, 1H, N–H). ¹³C NMR (75.5 MHz, DMSO-*d*₆): 14.6 (CH₃), 71.2 (CH₂), 104.4 (CH, thiazole), 114.8 (CH, Ar), 121.0 (CH, Ar),

125.7 (CH, Ar), 127.4 (CH, Ar), 127.9 (CH, Ar), 128.0 (CH, Ar), 128.4 (CH, Ar), 128.6 (CH, Ar), 129.6 (CH, Ar), 133.3 (Ar), 148.3 (CH=C), 149.4 (C=N), 158.1 (C-O, Ar), 169.6 (S-C=N). HRMS (ESI): 358.0909 [M + H]⁺. Anal. Calcd for C₁₈H₁₆SOClN₃: C, 60.41; H, 4.51; N, 11.74; S, 8.96; found: C, 61.01; H, 4.62; N, 12.03; S, 8.81.

2-((1-Phenoxypropan-2-ylidene)hydrazinyl)-4-(4-bromophenyl)-1,3-thiazole (34). Brownish crystals, yield = 0.8 g, 66%. Mp (°C): 171. IR (KBr): 3317 (N-H), 1615 and 1572 (C=N) cm⁻¹. ¹H NMR (400 MHz, DMSO-*d*₆): 2.02 (s, 3H, CH₃), 4.62 (s, 2H, CH₂), 6.92–7.01 (m, 3H, Ar), 7.26–7.35 (m, 2H, Ar), 7.35 (s, 1H, CH thiazole), 7.58 (d, 2H, J 7.5 Hz, Ar), 7.80 (d, 2H, J 7.5 Hz, Ar), 11.10 (s, 1H, N-H). ¹³C NMR (100 MHz, DMSO-*d*₆): 14.2 (CH₃), 71.3 (CH₂), 104.8, 114.7 (CH, Ar), 120.4 (CH, Ar), 120.9 (CH, Ar), 127.4 (CH, Ar), 129.4 (CH, Ar), 131.4 (CH, Ar), 133.9 (Ar), 147.1 (C=C, thiazole), 149.3 (C=N), 158.1 (C-O, Ar), 169.6 (S-C=N). HRMS (ESI): 402.0272 [M + H]⁺. Anal. Calcd for C₁₈H₁₆SOBrN₃: C, 53.74; H, 4.01; N, 10.44; S, 7.97; found: C, 53.72; H, 4.02; N, 10.55; S, 7.57.

2-((1-Phenoxypropan-2-ylidene)hydrazinyl)-4-(4-nitrophenyl)-1,3-thiazole (35). Crystallization from 2-propanol afforded yellowish crystals, yield = 0.3 g, 80%. Mp (°C): 171–173. IR (KBr): 3337 (N-H), 1598 and 1565 (C=N) cm⁻¹. ¹H NMR (300 MHz, DMSO-*d*₆): 2.03 (s, 3H, CH₃), 4.63 (s, 2H, CH₂), 6.92–7.01 (m, 3H, Ar), 7.29 (t, 2H, Ar), 7.70 (s, 1H, CH of thiazole), 8.07 (d, 2H, J 8.7 Hz, Ar), 8.29 (d, 2H, J 9.0 Hz, Ar), 11.26 (s, 1H, N-H). ¹³C NMR (75.5 MHz, DMSO-*d*₆): 14.3 (CH₃), 71.3 (CH₂), 108.9 (CH, thiazole), 114.8 (CH, Ar), 121.0 (CH, Ar), 124.1 (CH, Ar), 126.3 (CH, Ar), 129.5 (CH, Ar), 140.7 (CH, Ar), 146.1 (Ar), 147.6 (CH=C), 148.5 (C=N), 158.1 (C-O), 169.9 (S-C=N). HRMS (ESI): 369.1072 [M + H]⁺.

2-((1-Phenoxypropan-2-ylidene)hydrazinyl)-4-(3-nitrophenyl)-1,3-thiazole (36). Crystallization from toluene afforded yellowish crystals, yield = 0.18 g, 48%. Mp (°C): 159–160. IR (KBr): 3337 (N-H), 1598 and 1565 (C=N) cm⁻¹. ¹H NMR (400 MHz, DMSO-*d*₆): 2.64 (s, 3H, CH₃), 5.15 (s, 2H, CH₂), 7.40 (t, 1H, Ar), 7.49 (d, 2H, Ar), 7.75 (t, 2H, Ar), 7.89 (s, 1H, CH of thiazole), 8.10 (t, 1H, J 8.0 Hz, Ar), 8.56 (d, 1H, J 8.0 Hz, Ar), 8.70 (d, 1H, J 8.0 Hz, Ar), 10.58 (broad s, 1H, N-H). ¹³C NMR and DEPT (100 MHz, DMSO-*d*₆): 23.5 (CH₃), 82.0 (CH₂), 116.7 (CH, thiazole), 125.4 (CH, Ar), 130.8 (CH, Ar), 131.5 (CH, Ar), 132.3 (CH, Ar), 139.9 (CH, Ar), 140.3 (CH, Ar), 141.8 (Ar), 147.3 (Ar), 157.8 (CH=C), 159.3 (C=N), 169.2 (C-O, Ar), 180.1 (S-C=N). HRMS (ESI): 369.1042 [M + H]⁺.

2-((1-Phenoxypropan-2-ylidene)hydrazinyl)-4-(3,4-dichlorophenyl)-1,3-thiazole (37). Crystallization from methanol afforded reddish crystals, yield = 0.26 g, 66%. Mp (°C): 160. IR (KBr): 3338 (N-H), 1615 and 1565 (C=N) cm⁻¹. ¹H NMR (400 MHz, DMSO-*d*₆): 2.01 (s, 3H, CH₃), 4.61 (s, 2H, CH₂), 6.92–7.00 (m, 3H, Ar), 7.26–7.30 (m, 3H, Ar), 7.50 (s, 1H, 1H thiazole), 7.64 (d, 1H, J 8 Hz, Ar), 7.82 (d, 1H, J 8 Hz, Ar), 8.07 (s, 1H, Ar), 11.10 (broad s, 1H, N-H). ¹³C NMR and DEPT (100 MHz, DMSO-*d*₆): 14.2 (CH₃), 71.3 (CH₂), 106.2 (CH, thiazole), 114.7 (CH, Ar), 120.9 (CH, Ar), 125.5 (CH, Ar), 127.1 (CH, Ar), 129.4 (CH, Ar), 129.6 (CH, Ar), 130.8 (CH, Ar), 131.4 (Ar), 135.2 (Ar), 147.5 (CH=C), 147.7 (C=N), 158.1 (C-O, Ar), 169.7 (S-C=N). HRMS (ESI): 392.0378 [M + H]⁺.

2-((1-Phenoxypropan-2-ylidene)hydrazinyl)-4-(2,4-dichlorophenyl)-1,3-thiazole (38). Crystallization from methanol afforded reddish crystals, yield = 0.17 g, 55%. Mp (°C): 200. IR (KBr): 1568 (C=N) cm⁻¹. ¹H NMR (400 MHz, DMSO-*d*₆): 2.01 (s, 3H, CH₃), 4.63 (s, 2H, CH₂), 6.92–7.00 (m, 3H, Ar), 7.26–7.30 (m, 2H, Ar), 7.36 (s, 1H, CH of thiazole), 7.47–7.49 (d, 1H, J 8.4 Hz, Ar), 7.66 (s, 1H, Ar), 7.89 (d, 1H, J 8.4 Hz, Ar), 11.25 (broad s, 1H, N-H). ¹³C NMR (100 MHz, DMSO-*d*₆): 14.2 (CH₃), 71.3 (CH₂), 109.4 (CH, thiazole), 114.8 (CH, Ar), 120.9 (CH, Ar), 127.4 (CH, Ar), 129.4 (CH, Ar), 129.6 (CH, Ar), 131.5 (CH, Ar), 132.1 (CH, Ar), 132.2 (CH, Ar), 132.3 (Ar), 135.2 (Ar), 145.8 (CH=C), 147.2 (C=N), 158.1 (C-O, Ar), 168.6 (S-C=N). HRMS (ESI): 392.0378 [M + H]⁺.

2-((1-Phenoxypropan-2-ylidene)hydrazinyl)-4-(2,3,4-trichlorophenyl)-1,3-thiazole (39). Crystallization from toluene afforded reddish crystals, yield = 0.24 g, 50%. Mp (°C): 200 (decomp). IR (KBr): 3321 (N-H), 1615 and 1565 (C=N) cm⁻¹. ¹H NMR (300 MHz, DMSO-*d*₆): 2.01 (s, 3H, CH₃), 4.63 (s, 2H, CH₂), 6.92–7.01 (m, 3H, Ar), 7.29 (t, 2H, Ar), 7.40 (s, 1H, CH of thiazole), 7.72 (d, 1H, J 8.5 Hz, Ar),

7.81 (d, 1H, J 8.4 Hz, Ar), 11.17 (broad s, 1H, N-H). ¹³C NMR (75.5 MHz, DMSO-*d*₆): 14.2 (CH₃), 71.3 (CH₂), 110.2 (CH, thiazole), 114.8 (CH, Ar), 120.9 (CH, Ar), 128.7 (CH, Ar), 129.4 (CH, Ar), 129.9 (CH, Ar), 130.7 (Ar), 131.1 (Ar), 131.7 (Ar), 134.3 (Ar), 145.9 (CH=C), 147.3 (Ar), 158.1 (C-O), 168.7 (S-C=N). HRMS (ESI): 426.7810 [M + H]⁺.

2-((1-Phenoxypropan-2-ylidene)hydrazinyl)-4-(tert-butylphenyl)-1,3-thiazole (40). Crystallization from toluene afforded yellowish crystals, yield = 0.3 g, 79%. Mp (°C): 180–182. IR (KBr): 1610 and 1586 (C=N) cm⁻¹. ¹H NMR (300 MHz, DMSO-*d*₆): 1.23 (broad s, 9H, 3xCH₃), 2.00 (s, 3H, CH₃), 4.89 (s, 2H, CH₂), 6.92–7.00 (m, 3H, Ar), 7.16–7.20 (d, 2H, J 7.1 Hz, Ar), 7.37–7.42 (m, 3H, 2H Ar, J 7.1 Hz, and 1H of thiazole), 7.48–7.52 (m, 2H, Ar), 10.91 (broad s, 1H, N-H). ¹³C NMR (75.5 MHz, DMSO-*d*₆): 14.2 (CH₃), 31.1 (CH₃), 32.8 (CCH₃), 71.6 (CH₂), 103.6 (CH, thiazole), 115.2 (CH, Ar), 121.4 (CH, Ar), 126.0 (CH, Ar), 128.1 (CH, Ar), 128.2 (CH, Ar), 129.1 (CH, Ar), 129.2 (CH, Ar), 129.9 (Ar), 130.1 (Ar), 135.5 (Ar), 149.1 (C=N), 158.5 (C-O, Ar), 169.9 (S-C=N).

2-((1-Phenoxypropan-2-ylidene)hydrazinyl)-4-(2-naphthalenyl)-1,3-thiazole (41). Crystallization from toluene afforded brownish crystals, yield = 0.26 g, 70%. Mp (°C): 180–182 (decomp). IR (KBr): 1614 and 1490 (C=N) cm⁻¹. ¹H NMR (400 MHz, DMSO-*d*₆): 2.05 (s, 3H, CH₃), 4.64 (s, 2H, CH₂), 6.95–7.02 (m, 3H, Ar), 7.30 (s, 2H, 1H of Ar and 1H of thiazole), 7.47 (d, 3H, Ar), 7.91–8.01 (m, 4H, Ar), 8.39 (s, 1H, Ar), 11.14 (broad s, 1H, N-H). ¹³C NMR and DEPT (100 MHz, DMSO-*d*₆): 14.2 (CH₃), 71.4 (CH₂), 104.7 (CH, thiazole), 114.7 (CH, Ar), 120.9 (CH, Ar), 123.9 (CH, Ar), 124.0 (CH, Ar), 125.9 (CH, Ar), 126.3 (CH, Ar), 127.5 (CH, Ar), 128.0 (CH, Ar), 128.0 (CH, Ar), 129.4 (CH, Ar), 132.1 (CH, Ar), 132.3 (CH, Ar), 138.1 (Ar), 147.1 (CH=C), 158.1 (C-O, Ar), 169.5 (S-C=N). HRMS (ESI): 374.1270 [M + H]⁺. Anal. Calcd for C₂₂H₁₉SON₃: C, 70.75; H, 5.13; N, 11.25; S, 8.59; found: C, 70.68; H, 5.10; N, 11.27; S, 8.62.

2-((1-Phenoxypropan-2-ylidene)hydrazinyl)-4-(2-furanyl)-1,3-thiazole (42). Crystallization from methanol afforded brownish crystals, yield = 0.15 g, 50%. Mp (°C): 210. IR (KBr): 1600 and 1576 (C=N) cm⁻¹. ¹H NMR (400 MHz, DMSO-*d*₆): 2.02 (s, 3H, CH₃), 4.61 (s, 2H, CH₂), 6.58 (two s, 2H, Ar and CH thiazole), 7.00 (broad s, 4H Ar), 7.25 (d, 2H, Ar), 7.67 (s, 1H, Ar), 11.21 (s, 1H, N-H). ¹³C NMR and DEPT (100 MHz, DMSO-*d*₆): 14.2 (CH₃), 71.3 (CH₂), 102.9 (CH, thiazole), 106.0 (CH, Ar), 111.6 (CH, Ar), 114.7 (CH, Ar), 120.9 (CH, Ar), 129.5 (CH, Ar), 142.4 (CH, Ar), 147.2 (C-O, Ar), 150.3 (C=N), 158.1 (C-O, Ar), 170.0 (S-C=N).

2-((1-Phenoxypropan-2-ylidene)hydrazinyl)-4-(2-thiophenyl)-1,3-thiazole (43). Crystallization from methanol afforded brownish crystals, yield = 0.15 g, 53%. Mp (°C): 190–191. IR (KBr): 1620 and 1590 (C=N) cm⁻¹. ¹H NMR (400 MHz, DMSO-*d*₆): 2.02 (s, 3H, CH₃), 4.61 (s, 2H, CH₂), 6.58 (two s, 2H, Ar and CH thiazole), 7.00 (broad s, 4H Ar), 7.25 (d, 2H, Ar), 7.67 (s, 1H, Ar), 10.53 (s, 1H, N-H). ¹³C NMR (100 MHz, DMSO-*d*₆): 14.2 (CH₃), 71.3 (CH₂), 104.0 (CH, thiazole), 106.0 (CH, Ar), 111.6 (CH, Ar), 114.7 (CH, Ar), 120.9 (CH, Ar), 129.5 (CH, Ar), 141.3 (CH, Ar), 142.4 (CH, Ar), 147.2 (C-O, Ar), 150.3 (C=N), 158.1 (C-O, Ar), 170.0 (S-C=N).

2-((1-Phenoxypropan-2-ylidene)hydrazinyl)-3-methyl-4-phenyl-1,3-thiazole (44). Prepared from thiosemicarbazone 4b, crystallization from toluene afforded yellowish crystals, yield = 0.25 g, 73%. Mp (°C): 135. IR (KBr): 1591 (C=N) cm⁻¹. ¹H NMR (300 MHz, DMSO-*d*₆): 2.03 and 2.16 (s, 3H, CH₃), 3.47 (s, 3H, N-CH₃), 4.76 and 5.07 (s, 2H, CH₂), 6.91–6.99 (m, 3H, Ar), 7.02 (s, 1H, S-CH), 7.25–7.31 (m, 2H, Ar), 7.52 (m, 6H, Ar). ¹³C NMR (75.5 MHz, DMSO-*d*₆): 15.4 (CH₃), 35.4 (N-CH₃), 70.6 (CH₂), 114.3, 114.8, 121.0 (Ar), 128.9 (Ar), 129.1, 129.2, 129.5, 129.7, 129.8, 141.8 (CH=C), 158.0 (C=N), 158.7 (C-O, Ar), 169.6 (S-C=N). HRMS (ESI): 338.1326 [M + H]⁺. Anal. Calcd for C₁₉H₁₉SON₃: C, 67.63; H, 5.68; N, 12.45; S, 9.50; found: C, 67.70; H, 5.80; N, 12.53; S, 9.31.

2-((1-Phenoxypropan-2-ylidene)hydrazinyl)-3,4-diphenyl-1,3-thiazole (45). Prepared from thiosemicarbazone 4c, isolated as yellowish crystals, yield = 0.3 g, 75%. Mp (°C): 136. IR (KBr): 1622 and 1591 (C=N) cm⁻¹. ¹H NMR (400 MHz, DMSO-*d*₆): 1.84 (s, 3H, CH₃), 4.63 (s, 2H, CH₂), 6.58 (s, 1H, CH thiazole), 6.92–7.00 (m, 3H, Ar), 7.15 (d, 2H, Ar), 7.22–7.35 (m, 10H, Ar). ¹³C NMR (100 MHz,

DMSO-*d*₆): 14.6 (CH₃), 71.2 (CH₂), 101.3 (CH, thiazole), 114.7 (CH, Ar), 120.7 (CH, Ar), 127.5 (CH, Ar), 128.0 (CH, Ar), 128.20 (CH, Ar), 128.28 (CH, Ar), 128.3 (CH, Ar), 128.6 (CH, Ar), 129.4 (CH, Ar), 130.8 (Ar), 137.6 (Ar), 139.3 (C=CH), 156.9 (C=N), 158.2 (C–O, Ar), 168.6 (S–C=N). Anal. Calcd for C₂₄H₂₁SON₃: C, 72.15; H, 5.30; N, 10.52; S, 8.03; found: C, 72.14; H, 5.31; N, 10.42; S, 7.93.

Molecular Modeling. The optimized structures of all compounds were obtained by using the RMI⁴⁵ method, available as part of the SPARTAN '08 program,⁴⁶ using internal default settings for convergence criteria. Some of these new molecules were synthesized as racemic mixtures, so the molecular modeling treated the two isomers (R and S) independently, when appropriate, and the docking procedure used both isomers for each compound. Docking calculations and analysis were carried using the *T. cruzi* cruzain (PDB ID code: 3IUT) as the target,²³ in which there was a cocrystallized complex with inhibitor **54** (referred to as "KB2"). The active site was defined as all atoms within a radius of 6.0 Å from the cocrystallized ligand. The residues GLN19, CYS25, SER61, LEU67, MET68, ASN70, ASP161, HIS162, TRP184, and GLU208 were treated as flexible, using the conformation library for each one. The GOLD 5.1 program⁴⁷ was used for docking calculations, followed by the Binana program,⁴⁸ which was used to analyze the molecular interactions present in the best docking solutions, using the default setting, except for hydrogen bond distance, which was changed to a maximum of 3.5 Å. Figures were generated with Pymol.⁴⁹

Cruzain Inhibition. Recombinant cruzain was dissolved in acetate buffer (0.1 M; pH 5.5) to a concentration of 0.1 μM. Ten microliters of cruzain in DTT (5 mM) was distributed into a 96-well plate, and 150 μL of the test inhibitor (previously dissolved in DMSO) in phosphate buffer (in the presence of 0.001% EDTA, 100 mM NaCl, and DTT) was added to the respective wells. The plate was incubated at room temperature for 10 min. After this time, 340 μL of a solution containing the protease substrate Cbz-Phe-Arg-7-aminomethylcoumarin (Z-FR-AMC, Sigma-Aldrich Co., St. Louis, MO) was added to each well and the plate incubated. The plate was read 1, 5, and 10 min after the addition of the substrate (concentration of protein and substrate in the reaction was 0.5 nM and 2 μM, respectively). The percentage of cruzain inhibition was calculated using the following equation: $100 - (A_1/A \times 100)$, where A_1 means the RFU of the cruzain in the presence of the test inhibitor, and A means the RFU for the control well (cruzain plus substrate; no test inhibitor). Each test inhibitor concentration was measured in duplicate, and the IC₅₀ values were estimated employing nonlinear regression from at least nine different concentrations.

Cathepsins L and S Inhibition. Recombinant cathepsin L was dissolved in acetate buffer (0.1 M; pH 5.5) and activated with 1 mM of DTT. Test inhibitors were dissolved in DMSO and then diluted with phosphate buffer containing BSA (0.1%) and EDTA (1 mM) in 0.001% Tween. Protease substrate (Cbz-Phe-Arg-*p*-nitroanilide hydrochloride; denoted ZFR-pNA) in DMSO was suspended in phosphate buffer. Reactions were performed in 24-well plates. First, 90 μL of test inhibitor was distributed into the respective well, followed by the addition of 10 μL of cathepsin L. The plate was incubated for 45 min at room temperature. Then 100 μL of protease substrate was added, and the reaction was incubated for 5 min. The concentration of the protein in the reaction was 30 nM, and the concentration of the substrate was 5.0 μM. IC₅₀ values were calculated as described for cruzain. The same experiment was carried out for cathepsin S.

Animals. Female BALB/c mice (6–8 weeks old) were supplied by the animal breeding facility at Centro de Pesquisas Gonçalo Moniz (Fundação Oswaldo Cruz, Bahia, Brazil) and Centro de Pesquisas Aggeu Magalhães (Fundação Oswaldo Cruz, Pernambuco, Brazil) and maintained in sterilized cages under a controlled environment, receiving a balanced diet for rodents and water ad libitum. All experiments were carried out in accordance with the recommendations from Ethical Issues Guidelines and were approved by the local Animal Ethics Committee.

Parasites. Epimastigotes of *T. cruzi* (Y strain) were maintained at 26 °C in LIT medium (liver infusion tryptose) supplemented with 10% fetal bovine serum (FBS) (Cultilab, Brazil), 1% hemin (Sigma Co., St. Louis, MO), 1% R9 medium (Sigma Co), and 50 μg/mL gentamycin (Novafarma, Brazil). Bloodstream trypomastigote forms of *T. cruzi* were obtained from the supernatant of LLC-MK2 cells previously infected

and maintained in RPMI-1640 medium (Sigma Co.) supplemented with 10% FBS and 50 μg/mL gentamycin at 37 °C and 5% CO₂.

Toxicity to Mouse Splenocytes. Splenocytes from BALB/c mice were placed into 96-well plates at a cell density of 5×10^6 cells/well in RPMI-1640 medium supplemented with 10% of FBS and 50 μg mL⁻¹ of gentamycin. Each test inhibitor was used in at least three concentrations (1.0, 10, and 100 μg mL⁻¹) in triplicate. To each well, an aliquot of test inhibitor suspended in DMSO was added. Negative (untreated) and positive (saponin) controls were used with every plate. The plate was incubated for 24 h at 37 °C and 5% CO₂. After incubation, 1.0 μCi of ³H-thymidine (Perkin-Elmer, Waltham, MA) was added to each well, and the plate was returned to the incubator. The plate was then transferred to a β-radiation counter (Multilabel Reader, Finland), and the percent of ³H-thymidine was determined. Cell viability was measured as the percent of ³H-thymidine incorporation for treated cells in comparison to untreated cells. The highest nontoxic concentration was estimated.

Antiproliferative Activity for Splenocytes. BALB/c mouse splenocytes were placed into 96-well plates at a cell density of 5×10^6 cells/well in RPMI-1640 medium supplemented with 10% of FBS and 100 μg mL⁻¹ of gentamycin. Then 2.0 μg/mL of concanavalin A (con A) suspended in HEPES buffer and test inhibitors **5** and **18** (suspended in DMSO) were added to each well. Controls include untreated plus con A, without con A, and con A plus 0.01 μg/mL of cyclosporin A. Each concentration was assayed in triplicate. The plate was incubated for 72 h at 37 °C and 5% CO₂. According to manufacturer's recommendations, AlamarBlue was added and the plate was incubated for 1 h until AlamarBlue reduction by the living cells to the red fluorescent dye resorufin. After excitation at 530 nm and fluorescence at 590 nm, the signal was measured using a fluorescence microplate reader. Counts of untreated plus con A wells were subtracted from counts of untreated without con A wells. Inhibition (%) of cell proliferation was calculated in comparison to untreated cells. The concentration that results in 50% inhibition of cell proliferation (IC₅₀) was calculated from six different concentrations using nonlinear regression (Origin software).

Antiproliferative Activity for Epimastigotes. Epimastigotes were counted in a hemocytometer and then dispensed into 96-well plates at a cell density of 10^6 cells/well. Test inhibitors, dissolved in DMSO, were diluted to five different concentrations (1.23, 3.70, 11.11, 33.33, and 100 μg/mL) and added to respective wells in triplicate. The plate was incubated for 11 days at 26 °C, aliquots of each well were collected, and the number of viable parasites were counted in a Neubauer chamber and compared to untreated parasite culture. IC₅₀s were calculated using nonlinear regression on Prism 4.0 GraphPad software. Two independent experiments were carried out; benznidazole (LAFEPE, Brazil) and nifurtimox (Lampit, Roche) were used as the reference inhibitors.

Toxicity for Y Strain Trypomastigotes. Trypomastigotes collected from the supernatant of LLC-MK2 cells were dispensed into 96-well plates at a cell density of 4×10^5 cells/well. Test inhibitors, dissolved in DMSO, were diluted to five different concentrations and added into their respective wells, and the plate was incubated for 24 h at 37 °C and 5% of CO₂. Aliquots of each well were collected, and the number of viable parasites, based on parasite motility, was assessed in a Neubauer chamber. The percentage of inhibition was calculated in relation to untreated cultures. IC₅₀ calculation was also carried out using nonlinear regression with Prism 4.0 GraphPad software. Benznidazole and nifurtimox were used as the reference drugs.

Intracellular Parasite Development. Peritoneal exudate macrophages were seeded at a cell density of 2×10^5 cells/well in a 24-well plate with rounded coverslips on the bottom in RPMI supplemented with 10% FBS and incubated for 24 h. Cells were then infected with Y strain trypomastigotes at a ratio of 10 parasites per macrophage for 2 h. Free trypomastigotes were removed by successive washes using saline solution. Each test inhibitor was dissolved in DMSO at 10 μM and incubated for 6 h. The medium was replaced by a fresh medium, and the plate was incubated for 4 days. Cells were fixed in methanol, and the percentage of infected macrophages and the mean number of amastigotes/infected macrophages were determined by manual counting after Giemsa staining under an optical microscope (Olympus, Tokyo, Japan).

The percentage of infected macrophages and the number of amastigotes per macrophage were determined by counting 100 cells per slide. To estimate the IC₅₀ values, compounds were tested in triplicate at 1.0, 10, 25, and 50 μM.

Trypomastigote Invasion. Peritoneal macrophages (10⁵ cells) were plated onto 13-mm glass coverslips in a 24-well plate and allowed to stand for 24 h. The plate was washed with saline solution, and then trypomastigotes were added at a cell density of 1.25 × 10⁷ along with the addition of test inhibitor (at 50 μM). Amphotericin B (50 μM) was used as reference inhibitor. The plate was incubated for 2 h at 37 °C and 5% CO₂, followed by five washes with saline solution to remove extracellular trypomastigotes. Plates were maintained in RPMI medium supplemented with 10% FBS at 37 °C for 2 h. The number of infected cells was counted with optical microscopy using a standard Giemsa staining.

Infection in Mice. Female BALB/c mice (6–8 weeks old) were infected with bloodstream trypomastigotes by intraperitoneal injection of 10⁴ parasites in 100 μL of saline solution. Mice were then randomly divided into groups (six mice per group). After day 5 of postinfection, treatment with 250 μmol/kg weight of drug **18** was given orally by gavage once a day for five consecutive days. For the control group, benznidazole was also given orally at a dose of 250 μmol/kg weight. Infection was monitored daily by counting the number of motile parasites in 5 μL of fresh blood sample drawn from the lateral tail veins as recommended by standard protocols.³⁶

Statistical Analyses. To determine the statistical significance of each group in the in vitro/in vivo experiments of infection, the one-way ANOVA test and the Bonferroni for multiple comparisons were used. A *P* value <0.05 was considered significant. The data are representative of at least two experiments.

■ ASSOCIATED CONTENT

● Supporting Information

NMR, IR, and HRMS spectral data for intermediate compounds, and details for the electron microscopy studies and pharmacological tests. This material is available free of charge via the Internet at <http://pubs.acs.org>. Crystallographic data for compounds **2**, **4**, and **12** can be obtained free of charge from the Cambridge Crystallographic Data Centre (deposition numbers 874915, 874916, and 897962, respectively, www.ccdc.cam.ac.uk/data_request/cif).

■ AUTHOR INFORMATION

Corresponding Author

*Phone: +55 81-21268511, fax: +55 81-21268510; e-mail: diogollucio@gmail.com.

Notes

The authors declare no competing financial interest.

■ ACKNOWLEDGMENTS

This work received support from CNPq (grant 471461/2011-3 to A.C.L.L.), CAPES (grant 23038.003155/2011-37 to V.R.A.P.), FAPESB (PRONEX grant to M.B.P.S.), and European Union ChemBioFight (grant reference 269301 to M.B.P.S.). D.R.M.M. received a CNPq doctoral scholarship and a CAPES-Fulbright Foundation exchange doctoral sponsorship. A.C.L.L., C.A.S., and M.B.P.S. hold a CNPq senior fellowship. The authors acknowledge Prof. James McKerrow for providing recombinant cruzain and plasmid. C.A.S. also thanks the Instituto de Física de São Carlos (University of São Paulo, Brazil) for allowing the use of a Kappa CCD diffractometer.

■ REFERENCES

(1) World Health Organization. Fact sheet no. 340, June 2010. <http://www.who.int/mediacentre/factsheets/fs340/en/index.html> (accessed June 1, 2012).

(2) Rassi, A., Jr.; Rassi, A.; Marin-Neto, J. A. Chagas Disease. *Lancet* **2010**, *375*, 1388–402.

(3) Barrett, M. P.; Burchmore, R. J.; Stich, A.; Lazzari, J. O.; Frasch, A. C.; Cazzulo, J. J.; Krishna, S. The Trypanosomiasis. *Lancet* **2003**, *362*, 1469–1480.

(4) Marin-Neto, J. A.; Rassi, A., Jr.; Avezum, A., Jr.; Mattos, A. C.; Rassi, A. The BENEFIT Trial: Testing the Hypothesis That Trypanocidal Therapy is Beneficial for Patients with Chronic Chagas Heart Disease. *Mem. Inst. Oswaldo Cruz* **2009**, *104*, 319–324.

(5) Marin-Neto, J. A.; Rassi, A., Jr.; Morillo, C. A.; Avezum, A.; Connolly, S. J.; Sosa-Estani, S.; Rosas, F.; Yusuf, S. BENEFIT Investigators. Rationale and Design of a Randomized Placebo-Controlled Trial Assessing the Effects of Etiologic Treatment in Chagas' Cardiomyopathy: The BENznidazole Evaluation For Interrupting Trypanosomiasis (BENEFIT). *Am. Heart J.* **2008**, *156*, 37–43.

(6) Pinazo, M. J.; Muñoz, J.; Posada, E.; López-Chejade, P.; Gállego, M.; Ayala, E.; del Cacho, E.; Soy, D.; Gascon, J. Tolerance of Benznidazole in Treatment of Chagas' Disease in Adults. *Antimicrob. Agents Chemother.* **2010**, *54*, 4896–4899.

(7) Sajid, M.; Robertson, S. A.; Brinen, L. S.; McKerrow, J. H. Cruzain: the Path From Target Validation to the Clinic. In *Advances in Experimental Medicine and Biology, Proteases of Pathogenic Organisms*; Robinson, M. W.; Dalton, J. P., Eds.; Springer Science Business Media, LLC: New York, 2011; vol. 712, pp 100–115.

(8) Duschak, V. G.; Ciaccio, M.; Nassert, J. R.; Basombrio, M. A. Enzymatic Activity, Protein Expression, and Gene Sequence of Cruzain in Virulent and Attenuated *Trypanosoma cruzi* Strains. *J. Parasitol.* **2001**, *87*, 1016–1022.

(9) Doyle, P. S.; Zhou, Y. M.; Hsieh, I.; Greenbaum, D. C.; McKerrow, J. H.; Engel, J. C. The *Trypanosoma cruzi* Protease Cruzain Mediates Immune Evasion. *Plos Pathog.* **2011**, *7*, e1002139.

(10) Aoki, M. P.; Cano, R. C.; Pellegrini, A. V.; Tanos, T.; Guinázú, N. L.; Coso, O. A.; Gea, S. Different Signaling Pathways Are Involved in Cardiomyocyte Survival Induced by a *Trypanosoma cruzi* Glycoprotein. *Microbes Infect.* **2006**, *8*, 1723–1731.

(11) Monteiro, A. C.; Schmitz, V.; Svensjo, E.; Gazzinelli, R. T.; Almeida, I. C.; Todorov, A.; de Arruda, L. B.; Torrecilhas, A. C.; Pesquero, J. B.; Morrot, A.; Bouskela, E.; Bonomo, A.; Lima, A. P.; Müller-Esterl, W.; Scharfstein, J. Cooperative Activation of TLR2 and Bradykinin B2 Receptor is Required for Induction of Type 1 Immunity in a Mouse Model of Subcutaneous Infection by *Trypanosoma cruzi*. *J. Immunol.* **2006**, *177*, 6325–6735.

(12) Andrade, D.; Serra, R.; Svensjö, E.; Lima, A. P.; Ramos-Jr, E. S.; Fortes, F. S.; Morandini, A. C.; Morandi, V.; Soeiro, M. N.; Tanowitz, H. B.; Scharfstein, J. *Trypanosoma cruzi* Invades Host Cells Through the Activation of Endothelin and Bradykinin Receptors: A Converging Pathway Leading to Chagasic Vasculopathy. *Br. J. Pharmacol.* **2012**, *165*, 1333–1347.

(13) Du, X.; Guo, C.; Hansell, E.; Doyle, P. S.; Caffrey, C. R.; Holler, T. P.; McKerrow, J. H.; Cohen, F. E. Synthesis and Structure–Activity Relationship Study of Potent Trypanocidal Thio Semicarbazone Inhibitors of the Trypanosomal Cysteine Protease Cruzain. *J. Med. Chem.* **2002**, *45*, 2695–2707.

(14) Chiyanzu, I.; Hansell, E.; Gut, J.; Rosenthal, P. J.; McKerrow, J. H.; Chibale, K. Synthesis and Evaluation of Isatins and Thiosemicarbazone Derivatives Against Cruzain, Falcipain-2 and Rhodesain. *Bioorg. Med. Chem. Lett.* **2003**, *13*, 3527–3530.

(15) Greenbaum, D. C.; Mackey, Z.; Hansell, E.; Doyle, P.; Gut, J.; Caffrey, C. R.; Lehrman, J.; Rosenthal, P. J.; McKerrow, J. H.; Chibale, K. Synthesis and Structure–Activity Relationships of Parasiticidal Thiosemicarbazone Cysteine Protease Inhibitors against *Plasmodium falciparum*, *Trypanosoma brucei*, and *Trypanosoma cruzi*. *J. Med. Chem.* **2004**, *47*, 3212–3219.

(16) Fujii, N.; Mallari, J. P.; Hansell, E. J.; Mackey, Z.; Doyle, P.; Zhou, Y. M.; Gut, J.; Rosenthal, P. J.; McKerrow, J. H.; Guy, R. K. Discovery of Potent Thiosemicarbazone Inhibitors of Rhodesain and Cruzain. *Bioorg. Med. Chem. Lett.* **2005**, *15*, 121–123.

(17) Siles, R.; Chen, S. E.; Zhou, M.; Pinney, K. G.; Trawick, M. L. Design, Synthesis, and Biochemical Evaluation of Novel Cruzain

Inhibitors with Potential Application in the Treatment of Chagas Disease. *Bioorg. Med. Chem. Lett.* **2006**, *16*, 4405–4409.

(18) Porcal, W.; Hernández, P.; Boiani, M.; Aguirre, G.; Boiani, L.; Chidichimo, A.; Cazzulo, J. J.; Campillo, N. E.; Paez, J. A.; Castro, A.; Krauth-Siegel, R. L.; Davies, C.; Basombrió, M. A.; González, M.; Cerecetto, H. In Vivo Anti-Chagas Vinylthio-, Vinylsulfinyl-, and Vinylsulfonylbenzofuroxan Derivatives. *J. Med. Chem.* **2007**, *50*, 6004–6015.

(19) Guido, R. V.; Trossini, G. H.; Castilho, M. S.; Oliva, G.; Ferreira, E. I.; Andricopulo, A. D. Structure-Activity Relationships for a Class of Selective Inhibitors of the Major Cysteine Protease from *Trypanosoma cruzi*. *J. Enzyme Inhib. Med. Chem.* **2008**, *23*, 964–973.

(20) Pizzo, C.; Faral-Tello, P.; Salinas, G.; Flo, M.; Robello, C.; Wipf, P.; Mahler, S. G. Selenosemicarbazones as Potent Cruzipain Inhibitors and Their Antiparasitic Properties against *Trypanosoma cruzi*. *Med. Chem. Commun.* **2012**, *3*, 362–368.

(21) Merlino, A.; Benitez, M.; Campillo, N. E.; Páez, J. A.; Tinoco, L. W.; González, M.; Cerecetto, H. Amidines Bearing Benzofuroxan or Benzimidazole 1,3-Dioxide Core Scaffolds as *Trypanosoma cruzi*-Inhibitors: Structural Basis for Their Interactions with Cruzipain. *Med. Chem. Commun.* **2012**, *3*, 90–101.

(22) Brak, K.; Doyle, P. S.; McKerrow, J. H.; Ellman, J. A. Identification of a New Class of Nonpeptidic Inhibitors of Cruzain. *J. Am. Chem. Soc.* **2008**, *130*, 6404–6410.

(23) Brak, K.; Kerr, I. D.; Barrett, K. T.; Fuchi, N.; Debnath, M.; Ang, K.; Engel, J. C.; McKerrow, J. H.; Doyle, P. S.; Brinen, L. S.; Ellman, J. A. Nonpeptidic Tetrafluorophenoxymethyl Ketone Cruzain Inhibitors as Promising New Leads for Chagas Disease Chemotherapy. *J. Med. Chem.* **2010**, *53*, 1763–1773.

(24) Bryant, C.; Kerr, I. D.; Debnath, M.; Ang, K. K.; Ratnam, J.; Ferreira, R. S.; Jaishankar, P.; Zhao, D.; Arkin, M. R.; McKerrow, J. H.; Brinen, L. S.; Renslo, A. R. Novel Non-Peptidic Vinylsulfones Targeting the S2 and S3 Subsites of Parasite Cysteine Proteases. *Bioorg. Med. Chem. Lett.* **2009**, *19*, 6218–6221.

(25) Leite, A. C. L.; de Lima, R. S.; Moreira, D. R.; Cardoso, M. V. O.; Gouveia, A. C.; Santos, L. M.; Hernandes, M. Z.; Kiperstok, A. C.; de Lima, R. S.; Soares, M. B. P. Synthesis, Docking, and *In Vitro* Activity of Thiosemicarbazones, Aminoacyl-Thiosemicarbazides and Acyl-Thiazolidones Against *Trypanosoma cruzi*. *Bioorg. Med. Chem.* **2006**, *14*, 3749–3457.

(26) Leite, A. C.; Moreira, D. R.; Cardoso, M. V. O.; Hernandes, M. Z.; Pereira, V. R. A.; Silva, R. O.; Kiperstok, A. C.; Lima, M. S.; Soares, M. B. P. Synthesis, Cruzain Docking, and *In Vitro* Studies of Aryl-4-oxothiazolylhydrazones Against *Trypanosoma cruzi*. *ChemMedChem* **2007**, *2*, 1339–1345.

(27) Hernandes, M. Z.; Rabello, M. M.; Leite, A. C. L.; Cardoso, M. V. O.; Moreira, D. R. M.; Brondani, D. J.; Simone, C. A.; Reis, L. C.; Souza, M. A.; Pereira, V. R.; Ferreira, R. S.; McKerrow, J. H. Studies Toward the Structural Optimization of Novel Thiazolylhydrazone-Based Potent Antitrypanosomal Agents. *Bioorg. Med. Chem.* **2010**, *18*, 7826–7835.

(28) Lima, L. M.; Barreiro, E. J. Bioisosterism: a Useful Strategy for Molecular Modification and Drug Design. *Curr. Med. Chem.* **2005**, *23*–49.

(29) Zhang, D. N.; Li, J. T.; Song, Y. L.; Liu, H. M.; Li, H. Y. Efficient One-Pot Three-Component Synthesis of N-(4-arylthiazol-2-yl)-hydrazones in Water Under Ultrasound Irradiation. *Ultrason. Sonochem.* **2012**, *19*, 475–478.

(30) Chimenti, F.; Bizzarri, B.; Maccioni, E.; Secci, D.; Bolasco, A.; Chimenti, P.; Fioravanti, R.; Granese, A.; Carradori, S.; Tosi, F.; Ballario, P.; Vernarecci, S.; Filetici, P. A Novel Histone Acetyltransferase Inhibitor Modulating Gcn5 Network: Cyclopentylidene-[4-(4'-chlorophenyl)thiazol-2-yl]hydrazone. *J. Med. Chem.* **2009**, *52*, 530–536.

(31) Ferreira, R. S.; Bryant, C.; Ang, K. K.; McKerrow, J. H.; Shoichet, B. K.; Renslo, A. R. Divergent Modes of Enzyme Inhibition in a Homologous Structure–Activity Series. *J. Med. Chem.* **2009**, *52*, 5005–5058.

(32) Hernandes, M. Z.; Cavalcanti, S. M.; Moreira, D. R. M.; de Azevedo, W. F., Jr.; Leite, A. C. L. Halogen Atoms in the Modern

Medicinal Chemistry: Hints for the Drug Design. *Curr. Drug Targets* **2010**, *11*, 303–314.

(33) Engel, J. C.; Doyle, P. S.; Palmer, P.; Hsieh, I.; Bainton, D. F.; McKerrow, J. H. Cysteine Protease Inhibitors Alter Golgi Complex Ultrastructure and Function in *Trypanosoma cruzi*. *J. Cell Sci.* **1998**, *111*, 597–606.

(34) Pizzo, C.; Saiz, C.; Talevi, A.; Gavernet, L.; Palestro, P.; Bellera, C.; Blanch, L. B.; Benítez, D.; Cazzulo, J. J.; Chidichimo, A.; Wipf, P.; Mahler, S. G. Synthesis of 2-Hydrazolyl-4-Thiazolidinones Based on Multicomponent Reactions and Biological Evaluation Against *Trypanosoma cruzi*. *Chem. Biol. Drug Des.* **2011**, *77*, 162–177.

(35) Matsuo, A. L.; Silva, L. S.; Torrecilhas, A. C.; Pascoalino, B. S.; Ramos, T. C.; Rodrigues, E. G.; Schenkman, S.; Caires, A. C.; Travassos, L. R. *In Vitro* and *In Vivo* Trypanocidal Effects of the Cyclopalladated Compound 7a, a Drug Candidate for Treatment of Chagas' Disease. *Antimicrob. Agents Chemother.* **2010**, *54*, 3318–3325.

(36) Romanha, A. J.; Castro, S. L.; Soeiro, M. N.; Lannes-Vieira, J.; Ribeiro, I.; Talvani, A.; Bourdin, B.; Blum, B.; Olivieri, B.; Zani, C.; Spadafora, C.; Chiari, E.; Chatelain, E.; Chaves, G.; Calzada, J. E.; Bustamante, J. M.; Freitas-Jr, L. H.; Romero, L. I.; Bahia, M. T.; Lotrowska, M.; Soares, M. B. P.; Andrade, S. G.; Armstrong, T.; Degraeve, W.; Andrade, Z. A. *In Vitro* and *In Vivo* Experimental Models for Drug Screening and Development for Chagas Disease. *Mem. Inst. Oswaldo Cruz* **2010**, *105*, 233–238.

(37) Wilson, H. R.; Revankar, G. R.; Tolman, R. L. *In Vitro* and *In Vivo* Activity of Certain Thiosemicarbazones against *Trypanosoma cruzi*. *J. Med. Chem.* **1974**, *17*, 760–761.

(38) Otero, L.; Vieites, M.; Boiani, L.; Denicola, A.; Rigol, C.; Opazo, L.; Olea-Azar, C.; Maya, J. D.; Morello, A.; Krauth-Siegel, R. L.; Piro, O. E.; Castellano, E.; González, M.; Gambino, D.; Cerecetto, H. Novel Antitrypanosomal Agents Based on Palladium Nitrofurlythiosemicarbazone Complexes: DNA and Redox Metabolism as Potential Therapeutic Targets. *J. Med. Chem.* **2006**, *49*, 3322–3331.

(39) Vieites, M.; Otero, L.; Santos, D.; Toloza, J.; Figueroa, R.; Norambuena, E.; Olea-Azar, C.; Aguirre, G.; Cerecetto, H.; González, M.; Morello, A.; Maya, J. D.; Garat, B.; Gambino, D. Platinum(II) Metal Complexes as Potential Anti-*Trypanosoma cruzi* Agents. *J. Inorg. Biochem.* **2008**, *102*, 1033–1043.

(40) Maia, P. I.; Fernandes, A. G.; Silva, J. J.; Andricopulo, A. D.; Lemos, S. S.; Lang, E. S.; Abram, U.; Deflon, V. M. Dithiocarbazate Complexes With the $[M(PPh_3)]^{2+}$ (M = Pd or Pt) Moiety Synthesis, Characterization and Anti-*Trypanosoma cruzi* Activity. *J. Inorg. Biochem.* **2010**, *104*, 1276–1282.

(41) Caputto, M. E.; Ciccarelli, A.; Frank, F.; Moglioni, A. G.; Moltrasio, G. Y.; Vega, D.; Lombardo, E.; Finkielstein, L. M. Synthesis and Biological Evaluation of Some Novel 1-Indanone Thiazolylhydrazone Derivatives as Anti-*Trypanosoma cruzi* Agents. *Eur. J. Med. Chem.* **2012**, *55*, 155–163.

(42) Suryadevara, P. K.; Olepu, S.; Lockman, J. W.; Ohkanda, J.; Karimi, M.; Verlinde, C. L.; Kraus, J. M.; Schoepe, J.; Van-Voorhis, W. C.; Hamilton, A. D.; Buckner, F. S.; Gelb, M. H. Structurally Simple Inhibitors of Lanosterol 14 α -Demethylase Are Efficacious In a Rodent Model of Acute Chagas Disease. *J. Med. Chem.* **2009**, *52*, 3703–3715.

(43) Andriani, G.; Chessler, A. D.; Courtemanche, G.; Burleigh, B. A.; Rodriguez, A. Activity *In Vivo* of Anti-*Trypanosoma cruzi* Compounds Selected From a High Throughput Screening. *Plos Negl. Trop. Dis.* **2011**, *5*, e1298.

(44) Keenan, M.; Abbott, M. J.; Alexander, P. W.; Armstrong, T.; Best, W. M.; Berven, B.; Botero, A.; Chaplin, J. H.; Charman, S. A.; Chatelain, E.; Geldern, T. W.; Kerfoot, M.; Khong, A.; Nguyen, T.; McManus, J. D.; Morizzi, J.; Ryan, E.; Scandale, I.; Thompson, R. A.; Wang, S. Z.; White, K. L. Analogues of Fenarimol Are Potent Inhibitors of *Trypanosoma cruzi* and Are Efficacious in a Murine Model of Chagas Disease. *J. Med. Chem.* **2012**, *55*, 4189–4204.

(45) Rocha, G. B.; Freire, R. O.; Simas, A. M.; Stewart, J. J. P. RM1: A Reparameterization of AM1 for H, C, N, O, P, S, F, Cl, Br, and I. *J. Comput. Chem.* **2006**, *27*, 1101–1111.

(46) Spartan '08 Tutorial and user's guide; Wavefunction: Irvine, CA, 2008. <http://www.wavefun.com/products/spartan.html>.

(47) *Gold software, version 5.1*, Cambridge Crystallographic Data Centre. <http://www.ccdc.cam.ac.uk>.

(48) Durrant, J. D.; Mccammon, J. A. BINANA: A Novel Algorithm for Ligand-Binding Characterization. *J. Mol. Graph. Model.* **2011**, *29*, 888–893.

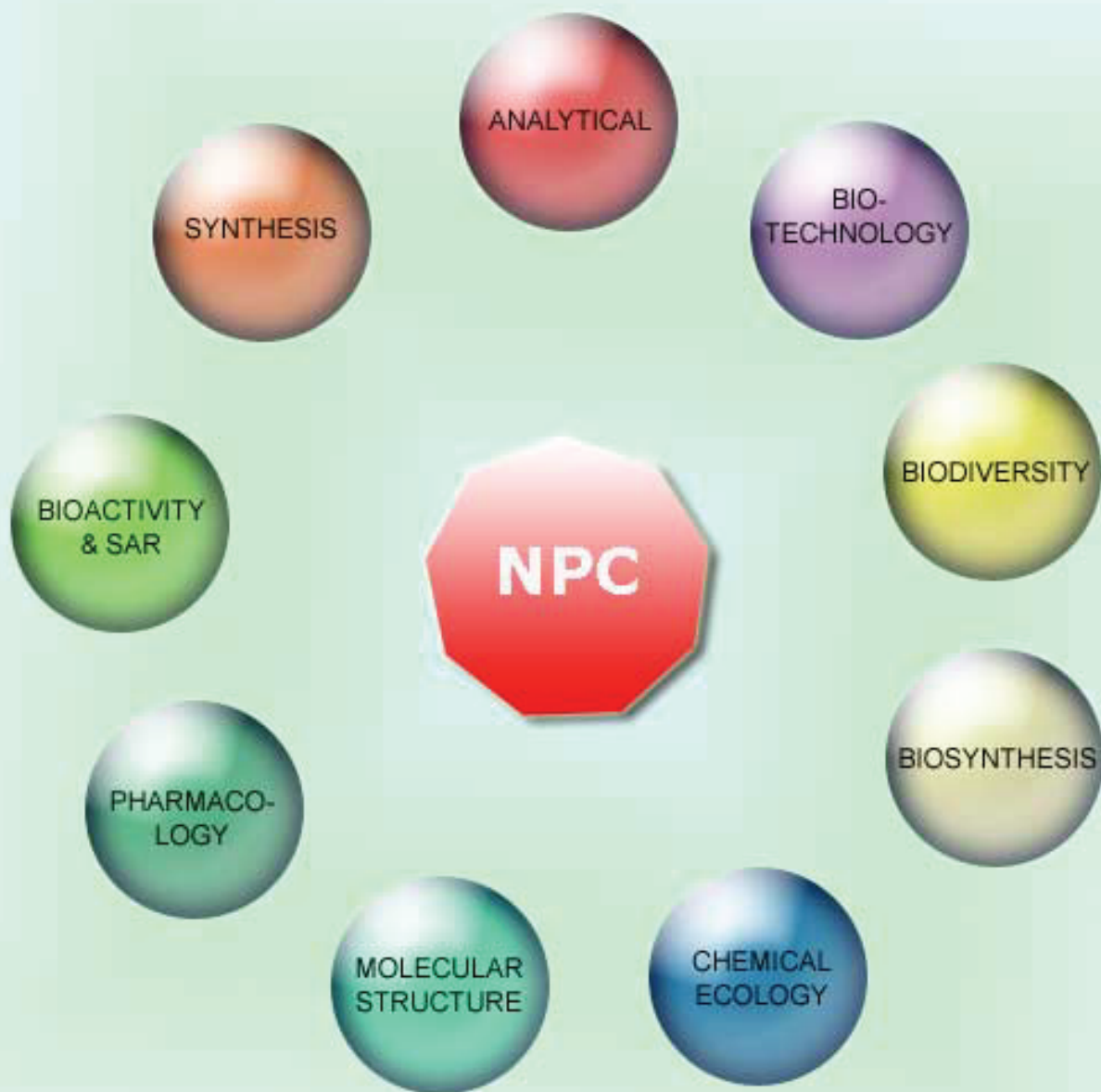
(49) DeLano, W. L. *The PyMOL Molecular Graphics System*, DeLano Scientific, San Carlos, CA, 2002. <http://www.pymol.org>.

ANEXO 3

Da Silva TB, Menezes LR, Sampaio MF, **Meira CS**, Guimarães ET, Soares MB, Prata AP, Nogueira PC, Costa EV. Chemical composition and anti-*Trypanosoma cruzi* activity of essential oils obtained from leaves of *Xylopia frutescens* and *X. laevigata* (Annonaceae). **Natural Product Communications**. v. 8, p. 403-406, 2013.

NATURAL PRODUCT COMMUNICATIONS

An International Journal for Communications and Reviews Covering all
Aspects of Natural Products Research



Volume 8. Issue 3. Pages 283-426. 2013
ISSN 1934-578X (printed); ISSN 1555-9475 (online)
www.naturalproduct.us

EDITOR-IN-CHIEF**DR. PAWAN K AGRAWAL**

Natural Product Inc.
7963, Anderson Park Lane,
Westerville, Ohio 43081, USA
agrawal@naturalproduct.us

EDITORS**PROFESSOR ALEJANDRO F. BARRERO**

Department of Organic Chemistry,
University of Granada,
Campus de Fuente Nueva, s/n, 18071, Granada, Spain
afbarre@ugr.es

PROFESSOR ALESSANDRA BRACA

Dipartimento di Chimica Bioorganica e Biofarmacia,
Università di Pisa,
via Bonanno 33, 56126 Pisa, Italy
braca@farm.unipi.it

PROFESSOR DEAN GUO

State Key Laboratory of Natural and Biomimetic Drugs,
School of Pharmaceutical Sciences,
Peking University,
Beijing 100083, China
gda5958@163.com

PROFESSOR YOSHIHIRO MIMAKI

School of Pharmacy,
Tokyo University of Pharmacy and Life Sciences,
Horinouchi 1432-1, Hachioji, Tokyo 192-0392, Japan
mimaki@ps.toyaku.ac.jp

PROFESSOR STEPHEN G. PYNE

Department of Chemistry
University of Wollongong
Wollongong, New South Wales, 2522, Australia
spyne@uow.edu.au

PROFESSOR MANFRED G. REINECKE

Department of Chemistry,
Texas Christian University,
Forts Worth, TX 76129, USA
m.reinecke@tcu.edu

PROFESSOR WILLIAM N. SETZER

Department of Chemistry
The University of Alabama in Huntsville
Huntsville, AL 35809, USA
wsetzer@chemistry.uah.edu

PROFESSOR YASUHIRO TEZUKA

Institute of Natural Medicine
Institute of Natural Medicine, University of Toyama,
2630-Sugitani, Toyama 930-0194, Japan
tezuka@inm.u-toyama.ac.jp

PROFESSOR DAVID E. THURSTON

Department of Pharmaceutical and Biological Chemistry,
The School of Pharmacy,
University of London, 29-39 Brunswick Square,
London WC1N 1AX, UK
david.thurston@pharmacy.ac.uk

HONORARY EDITOR**PROFESSOR GERALD BLUNDEN**

The School of Pharmacy & Biomedical Sciences,
University of Portsmouth,
Portsmouth, PO1 2DT U.K.
axuf64@dsl.pipex.com

ADVISORY BOARD

Prof. Berhanu M. Abegaz
Gaborone, Botswana

Prof. Viqar Uddin Ahmad
Karachi, Pakistan

Prof. Øyvind M. Andersen
Bergen, Norway

Prof. Giovanni Appendino
Novara, Italy

Prof. Yoshinori Asakawa
Tokushima, Japan

Prof. Lee Banting
Portsmouth, U.K.

Prof. Julie Banerji
Kolkata, India

Prof. Anna R. Bilia
Florence, Italy

Prof. Maurizio Bruno
Palermo, Italy

Prof. César A. N. Catalán
Tucumán, Argentina

Prof. Josep Coll
Barcelona, Spain

Prof. Geoffrey Cordell
Chicago, IL, USA

Prof. Ana Cristina Figueiredo
Lisbon, Portugal

Prof. Cristina Gracia-Viguera
Murcia, Spain

Prof. Duvvuru Gunasekar
Tirupati, India

Prof. Kurt Hostettmann
Lausanne, Switzerland

Prof. Martin A. Iglesias Arteaga
Mexico, D. F., Mexico

Prof. Leopold Jirovetz
Vienna, Austria

Prof. Vladimir I Kalinin
Vladivostok, Russia

Prof. Niel A. Koorbanally
Durban, South Africa

Prof. Karsten Krohn
Paderborn, Germany

Prof. Chiaki Kuroda
Tokyo, Japan

Prof. Hartmut Laatsch
Gottingen, Germany

Prof. Marie Lacaille-Dubois
Dijon, France

Prof. Shoei-Sheng Lee
Taipei, Taiwan

Prof. Francisco Macias
Cadiz, Spain

Prof. Imre Mathe
Szeged, Hungary

Prof. Ermino Murano
Trieste, Italy

Prof. M. Soledade C. Pedras
Saskatoon, Canada

Prof. Luc Pieters
Antwerp, Belgium

Prof. Peter Proksch
Düsseldorf, Germany

Prof. Phila Raharivelomanana
Tahiti, French Polynesia

Prof. Luca Rastrelli
Fisciano, Italy

Prof. Monique Simmonds
Richmond, UK

Dr. Bikram Singh
Palampur, India

Prof. John L. Sorensen
Manitoba, Canada

Prof. Valentin Stonik
Vladivostok, Russia

Prof. Winston F. Tinto
Barbados, West Indies

Prof. Sylvia Urban
Melbourne, Australia

Prof. Karen Valant-Vetschera
Vienna, Austria

INFORMATION FOR AUTHORS

Full details of how to submit a manuscript for publication in Natural Product Communications are given in Information for Authors on our Web site <http://www.naturalproduct.us>.

Authors may reproduce/republish portions of their published contribution without seeking permission from NPC, provided that any such republication is accompanied by an acknowledgment (original citation)-Reproduced by permission of Natural Product Communications. Any unauthorized reproduction, transmission or storage may result in either civil or criminal liability.

The publication of each of the articles contained herein is protected by copyright. Except as allowed under national "fair use" laws, copying is not permitted by any means or for any purpose, such as for distribution to any third party (whether by sale, loan, gift, or otherwise); as agent (express or implied) of any third party; for purposes of advertising or promotion; or to create collective or derivative works. Such permission requests, or other inquiries, should be addressed to the Natural Product Inc. (NPI). A photocopy license is available from the NPI for institutional subscribers that need to make multiple copies of single articles for internal study or research purposes.

To Subscribe: Natural Product Communications is a journal published monthly. 2013 subscription price: US\$2,395 (Print, ISSN# 1934-578X); US\$2,395 (Web edition, ISSN# 1555-9475); US\$2,795 (Print + single site online); US\$595 (Personal online). Orders should be addressed to Subscription Department, Natural Product Communications, Natural Product Inc., 7963 Anderson Park Lane, Westerville, Ohio 43081, USA. Subscriptions are renewed on an annual basis. Claims for nonreceipt of issues will be honored if made within three months of publication of the issue. All issues are dispatched by airmail throughout the world, excluding the USA and Canada.

Chemical Composition and Anti-*Trypanosoma cruzi* Activity of Essential Oils Obtained from Leaves of *Xylopia frutescens* and *X. laevigata* (Annonaceae)

Thanany Brasil da Silva^a, Leociley Rocha Alencar Menezes^a, Marília Fernanda Chaves Sampaio^a, Cássio Santana Meira^b, Elisalva Teixeira Guimarães^{b,c}, Milena Botelho Pereira Soares^{b,d}, Ana Paula do Nascimento Prata^e, Paulo Cesar de Lima Nogueira^a and Emmanoel Vilaça Costa^{a,*}

^aDepartamento de Química, Universidade Federal de Sergipe, São Cristóvão, Sergipe, Brazil, 49100-000

^bCentro de Pesquisas Gonçalo Moniz, Fundação Oswaldo Cruz, Salvador, Bahia, Brazil, 40296-710

^cDepartamento de Ciências da Vida, Universidade do Estado da Bahia, Salvador, Bahia, Brazil, 41150-000

^dCentro de Biotecnologia e Terapia Celular, Hospital São Rafael, Salvador, Bahia, Brazil, 41253-190

^eDepartamento de Biologia, Universidade Federal de Sergipe, São Cristóvão, Sergipe, Brazil, 49100-000

emmanoelvc@gmail.com

Received: November 7th, 2012; Accepted: January 7th, 2013

Essential oils from leaves of *Xylopia frutescens* (XFMJ) and two specimens of *Xylopia laevigata* (XLMC and XLSI) were obtained by hydrodistillation using a Clevenger-type apparatus, and analyzed by GC-MS and GC-FID. Sesquiterpenes dominated the essential oils. The main constituents of XFMJ were (*E*)-caryophyllene (24.8%), bicyclogermacrene (20.8%), germacrene D (17.0%), β -elemene (7.9%), and (*E*)- β -ocimene (6.8%). XLMC contained significant quantities of germacrene D (18.9%), bicyclogermacrene (18.4%), β -elemene (9.5%), δ -selinene (9.2%), (*E*)-caryophyllene (8.5%), germacrene B (5.7%) and γ -muurolene (5.7%), while germacrene D (27.0%), bicyclogermacrene (12.8%), (*E*)-caryophyllene (8.6%), γ -muurolene (8.6%), δ -cadinene (6.8%), and germacrene B (6.0%) were the main components of XLSI. The essential oils had trypanocidal activity against the Y strain of *Trypanosoma cruzi*, with IC₅₀ values lower than 30 $\mu\text{g}\cdot\text{mL}^{-1}$ and 15 $\mu\text{g}\cdot\text{mL}^{-1}$ against epimastigote and trypomastigote forms of *T. cruzi*, respectively, and were also able to reduce the percentage *in vitro* of *T. cruzi*-infected macrophages and the intracellular number of amastigotes at concentrations that were non-cytotoxic to macrophages.

Keywords: *Xylopia frutescens*, *Xylopia laevigata*, Essential oil, Trypanocidal activity.

Xylopia L. (Annonaceae) comprises approximately 157 species of trees and shrubs that are found predominantly in tropical regions [1]. This genus is known for the aromatic fragrance of its flowers and fruits and medicinal purposes [2a,b]. The fruits and seeds of some species of this genus, such as *X. aethiopica*, *X. sericea*, and *X. aromatica*, are also used as either condiments or mixed spices. As a spice, the fruit containing the seeds is usually pounded and used in cooked foods or in the spicing of beverages. As a component of herbal medicine, it is locally used as a carminative, stimulant, and additive to other remedies for the treatment of skin infections, as a digestive, appetizer, and antiemetic agent, and for the management of cough and fever [2a,3].

Recent phytochemical investigations of some species of *Xylopia* have indicated the presence of essential oils (monoterpenes and sesquiterpenes), diterpenes, steroids [4,5,6], alkaloids [7,8], and flavonoids [8], exhibiting several pharmacological activities, such as antifungal [4,6], antioxidant [3,7,8], antileishmanial [9], cytotoxic [10], antinociceptive [11], acaricidal [12], and insecticidal [6].

X. frutescens Aubl. and *X. laevigata* (Mart.) R. E. Fries are two Brazilian species commonly known as 'pindaíba' and 'meiu', respectively, found in the Northeast Region, mainly in Sergipe, Pernambuco, Bahia, and Paraíba States. Previous phytochemical and biological investigations of the stem of *X. laevigata* reported the isolation and identification of sesquiterpenes, steroids, and ent-kaurane diterpenoids with antimicrobial and larvicidal activities [6]. Phytochemical and biological investigations of fruits of *X. frutescens* have reported the presence of essential oils

(monoterpenes and sesquiterpenes), diterpenes and alkaloids, some of them with antimicrobial and anti-inflammatory activities [13]. Both species are used in traditional medicine. The seeds of *X. frutescens* are used as bladder stimulants and to trigger menstruation, as well as a treatment for rheumatism, halitosis, tooth decay, and intestinal diseases [13], whereas the leaves and flowers of *X. laevigata* are used to treat painful disorders, heart disease, and inflammatory conditions (oral communications received from local woodsmen known as 'mateiros', unpublished data).

In our continuous search for trypanocidal natural products from Annonaceous plants, herein we report the chemical composition of the essential oils from the leaves of *X. frutescens* and *X. laevigata*. There are no previous reports on the chemical composition of the essential oils from the leaves of these species or their trypanocidal action on Chagas' disease.

Hydrodistillation of the leaves of *X. frutescens* from 'Mata do Junco' (XFMJ) and two specimens of *X. laevigata* from 'Mata do Crasto' (XLMC) and 'Serra de Itabaiana' (XLSI) resulted in light yellow crude essential oils with yields of 1.1 \pm 0.0%, 0.9 \pm 0.1% and 1.5 \pm 0.0% (w/w), respectively, in relation to the dry weight of the plant material. As shown in Table 1, it was possible to identify 43 compounds: 23 in the essential oil of XFMJ (91.0%); and 33 in both XLMC and XLSI (97.3 and 97.6%, respectively). The essential oils were dominated by sesquiterpenes, with 83.1% in XFMJ, 96.3% in XLMC and 93.5% in XLSI. The major compounds identified in the essential oil of XFMJ were (*E*)-caryophyllene (24.8%), bicyclogermacrene (20.8%), germacrene D (17.0%), β -elemene (7.9%),

Table 1: Essential oil composition of the leaves of *Xylopi frutescens* (XFMJ) and *X. laevigata* (XLMC and XLSI).

Compound	Peak area %					
	RF ^a	RI ^b	XFMJ	XLMC	XLSI	
1	α -Pinene	931	932	0.6±0.1	0.3±0.5	1.3±0.4
2	Camphene	947	946	0.3±0.0	0.1±0.1	0.3±0.1
3	β -Pinene	975	974			0.3±0.1
4	Myrcene	988	988	0.2±0.0		
5	Limonene	1028	1024		0.4±0.3	1.7±0.4
6	(Z)- β -Ocimene	1036	1032		0.2±0.2	0.4±0.1
7	(E)- β -Ocimene	1046	1044	6.8±0.4		0.1±0.1
8	Bicycloelemene	1332	1335	0.2±0.0	0.2±0.0	0.3±0.0
9	δ -Elemene	1335	1335		2.9±0.1	2.7±0.0
10	α -Cubebene	1347	1345	0.3±0.0	0.6±0.1	1.3±0.1
11	α -Ylangene	1370	1373	0.4±0.0	0.3±0.0	0.6±0.1
12	α -Copaene	1376	1374	1.4±0.0	2.5±0.2	4.8±0.4
13	β -Bourbonene	1384	1387		0.1±0.1	0.3±0.0
14	β -Cubebene	1388	1387			1.0±0.0
15	β -Elemene	1390	1389	7.9±0.3	9.5±0.5	
16	(E)-Caryophyllene	1421	1417	24.8±0.2	8.5±0.5	8.6±0.3
17	γ -Elemene	1429	1430		1.0±0.0	
18	β -Copaene	1431	1430	0.3±0.0		1.6±0.0
19	α -Guaiene	1435	1437		0.3±0.0	
20	Aromadendrene	1440	1439		1.0±0.1	1.6±0.1
21	trans-Muurolo-3,5-diene	1450	1451	0.3±0.0		
22	α -Humulene	1457	1452	2.4±0.0	2.0±0.0	1.1±0.0
23	allo-Aromadendrene	1461	1458		0.3±0.0	
24	γ -Muurolole	1476	1478	2.1±0.1	5.7±0.3	8.6±0.2
25	Germacrene D	1483	1484	17.0±0.3	18.9±0.4	27.0±0.4
26	δ -Selinene	1488	1492		9.2±0.2	0.2±0.0
27	trans-Muurolo-4(14),5-diene	1493	1493		0.7±0.0	1.8±0.1
28	Bicyclogermacrene	1497	1500	20.8±0.1	18.4±0.2	12.8±0.4
29	δ -Amorphene	1503	1509		0.6±0.2	0.6±0.1
30	Germacrene A	1508	1509	1.0±0.0	1.1±0.1	
31	γ -Cadinene	1514	1513	0.7±0.0	1.2±0.1	2.5±0.1
32	δ -Cadinene	1519	1522	2.4±0.0	3.3±0.0	6.8±0.2
33	trans-Cadina-1,4-diene	1534	1533	0.3±0.0		0.3±0.0
34	α -Cadinene	1538	1537		0.1±0.1	0.7±0.0
35	Selina-3,7(11)-diene	1543	1545			0.3±0.0
36	Germacrene B	1561	1559	0.1±0.1	5.7±0.3	6.0±0.5
37	Spathulenol	1578	1577	0.3±0.1	0.8±0.1	0.9±0.3
38	Caryophyllene oxide	1584	1582		0.4±0.0	0.4±0.1
39	Viridiflorol	1588	1592	0.4±0.0		
40	epi- α -Muurolo	1645	1640			0.2±0.3
41	α -Cadinol	1657	1652		0.1±0.2	0.5±0.2
42	neo-Intermedeol	1660	1658		0.7±0.3	
43	Abietadiene	2084	2087		0.2±0.2	
	Monoterpenes			7.9	1.0	4.1
	Sesquiterpenes			83.1	96.3	93.5
	Total Identified			91.0	97.3	97.6

RF^a (calc.), retention indices on DB-5MS column calculated according to ref. [20a]. RI^b retention indices according to ref. [20b]. Data are expressed as mean \pm SD of three analyses.

and (E)- β -ocimene (6.8%). Germacrene D (18.9%), bicyclogermacrene (18.4%), β -elemene (9.5%), δ -selinene (9.2%), (E)-caryophyllene (8.5%), germacrene B (5.7%), and γ -muurolole (5.7%) were the main compounds in the essential oil of XLMC, whereas germacrene D (27.0%), bicyclogermacrene (12.8%), (E)-caryophyllene (8.6%), γ -muurolole (8.6%), δ -cadinene (6.8%), and germacrene B (6.0%) were the major compounds in the essential oil of XLSI (Table 1).

Table 1 shows the chemical composition of the essential oils from the leaves of XFMJ, XLMC and XLSI, which were very similar, differing only in the concentrations of their constituents. These results confirm that *X. laevigata* and *X. frutescens* are typical members of the Annonaceae family, because the chemical constituents identified have been reported in the essential oils of other species of *Xylopi* [5,14]. Although the chemical constituents in the essential oils of *X. frutescens* and *X. laevigata* specimens

have been found in other essential oils of *Xylopi* species, recent studies have demonstrated significant variations in the chemical composition of the essential oils of the species of this genus.

Maia et al. [5] analyzed the chemical composition of four Amazon *Xylopi* species (*X. aromatica*, *X. cayennensis*, *X. emarginata*, and *X. nitida*) and observed variations in their chemical composition. The main compounds found in the leaf oil of *X. aromatica* were bicyclogermacrene (36.5%), spathulenol (20.5%), and limonene (4.6%); for *X. cayennensis*, α -pinene (29.2%), β -pinene (16.5%), caryophyllene oxide (14.5%), bicyclogermacrene (12.5%), germacrene D (4.7%), and 1,8-cineole (4.5%); for *X. emarginata*, spathulenol (73.0%); and for *X. nitida*, γ -terpinene (44.1%), *p*-cymene (13.7%), α -terpinene (12.6%), and limonene (11.3%). Lago et al. [14] analyzed the chemical composition of the leaves of *X. aromatica* from the Savannah region, and verified that the major compounds were α -pinene (26.1%), limonene (22.3%), bicyclogermacrene (20.4%), and β -pinene (19.0%). Tavares et al. [15] investigated the chemical constituents from the leaves of *X. langsdorffiana*, a species from northeastern Brazil, and observed that the major compounds were germacrene D (22.9%), trans- β -guaiene (22.6%), (E)-caryophyllene (15.7%), and α -pinene (7.3%). These variations in the composition of the major constituents, as well as the contents of all components, can be related to soil and climate conditions, water stress, collection place, nutrition, and other abiotic factors.

The difference between the chemical composition of species of *Xylopi* collected in the Amazon and Savannah regions has been investigated to evaluate the influence of the climatic differences [5,14], but for the species of *Xylopi* from northeastern Brazil there have been few investigations. For species of the Amazon region it has been suggested that there is a dominance of oxygenated constituents (mono- and sesquiterpenes) when compared with the species of the Savannah region [5,14]. According to our results and those of Tavares et al. [15], the *Xylopi* species from northeastern Brazil are dominated by non-oxygenated constituents (mono- and sesquiterpenes), such as (E)-caryophyllene, bicyclogermacrene, and germacrene D.

The *in vitro* trypanocidal activity against epimastigote and trypomastigote forms of *T. cruzi* is presented in Table 2. All essential oils showed significant trypanocidal action with IC₅₀ values lower than 30 $\mu\text{g}\cdot\text{mL}^{-1}$ and 15 $\mu\text{g}\cdot\text{mL}^{-1}$ against epimastigote and trypomastigote forms, respectively.

In the *in vitro* model of macrophage infection, the essential oils showed trypanocidal activity against intracellular forms of *T. cruzi* at concentrations that were non-toxic to macrophages (10 $\mu\text{g}\cdot\text{mL}^{-1}$). As shown in Figure 1, the essential oils significantly reduced ($P < 0.05$) the percentage of infected macrophages and the number of intracellular parasites, although less than the reference drug (benznidazole).

Although the oils were less effective than benznidazole, it is important to say that this drug is highly toxic to mammalian cells and its action results in a cure rate of approximately 70–80% in the acute phase and 10–20% in the chronic phase. Even after decades of research there are still no compounds able to cure all Chagas' disease patients, and no substitute for benznidazole has been developed [16].

The trypanocidal activities of the essential oils were considered very closely and could be explained by the similarity in their chemical compositions. In all the essential oils, bicyclogermacrene,

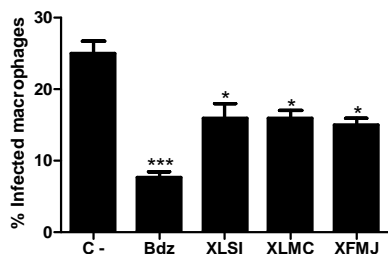
Table 2: IC₅₀ values for anti-*T. cruzi* activity.

Essential Oil	IC ₅₀ µg.mL ⁻¹	
	Epimastigote forms	Trypomastigote forms
XFMJ	20.2 (±1.4)	11.9 (±0.6)
XLMC	22.2 (±1.7)	12.7 (±1.9)
XLSI	27.7 (±0.4)	13.4 (±2.1)
Benznidazole ^a	2.8 (±0.7)	2.8 (±0.5)

Data are expressed as mean ± SD of three independent experiments.

^a Reference drug (positive control).

A



B

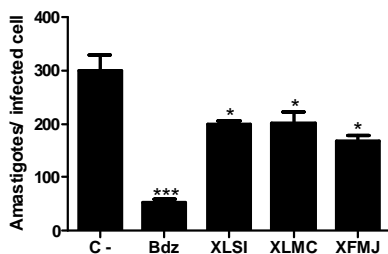


Figure 1: *Xylopiia* oils inhibited *T. cruzi* trypomastigote development in macrophages at a concentration of 10 µg.mL⁻¹. Peritoneal macrophages were infected with Y strain trypomastigotes and treated with either benznidazole (10 µg.mL⁻¹) or the essential oils (10 µg.mL⁻¹) or neither (negative control) for 6 hours. The percentage of infected macrophages (A) and the relative number of amastigotes in infected cells (B) were higher in untreated infected controls than in cultures treated the test-inhibitor XLSI, XLMC and XFMJ. Bdz (Benznidazole) was used as a positive control. Standard error of the mean is shown as error bars. ***, *P* < 0.001 vs control; *, *P* < 0.05 vs control.

(*E*)-caryophyllene and germacrene D were detected in high concentration. The significant trypanocidal activity against the different forms of *T. cruzi* could be attributed to the high concentration of these compounds. Recent works have demonstrated that essential oils with high concentration of these compounds possess antiprotozoal properties, in particular against *T. cruzi* [17,18a,b]. The results obtained in this work are considered very promising when compared with other essential oils with trypanocidal activity [17,18a,b,19a,b] and confirm that species of Annonaceae are a natural source of compounds that are biologically active with antiprotozoal properties.

This is the first report of the volatile constituents from the leaves of *X. frutescens* and *X. laevigata* and their trypanocidal action. The significant trypanocidal properties presented by the essential oils suggest that these species are a rich source of biologically active compounds. The presence of (*E*)-caryophyllene, bicyclogermacrene and germacrene D in high concentration in the essential oils could be responsible for the significant trypanocidal activity, because these compounds have been found in other essential oils with trypanocidal action. In addition, this study confirms the importance of chemical and biological investigations of essential oils of Annonaceous species, in particular *Xylopiia* spp., in the search for new and safer trypanocidal agents.

Experimental

Plant material: The leaves of *X. laevigata* were collected in January and August 2011 at the 'Parque Nacional Serra de

Itabaiana', city of Itabaiana [coordinates: S 10° 44' 53" W 37° 20' 21"] and 'Mata do Crasto' [coordinates: S 11° 24' 05" W 37° 25' 45"], city of Santa Luzia do Itanhy, respectively, whereas the leaves of *X. frutescens* were collected in January 2011 at the 'Mata do Junco, city of Capela [coordinates: S 10° 31' 45" W 37° 03' 32"], all in Sergipe State, Brazil. The identity of the plants was confirmed by Dr Ana Paula do Nascimento Prata, Departamento de Biologia, Universidade Federal de Sergipe (UFS), Brazil, and voucher specimens (24792, 21510, and 19796, respectively) have been deposited in the Herbarium of the Universidade Federal de Sergipe (ASE/UFS).

Hydrodistillation of the essential oils: The essential oils from dried leaves (for 24 h) of *X. laevigata* specimens and *X. frutescens* (200 g each) were obtained by hydrodistillation for 3 h using a Clevenger-type apparatus. The essential oils were dried over anhydrous sodium sulfate and the percentage content was calculated on the basis of the dry weight of plant material. The essential oils were stored in a freezer until analysis. The hydrodistillation was performed in triplicate.

GC-FID and CG-MS analysis of the essential oils: GC-FID analyses were carried out using a Shimadzu GC-17A fitted with a flame ionization detector (FID) and an electronic integrator. Separation of the compounds was achieved employing a ZB-5MS fused capillary column (30m X 0.25mm X 0.25µm film thickness) coated with 5%-phenyl-arylene-95%-dimethylpolysiloxane. Helium was the carrier gas at 1.0 mL.min⁻¹ flow rate. The column temperature program was 40°C/4min, at a rate of 4°C/min to 240°C, then at 10°C/min to 280°C, and at 280°C/2min. The injector and detector temperatures were 250°C and 280°C, respectively. Samples (10 mg.mL⁻¹ in CH₂Cl₂) were injected with a 1:50 split ratio. Retention indices were generated with a standard solution of *n*-alkanes (C₈-C₁₈). Peak areas and retention times were measured by an electronic integrator. The relative amounts of individual compounds were computed from GC peak areas without a FID response factor correction. GC-MS analyses were performed on a Shimadzu QP5050A GC-MS system equipped with an AOC-20i auto-injector. A J&W Scientific DB-5MS (coated with 5%-phenyl-95%-dimethylpolysiloxane) fused capillary column (30 m X 0.25 mm X 0.25 µm film thickness) was used as the stationary phase. MS were taken at 70 eV with scan intervals of 0.5s and fragments from 40-550 Da. The other conditions were similar to the GC analysis. Essential oil components were identified by comparing the retention times of the GC peaks with standard compounds run under identical conditions, and by comparison of retention indices [20a,b] and MS [20b] with those in the literature and by comparison of MS with those stored in the NIST and Wiley libraries.

In vitro trypanocidal activity: Epimastigotes of *T. cruzi* (Y strain) were maintained at 26°C in LIT medium (Liver Infusion Tryptose), supplemented with 10% fetal bovine serum (FBS; Cultilab, Campinas, SP, Brazil), 1% hemin (Sigma, Chemical Co., MO, USA), 1% R9 medium (Sigma), and 50 µg.mL⁻¹ of gentamycin (Novafarma, Anápolis, GO, Brazil). Parasites (1 × 10⁶ cells.well⁻¹) were cultured in fresh medium in the absence or presence of the essential oils at various concentrations (100 to 1.23 µg.mL⁻¹), in triplicate. Cell growth was determined after culture for 5 days by counting viable forms in a Neubauer chamber. Bloodstream trypomastigote forms of *T. cruzi* were obtained from supernatants of LLC-MK2 cells previously infected and cultured in 96-well plates (4 × 10⁵ cells.well⁻¹) in RPMI (Sigma), supplemented with 10% FBS and 50 µg.mL⁻¹ of gentamycin in the absence or presence of different concentrations of the essential oils, in triplicate. Viable (motile) parasites were counted in a Neubauer chamber 24 h later.

The percentage of inhibition was calculated in relation to untreated cultures. To determine the 50% inhibitory concentration (IC₅₀) of the epimastigote and trypomastigote forms of *T. cruzi*, nonlinear regression on Prism 5.02 GraphPad software was used.

In vitro macrophage infection and treatment with essential oils: Peritoneal exudate macrophages (2 x 10⁵ cells.well⁻¹) obtained from BALB/c mice were placed in a 24-well plate with rounded coverslips on the bottom in RPMI supplemented with 10% FBS and incubated for 24 h. Cells were then infected with trypomastigotes at a ratio of 10 parasites per macrophage for 2 h. Free trypomastigotes were removed by successive washes using saline solution. Cultures were incubated in complete medium alone or with the essential oils (10 µg.mL⁻¹) or benznidazole at the same concentration for 6 h. The medium was replaced by a fresh medium and the plate was incubated for 72 h. Cells were fixed in absolute EtOH and the

percentage of infected macrophages and the mean number of amastigotes/infected macrophages was determined by manual counting after hematoxylin and eosin staining using an optical microscope (Olympus, Tokyo, Japan). The percentage of infected macrophages and the number of amastigotes per macrophage was determined by counting 100 cells per slide. One-way ANOVA and Bonferroni tests were used to determine the statistical significance of the group comparisons.

Acknowledgments - The authors are grateful to Dr Thomas Henry from the United States National Museum (USNM), Washington DC, USA and Dr Daniela Maeda Takiya from Universidade Federal do Rio de Janeiro (UFRJ), Rio de Janeiro, Brazil for revision of the English language, and to FAPITEC/SE (Editais 07/2009 and 10/2009), FAPESB, CNPq and CAPES for financial support.

References

- [1] Chatrou LW, Pirie MD, Erkens RHJ, Couvreur TLP, Neubig KM, Abbott JR, Mols JB, Maas JW, Saunders RMK, Chase MW. (2012) A new subfamilial and tribal classification of the pantropical flowering plant family Annonaceae informed by molecular phylogenetics. *Botanical Journal of the Linnean Society*, **169**, 5-40.
- [2] (a) Corrêa MP. (1984) *Dicionário das plantas úteis do Brasil e das exóticas cultivadas*. IBDF, Rio de Janeiro, RJ; (b) Pontes AF, Mello-Silva R. (2005) Annonaceae do Parque Nacional da Serra da Canastra, Minas Gerais, Brasil. *Boletim de Botânica da Universidade de São Paulo*, **23**, 71-84.
- [3] Karioti A, Hadjipavlou-Litina D, Mensah, MLK, Fleischer TC, Skaltsa H. (2004) Composition and antioxidant activity of the essential oils of *Xylopiya aethiopyca* (Dun) A. Rich. (Annonaceae) leaves, stem bark, root bark, and fresh and dried fruits, growing in Ghana. *Journal of Agricultural and Food Chemistry*, **52**, 8094-8098.
- [4] Moreira IC, Lago JHG, Young MCM, Roque NF. (2003) Antifungal aromadendrane sesquiterpenoids from the leaves of *Xylopiya brasiliensis*. *Journal of the Brazilian Chemical Society*, **14**, 828-831.
- [5] Maia JGS, Andrade EHA, Da Silva ACM, Oliveira J, Carreira LMM, Araújo JS. (2005) Leaf volatile oils from four Brazilian *Xylopiya* species. *Flavour and Fragrance Journal*, **20**, 474-477.
- [6] Silva DM, Costa EV, Nogueira PCL, Moraes VRS, Cavalcanti SCH, Salvador MJ, Ribeiro LHG, Gadelha FR, Barison A, Ferreira AG. (2012) *Química Nova*, **35**, 1570-1576.
- [7] Puvanendran S, Wickramasinghe A, Karunaratne DN, Carr G, Wijesundara DSA, Andersen R, Karunaratne V. (2008) Antioxidant constituents from *Xylopiya championii*. *Pharmaceutical Biology*, **46**, 352-355.
- [8] Da Silva MS, Tavares JF, Queiroga KF, Agra MF, Barbosa-Filho JM, Almeida JRGS, Da Silva SAS. (2009) Alcalóides e outros constituintes de *Xylopiya langsdorffiana* (Annonaceae). *Química Nova*, **32**, 1566-1570.
- [9] López R, Cuca LE, Delgado G. (2009) Antileishmanial and immunomodulatory activity of *Xylopiya discreta*. *Parasite Immunology*, **31**, 623-630.
- [10] Castelo-Branco MVS, Tavares JF, Silva MS, Barbosa Filho JM, Anazetti MC, Frungillo L, Haun M, Diniz MFFM, Melo PS. (2011) Xyloidiol from *Xylopiya langsdorffiana* induces apoptosis in HL60 cells. *Revista Brasileira de Farmacognosia*, **21**, 1035-1042.
- [11] Nishiyama Y, Moriyasu M, Ichimaru M, Iwasa K, Kato A, Mathenge SG, Mutiso PBC, Juma FD. (2010) Antinociceptive effects of the extracts of *Xylopiya parviflora* bark and its alkaloidal components in experimental animals. *Journal of Natural Medicines*, **64**, 9-15.
- [12] Pontes WJT, Oliveira JCS, Câmara CAG, Gondim Jr. MGC, Oliveira JV, Schwartz MOE. (2007) Atividade acaricida dos óleos essenciais de folhas e frutos de *Xylopiya sericea* sobre o ácaro rajado (*Tetranychus urticae* Koch). *Química Nova*, **30**, 838-841.
- [13] Sena Filho JG, Durringer JM, Craig AM, Schuler ARP, Xavier HS. (2008) Preliminary phytochemical profile and characterization of the extract from the fruits of *Xylopiya frutescens* Aubl. (Annonaceae). *Journal of Essential Oil Research*, **20**, 536-538.
- [14] Lago JHG, De Ávila Jr. P, Moreno PRH, Limberger RP, Apel MA, Henriques AT. (2003) Analysis, comparison and variation on the chemical composition from the leaf volatile oil of *Xylopiya aromatica* (Annonaceae). *Biochemical Systematics and Ecology*, **31**, 669-672.
- [15] Tavares JF, Silva MVB, Queiroga KF, Martins RM, Silva TMS, Camara CA, Agra MF, Barbosa-Filho JM, Da Silva MS. (2007) Composition and molluscicidal properties of essential oils from leaves of *Xylopiya langsdorffiana* A. St. Hil. et Tul. (Annonaceae). *Journal of Essential Oil Research*, **19**, 282-284.
- [16] Izumi E, Ueda-Nakamura T, Dias Filho BP, Veiga Júnior VF, Nakamura CV. (2011) Natural products and Chagas' disease: a review of plant compounds studied for activity against *Trypanosoma cruzi*. *Natural Product Reports*, **28**, 809-823.
- [17] Siqueira CAT, Oliani J, Sartoratto A, Queiroga CL, Moreno, PRH, Reimão JQ, Tempone AG, Fischer DCH. (2011) Chemical constituents of the volatile oil from leaves of *Annona coriacea* Mart., Annonaceae, and *in vitro* antiprotozoal activity. *Revista Brasileira de Farmacognosia*, **21**, 33-40.
- [18] (a) Costa EV, Dutra LM, Nogueira PCL, Moraes VRS, Salvador MJ, Ribeiro LHG, Gadelha FR. (2012) Essential oil from the leaves of *Annona vepretorum*: chemical composition and bioactivity. *Natural Product Communications*, **7**, 265-266; (b) Costa EV, Dutra LM, Salvador MJ, Ribeiro LHG, Gadelha FR, Carvalho JE. (2012) Chemical composition of the essential oils of *Annona pickelii* and *Annona salzmannii* (Annonaceae), and their antitumour and trypanocidal activities. *Natural Product Research*, DOI:10.1080/14786419.2012.686913
- [19] (a) Santoro GF, Cardoso MG, Guimarães LGL, Mendonça LZ, Soares MJ. (2007) *Trypanosoma cruzi*: Activity of essential oils from *Achillea millefolium* L., *Syzygium aromaticum* L. and *Ocimum basilicum* L. on epimastigotes and trypomastigotes. *Experimental Parasitology*, **116**, 283-290; (b) Santoro GF, Cardoso MG, Guimarães LGL, Salgado APSP, Menna-Barreto RFS, Soares MJ. (2007) Effect of oregano (*Origanum vulgare* L.) and thyme (*Thymus vulgaris* L.) essential oils on *Trypanosoma cruzi* (Protozoa: Kinetoplastida) growth and ultrastructure. *Parasitology Research*, **100**, 783-790.
- [20] (a) van Den Dool H, Kratz PD. (1963) A generalization of the retention index system including linear temperature programmed gas-liquid partition chromatography. *Journal of Chromatography*, **11**, 463-471; (b) Adams RP. (2007) *Identification of Essential Oil Components by Gas Chromatography/Mass Spectrometry*. 4th ed. Allured Publ. Corp., Carol Stream, IL.

Antimicrobials from the Marine Algal Endophyte <i>Penicillium</i> sp. Andrew J. Flewelling, John A. Johnson and Christopher A. Gray	373
Antioxidant and Cytoprotective Effects of an Ethanol Extract of <i>Acalypha wilkesiana</i> var. <i>macafeana</i> from Malaysia Wardah M. Din, Jessica Chu, Garry Clarke, Khoo T. Jin, Tracey D. Bradshaw, Jeff R. Fry and Christophe Wiart	375
A New Antimicrobial and Anticancer Peptide Producing by the Marine Deep Sediment Strain “<i>Paenibacillus profundus</i>” sp. nov. SI 79 Nataliya I. Kalinovskaya, Lyudmila A. Romanenko, Anatoly I. Kalinovskiy, Pavel S. Dmitrenok and Sergey A. Dyshlovoy	381
Potential Applications for <i>Annona squamosa</i> Leaf Extract in the Treatment and Prevention of Foodborne Bacterial Disease Achara Dholvitayakhun, Nathanon Trachoo, Uthai Sakee and T.P. Tim Cushman	385
Genoprotective Effect of the Chinese Herbal Decoction Xiao Jian Zhong Tang Yim-Tong Szeto, Ngok-Fung Cheng, Sok-Cheon Pak and Wouter Kalle	389
Effect of Nine Plant Volatiles in the Field on the Sex Pheromones of <i>Leguminivora glycinivorella</i> Daihua Hu, Juntao Feng, Zhihui Wang, Hua Wu and Xing Zhang	393
Induction of Defensive Response in <i>Eucalyptus globulus</i> Plants and its Persistence in Vegetative Propagation Christian Troncoso, Claudia Perez, Victor Hernandez, Manuel Sanchez-Olate, Darcy Rios, Aurelio San Martin and José Becerra	397
Chemical Composition of the Essential Oil of <i>Baccharoides lilacina</i> from India Rajesh K. Joshi	401
Chemical Composition and Anti-<i>Trypanosoma cruzi</i> Activity of Essential Oils Obtained from Leaves of <i>Xylopi frutescens</i> and <i>X. laevigata</i> (Annonaceae) Thanany Brasil da Silva, Leociley Rocha Alencar Menezes, Marília Fernanda Chaves Sampaio, Cássio Santana Meira, Elisalva Teixeira Guimarães, Milena Botelho Pereira Soares, Ana Paula do Nascimento Prata, Paulo Cesar de Lima Nogueira and Emmanoel Vilaça Costa	403
Chemical Composition and Biological Activities of the Essential Oil from <i>Artemisia herba-alba</i> Growing Wild in Tunisia Ismail Amri, Laura De Martino, Aurelio Marandino, Hamrouni Lamia, Hanana Mohsen, Elia Scandolera, Vincenzo De Feo and Emilia Mancini	407
<i>Aloe ferox</i> Seed: A Potential Source of Oil for Cosmetic and Pharmaceutical Use Rachael Dangarembizi, Eliton Chivandi and Kennedy Erlwanger	411
<u>Review/Account</u>	
Therapeutic Effects of Glycyrrhizic Acid Lee Jia Ming and Adeline Chia Yoke Yin	415
Natural Products of Mineral Origin Massimiliano Laudato, Luigi Pescitelli and Raffaele Capasso	419
<u>Addition/Correction</u>	
Chemical Composition and Biological Activities of Soldiers of the Brazilian Termite Species, <i>Nasutitermes macrocephalus</i> (Isoptera: Natutitermitinae) Márcia N. S. de la Cruz, Helvécio M. S. Júnior, Denilson F. Oliveira, Letícia V. Costa-Lotufo, Antonio G. Ferreira, Daniela S. Alviano and Claudia M. Rezende	424

Natural Product Communications

2013

Volume 8, Number 3

Contents

<u>Original Paper</u>	<u>Page</u>
Metabolites from the Aerial Parts of the Sicilian Population of <i>Artemisia alba</i> Antonella Maggio, Sergio Rosselli, Celeste Laura Brancazio, Vivienne Spadaro, Francesco Maria Raimondo and Maurizio Bruno	283
New Bioactive Secondary Metabolites from Bornean Red Alga, <i>Laurencia similis</i> (Ceramiales) Takashi Kamada and Charles Santharaju Vairappan	287
A New Bioactive Sesquiterpenoid Quinone from the Mediterranean Sea Marine Sponge <i>Dysidea avara</i> Ashraf Nageeb El-Sayed Hamed, Wim Wätjen, Roland Schmitz, Yvonne Chovolou, RuAngelie Edrada-Ebel, Diaa T. A. Youssef, Mohammed Salah Kamel and Peter Proksch	289
An Efficient Oxyfunctionalization of Quinopimaric Acid Derivatives with Ozone Oxana B. Kazakova, Elena V. Tretyakova, Irina E. Smirnova, Timur I. Nazyrov, Ol'ga S. Kukovinets, Genrikh A. Tolstikov and Kiryll Yu. Suponitskii	293
Plants from Northeast Mexico with Anti-HSV Activity David Silva-Mares, Ernesto Torres-López, Ana M Rivas-Estilla, Paula Cordero-Pérez, Noemí Waksman-Minsky and Verónica M Rivas-Galindo	297
The True Identity of the Triterpene Component of <i>Wyethia mollis</i>, a Lanosta-diene Containing a Tetrahydropyran E-ring Cole T. Smith, Bruce Noll, Thomas G. Waddell and Kyle S. Knight	299
Structures and Biological Activities of Typicosides A₁, A₂, B₁, C₁ and C₂, Triterpene Glycosides from the Sea Cucumber <i>Actinocucumis typica</i> Alexandra S. Silchenko, Anatoly I. Kalinovskiy, Sergey A. Avilov, Pelageya V. Andryjaschenko, Pavel S. Dmitrenko, Ekaterina A. Martyyas, Vladimir I. Kalinin, P. Jayasandhya, Gigi C. Rajan and Krishna P. Padmakumar	301
Preparation and Application of Reversed Phase Chromatorotor™ for the Isolation of Natural Products by Centrifugal Preparative Chromatography Ilias Muhammad, Volodymyr Samoylenko, Francis Machumi, Mohamed Ahmed Zaki, Rabab Mohammed, Mona H. Hetta and Van Gillum	311
Chemical Constituents of the Leaves of <i>Dracaena thalioides</i> Akihito Yokosuka, Atsushi Sekiguchi and Yoshihiro Mimaki	315
7-Oxidioscin, a New Spirostan Steroid Glycoside from the Rhizomes of <i>Dioscorea nipponica</i> Zulfiqar Ali, Troy J. Smillie and Ikhlās A. Khan	319
Two Spirostan Steroid Glycoside Fatty Esters from <i>Dioscorea cayenensis</i> Zulfiqar Ali, Troy J. Smillie and Ikhlās A. Khan	323
GC-MS Investigation of Amaryllidaceae Alkaloids in <i>Galanthus xvalentinei</i> nothosubsp. <i>subplicatus</i> Buket Bozkurt Sarikaya, Strahil Berkov, Jaime Bastida, Gulen Irem Kaya, Mustafa Ali Onur and Nehir Unver Somer	327
Antifouling Indole Alkaloids from Two Marine Derived Fungi Fei He, Zhuang Han, Jiang Peng, Pei-Yuan Qian and Shu-Hua Qi	329
Andrographidine G, a New Flavone Glucoside from <i>Andrographis paniculata</i> Swarna D. Hapuarachchi, Zulfiqar Ali, Naohito Abe, Suresh T. Sugandhika, Senerath T. P. Sandun and Ikhlās A. Khan	333
Geranyl Flavonoids from <i>Robinia pseudoacacia</i> Lai-Bin Zhang, Jie-Li Lv and Hui Zhang	335
Antibacterial Activity Against <i>Ralstonia solanacearum</i> of Phenolic Constituents Isolated from Dragon's Blood Hui Wang, Ying Luo, Haofu Dai and Wenli Mei	337
Interaction of Dihydromyricetin and α-Amylase Lei Chen, Chao Wang, Qingyi Wei, Zhengxiang Ning and Erdong Yuan	339
Effect of the Isoflavone Genistein on Tumor Size, Metastasis Potential and Melanization in a B16 Mouse Model of Murine Melanoma Corina Danciu, Florin Borcan, Florina Bojin, Istvan Zupko and Cristina Dehelean	343
Quantitative Analysis of Total Flavonoids and Total Phenolic Acids in Thirty <i>Hypericum</i> Taxa Kroata Hazler Pilepić, Željko Maleš and Maja Crkvenčić	347
New Diarylheptanoids and a Hydroxylated Otelione from <i>Ottelia alismoides</i> Thomas R. Hoye, Seif-Eldin N. Ayyad, Hollie J. Beckord and Susan G. Brown	351
Evaluation of the <i>in vivo</i> Anti-inflammatory and Analgesic and <i>in vitro</i> Anti-cancer Activities of Curcumin and its Derivatives James N. Jacob, Dinesh K. Badyal, Suman Bala and Masoud Toloué	359
Chemical Constituents from <i>Dendropanax dentiger</i> Yi-Chun Lai and Shoen-Sheng Lee	363
Six New Phenolic Glycosides and a New Ceramide from the Flowers of <i>Wedelia biflora</i> and Their Cytotoxicity Against Some Cancer Cell Lines Nguyen T. H. Thu, Le T. Ha, Vo T. Nga, Pham N. K. Tuyen, Ton T. Quang, Forde-Riddick Danielle, Pratt Lawrence M. and Nguyen K. P. Phung	367

Continued Inside Backcover

ANEXO 4

Vasconcelos JF, Souza BF, Lins TF, Garcia LM, Kaneto CM, Sampaio GP, de Alcântara AC, **Meira CS**, Macambira SG, Ribeiro-dos-Santos R, Soares MB. Administration of granulocyte colony-stimulating factor induces immunomodulation, recruitment of T regulatory cells, reduction of myocarditis and decrease of parasite load in a mouse model of chronic Chagas disease cardiomyopathy. **FASEB Journal**. v. 27, p. 4691-4702, 2013.

Administration of granulocyte colony-stimulating factor induces immunomodulation, recruitment of T regulatory cells, reduction of myocarditis and decrease of parasite load in a mouse model of chronic Chagas disease cardiomyopathy

Juliana F. Vasconcelos,^{*,†} Bruno S. F. Souza,^{*,†} Thayse F. S. Lins,^{*}
Letícia M. S. Garcia,[†] Carla M. Kaneto,^{†,‡} Geraldo P. Sampaio,[†]
Adriano C. de Alcântara,[†] Cássio S. Meira,^{*} Simone G. Macambira,^{*,†,§}
Ricardo Ribeiro-dos-Santos,[†] and Milena B. P. Soares^{*,†,1}

^{*}Centro de Pesquisas Gonçalo Moniz, Fundação Oswaldo Cruz, Salvador, Bahia, Brazil; [†]Centro de Biotecnologia e Terapia Celular, Hospital São Rafael, Salvador, Bahia, Brazil; [‡]Universidade Estadual de Santa Cruz, Ilhéus, Bahia, Brazil; and [§]Universidade Federal da Bahia, Salvador, Bahia, Brazil

ABSTRACT Chagas disease, caused by *Trypanosoma cruzi* infection, is a leading cause of heart failure in Latin American countries. In a previous study, we showed beneficial effects of granulocyte colony-stimulating factor (G-CSF) administration in the heart function of mice with chronic *T. cruzi* infection. Presently, we investigated the mechanisms by which this cytokine exerts its beneficial effects. Mice chronically infected with *T. cruzi* were treated with human recombinant G-CSF (3 courses of 200 µg/kg/d for 5 d). Inflammation and fibrosis were reduced in the hearts of G-CSF-treated mice, compared with the hearts of vehicle-treated mice, which correlated with decreased syndecan-4, intercellular adhesion molecule-1, and galectin-3 expressions. Marked reductions in interferon-γ and tumor necrosis factor-α and increased interleukin-10 and transforming growth factor-β were found after G-CSF administration. Because the therapy did not induce a Th1 to Th2 immune response deviation, we investigated the role of regulatory T (T_{reg}) cells. A significant increase in CD3⁺Foxp3⁺ cells was observed in the hearts of G-CSF-treated mice. In addition, a reduction of parasitism was observed after G-CSF treatment. Our results indicate a role of T_{reg} cells in the immunosuppression induced by G-CSF treatment and reinforces its potential therapeutic use for patients with Chagas disease.—Vasconcelos, J. F., Souza, B. S. F., Lins, T. F. S., Garcia,

L. M. S., Kaneto, C. M., Sampaio, G. P., de Alcântara, A. C., Meira, C. S., Macambira, S. G., Ribeiro-dos-Santos, R., Soares, M. B. P. Administration of granulocyte colony-stimulating factor induces immunomodulation, recruitment of T regulatory cells, reduction of myocarditis and decrease of parasite load in a mouse model of chronic Chagas disease cardiomyopathy. *FASEB J.* 27, 4691–4702 (2013). www.fasebj.org

Key Words: *Trypanosoma cruzi* • cytokine therapy • inflammation • fibrosis • Th1 modulation

CHAGAS DISEASE, CAUSED BY infection with *Trypanosoma cruzi*, is considered a neglected tropical disease endemic in Latin American countries that mainly affects the poorest populations (1, 2). Although recent data indicate a reduction in the number of infected people as a result of vector transmission control, it is estimated that 10 million individuals are infected and 25 million are at risk of acquiring the disease (3, 4). About 70% of infected individuals remain asymptomatic, whereas 30% will develop the chronic symptomatic form of Chagas disease. Chronic chagasic cardiomyopathy (CCC), the most common symptomatic form of the disease, is one of the leading causes of heart failure. The only available treatment is heart transplantation, a high-cost procedure, that is limited by organ donation and presents severe complications in patients with Chagas disease due to infection reactivation after immunosuppressant administration (5).

Abbreviations: CCC, chronic chagasic cardiomyopathy; DAPI, 4,6-diamidino-2-phenylindole dihydrochloride; DMEM, Dulbecco's modified Eagle's medium; ELISA, enzyme-linked immunosorbent assay; FBS, fetal bovine serum; Foxp3, forkhead box P3; G-CSF, granulocyte colony-stimulating factor; ICAM-1, intercellular adhesion molecule 1; IL, interleukin; IFN-γ, interferon-γ; RT-qPCR, reverse transcription-quantitative polymerase chain reaction; PBS, phosphate-buffered saline; TGF-β, transforming growth factor-β; TNF-α, tumor necrosis factor-α; T_{reg}, regulatory T

¹ Correspondence: Centro de Pesquisas Gonçalo Moniz, Fundação Oswaldo Cruz, Rua Waldemar Falcão, 121, Candé, Salvador, Bahia, Brazil 40296-710. E-mail: milena@bahia.fiocruz.br

doi: 10.1096/fj.13-229351

Granulocyte colony-stimulating factor (G-CSF) is a pleiotropic cytokine that stimulates the production of neutrophils and releases bone marrow stem cells into the peripheral circulation. It has been in clinical use for nearly 2 decades, mainly as an adjunctive medication to chemotherapy or to mobilize stem cells for bone marrow transplantation (6). In addition to neutrophils and their precursors, monocytes are direct target cells of G-CSF action (7, 8). The administration of G-CSF in models of cardiac ischemic diseases has also shown the potential use of this cytokine in regenerative medicine (9–11).

Evidence is now accumulating that G-CSF also has immunomodulatory effects on adaptive immune responses mediated through several mechanisms, including activation of regulatory T (T_{reg}) cells (12). T_{reg} cells express the regulatory lineage factor forkhead box P3 (Foxp3), comprise 5–10% of peripheral $CD4^+$ T cells, and are known as natural T_{reg} cells (13). $CD4^+$ T cells from G-CSF-mobilized stem cell donors are able to suppress alloproliferative responses of autologous T cells in a cell contact-independent manner, by acquiring a T_{reg} -like cytokine profile (14). G-CSF drives the *in vitro* differentiation of human dendritic cells that express tolerogenic markers involved in T_{reg} cell induction (15).

We have previously demonstrated that administration of G-CSF in mice with chronic heart lesions caused by *T. cruzi* infection improved cardiac structure and function (16). Here we investigate the immunomodulatory effects of G-CSF in a mouse model of chronic Chagas disease, by investigating the modulation of key inflammatory mediators and the participation of T_{reg} cells.

MATERIALS AND METHODS

Animals

Four-week-old male C57BL/6 mice were used for *T. cruzi* infection and as normal controls. All animals were raised and maintained at the Gonçalo Moniz Research Center, Fundação Oswaldo Cruz (FIOCRUZ) in rooms with controlled temperature ($22 \pm 2^\circ\text{C}$) and humidity ($55 \pm 10\%$) and continuous air flow. Animals were housed in a 12 h-light-dark cycle (6:00 AM–6:00 PM) and provided with rodent diet and water *ad libitum*. Animals were handled according to the U.S. National Institutes of Health guidelines for animal experimentation. All procedures described had prior approval

from the local animal ethics committee under number L-002/11 (FIOCRUZ, Bahia, Brazil).

T. cruzi infection and G-CSF administration

Trypomastigotes from the myotropic Colombian *T. cruzi* strain (17) were obtained from culture supernatants of infected LLC-MK2 cells. Infection of C57BL/6 mice was performed by intraperitoneal injection of 100 *T. cruzi* trypomastigotes in saline. Parasitemia of infected mice was evaluated at different time points after infection by counting the number of trypomastigotes in peripheral blood aliquots. Groups of chronic chagasic mice (6 mo after infection) were treated intraperitoneally ($200 \mu\text{g}/\text{kg}/\text{d}$) with 3 administered courses of human recombinant G-CSF (Filgrastim; Bio Sidus S.A., Buenos Aires, Argentina) for 5 consecutive d with an interval of 9 d between the courses (Fig. 1). Control chagasic mice received saline solution in the same regimen.

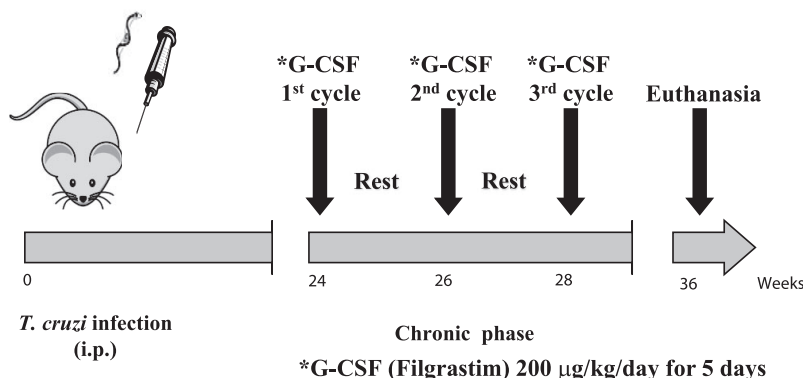
Morphometric analyses

Groups of mice were euthanized 2 mo after the therapy under anesthesia [5% ketamine (Vetanarcol; König, Santana de Parnaíba, Brazil) and 2% xylazine (Sedomin; König)], and hearts were removed and fixed in 10% buffered formalin. Heart sections were analyzed by light microscopy after paraffin embedding, followed by standard hematoxylin and eosin staining. Inflammatory cells infiltrating heart tissue were counted using a digital morphometric evaluation system. Images were digitized using a color digital video camera (CoolSnap, Photometrics, Montreal, QC, Canada) adapted to a BX41 microscope (Olympus, Tokyo, Japan). Morphometric analyses were performed using the software Image-Pro Plus v.7.0 (Media Cybernetics, San Diego, CA, USA). The inflammatory cells were counted in 10 fields ($\times 400$ view)/heart. The percentage of fibrosis was determined using Sirius red-stained heart sections and Image-Pro Plus v.7.0 to integrate the areas; 10 fields per animal were captured using $\times 200$ view. All of the analyses were performed in a blinded fashion.

Confocal immunofluorescence analyses

Frozen or formalin-fixed paraffin-embedded hearts were sectioned, and 4- μm -thick sections were used for detection of syndecan-4, intercellular adhesion molecule-1 (ICAM-1), galectin-3, CD3, Foxp3, and interleukin (IL)-10 expression by immunofluorescence. First, paraffin-embedded sections were deparaffinized and submitted to a heat-induced antigen retrieval step by incubation in citrate buffer (pH 6.0). Then, sections were incubated overnight with the following primary antibodies: anti-syndecan-4 (1:50; Santa Cruz Biotechnology,

Figure 1. Experimental design. C57BL/6 mice were infected with 100 Colombian strain *T. cruzi* trypomastigotes and treated during the chronic phase of infection with human recombinant G-CSF, as indicated.



Santa Cruz, CA, USA), anti-ICAM-1 (1:50; BD Biosciences, San Jose, CA, USA), anti-CD3 (1:400; BD Biosciences), anti-Foxp3 (1:400; Dako, Glostrup, Denmark), or anti-IL-10 (1:100; BD Biosciences). On the following day, sections were incubated for 1 h with Alexa Fluor 633- or Alexa Fluor 488-conjugated phalloidin (1:200), mixed with one of the following secondary antibodies: Alexa Fluor 594-conjugated anti-goat IgG (1:200) or Alexa Fluor 488-conjugated anti-rabbit IgG (1:200; Molecular Probes, Carlsbad, CA, USA). Nuclei were stained with 4,6-diamidino-2-phenylindole (DAPI; VectaShield Hard Set mounting medium with DAPI H-1500; Vector Laboratories, Burlingame, CA, USA). The presence of fluorescent cells was determined by observation on a FluoView 1000 confocal microscope (Olympus). Quantifications of galectin-3⁺ cells, syndecan-4⁺ blood vessels, and ICAM-1⁺ percentual area were performed in 10 random fields captured under $\times 400$ magnification, using Image-Pro Plus v.7.0.

Real-time reverse transcription-quantitative polymerase chain reaction (RT-qPCR)

Total RNA was isolated from heart samples with TRIzol reagent (Molecular Probes) and concentration was determined by photometric measurement. A High Capacity cDNA Reverse Transcription Kit (Applied Biosystems, Foster City, CA, USA) was used to synthesize cDNA from 1 μ g of RNA following the manufacturer's recommendations. RT-qPCR assays were performed to detect the expression levels of *Tbet* (Mm_00450960_m1), *GATA3* (Mm_00484683_m1), and *G-CSF* (Mm_00438334_m1). The RT-qPCR amplification mixtures contained 20 ng of template cDNA, TaqMan Master Mix (10 μ l), and probes in a final volume of 20 μ l (all from Applied Biosystems). All reactions were run in duplicate on an ABI 7500 sequence detection system (Applied Biosystems) under standard thermal cycling conditions. The mean C_t (cycle threshold) values from duplicate measurements were used to calculate expression of the target gene, with normalization to an internal control (*GAPDH*) using the $2^{-\Delta\Delta C_t}$ formula. Experiments with coefficients of variation $> 5\%$ were excluded. A nontemplate control and nonreverse transcription controls were also included.

Flow cytometry analysis

Quantitative analysis of T_{reg} cells was performed in the bone marrow and spleen of G-CSF- or saline-treated chronic chagasic mice, by flow cytometry. In brief, mice were treated with one course of G-CSF or saline and were euthanized under anesthesia the day after the final dose. Bone marrow cells were obtained from mice femurs. The bone marrow was collected by flushing the bones with Dulbecco's modified Eagle's medium (DMEM), followed by cell purification by centrifugation in Ficoll (Histopaque 1119 and 1077, 1:1; Sigma-Aldrich, St. Louis, MO, USA) gradient at 1000 g for 15 min. The spleens were collected, washed in DMEM, and homogenized by pressing through a 40-mm cell strainer. Bone marrow and spleen cells were counted and resuspended in phosphate-buffered saline (PBS) buffer [1% fetal bovine serum (FBS) in PBS]. For flow cytometry, cells were stained with labeled anti-CD4 PE-Cy5.5 and CD25 APC antibodies (BD Biosciences) for 20 min at room temperature. Cells were washed and analyzed using a cell analyzer (LSRFortessa; BD Biosciences) with FACSDiva software (version 6.1.3; BD Biosciences).

Cytokine assessment

Cytokine concentrations were measured in total spleen or heart protein extracts and in sera. Tissue proteins were

extracted at 50 mg of tissue/500 ml of PBS to which 0.4 M NaCl, 0.05% Tween 20, and protease inhibitors (0.1 mM phenylmethylsulfonyl fluoride, 0.1 mM benzethonium chloride, 10 mM EDTA, and 20 kIU of aprotinin A/100 ml) were added. The samples were centrifuged for 10 min at 3000 g , and the supernatants were immediately used in enzyme-linked immunosorbent assays (ELISAs) or frozen at -70°C for later quantification. Interferon- γ (IFN- γ), tumor necrosis factor- α (TNF- α), transforming growth factor- β (TGF- β), IL-4, IL-6, IL-10, or IL-17 was quantified from individual mice by ELISA using specific antibody kits (R&D Systems, Minneapolis, MN, USA), according to the manufacturer's instructions. In brief, 96-well plates were blocked and incubated at room temperature for 1 h. Samples were added in duplicate and incubated overnight at 4°C . Biotinylated antibodies were added, and plates were incubated for 2 h at room temperature. A 0.5-h incubation with streptavidin-horseradish peroxidase conjugate was followed by detection using 3,3',5,5'-tetramethylbenzidine peroxidase substrate and reading at 450 nm.

Quantification of parasite load

T. cruzi DNA was quantified in heart samples by qPCR analysis. For DNA extraction, heart fragments were submitted to DNA extraction using the NucleoSpin Tissue Kit (Machenerey-Nagel, Düren, Germany), as recommended by the manufacturer. In brief, 10 mg of each heart sample was submitted to DNA extraction, and the DNA amount and purity (260/280 nm) were analyzed by Nanodrop 2000 spectrophotometry (Thermo Fisher Scientific, Waltham, MA, USA). Kapa Probe Fast Universal 2X qPCR Master Mix was used to perform the qPCR in 20- μ l reactions, including ROX low as the passive reference, as recommended by the manufacturer (Kapa Biosystems Inc., Woburn, MA, USA). Primers were designed based on the report by Schijman *et al.* (18), and the amounts used per reaction were 0.4 μ M concentrations of both primers (primer 1, 5'-GTTCA-CACACTGGACACCAA-3' and primer 2, 5'-TCGAAAACGAT-CAGCCGAST-3') and a 0.2 μ M concentration of the probe (SatDNA specific probe, 5'-/56-FAM/AATTCCTCC/ZEN/AAGCAGCGGATA/3IABkFQ/-3'), all included in a Mini PrimeTime qPCR assay (Integrated DNA Technologies, Inc., Coralville, IA, USA). Amounts of 1 μ l for each point of the standard curve, samples, and controls were applied to different wells of a PCR microplate (Axygen, Union City, CA, USA), film sealed, and submitted to amplification. Cycles were performed in an ABI 7500 system (Applied Biosystems) as follows: first, 3 min at 95°C for *Taq* activation; and second, 45 cycles at 95°C for 10 s followed by 55°C for 30 s. To calculate the number of parasites per milligram of tissue, each plate contained an 8-log standard curve of DNA extracted from trypomastigotes of the Colombian *T. cruzi* strain (ranging from 4.7×10^{-1} to 4.7×10^6) in duplicate. Data were analyzed using 7500 software 2.0.1 (Applied Biosystems).

Assessment of trypanocidal activity

T. cruzi epimastigotes (Colombian strain) were maintained at 26°C in liver infusion tryptose medium supplemented with 10% FBS, 1% hemin (Sigma-Aldrich), 1% R9 medium (Sigma-Aldrich), and 50 μ g/ml gentamicin. Parasites were counted in a hemocytometer and then dispensed into 96-well plates at a cell density of 5×10^6 cells/ml in the absence or presence of the human recombinant G-CSF at 3, 10, or 30 μ g/ml in triplicate. The plate was incubated for 5 d at 26°C , aliquots of each well were collected, and the number of viable parasites was counted in a Neubauer chamber. Trypomastigote forms of *T. cruzi* were obtained from supernatants of LLC-MK2 cells previously infected and cultured in 96-well plates at a cell

density of 2×10^6 cells/ml in RPMI 1640 medium (Sigma-Aldrich) supplemented with 10% FBS and 50 $\mu\text{g/ml}$ gentamicin in the absence or presence of human recombinant G-CSF. After 24 h of incubation, the number of viable parasites, based on parasite motility, was assessed in a Neubauer chamber and compared with that of an untreated parasite culture to calculate the percentage of inhibition. Benznidazole (30 $\mu\text{g/ml}$) was used as a positive control. For *in vitro* infection, peritoneal macrophages obtained from C57BL/6 mice were seeded at a cell density of 2×10^5 cells/ml in a 24-well plate with rounded coverslips on the bottom in RPMI 1640 medium supplemented with 10% FBS and 50 $\mu\text{g/ml}$ gentamicin and incubated for 24 h. Cells were then infected with trypomastigotes (1:10) for 2 h. Free trypomastigotes were removed by successive washes using saline solution. Cultures were incubated in complete medium alone or with G-CSF (2, 6, or 10 $\mu\text{g/ml}$) or benznidazole (10 $\mu\text{g/ml}$) for 6 h. The medium was then replaced by fresh medium, and the plate was incubated for 3 d at 37°C. Cells were fixed in absolute alcohol, and the percentage of infected macrophages and the mean number of amastigotes/100 infected macrophages was determined by manual counting after hematoxylin and eosin staining using an optical microscope (Olympus).

Evaluation of anti-*T. cruzi* antibodies

T. cruzi-specific, total IgG, IgG1, and IgG2 antibodies were detected in the sera of naive or G-CSF- or saline-treated chronic chagasic mice by ELISA. Microtiter plates were coated overnight at 4°C with *T. cruzi* trypomastigote antigen (3 $\mu\text{g/ml}$) in 50 μl of carbonate-bicarbonate buffer (pH 9.6). The plates were washed 3 times with PBS containing 0.05% Tween 20 and then blocked by incubation at room temperature for 1 h with PBS-5% nonfat milk. After washing, the plates were incubated with 50 μl of a 1:200 (IgG) or 1:100 (IgG1 or IgG2a) dilution of each serum sample at 37°C for 2 h. The plates were washed, and a 1:1000 dilution of goat anti-mouse IgG (Sigma-Aldrich) or rat anti-mouse IgG1 or IgG2a (BD Biosciences) was incubated for 1 h at room temperature. After washing, peroxidase-conjugated anti-mouse polyvalent immunoglobulins (Sigma-Aldrich) diluted 1:1000 were dispensed into each well, and the plate was incubated for 30 min at room temperature followed by detection using 3,3',5,5'-tetramethylbenzidine peroxidase substrate and read at 450 nm.

Statistical analyses

All continuous variables are presented as means \pm SEM. Morphometric and cytokine levels were analyzed using 1-way analysis of variance, followed by a Newman-Keuls multiple comparison test with Prism 3.0 (GraphPad Software, San Diego, CA, USA). All differences were considered significant at values of $P < 0.05$.

RESULTS

Administration of G-CSF reduces inflammation and fibrosis in hearts of chronic chagasic mice

Multifocal inflammation, mainly composed of mononuclear cells, and fibrosis were found in the hearts of *T. cruzi*-infected mice during the chronic phase of the disease (Fig. 2A, B). Administration of G-CSF reduced

the number of inflammatory cells and the fibrotic area in chronic chagasic hearts (Fig. 2C, D). Morphometric analysis showed a statistically significant reduction of inflammation and fibrosis after G-CSF treatment, compared with the saline-treated controls (Fig. 2E, F).

Reduction of syndecan-4, ICAM-1, and galectin-3 expression in the hearts of G-CSF-treated mice

We have previously shown the overexpression of syndecan-4, ICAM-1, and galectin-3 in the hearts of chronic chagasic mice (19). To evaluate the effects of G-CSF on the expression of these inflammation markers, we performed confocal microscopy analysis in heart sections of mice from the 3 different groups. A marked decrease in syndecan-4 production, which is highly expressed in blood vessels of chagasic hearts, was seen after G-CSF treatment (Fig. 3A, B). Morphological analyses revealed a statistically significant difference (Fig. 3C). Similarly, the expression of ICAM-1, mainly in inflammatory cells and cardiomyocytes in hearts of chronic chagasic mice, was significantly decreased after G-CSF treatment (Fig. 3D–F). Moreover, the high expression of galectin-3 in inflammatory cells was down-regulated in mouse hearts treated with G-CSF, which correlated to decreased inflammation (Fig. 3G–I).

Modulation of cytokine production after G-CSF administration

CCC has been associated with increased IFN- γ and TNF- α production in mice and in humans (19, 20). The concentrations of these two proinflammatory cytokines were increased in heart extracts from saline-treated chagasic mice, compared with those in normal mice. The administration of G-CSF promoted a statistically significant reduction in the concentrations of both cytokines (Fig. 4A, B). In contrast, a significant increase in TGF- β and IL-10 concentrations was observed in G-CSF-treated chagasic mice hearts compared with that in saline-treated controls (Fig. 4C, D). No significant differences were measured in IL-17 and IL-4 concentrations (Fig. 4E, F). Moreover, RT-qPCR analysis showed a significant decrease in *Tbet* gene expression after G-CSF administration (Fig. 4G), but no significant alterations in *GATA3* gene expression were observed in the hearts of chronic chagasic mice (Fig. 4H).

The systemic effects of G-CSF on cytokine production were also investigated. G-CSF increased IL-10 production in the spleens of chagasic mice compared with that in uninfected and saline-treated mice (Fig. 5A). This effect was also correlated with a reversion in the overexpression of IL-17, TNF- α , and IFN- γ in sera or in the spleens of G-CSF-treated mice (Fig. 5B–E). In addition, G-CSF administration also induced an increase in *G-CSF* gene expression in the spleens of chagasic mice (Fig. 5F).

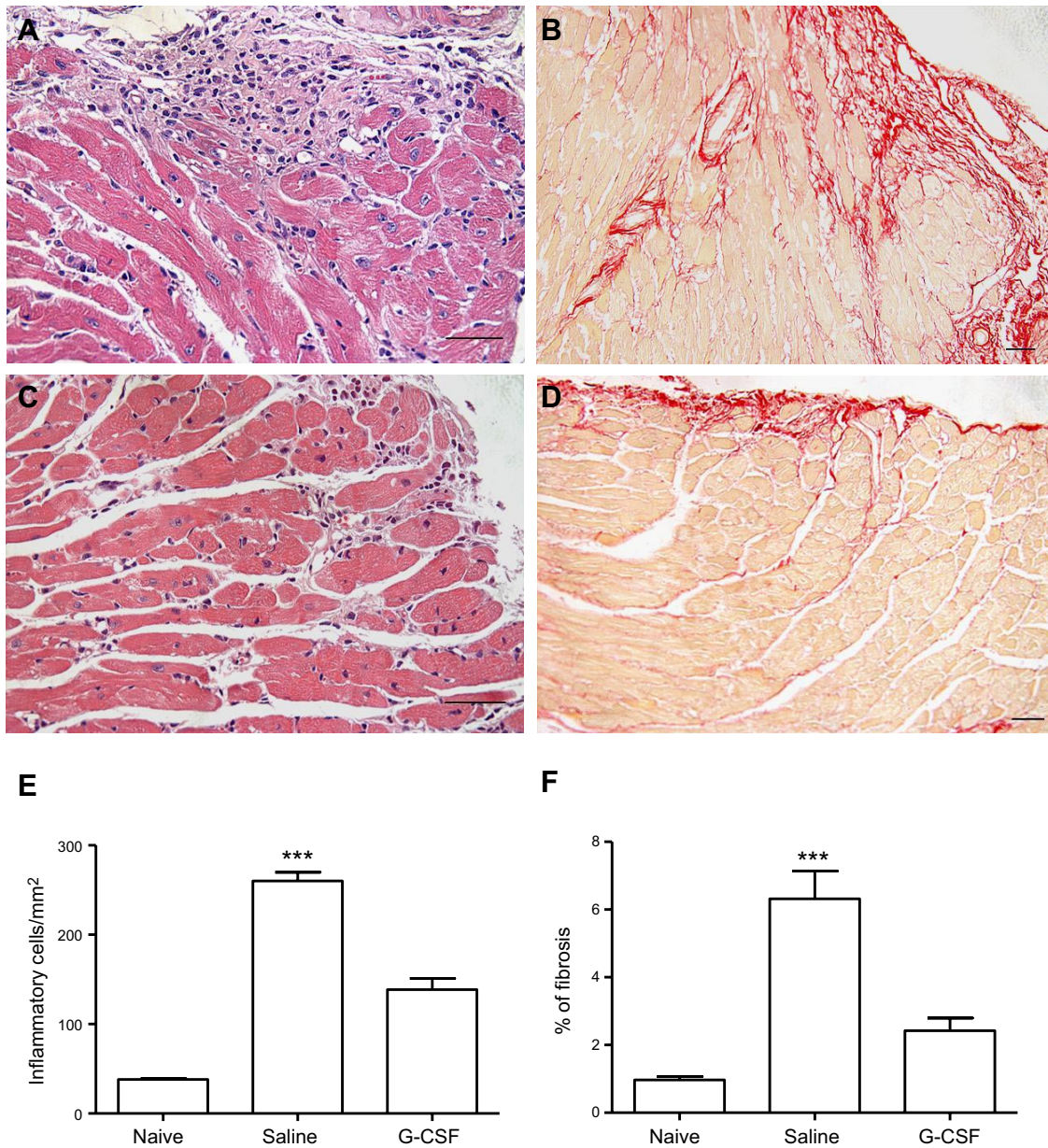


Figure 2. Reduction of inflammation and fibrosis in the hearts of chagasic mice after G-CSF administration. Groups of C57BL/6 mice in the chronic phase of infection (6 mo) were treated with saline (*A, B*) or G-CSF (*C, D*). *A, C*) heart sections stained with hematoxylin and eosin. *B, D*) Heart sections stained with Sirius red. *E*) Inflammatory cells were quantified in heart sections of naive mice, saline-treated chagasic mice, or G-CSF-treated chagasic mice and integrated by area. *F*) Fibrotic area is represented by percentage of collagen deposition in heart sections. Bars represent means \pm SEM of 9–10 mice/group. *** $P < 0.001$.

G-CSF therapy increases the percentage of T_{reg} cells in the hearts of chagasic mice

Next, we examined whether G-CSF administration altered the number of T_{reg} cells in chagasic mice. G-CSF caused a decrease in the percentage of $CD4^+CD25^+$ cells in the bone marrow of chagasic mice (**Fig. 6A–C**). Foxp3 expression was analyzed in cardiac $CD3^+$ cells by immunofluorescence. A higher percentage of $CD3^+$ Foxp3⁺ T-cell expression was found in the hearts of G-CSF-treated mice compared with those of saline-treated mice (**Fig. 6D–F**). A partial recovery of $CD4^+CD25^+$ cells in the spleens of chagasic mice was observed after G-CSF

administration (**Fig. 6G**), and splenic Foxp3⁺ cells coexpressed IL-10 (**Fig. 6H**).

Effects of G-CSF administration on *T. cruzi* infection

To investigate whether the suppressive response induced by G-CSF treatment affected the immune response against the parasite, we first analyzed parasite-specific antibody levels in the sera of mice from the different experimental groups. Total IgG anti-*T. cruzi* antibody levels were similar between G-CSF and saline-treated chagasic mice (**Fig. 7A**). A significant increase in IgG1 but not in IgG2 anti-*T. cruzi* antibodies was

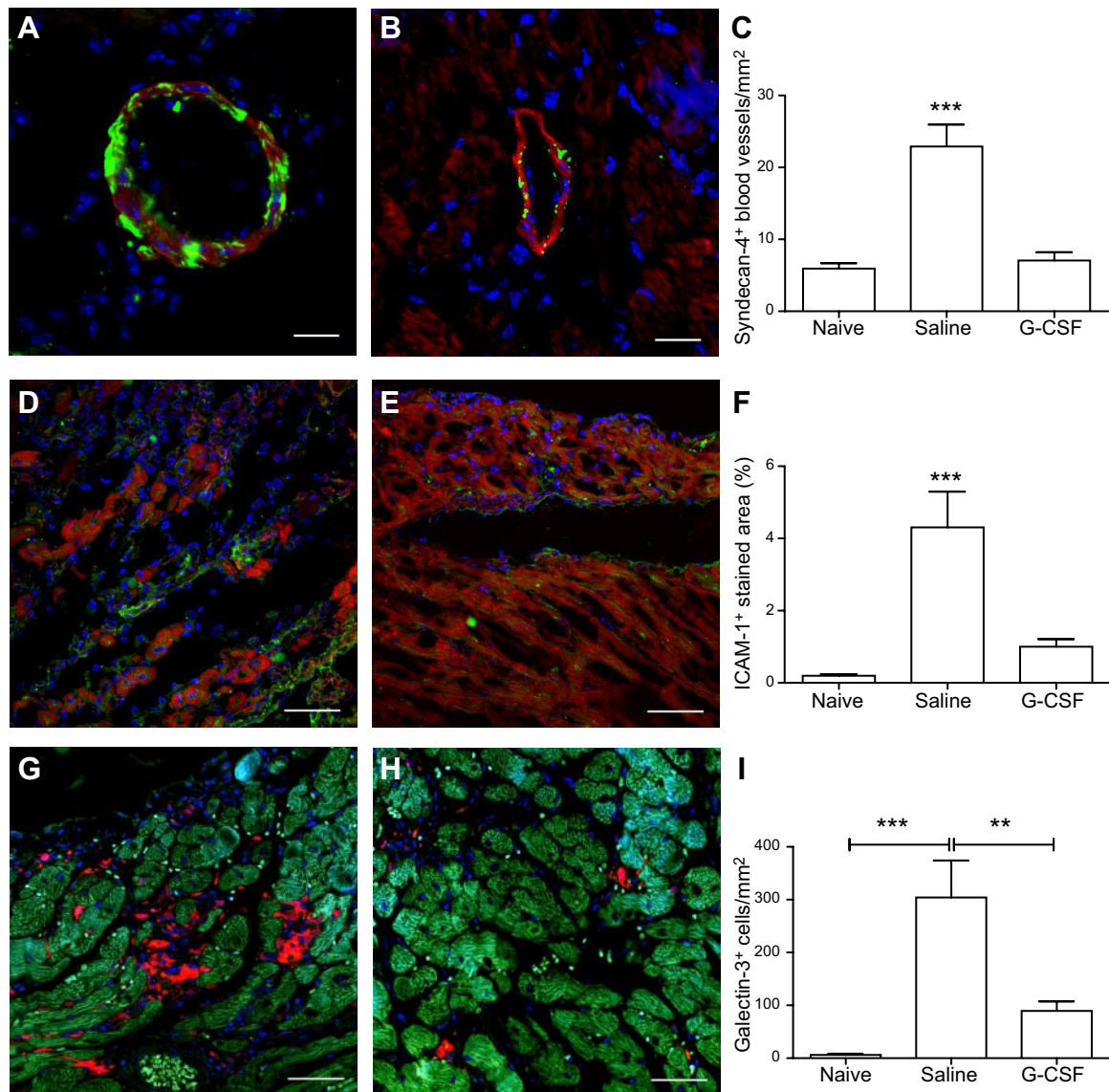


Figure 3. Reduction of syndecan-4, ICAM-1, and galectin-3 in hearts of chronic chagasic mice after G-CSF administration. Heart sections of saline-treated (A, D, G) or G-CSF-treated (B, E, H) mice were stained with anti-syndecan-4 (green; A, B), anti-ICAM-1 (green; D, E), or anti-galectin-3 (red; G, H) antibodies. F-actin stained with phalloidin 633 (red; A, B, D, E) or 488 (green; G, H). All sections were stained with DAPI for nuclear visualization (blue). Scale bars = 50 μ m. C, F, I) Morphometric analyses in heart sections of naive mice or chagasic mice treated with saline or G-CSF. Bars represent means \pm SEM of 3 animals/group. ** $P < 0.01$; *** $P < 0.001$.

found in the group treated with G-CSF compared with the saline-treated controls (Fig. 7B, C).

To evaluate whether G-CSF administration in chronic chagasic mice affected the residual *T. cruzi* infection, we performed RT-qPCR analysis to quantify the parasite load in the hearts of the mice. As shown in Fig. 7D, a significant reduction in the parasite load was observed in the hearts of G-CSF-treated mice compared with that in saline-treated controls. To determine whether G-CSF acts directly on the parasite, we analyzed the effects of G-CSF on *T. cruzi* cultures. Addition of G-CSF at various concentrations in axenic cultures of *T. cruzi* epimastigotes had little effect on viability at 30 μ g/ml (Table 1). In contrast, a concentration-dependent trypanocidal effect was seen in cultures of isolated trypomastigotes (Table 1). In addition, when G-CSF was

added to macrophage cultures infected with *T. cruzi*, a concentration-dependent decrease in the percentage of infected cells, as well as in the number of intracellular amastigotes, was observed (Fig. 7E, F).

DISCUSSION

The hallmark of CCC is the presence of a multifocal inflammatory response mainly composed of lymphocytes and macrophages, which promotes myocytolysis, fibrosis deposition, and myocardial remodeling (21). This is a progressively debilitating condition that occurs during a phase of the disease when parasitism is very scarce. Although the pathogenic mechanisms are still a matter of debate (22), the correlation of disease

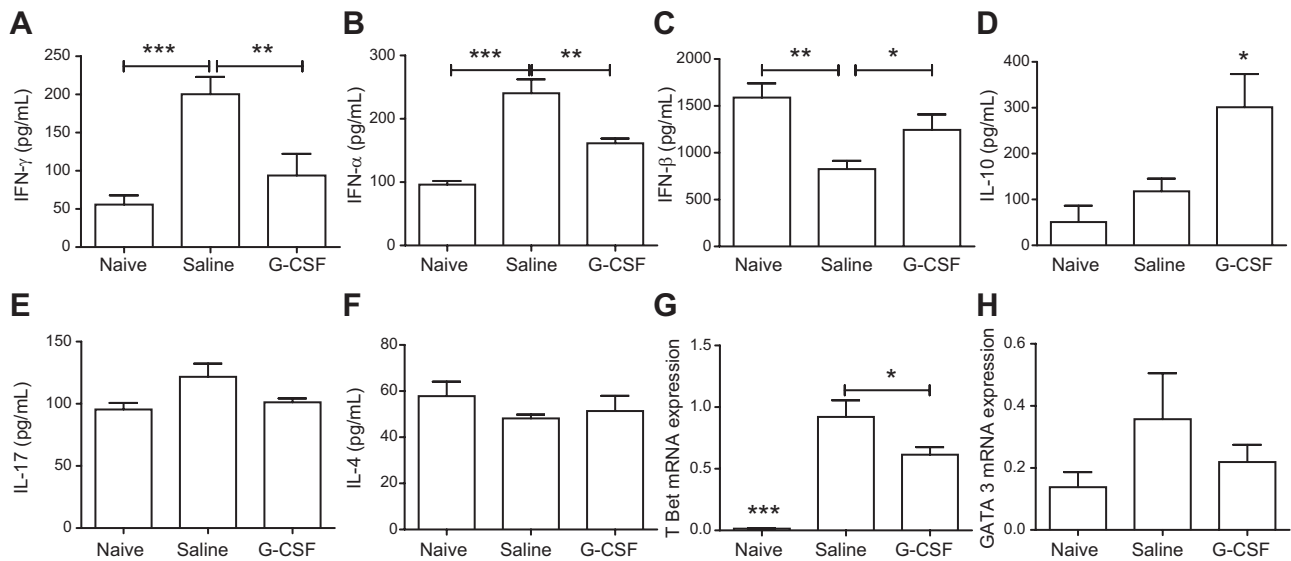


Figure 4. Modulation of cytokine production after G-CSF treatment. Concentrations of IFN- γ (A), TNF- α (B), TGF- β (C), IL-10 (D), IL-17 (E), and IL-4 (F) were determined in heart homogenates from naive ($n=3$) or chagasic mice treated with saline ($n=7$) or G-CSF ($n=10$), by ELISA. Analysis of *Tbet* (G) and *GATA3* (H) was performed by real-time RT-qPCR using cDNA samples prepared from mRNA extracted from hearts of naive and chronic chagasic mice treated with saline or G-CSF ($n=9-10$ mice/group). Values represent means \pm SEM. * $P < 0.05$; ** $P < 0.01$; *** $P < 0.001$.

severity and IFN- γ production has been well demonstrated (23, 24). The fact that the parasite persists in *T. cruzi*-infected individuals renders any immunosuppressive condition a risk for reactivation of parasitemia (25, 26).

In the present study, we have demonstrated that systemic administration of G-CSF, a cytokine widely used in the clinical setting, modulates the inflammatory

response, decreasing the production of key inflammatory mediators such as IFN- γ and TNF- α , in the main target organ, the heart. Different cytokine profiles are involved in the control of both the immune response and pathology during *T. cruzi* infection. The control of parasitism during the acute phase of Chagas disease is critically dependent on effective macrophage activation by cytokines, such as IFN- γ and TNF- α , which are

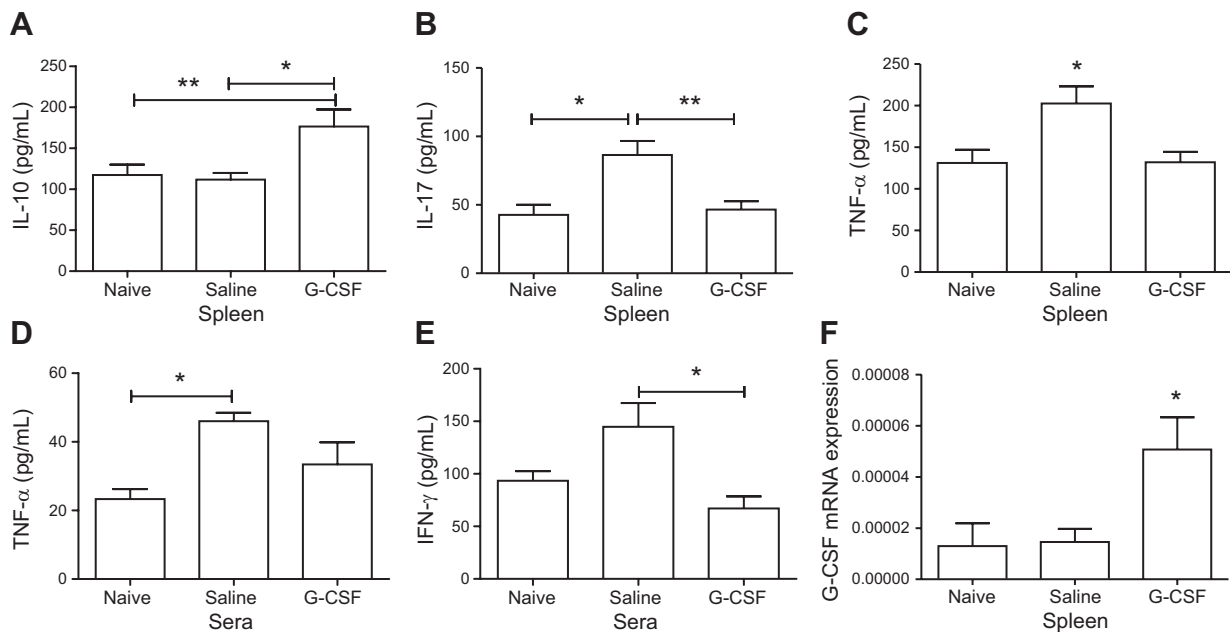


Figure 5. Modulation of systemic cytokine production in chronic chagasic mice treated with G-CSF. A–E) Concentrations of IL-10 (A), IL-17 (B), and TNF- α (C) were determined by ELISA in spleen homogenates and TNF- α (D) and IFN- γ (E) in the sera from naive ($n=3$) and chagasic mice treated with saline ($n=7$) or G-CSF ($n=10$). F) G-CSF mRNA expression was determined by real-time RT-qPCR using cDNA samples prepared from mRNA extracted from spleens of naive and chronic chagasic mice treated with saline or G-CSF. Values represent means \pm SEM. * $P < 0.05$; ** $P < 0.01$.

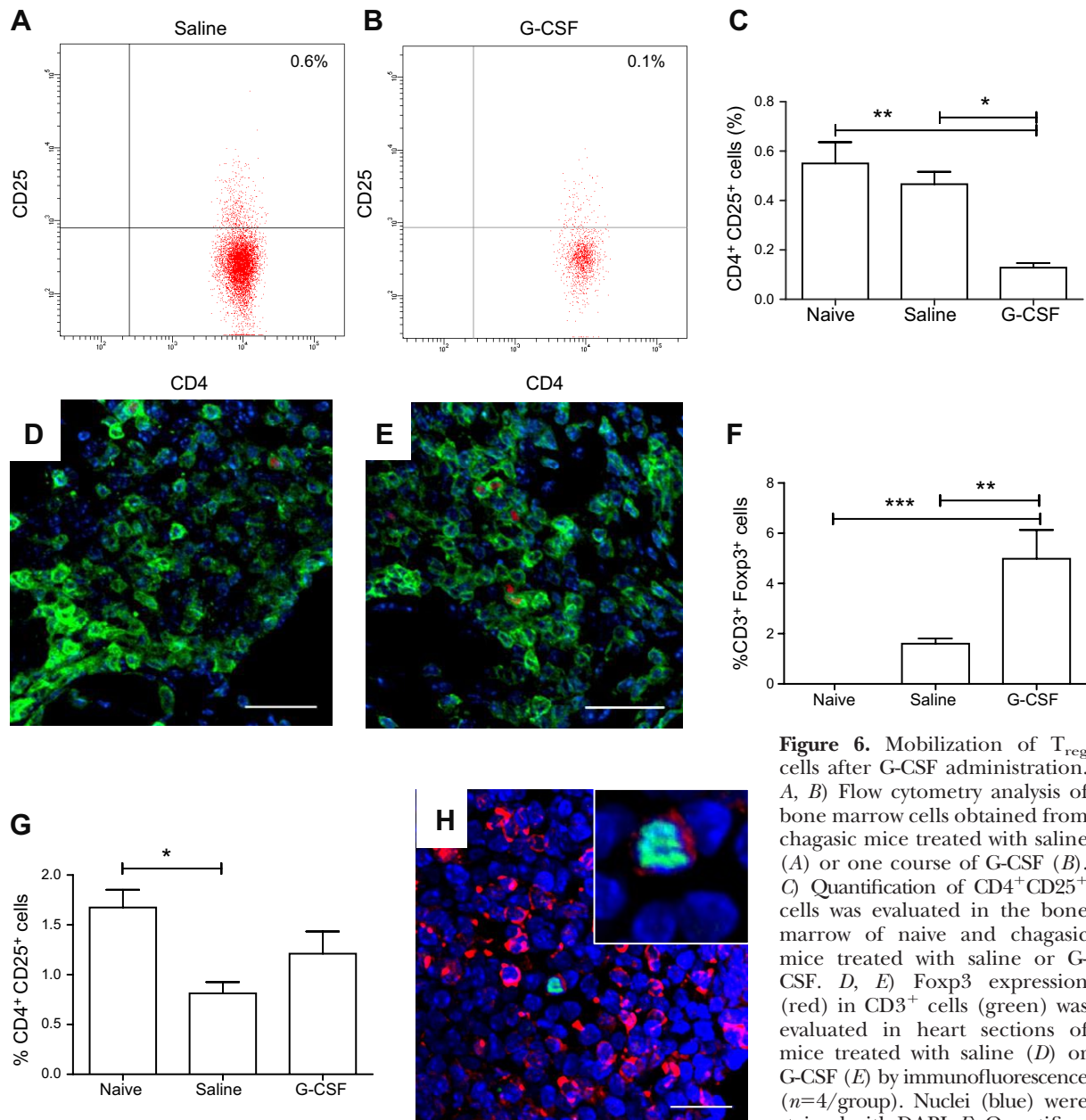


Figure 6. Mobilization of T_{reg} cells after G-CSF administration. *A, B*) Flow cytometry analysis of bone marrow cells obtained from chagasic mice treated with saline (*A*) or one course of G-CSF (*B*). *C*) Quantification of $CD4^+CD25^+$ cells was evaluated in the bone marrow of naive and chagasic mice treated with saline or G-CSF. *D, E*) Foxp3 expression (red) in $CD3^+$ cells (green) was evaluated in heart sections of mice treated with saline (*D*) or G-CSF (*E*) by immunofluorescence ($n=4$ /group). Nuclei (blue) were stained with DAPI. *F*) Quantification of $CD3^+Foxp3^+$ cells in hearts of naive and chagasic mice treated with saline or G-CSF. *G*) Quantification of $CD4^+CD25^+$ cells was evaluated in the spleens of naive and chagasic mice treated with saline or G-CSF. Bars represent means \pm SEM. *H*) Spleen section of a G-CSF-treated mouse, stained with anti-Foxp3 (green) and anti-IL-10 (red) antibodies. Nuclei (blue) were stained with DAPI. * $P < 0.05$; ** $P < 0.01$; *** $P < 0.001$.

crucial for limiting parasite replication (20, 27). On the other hand, an intense Th1 response will enhance heart inflammation (23), and elevated $TNF-\alpha$ may affect cardiomyocyte contraction (28). Exacerbated production of $IFN-\gamma$ against *T. cruzi* antigens favors the development of a strong Th1 response in symptomatic cardiac patients, which leads to the progression of heart disease (20, 29). Despite the observed suppression of $IFN-\gamma$ and $TNF-\alpha$ after G-CSF administration in chagasic mice, this therapy did not increase the parasite load, suggesting that the immune response against the parasite is still effective.

Previous reports have shown immune deviation induced after G-CSF treatment (30). In our model of

Chagas disease, we did not observe an increase in IL-4, a marker of the Th2-type response. In addition, we found a significant decrease in *Tbet* mRNA, a transcriptional factor essential for Th1-polarized immune responses, but we did not observe a significant difference in gene expression levels for GATA3, essential for Th2 responses, in the hearts of G-CSF-treated mice. Therefore, our results do not indicate a shift toward a Th2 profile after G-CSF administration in chagasic mice, but rather a suppression of the Th1-type immune response found in chronic chagasic mice.

In addition to cytokines, the expression of adhesion molecules important to cell migration, such as syndecan-4 and ICAM-1, already shown to be elevated in the

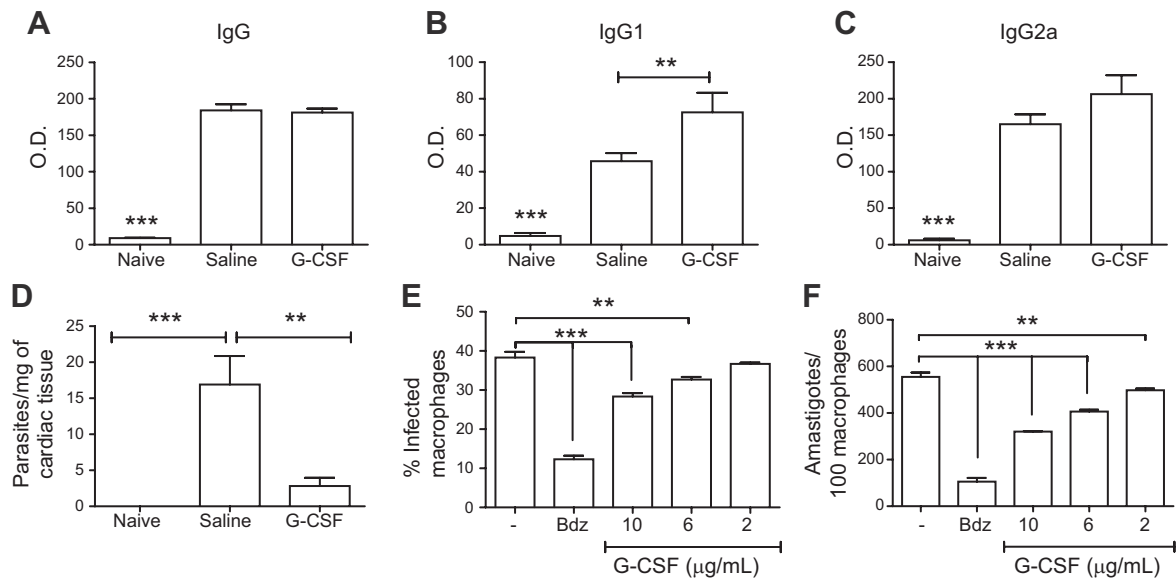


Figure 7. Effects of G-CSF on anti-*T. cruzi* antibody production and on the parasite. *A–C*) Serum samples from normal and *T. cruzi*-infected mice treated with saline or G-CSF (3 courses) were obtained 2 mo after treatment. Anti-*T. cruzi* levels of total IgG (*A*), IgG1 (*B*), and IgG2 (*C*) antibodies were determined by ELISA. Bars represent means \pm SEM of 5–10 mice/group. *D*) Heart fragments obtained from normal and *T. cruzi*-infected mice treated with saline or G-CSF (3 courses) were used for DNA extraction and RT-qPCR analysis for quantification of parasite load. *E, F*) Mouse peritoneal macrophages were infected with *T. cruzi* and treated with G-CSF (3 and 10 μ g/ml) or benznidazole (10 μ g/ml), a standard drug. Numbers of infected cells (*E*) and amastigotes (*F*) were determined by counting hematoxylin and eosin-stained cultures. Values represent means \pm SEM of triplicate determinations obtained in 1 of 2 experiments performed. ** $P < 0.01$; *** $P < 0.001$.

hearts of chronic chagasic mice (19, 29), was reduced after G-CSF therapy. TNF- α induces ICAM-1 expression, thus increasing endothelial adhesiveness for leukocytes (31). Syndecan-4 is a transmembrane heparan sulfate proteoglycan that acts cooperatively with integrins in generating signals necessary for the assembly of actin stress fibers and focal adhesions (32–34). Because TNF- α up-regulates syndecan-4 expression (35), the decreased expression in endothelial cells in the hearts of chagasic mice may be a consequence of the TNF- α down-regulation observed after G-CSF administration. Taken together, the decreases in syndecan-4 and ICAM-1 may contribute to a reduction in cell migration into the myocardium and, consequently, reduced inflammation.

Another important action of G-CSF in the Chagas disease model, as well as in other models of ischemic heart disease, is reduced fibrosis (17, 36). This may be due to the modulation in the heart of fibrogenic

mediators, such as galectin-3, which have been shown to play important roles in fibrosis deposition and in heart failure (37). Galectin-3 expression was found in activated myocardial macrophages and is increased by IFN- γ (38, 39). In addition, the administration of recombinant galectin-3 in rats induced cardiac fibroblast proliferation, collagen production, and left ventricular dysfunction (38). Moreover, galectin-3 is known to play important roles in the regulation of inflammatory responses, including suppression of T-cell apoptosis (40). In fact, in our previous study, we observed an increase in apoptosis in the hearts of chagasic mice treated with G-CSF (16), correlating with the decrease of galectin-3 found herein.

We observed suppression of inflammatory mediators after G-CSF administration, which was accompanied by an increase in IL-10 production in the hearts and spleens of chagasic mice. This is an important regulatory cytokine already shown to be associated with an improved outcome in chronic chagasic patients (20). Studies in noninfectious disease models have shown that G-CSF administration can induce both increases in IL-10 and TGF- β and mobilization of T_{reg} cells from the bone marrow (12, 41, 42). Evidence for the suppressive effects of G-CSF-mobilized T_{reg} cells are shown in a model of diabetes, in which isolated G-CSF-mobilized T_{reg} cells protected naive recipients against diabetogenic lymphocytes (42). Natural T_{reg} cells have emerged as potential immune tolerance mediators after immunotherapy in allergic diseases, comprising a population of circulating T cells that express the IL-10⁺CD4⁺CD25⁺ phenotype involved in the ameliora-

TABLE 1. Effects of G-CSF in axenic cultures of *T. cruzi* (Colombian strain)

Drug	Conc. (μ g/ml)	% Inhibition	
		Epimastigotes	Trypomastigotes
G-CSF	3	0.52 \pm 0.52	1.90 \pm 0.90
	10	2.58 \pm 0.66	12.85 \pm 1.43*
	30	9.60 \pm 1.34**	24.28 \pm 2.51***
Benznidazole	30	96.78 \pm 0.06***	100***

Values are means \pm SEM of 3 independent experiments. * $P < 0.05$; ** $P < 0.01$; *** $P < 0.001$.

tion of symptoms (43–45). The coexpression of IL-10 in T_{reg} cells, which demonstrated increased frequency after G-CSF treatment, suggests that these cells are a source of IL-10. In fact, the production of IL-10 has been described as one of the mechanisms by which T_{reg} cells exert their suppressive activity (46).

G-CSF administration had a systemic effect on the immune response, as shown by the reduction in inflammatory mediators such as TNF- α and IFN- γ in the spleen and sera of chagasic mice. Although we did not observe significant alterations in IL-17 in the hearts of G-CSF-treated mice, G-CSF administration did affect splenic IL-17 levels. In contrast to the work in naive mice performed by Hill *et al.* (47), we did not observe IL-17 induction after G-CSF administration in chronically infected mice. Concomitant with the reduction in inflammatory mediators, we observed increased production of IL-10 in the spleens of G-CSF-treated mice. FoxP3⁺ cells also were costained for IL-10 in the spleens of chagasic mice treated with G-CSF, suggesting a role of this cell population in the modulatory action induced by G-CSF.

T_{reg} cells constitute an anti-inflammatory T-cell population associated with immune regulation, which may prevent tissue damage caused by parasite-triggered immune responses (48). T_{reg} cells expressing CD4⁺CD25⁺ cells have recently been associated with the expression of the regulatory lineage factor Foxp3 and are responsible for maintaining self-tolerance (49, 50). The increased percentage of T_{reg} cells in the spleens and lymph nodes of G-CSF-treated mice caused by mobilization of bone marrow-resident T_{reg} cells has been described previously (41). This mobilization of T_{reg} cells after G-CSF administration seems to be due to the reduced expression of SDF1, the CXCR4 ligand, in the bone marrow. Rutella *et al.* (51) reported that G-CSF induces an increase in T_{reg} cells in the peripheral blood of normal human recipients. Recent investigations evaluating the frequency of T_{reg} cells during early and late indeterminate forms of Chagas disease have shown a correlation between the severity of the CCC and a lower frequency or suppressive activity of CD4⁺CD25⁺ cells (52–54). Thus, our data corroborate these findings, because an inverse correlation between the percentage of T_{reg} cells, inflammatory cells, and cytokines in the heart of chagasic mice was found when G-CSF- and saline-treated mice were compared.

One important issue raised was whether the suppressive effects of G-CSF could interfere with the control of *T. cruzi* infection. The levels of anti-*T. cruzi* IgG antibodies in the sera of chagasic mice were not reduced after G-CSF treatment. More importantly, by using a very sensitive quantification method (18), we found a decrease in parasite load in the hearts of chronic chagasic mice treated with G-CSF compared with that in saline-treated mice, suggesting that this cytokine could have a direct effect on parasite elimination. To address this question, we evaluated the effects of G-CSF *in vitro*, in 3 parasitic forms. Although G-CSF had little effect on the viability of epimastigote form, it did

significantly affect the forms found in the mammalian hosts (trypomastigotes and amastigotes) in a concentration-dependent manner. In fact, previous reports have shown that other cytokines, such as GM-CSF and TNF- α , can have direct effects on the parasite and interfere with *T. cruzi* infection (55). Taken together, our data indicate that parasitism reduction may be a positive effect of G-CSF therapy.

In conclusion, the present study reinforces our previous work, in which we demonstrated improvement in cardiopulmonary function after G-CSF administration, by revealing its potent anti-inflammatory properties in a model of parasite-driven heart disease. More importantly, we demonstrated the modulation of pathogenic immune responses without affecting the control of infection, a feature highly desired in the clinical setting. Finally, our results reinforce the possibility of clinical applications of G-CSF, a well-tolerated drug with few side effects, in the treatment of patients with CCC. **[F]**

The authors thank Kyan Allahdadi for careful review of the article. This work was supported by grants from the Brazilian Ministry of Sciences and Technology (MCT), Conselho Nacional de Pesquisas (CNPq), Financiadora de Estudos e Projetos (FINEP), Fundação Oswaldo Cruz (FIOCRUZ), and Fundação de Amparo as Pesquisas do Estado da Bahia (FAPESB). J.F.V. and A.C.D.A. were recipients of a Coordination for the Improvement of Higher Education Personnel (CAPES) doctoral scholarship from the Universidade Estadual de Feira de Santana/Programa de Pós-graduação em Biotecnologia (UEFS/PPgBIOTEC) and Rede Nordeste de Biotecnologia (RENORBIO) graduate programs, respectively. B.S.F.S. holds a CNPq doctoral scholarship, and C.S.M. holds a FAPESB master scholarship. M.B.P.S. and R.R.-D.-S. are recipients of CNPq senior fellowships.

REFERENCES

1. Franco-Paredes, C., Von, A., Hidron, A., Rodríguez-Morales, A. J., Tellez, I., Barragán, M., Jones, D., Náquira, C. G., and Mendez, J. (2007) Chagas disease: an impediment in achieving the millennium development goals in Latin America. *BMC Int. Health Hum. Rights* **7**, 1–6
2. Hotez, P. J., Bottazzi, M. E., Franco-Paredes, C., Ault, S. K., and Roses-Periágo, M. (2008) The neglected tropical diseases of Latin America and the Caribbean: estimated disease burden and distribution and a roadmap for control and elimination. *PLoS Negl. Trop. Dis.* **2**, 1–11
3. Franco-Paredes, C., Bottazzi, M. E., and Hotez, P. J. (2009) The unfinished public health agenda of Chagas disease in the era of globalization. *PLoS Negl. Trop. Dis.* **3**, 1–4
4. World Health Organization. Chagas disease. Retrieved November 1, 2012, from <http://www.who.int/mediacentre/factsheets/fs340/en/index.html>
5. Bocchi, E. A., Bellotti, G., Mocelin, A., Uip, D., Bacal, F., Higuchi, M. L., Amato-Neto, V., Fiorelli, A., Stolf, N. A., Jatene, A. D., and Pileggi, F. (1996) Heart transplantation for chronic Chagas' heart disease. *Ann. Thorac. Surg.* **61**, 1727–1733
6. Von-Aulock, S., Boneberg, E. M., Diterich, I., and Hartung, T. (2004) Granulocyte colony-stimulating factor (filgrastim) treatment primes for increased ex vivo inducible prostanoid release. *J. Pharmacol. Exp. Ther.* **308**, 754–759
7. Hartung, T., Docke, W. D., Gantner, F., Krieger, G., Sauer, A., Stevens, P., Volk, H. D., and Wendel, A. (1995) Effect of granulocyte colony-stimulating factor treatment on ex vivo blood cytokine response in human volunteers. *Blood* **85**, 2482–2489

8. Boneberg E. M., and Hartung, T. (2002) Molecular aspects of anti-inflammatory action of G-CSF. *Inflamm. Res.* **51**, 119–128
9. Iwanaga, K., Takano, H., Ohtsuka, M., Hasegawa, H., Zou, Y., Qin, Y., Odaka, K., Hiroshima, K., Tadokoro, H., and Komuro, I. (2004) Effects of G-CSF on cardiac remodeling after acute myocardial infarction in swine. *Biochem. Biophys. Res. Commun.* **325**, 1353–1359
10. Harada, M., Qin, Y., Takano, H., Minamino, T., Zou, Y., Toko, H., Ohtsuka, M., Matsuura, K., Sano, M., Nishi, J., Iwanaga, K., Akazawa, H., Kunieda, T., Zhu, W., Hasegawa, H., Kunisada, K., Nagai, T., Nakaya, H., Yamauchi-Takahara, K., and Komuro, I. (2005) G-CSF prevents cardiac remodeling after myocardial infarction by activating the Jak-Stat pathway in cardiomyocytes. *Nat. Med.* **11**, 305–311
11. Higuchi, T., Yamauchi-Takahara, K., Matsumiya, G., Fukushima, N., Ichikawa, H., Kuratani, T., Maehata, Y., and Sawa, Y. (2008) Granulocyte colony-stimulating factor prevents reperfusion injury after heart preservation. *Ann. Thorac. Surg.* **85**, 1367–1373
12. Rutella, S., Zavala, F., Danese, S., Kared, H., and Leone, G. (2005) Granulocyte colony-stimulating factor: a novel mediator of T cell tolerance. *J. Immunol.* **175**, 7085–7091
13. Sakaguchi, S. (2005) Naturally arising Foxp3-expressing CD25⁺CD4⁺ regulatory T cells in immunological tolerance to self and non-self. *Nat. Immunol.* **6**, 345–352
14. Rutella, S., Pierelli, L., Bonanno, G., Sica, S., Ameglio, F., Capoluongo, E., Mariotti, A., Scambia, G., d'Onofrio, G., and Leone, G. (2002) Role for granulocyte colony-stimulating factor in the generation of human T regulatory type 1 cells. *Blood* **100**, 2562–2571
15. Rossetti, M., Gregori, S., and Roncarolo, M. G. (2010) Granulocyte-colony stimulating factor drives the in vitro differentiation of human dendritic cells that induce anergy in naive T cells. *Eur. J. Immunol.* **40**, 3097–3106
16. Macambira, S. G., Vasconcelos, J. F., Costa, C. R., Klein, W., Lima, R. S., Guimarães, P., Vidal, D. T., Mendez, L. C., Ribeiro-Dos-Santos, R., and Soares, M. B. (2009) Granulocyte colony-stimulating factor treatment in chronic Chagas disease: preservation and improvement of cardiac structure and function. *FASEB J.* **23**, 3843–3850
17. Federici, E. E., Abelmann, W. H., and Neva, F. A. (1964) Chronic and progressive myocarditis and myositis in C3H mice infected with *Trypanosoma cruzi*. *Am. J. Trop. Med. Hyg.* **13**, 272–280
18. Schijman, A. G., Bisio, M., Orellana, L., Sued, M., Duffy, T., Mejía Jaramillo, A. M., Cura, C., Auter, F., Veron, V., Qvarnstrom, Y., Deborggraave, S., Hajar, G., Zulantay, I., Lucero, R. H., Velazquez, E., Tellez, T., Sanchez Leon, Z., Galvão, L., Nolder, D., Monje Rumi, M., Levi, J. E., Ramirez, J. D., Zorrilla, P., Flores, M., Jercic, M. I., Crisante, G., Añez, N., De Castro, A. M., Gonzalez, C. I., Acosta Viana, K., Yachelini, P., Torrico, F., Robello, C., Diosque, P., Triana Chavez, O., Aznar, C., Russo-mando, G., Büscher, P., Assal, A., Guhl, F., Sosa Estani, S., DaSilva, A., Britto, C., Luquetti, A., and Ladzins, J. (2011) International study to evaluate PCR methods for detection of *Trypanosoma cruzi* DNA in blood samples from Chagas disease patients. *PLoS Negl. Trop. Dis.* **5**, 1–13
19. Soares, M. B., de Lima, R. S., Rocha, L. L., Vasconcelos, J. F., Rogatto, S. R., dos Santos, R. R., Iacobas, S., Goldenberg, R. C., Iacobas, D. A., Tanowitz, H. B., de Carvalho, A. C., and Spray, D. C. (2010) Gene expression changes associated with myocarditis and fibrosis in hearts of mice with chronic chagasic cardiomyopathy. *J. Infect. Dis.* **202**, 416–426
20. Gomes, J. A., Bahia-Oliveira, L. M., Rocha, M. O., Martins-Filho, O. A., Gazzinelli, G., and Correa-Oliveira, R. (2003) Evidence that development of severe cardiomyopathy in human Chagas' disease is due to a Th1-specific immune response. *Infect. Immun.* **71**, 1185–1193
21. Köberle, F. (1968) Chagas' disease and Chagas' syndromes: the pathology of American trypanosomiasis. *Adv. Parasitol.* **6**, 63–116
22. Soares, M.B., Silva-Mota, K.N., Lima, R.S., Bellintani, M.C., Pontes-de-Carvalho, L., and Ribeiro-dos-Santos, R. (2001) Modulation of chagasic cardiomyopathy by IL-4: dissociation between inflammatory and tissue parasitism. *Am. J. Pathol.* **159**, 703–709
23. Soares, M. B. P., Pontes-de-Carvalho, L., and Ribeiro-dos-Santos, R. (2001) The pathogenesis of Chagas' disease: when autoimmune and parasite-specific immune responses meet. *An. Acad. Bras. Cienc.* **73**, 547–559
24. Bahia-Oliveira, L. M. G., Gomes, J. A. S., Rocha, M. O. S., Moreira, M. C., Lemos, E. M., Luz, Z. M., Pereira, M. E., Coffman, R. L., Dias, J. C., Cançado, J. R., Gazzinelli, G., and Corrêa-Oliveira, R. (1998) IFN- γ in human Chagas' disease: protection or pathology? *Braz. J. Med. Biol. Res.* **31**, 127–131
25. Galhardo, M. C. G., Martins, I. A., Hasslocher-Moreno, A., Xavier, S. S., Coelho, J. M., Junqueira, A. C., and dos Santos, R. R. (1999) Reactivation of *Trypanosoma cruzi* infection in a patient with acquired immunodeficiency syndrome. *Rev. Soc. Bras. Med. Trop.* **32**, 291–294
26. Campos, S. V., Strabelli, T. M., Amato Neto, V., Silva, C. P., Bacal, F., Bocchi, E. A., and Stolf, N. A. (2008) Risk factors for Chagas' disease reactivation after heart transplantation. *J. Heart Lung Transplant.* **27**, 597–602
27. Tadokoro, C. E., and Abrahamsohn, I. A. (2001) Bone marrow-derived macrophages grown in GM-CSF or M-CSF differ in their ability to produce IL-12 and to induce IFN- γ production after stimulation with *Trypanosoma cruzi* antigens. *Immunol. Lett.* **77**, 31–38
28. Ferrari, R. (1999) The role of TNF in cardiovascular disease. *Pharmacol. Res.* **40**, 97–105
29. Soares, M. B., Lima, R. S., Souza, B. S. F., Vasconcelos, J. F., Rocha, L. L., Dos Santos, R. R., Iacobas, S., Goldenberg, R. C., Lisanti, M. P., Iacobas, D. A., Tanowitz, H. B., Spray, D. C., and Campos de Carvalho, A. C. (2011) Reversion of gene expression alterations in hearts of mice with chronic chagasic cardiomyopathy after transplantation of bone marrow cells. *Cell Cycle* **10**, 1448–1455
30. Sloand, E., Kim, S., Maciejewski, J., Van Rhee, F., Chaudhuri, A., Barrett, J., and Young, N. S. (2000) Pharmacologic doses of granulocyte colony stimulating factor affect cytokine production by lymphocytes in vitro and in vivo. *Blood* **95**, 2269–2274
31. Ledebur, H. C., and Parks, T. P. (1995) Transcriptional regulation of the intercellular adhesion molecule-1 gene by inflammatory cytokines in human endothelial cells. Essential roles of a variant NF- κ B site and p65 homodimers. *J. Biol. Chem.* **270**, 933–943
32. Horowitz, A., Tkachenko, E., and Simons, M. (2002) Fibroblast growth factor-specific modulation of cellular response by syndecan-4. *J. Cell Biol.* **157**, 715–725
33. Ishiguro, K., Kojima, T., and Muramatsu, T. (2003) Syndecan-4 as a molecule involved in defense mechanisms. *Glycoconj. J.* **19**, 315–318
34. Hamon, M., Mbemba, E., Charnaux, N., Slimani, H., Brule, S., Saffar, L., Vassy, R., Prost, C., Lievre, N., Starzec, A., and Gattegno, L. (2004) A syndecan-4/CXCR4 complex expressed on human primary lymphocytes and macrophages and HeLa cell line binds the CXCR4 chemokine stromal cell-derived factor-1 (SDF-1). *Glycobiology* **14**, 311–313
35. Zhang, Y., Pasparakis, M., Kollias, G., and Simons, M. (1999) Myocyte-dependent regulation of endothelial cell syndecan-4 expression. Role of TNF- α . *J. Biol. Chem.* **274**, 14786–14790
36. Angeli, F. S., Amabile, N., Shapiro, M., Mirsky, R., Bartlett, L., Zhang, Y., Virmani, R., Chatterjee, K., Boyle, A., Grossman, W., and Yeghiazarians, Y. (2010) Cytokine combination therapy with erythropoietin and granulocyte colony stimulating factor in a porcine model of acute myocardial infarction. *Cardiovasc. Drugs Ther.* **24**, 409–420
37. Joo, H. G., Goedegebuure, P. S., Sadanaga, N., Nagoshi, M., and Von Bernstorff, W., and Eberlein, T. J. (2001) Expression and function of galectin-3, a β -galactoside-binding protein in activated T lymphocytes. *J. Leukoc. Biol.* **69**, 555–564
38. Sharma, U. C., Pokharel, S., Brakel, T. J. V., van Berlo, J. H., Cleutjens, J. P., Schroen, B., André, S., Crijns, H. J., Gabius, H. J., Maessen, J., and Pinto, Y. M. (2004) Galectin-3 marks activated macrophages in failure-prone hypertrophied hearts and contributes to cardiac dysfunction. *Circulation* **110**, 3121–3128
39. Reifenberg, K., Lehr, H. A., Torzewski, M., Steige, G., Wiese, E., Kötter, I., Becker, C., Ott, S., Nusser, P., Yamamura, K., Rechtssteiner, G., Warger, T., Pautz, A., Kleinert, H., Schmidt, A., Pieske, B., Wenzel, P., Münzel, T., and Löhler, J. (2007) Interferon- γ induces chronic active myocarditis and cardiomyopathy in transgenic mice. *Am. J. Pathol.* **171**, 463–472

40. Rabinovich, G. A., Ramhorst, R. E., Rubinstein, N., Corigliano, A., Daroqui, M. C., Kier-Joffé, E.B., and Fainboim, L. (2002) Induction of allogenic T-cell hyporesponsiveness by galectin-I-mediated apoptotic and non-apoptotic mechanisms. *Cell Death Differ.* **9**, 661–670
41. Zou, L., Barnett, B., Safah, H., Larussa, V. F., Evdemon-Hogan, M., Mottram, P., Wei, S., David, O., Curiel, T. J., and Zou, W. (2004) Bone marrow is a reservoir for CD4⁺CD25⁺ regulatory T cells that traffic through CXCL12/CXCR4 signals. *Cancer Res.* **64**, 8451–8455
42. Kared, H., Masson, A., Adle-Biassette, H., Bach, J. F., Chatenoud, L., and Zavala, F. (2005) Treatment with granulocyte colony-stimulating factor prevents diabetes in NOD mice by recruiting plasmacytoid dendritic cells and functional CD4⁺CD25⁺ regulatory T-cells. *Diabetes* **54**, 78–84
43. Francis, J. N., Till, S. J., and Durham, S. R. (2003) Induction of IL-10⁺CD4⁺CD25⁺ T cells by grass pollen immunotherapy. *J. Allergy Clin. Immunol.* **111**, 1255–1261
44. Gardner, L. M., Thien, F. C., Douglass, J. A., Rolland, J. M., and O’Hehir, R. E. (2004) Induction of T⁺regulatory⁺ cells by standardized house dust mite immunotherapy: an increase in CD4⁺CD25⁺interleukin-10⁺ T cells expressing peripheral tissue trafficking markers. *Clin. Exp. Allergy* **34**, 1209–1219
45. Urry, Z., Chambers, E. S., Xystrakis, E., Dimeloe, S., Richards, D. F., Gabryšová, L., Christensen, J., Gupta, A., Saglani, S., Bush, A., O’Garra, A., Brown, Z., and Hawrylowicz, C. M. (2012) The role of 1 α ,25-dihydroxyvitamin D₃ and cytokines in the promotion of distinct Foxp3⁺ and IL-10⁺ CD4⁺ T cells. *Eur. J. Immunol.* **42**, 2697–2708
46. Morris, E. S., MacDonald, K. P., Rowe, V., Johnson, D. H., Banovic, T., Clouston, A. D., and Hill, G. R. (2004) Donor treatment with pegylated G-CSF augments the generation of IL-10-producing regulatory T cells and promotes transplantation tolerance. *Blood* **103**, 3573–3581
47. Hill, G. R., Olver, S. D., Kuns, R. D., Varelias, A., Raffelt, N. C., Don, A. L., Markey, K. A., Wilson, Y. A., Smyth, M. J., Iwakura, Y., Tocker, J., Clouston, A. D., and Macdonald, K. P. (2010) Stem cell mobilization with G-CSF induces type 17 differentiation and promotes scleroderma. *Blood* **116**, 819–828
48. Belkaid, Y., Blank, R. B., and Suffia, I. (2006) Natural regulatory T cells and parasites: a common quest for host homeostasis. *Immunol. Rev.* **212**, 287–300
49. Itoh, M., Takahashi, T., Sakaguchi, N., Kuniyasu, Y., Shimizu, J., Otsuka, F., and Sakaguchi, S. (1999) Thymus and autoimmunity: production of CD25⁺CD4⁺ naturally anergic and suppressive T cells as a key function of the thymus in maintaining immunologic self-tolerance. *J. Immunol.* **162**, 5317–5326
50. Shevach, E. M. (2009) Mechanisms of foxp3⁺ T regulatory cell-mediated suppression. *Immunity* **30**, 636–645
51. Rutella, S., Bonanno, G., Pierelli, L., Mariotti, A., Capoluongo, E., Contemi, A. M., Ameglio, F., Curti, A., De Ritis, D. G., Voso, M. T., Perillo, A., Mancuso, S., Scambia, G., Lemoli, R. M., and Leone, G. (2004) Granulocyte colony-stimulating factor promotes the generation of regulatory DC through induction of IL-10 and IFN- α . *Eur. J. Immunol.* **34**, 1291–1302
52. Vitelli-Avelar, D. M., Sathler-Avelar, R., Dias, J. C. P., Pascoal, V. P., Teixeira-Carvalho, A., Lage, P. S., Elói-Santos, S. M., Corrêa-Oliveira, R., and Martins-Filho, O. A. (2005) Chagasic patients with indeterminate clinical form of the disease have high frequencies of circulating CD3⁺CD16⁺CD56⁺ natural killer T cells and CD4⁺CD25^{High} regulatory T lymphocytes. *Scand. J. Immunol.* **62**, 297–308
53. De-Araújo, F. F., Vitelli-Avelar, D. M., Teixeira-Carvalho, A., Antas, P. R., Assis Silva Gomes, J., Sathler-Avelar, R., Otávio Costa Rocha, M., Elói-Santos, S. M., Pinho, R. T., Correa-Oliveira, R., and Martins-Filho, O. A. (2011) Regulatory T cells phenotype in different clinical forms of Chagas’ disease. *PLoS Negl. Trop. Dis.* **5**, 1–8
54. Guedes, P. M., Gutierrez, F. R., Silva, G. K., Dellalibera-Joviliano, R., Rodrigues, G. J., Bendhack, L. M., Rassi, A. Jr., Rassi, A., Schmidt, A., Maciel, B. C., Marin Neto, J. A., and Silva, J. S. (2012) Deficient regulatory T cell activity and low frequency of IL-17-producing T cells correlate with the extent of cardiomyopathy in human Chagas’ disease. *PLoS Negl. Trop. Dis.* **6**, 1–11
55. Olivares-Fontt, E. O., de Baetselier, P., Heirman, C., Thielemans, K., Lucas, R., and Vray, B. (1998) Effects of granulocyte-macrophage colony-stimulating factor and tumor necrosis factor alpha on *Trypanosoma cruzi* trypomastigotes. *Infect. Immun.* **66**, 2722–2727

Received for publication February 20, 2013.

Accepted for publication August 5, 2013.

ANEXO 5

Moreira DR, Lima Leite AC, Cardoso MV, Srivastava RM, Hernandez MZ, Rabello MM, da Cruz LF, Ferreira RS, de Simone CA, **Meira CS**, Guimaraes ET, da Silva AC, Dos Santos TA, Pereira VR, Soares MB. Structural design, synthesis and structure-activity relationships of thiazolidinones with enhanced anti-Trypanosoma cruzi activity. **ChemMedChem**. v. 9, p. 177-188, 2014.

DOI: 10.1002/cmdc.201300354

Structural Design, Synthesis and Structure–Activity Relationships of Thiazolidinones with Enhanced Anti-*Trypanosoma cruzi* Activity

Diogo Rodrigo Magalhães Moreira,^{*[a, e]} Ana Cristina Lima Leite,^[b] Marcos Verissimo Oliveira Cardoso,^[b] Rajendra Mohan Srivastava,^[a] Marcelo Zaldini Hernandez,^[b] Marcelo Montenegro Rabello,^[b] Luana Faria da Cruz,^[c] Rafaela Salgado Ferreira,^[c] Carlos Alberto de Simone,^[d] Cássio Santana Meira,^[e] Elisalva Teixeira Guimaraes,^[e, f] Aline Caroline da Silva,^[g] Thiago André Ramos dos Santos,^[g] Valéria Rêgo Alves Pereira,^[g] and Milena Botelho Pereira Soares^[e, h]

Pharmacological treatment of Chagas disease is based on benznidazole, which displays poor efficacy when administered during the chronic phase of infection. Therefore, the development of new therapeutic options is needed. This study reports on the structural design and synthesis of a new class of anti-*Trypanosoma cruzi* thiazolidinones (**4a–p**). (2-[2-Phenoxy-1-(4-bromophenyl)ethylidene]hydrazono]-5-ethylthiazolidin-4-one (**4h**) and (2-[2-phenoxy-1-(4-phenylphenyl)ethylidene]hydrazono]-5-ethylthiazolidin-4-one (**4l**) were the most potent compounds, resulting in reduced epimastigote proliferation and were toxic for trypomastigotes at concentrations below 10 μM , while they did not display host cell toxicity up to 200 μM . Thiazolidinone **4h** was able to reduce the in vitro parasite burden and the blood parasitemia in mice with similar potency to

benznidazole. More importantly, *T. cruzi* infection reduction was achieved without exhibiting mouse toxicity. Regarding the molecular mechanism of action, these thiazolidinones did not inhibit cruzain activity, which is the major trypanosomal protease. However, investigating the cellular mechanism of action, thiazolidinones altered Golgi complex and endoplasmic reticulum (ER) morphology, produced atypical cytosolic vacuoles, as well as induced necrotic parasite death. This structural design employed for the new anti-*T. cruzi* thiazolidinones (**4a–p**) led to the identification of compounds with enhanced potency and selectivity compared to first-generation thiazolidinones. These compounds did not inhibit cruzain activity, but exhibited strong antiparasitic activity by acting as parasitocidal agents and inducing a necrotic parasite cell death.

Introduction

Chagas disease, caused by *Trypanosoma cruzi* parasite infection, affects approximately 5–10% of the Latin American population.^[1,2] The standard treatment is based on benznidazole, a compound able to eliminate the parasite during the acute phase.^[3] However, during the chronic phase, in which the parasite remains located inside various cell types, benznidazole is

not able to eliminate the parasitism even following long-term administration.^[4] Human vaccination against *T. cruzi* infection is not available,^[5] and thus other therapies aiming to control infection or reduce clinical symptoms are being investigated.^[6–8]

Aiming at the development of more effective medicines, a large number of anti-*T. cruzi* small molecules have been eval-

[a] Dr. D. R. M. Moreira, Prof. R. M. Srivastava
Universidade Federal de Pernambuco (UFPE)
Departamento de Química Fundamental
50670-901, Recife, PE (Brazil)
E-mail: diogollucio@gmail.com

[b] Prof. A. C. Lima Leite, Dr. M. V. O. Cardoso, Prof. M. Z. Hernandez,
M. M. Rabello
UFPE, Departamento de Ciências Farmacêuticas
50740-520, Recife, PE (Brazil)

[c] L. F. da Cruz, Prof. R. S. Ferreira
Universidade Federal de Minas Gerais (UFMG)
Departamento de Bioquímica e Imunologia
31270-901, Belo Horizonte, MG (Brazil)


[d] Prof. C. A. de Simone
Universidade de São Paulo (USP)
Departamento de Física e Informática, Instituto de Física
CEP 13560-970, São Carlos, SP (Brazil)

[e] Dr. D. R. M. Moreira, C. S. Meira, Dr. E. T. Guimaraes, Dr. M. B. Pereira Soares
Fundação Oswaldo Cruz (Fiocruz), Centro de Pesquisas Gonçalo Moniz
CEP 40296-710, Salvador, BA (Brazil)

[f] Dr. E. T. Guimaraes
Universidade do Estado da Bahia (UNEB)
Departamento de Ciências da Vida
41150-000, Salvador, BA (Brazil)

[g] A. C. da Silva, T. A. R. dos Santos, Dr. V. R. A. Pereira
FIOCRUZ, Centro de Pesquisas Aggeu Magalhaes
50670-420, Recife, PE (Brazil)

[h] Dr. M. B. Pereira Soares
Centro de Biotecnologia e Terapia Celular, Hospital São Rafael
41253-190, Salvador, BA (Brazil)

 Supporting information for this article is available on the WWW under <http://dx.doi.org/10.1002/cmdc.201300354>.

uated. To date, compounds that in some way inhibit either the trypanosomal protease cruzain or the ergosterol biosynthesis are the most outstanding *T. cruzi* growth inhibitors.^[9–12] In fact, some of these compounds have exhibited strong activity in reducing parasitemia in *T. cruzi*-infected mice as well as low toxicity in these animal models.^[13–16] Given this promising outlook, the structural design of new molecules based on these *T. cruzi* molecular targets is an attractive line of research.

Hydrazones are well-known antiparasitic compounds.^[17,18] Based on this, our research group has been investigating cruzain-inhibiting hydrazones to obtain novel and potent anti-*T. cruzi* agents. At least five distinct classes were investigated: thiosemicarbazones,^[19] *N*-acylhydrazones,^[20,21] thiazolidinones^[22–24] and their transition metal complexes.^[25] Within the thiazolidinone class of compounds, we identified compound **18** after examining the importance of modifications at every atom of the thiazolidinic ring (Figure 1). Compound **18** displayed an IC_{50} value of $10.1 \pm 0.09 \mu\text{M}$ to reduce the percentage of infected host cells, which is similar to the observed value for benznidazole. However, thiazolidinone **18** was less efficient in reducing blood parasitemia in *T. cruzi*-infected mice than benznidazole.^[24] To identify new anti-*T. cruzi* thiazolidinones with enhanced *in vivo* efficacy, we reasoned that some molecular modifications in this class of compounds are necessary.

Previously, it was observed that thiazolidinone **18** inhibits cruzain activity but not its homologous in mammalian cells (cathepsin L).^[24] However, it was several times less potent than KB2, a high-efficient cruzain inhibitor.^[13] A comparison of cruzain docking between **18** and KB2 has revealed that the major difference is that KB2 assumes a T-shaped conformation. Therefore, we hypothesized that thiazolidinones displaying a conformation resembling the KB2 might enhance activity against cruzain, and consequently, against parasite cells. To achieve this, it was necessary to disrupt the existent planarity between the phenoxy group and the thiazolidinic ring. Based on literature findings,^[26,27] the attachment of an aryl ring to the iminic carbon should produce thiazolidinones with greater conformational restriction (i.e., high rotational energy barrier) than observed in **18**, and, consequently, produce thiazolidinones with the desirable T-shaped conformation (Figure 2).

Based on this structural design, new thiazolidinones denoted as compounds **4a–p** were synthesized and evaluated as antiparasitic agents as well as cruzain inhibitors. Initially, compound **4a** was prepared, which contains a phenyl ring attached to the iminic carbon. To determine the importance of this phenyl for the activity, compounds containing a pyridinyl instead of a phenyl ring were synthesized. Thereafter, substituents attached to the phenyl ring were examined, such as, alkyl,

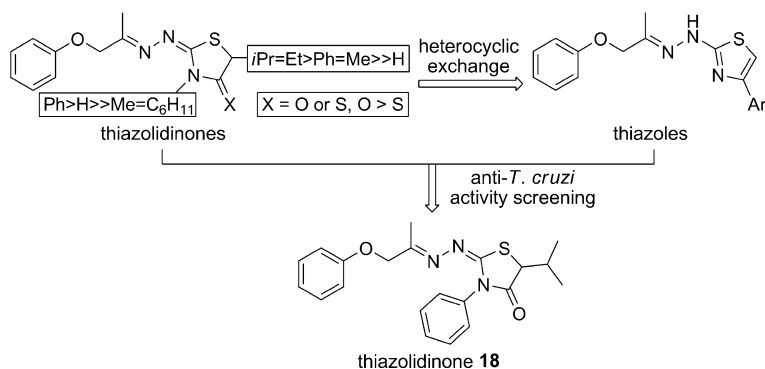


Figure 1. SARs of the previously studied anti-*T. cruzi* agents. Thiazolidinone **18** was identified as the most potent compound among them.

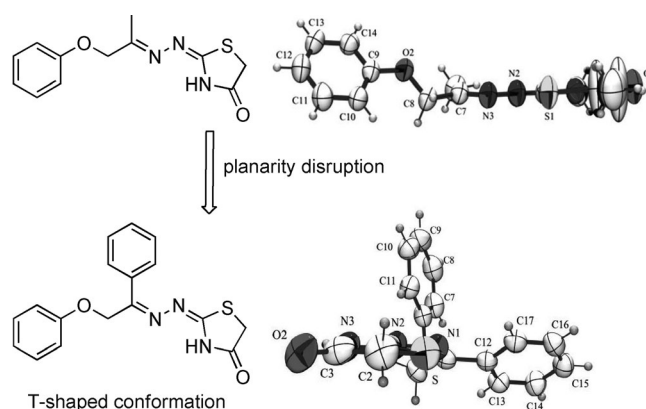


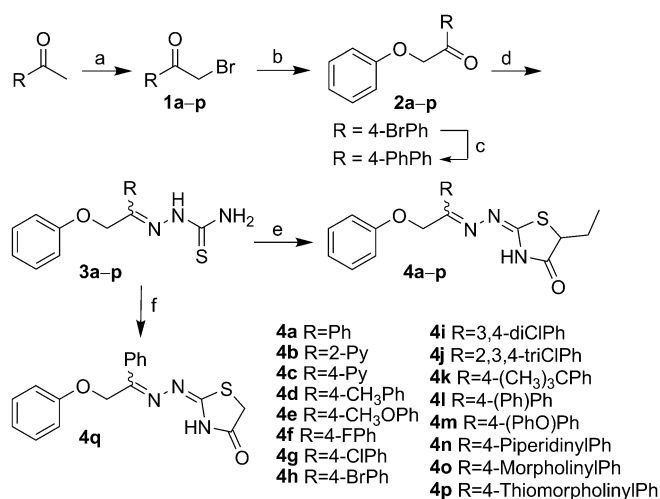
Figure 2. Thiazolidinones previously investigated (top) and proposed here (bottom). Crystal structures (Ortep-3) highlight the difference of molecular planarity between the two series.

alkoxy, halogen atoms and six-membered rings. In addition, compounds containing two or three substituents attached to the phenyl ring were prepared. By evaluating the antiparasitic activity of compounds **4a–p**, we identified that thiazolidinones had stronger anti-*T. cruzi* activity compared with the previously reported thiazolidinone **18**. More importantly, we found that compounds **4h** and **4i** are as potent as benznidazole in the inhibition of *T. cruzi* infection in host cells. As expected, based on its high *in vitro* antiparasitic activity, mice treated orally with thiazolidinone **4h** had substantially reduced blood parasitemia, similar to the observations made with benznidazole-treated mice.

Results

Synthesis

The route used for synthesizing thiazolidinones **4a–p** is shown in Scheme 1. The synthesis was initiated with the reaction between commercially available ketones and bromines, which yielded α -bromoketones **1a–p**.^[28] These were reacted with phenol in basic conditions to give the respective β -ketoethers **2a–p**. To prepare biphenyl compound **2i**, a Suzuki cross-cou-



Scheme 1. Synthesis of thiazolidinones **4a–q**. *Reagents and conditions:* a) Br₂, Et₂O/dioxane (1:1), –5 °C, 5 h. b) Phenol, K₂CO₃, butanone, reflux, 5–10 h, 42–72 %. c) Phenylboronic acid, Pd(OAc)₂, P(Ph)₃, MeOH, dioxane, 90 °C, 20 h, 50%. d) Thiosemicarbazide, EtOH, AcOH, reflux, 2 h, 43–83 %. e) Ethyl 2-bromobutyrate, KOAc, EtOH, reflux, 6–8 h, 40–81 %. f) Ethyl 2-bromoacetate, KOAc, EtOH, reflux, 6 h, 75%. Ph = phenyl, Py = pyridinyl.

pling reaction was performed between the bromophenyl **2h** and phenylboronic acid by using Pd(OAc)₂ and P(Ph)₃ as catalysts.^[29] Reactions of β-ketoethers **2a–p** with thiosemicarbazide under acidic conditions at reflux provided thiosemicarbazones **3a–p** with yields varying from 43 to 83% and acceptable purities (approx. 95%) by simple precipitation following recrystallization. Cyclizations of thiosemicarbazones **3a–p** to thiazolidinones **4a–p** were carried out with ethyl-2-bromobutyrate in the presence of potassium acetate at reflux for six to eight hours, and thiazolidinones **4a–p** were isolated as colorless solids with purities > 98% determined by elemental analysis. The compounds were chemically characterized by ¹H and ¹³C NMR, IR and HRMS (ESI). The ¹H NMR spectra showed that thiazolidinones **4a–p** are composed of two diastereomers, and through analysis of the HPLC chromatograms, we determined that the ratio of the isomer mixture **4a/4h** is 90:10.

Next, we aimed to define the configuration of the major isomer by crystallographic analysis. We did not succeed in crystallizing thiazolidinones **4a–p** suitable for X-ray analysis. Because previously we observed that thiazolidinic derivatives without substituents attached to the heterocyclic ring are more prone to afford crystals suitable for X-ray measurements, we decided to prepare thiazolidinone **4q** for X-ray analysis. After recrystallization and chromatographic purification of **4q**, its major isomer was isolated, and a single crystal suitable for X-ray analysis was collected. As shown in the Ortep-3 representation of thiazolidinone **4q**, carbon C5 and nitrogen N2 are on the same side, characteristic of a Z configuration in regard to the C4=N1 bond (Figure 3). Interestingly, the phenyl ring attached to the iminic carbon is coplanar to the thiazolidinic ring, while the phenoxy ring is oriented to a different side. Another interesting observation is that the double bond of C1 is located in an exocyclic position in relation to the heterocyclic ring, which gives rise to an isomerism in the C1=N2 bond.^[30–32]

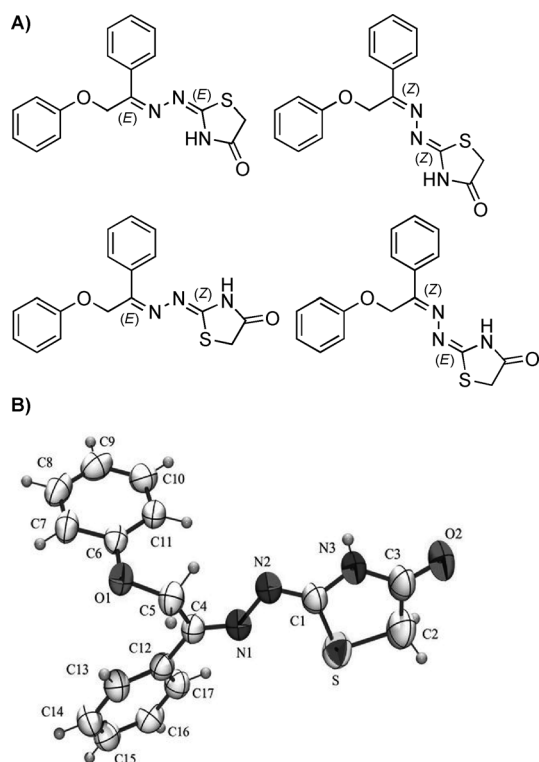


Figure 3. A) Structures of the possible diastereoisomers and B) Ortep-3 representation for the crystal structure of thiazolidinone **4q**.

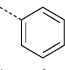
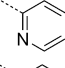
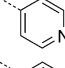
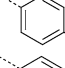
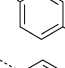
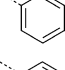
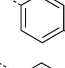
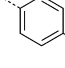
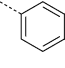
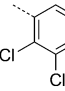
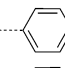
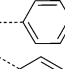
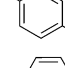
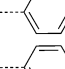
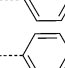
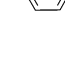
In the crystalline structure depicted in Figure 3, N2 and the sulfur atom are on the same side, characterizing a Z configuration for the C1=N2 bond. Thiazolidinone **4q** showed ¹H NMR chemical shifts similar to thiazolidinones **4a–p**; therefore, it is fair to suggest that the major isomer for thiazolidinones **4a–p** has a Z configuration in regard to the C4=N1 bond. Important to note is that all compounds were used in the pharmacological tests as isomer mixtures.

Antiparasitic activity against extracellular forms and cytotoxicity against host cells

First, compounds **4a–p** were evaluated against epimastigotes and trypomastigotes of *T. cruzi*. Antiparasitic activity was determined by counting the parasite number in a Neubauer chamber and calculating the concentration of the test compound resulting in 50% inhibition (IC₅₀, epimastigotes) or 50% cytotoxicity (CC₅₀, trypomastigotes). Cytotoxicity in host cells was determined in mouse splenocytes, measured by the incorporation of [³H]-thymidine, and results were expressed as the highest non-cytotoxic concentration (HNC). Benznidazole was used as reference antiparasitic drug and exhibited a CC₅₀ value of 6.0 μM against trypomastigotes. As cut-off, compounds with CC₅₀ values ≤ 6.0 μM against trypomastigotes were considered potent anti-*T. cruzi* compounds. The results are reported in Table 1.

We first analyzed the antiparasitic activity against trypomastigotes. The nonsubstituted phenyl derivative **4a** was active but was less potent than benznidazole. The replacement of

Table 1. Anti-*T. cruzi* activity, cytotoxicity and cruzain inhibition.

Compd	R	<i>T. cruzi</i>		Splenocytes HNC [μM] ^[c]	Cruzain Inhibition [%] ^[d]
		CC ₅₀ [μM] ^[a] trypomastigotes	IC ₅₀ [μM] ^[b] epimastigotes		
4a		17.7	25.0	> 283	64 ± 2
4b		> 100	> 100	28	5 ± 5
4c		> 100	67.8	28	11 ± 2
4d		97.2	ND	> 272	36.1 ± 0.6
4e		82.0	ND	> 261	58 ± 5
4f		78.9	> 100	> 269	37 ± 2
4g		17.3	11.3	258	50.4 ± 0.3
4h		4.0	3.9	> 231.4	40 ± 13
4i		50.8	ND	237	25 ± 2
4j		ND	> 100	21.9	13 ± 3
4k		74.9	> 100	> 244	0
4l		10.8	11.1	> 233	18 ± 2
4m		68.5	> 100	> 244	31 ± 2
4n		12.7	1.8	57.3	78 ± 2 (0.7 ± 0.4)
4o		15.9	> 100	22.8	15 ± 2
4p		10.8	31.9	22.0	94.3 ± 0.9 (4.0 ± 0.5)
Bdz		6.0	4.8	96.1	-
Sap		-	-	1.0 $\mu\text{g mL}^{-1}$	-

[a] Determined 24 h after incubation of Y strain trypomastigotes with the test compounds. [b] Determined 5 days after incubation of Dm28c-strain epimastigotes with the test compounds. [a,b] Only values with a standard deviation < 10% were included. [c] Highest noncytotoxic (HNC) concentration for mouse splenocytes after 24 h of incubation in the presence of the test compounds. [d] Compounds were tested at 100 μM and the percent inhibition of catalytic activity was determined; values in parenthesis are IC₅₀ values [nM] and represent the mean ± SD of three measurements. ND = not determined due to lack of activity; NT = not tested; Bdz = benznidazole; Sap = saponin.

the phenyl ring (**4a**) by 2- and 4-pyridinyl (**4b** and **4c**, respectively) produced inactive thiazolidinones. The attachment of a methyl (**4d**), methoxy (**4e**) and *tert*-butyl (**4k**) substituent at the 4-position of the phenyl ring decreased the antiparasitic activity. The attachment of 4-fluoro (**4f**) also decreased the activity; however, attaching a 4-chloro (**4g**) produced a compound as active as the nonsubstituted phenyl derivative (**4a**). A further increase in potency was achieved by replacing the nonsubstituted phenyl ring (**4a**) with a 4-bromo (**4h**), which

resulted in a fourfold increase in activity and produced a derivative that was as potent as benznidazole. In contrast, attaching two (**4i**) or three chloro (**4j**) substituents decreased anti-*T. cruzi* activity.

Compound **4l**, carrying a biphenyl group, displayed an activity similar to benznidazole-treated parasites. In practice, the 4-bromophenyl derivative **4h** and biphenyl derivative **4l** are equipotent antitrypanosomal agents. The 4-phenoxy derivative **4m** exhibited a CC₅₀ value of 68.5 μM , being inactive in practice. In comparison to the non-substituted phenyl derivative **4a**, the piperidinyl derivative **4n** was slightly more active. The same was observed when a morpholinyl (**4o**) or a thiomorpholinyl (**4p**) substituent was attached. Overall, **4h** was identified as the most potent cidal agent against trypomastigote, while six other compounds (**4a**, **4g**, **4l**, and **4n–p**) also showed considerable antiparasitic activity (CC₅₀ < 10 μM), but they were less potent than benznidazole.

Next, we analyzed the antiparasitic activity against epimastigotes. Benznidazole, which was used as the reference drug, exhibited an IC₅₀ value of 4.8 μM . In comparison, the nonsubstituted phenyl derivative **4a** was several times less potent (IC₅₀ = 25 μM). The 4-bromo derivative **4h** was very active in inhibiting epimastigote and displayed an IC₅₀ value of 3.9 μM . In fact, this compound was as potent as benznidazole. In contrast, the biphenyl derivative **4l** was active in inhibiting epimastigotes

(IC₅₀ = 11.1 μM) but was only half as potent as benznidazole.

After determining the antiparasitic activity, we evaluated the cytotoxicity in host cells. Saponin was used as the reference drug in this assay, while benznidazole was evaluated to compare the cytotoxicity. As shown in Table 1, compounds **4a–p** were less cytotoxic than saponin. In comparison to benznidazole, only five derivatives **4b**, **4c**, **4n**, **4o**, and **4p** were equally or more cytotoxic, whereas the rest of the derivatives were less cytotoxic. Derivatives **4h** and **4l**, which are the most potent

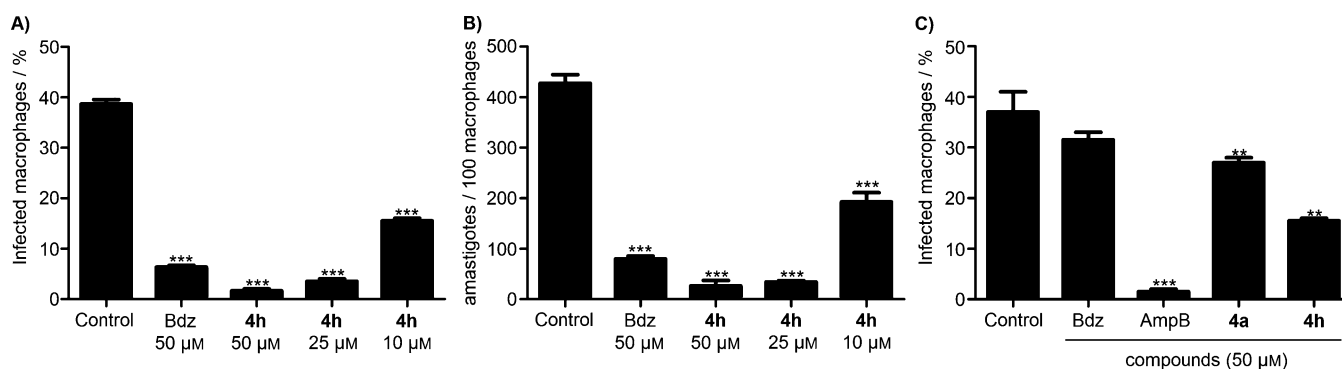


Figure 4. Thiazolidinone **4h** reduces the parasite development and invasion process in host cells. A, B) *T. cruzi*-infected macrophages were treated and incubated for 4 days. A) Infected cells in percent. B) Mean number of intracellular amastigotes per 100 infected macrophages. C) Macrophages were simultaneously exposed to trypomastigotes and treatment. The cell culture was incubated for 2 h, washed and the percent of infected cells was determined after 2 h. Bdz = benznidazole, AmpB = amphotericin B. Data are the mean \pm S.E.M. (error bars) of two independent experiments performed. Panels A and B: ***, $p < 0.001$; panel C: ***, $p < 0.001$; **, $p < 0.01$.

anti-*T. cruzi* compounds among the series, did not exhibit cytotoxicity for splenocytes at concentrations up to 200 μ M.

In vitro infection and selectivity index

After evaluating the antiparasitic activity against the extracellular parasite, we analyzed the activity against the intracellular parasite. In this assay, *T. cruzi*-infected macrophages were treated and incubated for 96 h. Benznidazole was used as a reference drug, and the results are summarized in Figure 4A,B. In comparison to untreated cells, treatment with **4h** reduced the percentage of infected cells ($p < 0.001$) as well as the mean number of intracellular amastigotes per 100 macrophages. Next, we investigated whether **4h** inhibits the *T. cruzi* invasion process in macrophages. To study this, macrophages were infected with trypomastigotes and simultaneously treated. After 2 h, unbound parasites were removed, and the cells were incubated for 2 h. Benznidazole and amphotericin B were used as reference drugs (Figure 4C). In comparison to untreated cells, treatment with **4h** or **4l** reduced the percentage of infected macrophages ($p < 0.01$); however, this reduction was smaller than observed under amphotericin B treatment ($p < 0.001$). In this parasite invasion assay, benznidazole did not show significant activity.

Because the activity of **4h** was concentration-dependent, we determined its IC_{50} value and selectivity index (SI) in the in vitro infection assay (see Table 2). Compound **4h** was twice as potent as benznidazole in reducing the percentage of infected cells. In contrast, **4l** was less potent, exhibiting the same potency as benznidazole. Compound **4h** has an SI value of 44, which is two times higher than the value for **4l** as well as benznidazole.

Cruzain inhibition and docking analysis

To investigate the mechanism of action, compounds were tested against cruzain. The inhibition of cruzain enzymatic activity by all compounds was measured using a competition-based assay with the substrate Z-Phe-Arg-aminomethylcou-

Compd	IC_{50} [μ M] ^[a]	CC_{50} [μ M] ^[b]	SI ^[c]
4h	5.2 \pm 0.54	230.5 \pm 5	44
4l	10.1 \pm 0.09	233.3 \pm 9	23
Bdz	13.9 \pm 0.39	250 \pm 9	18

[a] IC_{50} determined in *T. cruzi*-infected macrophages after incubation for 4 days. [b] CC_{50} determined in mouse splenocytes after incubation for 24 h. Data represent the mean \pm SD of two independent experiments performed in duplicate. [c] Determined as CC_{50}/IC_{50} . Bdz = benznidazole.

marin (Z-FR-AMC).^[33] Initially, compounds were screened at 100 μ M, and only compounds with an inhibition value $> 70\%$ were chosen for IC_{50} value determination (see Table 1). We observed that cruzain activity was not substantially inhibited by the presence of most thiazolidinones, except for derivatives **4n** and **4p**, which showed IC_{50} values of 0.7 \pm 0.4 nM and 4.0 \pm 0.5 nM, respectively.

To define the structural determinants for cruzain inhibition observed for compounds **4n** and **4p**, molecular docking was performed. The binding mode for these ligands was determined by the highest (most positive) score among the possible solutions for each ligand. These calculations were generated according to the Goldscore fitness function. In order to identify the molecular reasons for the two extreme affinities towards the cruzain target, we selected the two most potent compound, (*R*)-**4n** and (*R*)-**4p**, in addition to the weak cruzain inhibitor (*S*)-**4b**. We performed a detailed analysis of the intermolecular interactions observed in the docking solutions, for these molecules. Although the two most potent molecules are very similar to each other, they differ by the replacement of a carbon atom on (*R*)-**4n** for a sulfur atom on (*R*)-**4p**. The difference between the active (*R*)-**4n** and the inactive cruzain inhibitor (*S*)-**4b** is the presence of a 2-pyridinyl instead of a 4-(piperidinyl)phenyl ring, in addition to the inversion of the chiral center. The comparative results can be found in Figure 5.

The difference between the binding modes of (*R*)-**4n** and (*S*)-**4b** is shown in Figure 6 and Table 3. The residues of cruzain,

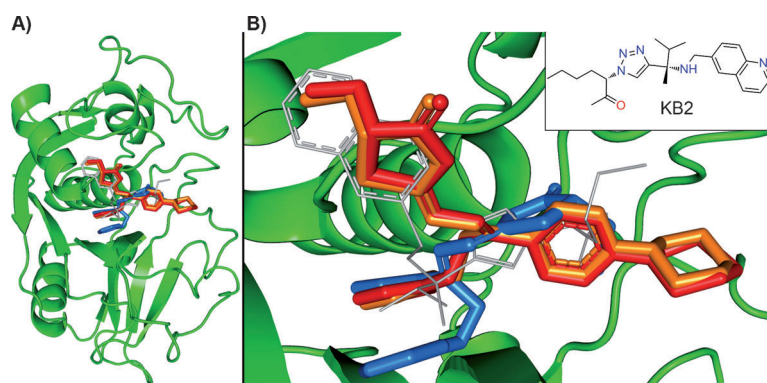


Figure 5. Superimposition of the docking solutions on cruzain for compounds (*R*)-**4n** (orange stick), (*R*)-**4p** (red stick), (*S*)-**4b** (blue stick) and the crystal structure of “KB2” co-crystallized ligand (gray line). A) Full and B) active site view. Inset: chemical structure of KB2.^[13]

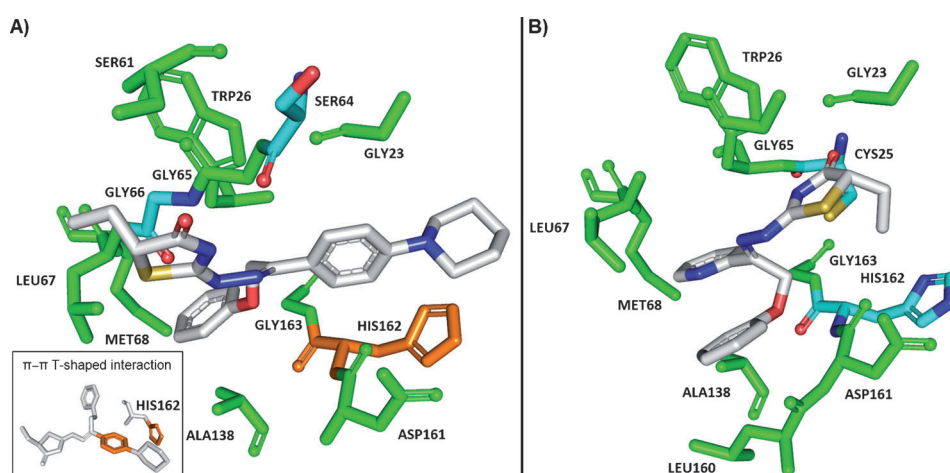


Figure 6. Detailed view of the docking solutions on cruzain, for A) (*R*)-**4n** and B) (*S*)-**4b**. Residues involved in hydrophobic interactions (green), hydrogen bonds (cyan), and π - π T-shaped interactions (orange) are highlighted. A detailed view of the π - π T-shaped interaction (orange) of the HIS162 residue with (*R*)-**4n** is shown in the box.

which participate in hydrophobic interactions, are highlighted in green, whereas those that participate in hydrogen bonds are highlighted in cyan. Finally, the residues involved in π - π T-shaped interactions are highlighted in orange. As shown in Figure 5, the cruzain binding mode for (*R*)-**4n** and (*R*)-**4p** is very similar. Table 3 provides a list of the molecular interactions and shows that the two compounds have many interactions in common. This similarity is also revealed when we analyze the docking score values for (*R*)-**4n** and (*R*)-**4p**, which are 55.39 and 56.48, respectively. In contrast, through comparison with the values for (*R*)-**4n** and (*R*)-**4p**, the lower affinity of (*S*)-**4b** for cruzain can also be identified. The data presented in Table 3 demonstrates that the π - π T-shaped interaction seems to be mainly responsible for the greater stability and the positioning of the complex formed between (*R*)-**4n** or (*R*)-**4p** and cruzain. The docking score calculated for (*S*)-**4b** is lower (49.59) than those calculated for the potent compounds (*R*)-**4n** or (*R*)-**4p**. Therefore, this result indicates that the most potent cruzain inhibitors (*R*)-**4n** and (*R*)-**4p** are also those with the highest

docking scores, demonstrating that the molecules with more stable or positive docking scores (in silico affinity) are the most potent cruzain inhibitors.

Electron microscopy of parasite morphology

We analyzed the *T. cruzi* cellular membranes and organelles following thiazolidinone treatment. In this assay, trypomastigotes were treated with **4h** (4.0 μ M; CC₅₀ value), incubated for 24 h and then cells were analyzed by transmission electron microscopy (TEM). In comparison to untreated parasites, the treatment induced the formation of an atypical dilatation of the Golgi complex and endoplasmic reticulum (ER), as well as some distentions of the ER perinuclear membrane (Figure 7). In addition, treatment produced the formation of numerous and atypical vacuoles within the cytoplasm and in close proximity to the Golgi complex, which is commonly observed within parasite autophagy. In comparison to untreated parasites, no alterations were observed in the kinetoplast and cell nucleus in the treated parasites.

Table 3. Molecular interaction of cruzain with (*R*)-**4n**, (*R*)-**4p** and (*S*)-**4b**.

Residues	Compounds ^[a]		
	(<i>R</i>)- 4n	(<i>R</i>)- 4p	(<i>S</i>)- 4b
Gly 23	HC	HC	HC
Cys 25	-	-	2.4 ^[b]
Trp 26	HC	HC	HC
Ser 61	HC	HC	-
Ser 64	3.1 ^[b]	2.9 ^[b]	-
Gly 65	HC	HC	HC
Gly 66	3.1 ^[b]	3.0 ^[b]	-
Leu 67	HC	HC	HC
Met 68	HC	HC	HC
Ala 138	HC	HC	HC
Leu 160	-	-	HC
Asp 161	HC	HC	HC
His 162	PIT	PIT	2.6 ^[b]
Gly 163	HC	HC	HC
Scores	55.39	56.48	49.59

[a] HC = hydrophobic contacts, PIT = π - π T-shaped interaction. [b] Hydrogen bond distances [Å] between donor and acceptor.

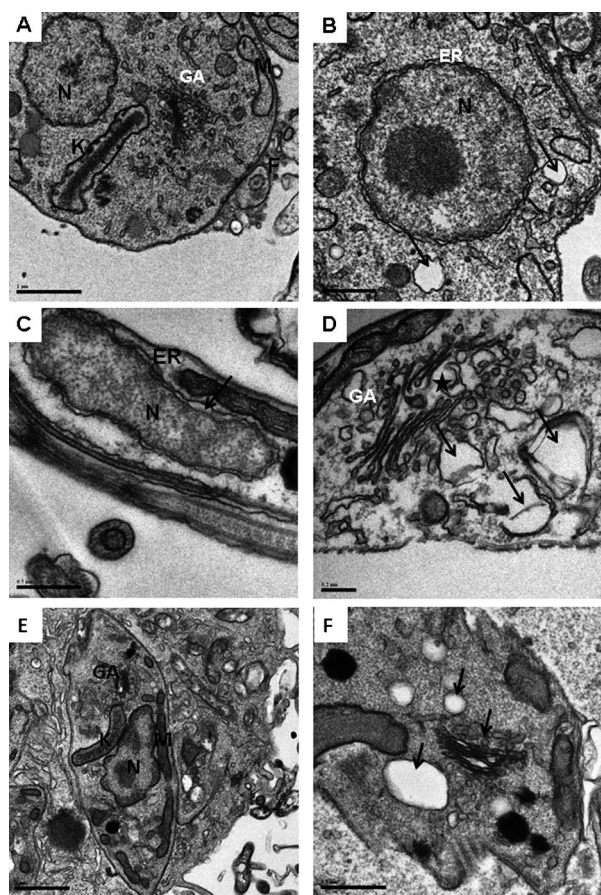


Figure 7. Electron microscopy analysis of parasite morphology. A) Untreated trypomastigotes analyzed by TEM. B–D) Trypomastigotes incubated for 24 h with **4h** (4.0 μm). The formation of atypical vacuoles in the cytoplasm is shown (B). Arrows highlight alterations in the ER membrane (C). Alterations in the Golgi complex is indicated by stars (D). Untreated infected macrophages are observed after 6 h of infection (E). F) Infected macrophages incubated for 6 h with **4h** (5.0 μm). Alterations in the Golgi apparatus and the formation of atypical vacuoles are visible (indicated by arrows). N = nucleus; K = kinetoplast; GA = Golgi apparatus; ER = endoplasmic reticulum. Scale bars: A) 1 μm; B, C) 0.5 μm; D) 0.2 μm; E) 1 μm; F) 0.5 μm.

Next, infected macrophages were analyzed by TEM. In comparison to untreated infected macrophages, thiazolidinone treatment led to the formation of atypical cytosolic vacuoles as well as alterations in the Golgi complex morphology. These results indicate that **4h** is a parasitocidal agent.^[34]

Parasite death process

After ascertaining that **4h** is a parasitocidal agent, the process of parasite death induction was studied more closely. Trypomastigotes were treated with different concentrations of **4h** during 24, 48 and 72 h incubation and then labeled with annexin V and propidium iodide (PI). Experiments were analyzed by flow cytometry (Figure 8). In untreated parasites, most cells were negative for annexin V and PI staining, demonstrating cell viability. In comparison to untreated parasites, a significant and concentration-dependent increase in the number of PI-positive parasites was observed under treatment with **4h**. Treatment

with 12 μm of **4h** for 48 h resulted in 9.56 and 16.2% of parasites positively stained for PI and PI+annexin V, respectively; whereas 1.94% parasite cells were stained only for annexin V. These results indicate that thiazolidinone treatment increases the number of PI staining, which is characteristic of a parasite cell death caused by a necrotic process.

Toxicology in mice

A single-dose toxicological study was carried out for thiazolidinone **4h**. The compound was given orally by gavage in uninfected female BALB/c mice ($n=3/\text{group}$) at the doses of 150, 300 or 600 mg kg⁻¹. Mice were monitored during 14 days. To the tested doses, neither mortality nor gross signs associated to toxicity were observed (data not shown). Doses higher 600 mg kg⁻¹ could not be tested due to the limited solubility of **4h** in 20% DMSO/saline, so the maximum tolerated dose in BALB/c mice was not calculated.

In another experiment, 600 mg kg⁻¹ of **4h** was administered to a group of uninfected mice ($n=6$) and blood samples were collected 24 h after treatment. Fourteen biochemical components of the sera were measured and the levels were compared to the negative control group (receiving vehicle; data are summarized in table S1 of the Supporting Information). In comparison to the negative control, treatment with **4h** altered three biochemical components of the sera ($p<0.05$): alanine aminotransferase, amylase and creatine. Alanine aminotransferase and amylase are biochemical components involved in liver function, suggesting that in this dose, compound **4h** is potentially hepatotoxic. However, between untreated and treated groups, no statistical differences were observed for other analyzed components.

Infection in mice

Given the potent in vitro antiparasitic activity as well as low toxicity in mice, we tested thiazolidinone **4h** in *T. cruzi*-infected mice (acute model). In this assay, Y strain trypomastigotes were inoculated in female BALB/c mice ($n=6/\text{group}$). Five days after infection, mice were treated orally by gavage once a day for five consecutive days. Compound **4h** was administered at a dose of 125 μmol kg⁻¹ (55 mg kg⁻¹) and 250 μmol kg⁻¹ (110 mg kg⁻¹). The positive and negative control groups received benznidazole (250 μmol kg⁻¹, 65 mg kg⁻¹) and 20% DMSO/saline, respectively. Blood parasitemia was analyzed, and the results are shown in Figure 9.

In the negative control group, blood parasitemia was observed after day 6 of parasite inoculation and peaked on day 10. In the positive control group, which received benznidazole, very low blood parasitemia was observed during the experiment, indicating that infection eradication was achieved. In comparison to the negative control group, treatment with **4h** significantly reduced blood parasitemia in all tested doses ($p<0.001$). All infected and treated mice survived and did not show any behavioral alterations until the end of the experiment (data not shown).

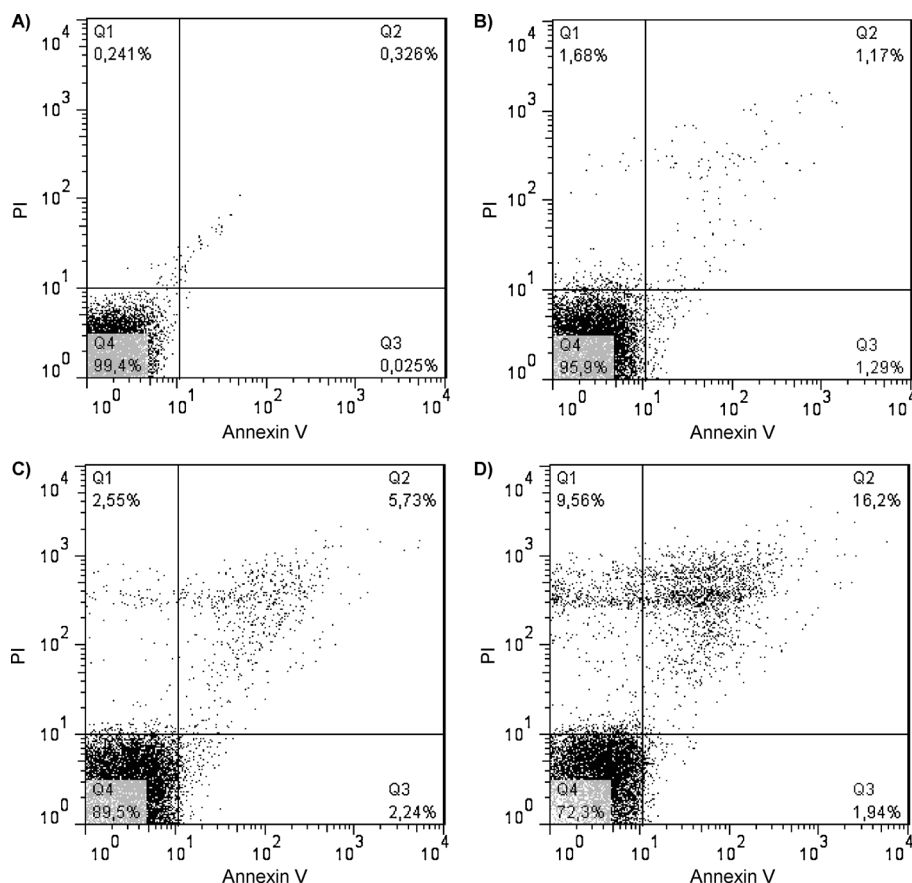


Figure 8. Thiazolidinones cause *T. cruzi* death by a necrotic process. Flow cytometry examination of trypanomastigotes treated with **4h** within 48 h incubation. A) Untreated trypanomastigotes; B) 4.0 μM ; C) 8.0 μM ; D) 12 μM . Two independent experiments were performed. Data are representative of one experiment.

a dose of 250 $\mu\text{mol kg}^{-1}$, 97% of blood parasitemia was reduced ($p < 0.001$).

Drug combination

In another set of experiments, the antiparasitic activity of thiazolidinone **4h** alone and in combination with benznidazole was investigated in the in vitro infection assay. For this assay, compound concentrations were selected based on the IC_{50} values. As shown in Table 5, neither thiazolidinone **4h** nor benznidazole alone were unable to cure the infection in macrophage culture. In contrast, the combination of **4h** plus benznidazole reduced the number of infected macrophages to greater extent than each compound used alone. The combination of the two compounds each at a concentration of 40 μM cured the infection in macrophages. More importantly, this was achieved without affecting host cell viability (data not shown).

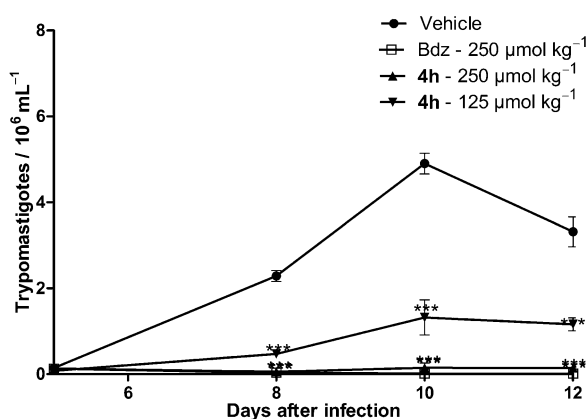


Figure 9. Course of acute infection and response to treatment in *T. cruzi*-infected mice. Female BALB/c mice ($n = 6/\text{group}$) were infected with trypanomastigotes and treated for five consecutive days with thiazolidinone **4h** by oral gavage once a day. Blood parasitemia was monitored by counting the number of trypanomastigotes. One single experiment. Error bars for S.E.M.; significance: ***, $p < 0.001$ compared to untreated (vehicle) group.

The peak parasitemia was employed to calculate the percentage of parasitemia reduction (Table 4). In comparison to the negative control, treatment with **4h** at a dose of 125 $\mu\text{mol/kg}$ reduced blood parasitemia by 75.4% ($p < 0.001$). At

Table 4. Summary of the in vivo antiparasitic activity.

Compd	Dose [$\mu\text{mol kg}^{-1}$]	Blood parasitemia reduction in mice [%] ^[a]	
		8 dpi	10 dpi
4h	125	79.4	75.4
4h	250	97.7	97
Bdz	250	98.6	> 99

[a] Data taken from Figure 9, and values were calculated using the equation (vehicle group – treated group)/vehicle group $\times 100\%$. Dpi = days post-infection; Bdz = benznidazole.

Table 5. Summary of the in vitro antiparasitic activity of the drug combination.

4h [μM]	Bdz [μM]	Cell infection inhibition [%] ^[a]
none	14	49.7
5.5	none	45.2
5.5	14	81.5
11	28	94.9
40	40	100

[a] Determined 4 days after macrophage infection with Y strain trypanomastigotes. Inhibition [%] was determined in comparison to untreated infected cells. Data are from one single experiment. Bdz = benznidazole.

Discussion

There is a need for novel anti-*T. cruzi* drugs. Thiazolidinones are heterocyclic compounds well known for their antiprotozoal activities.^[35–38] After screening the activity of 60 thiazolidinic derivatives, we previously identified a potent anti-*T. cruzi* thiazolidinone (**18**).^[24] This compound selectively inhibited the trypanosomal protease cruzain but not its mammalian homologous cathepsin L. Of note, compound **18** achieved inhibitory property against cruzain without exhibiting nonspecific and promiscuous binding properties, a characteristic observed for thiazolidinones of very low molecular weight.^[39] Moreover, this compound presented low cytotoxicity towards host cells, no apparent toxicity in mice and reduced blood parasitemia in mice when administrated orally. As a limitation, thiazolidinone **18** was less efficient in reducing acute infection than benznidazole. Therefore, compound **18** was used here as a structural prototype for the synthesis of a series of novel thiazolidinones.

The employed structural planning for the design of compounds **4a–p** aimed at causing a disruption in the molecular planarity between the phenoxy group and the thiazolidinic ring. This was achieved by the attachment of an aryl group in the iminic carbon of this class of compounds. As highlighted in Figure 2, this produced derivatives with higher conformational restriction compared with the prototype (**18**). The pharmacological evaluation of compounds **4a–p** confirmed that the disruption of the planarity changed the bioactive profile of this compound class. Importantly, this led to the identification of derivatives with an enhanced antiparasitic activity compared with known thiazolidinones, such as compound **18**.

Regarding the antiparasitic activity for trypomastigotes, we found that the attachment of a phenyl ring produced an active thiazolidinone, which was, however, less potent than benznidazole. Replacing the phenyl with a pyridinyl ring was deleterious for antiparasitic activity, suggesting certain structural requirements for placing an aryl ring at the iminic carbon. In fact, the investigation of substituents attached to the phenyl ring revealed interesting SARs. We found substituents that retained (4-Cl, 4-morpholinyl), enhanced (4-Br, 4-phenyl, 4-thiomorpholinyl) or removed (4-CH₃, 4-CH₃O, 4-F) activity against trypomastigotes in comparison to the nonsubstituted thiazolidinone. Among the substituents that led to an enhanced anti-*T. cruzi* activity, 4-bromo (**4h**) and biphenyl (**4l**) were the most promising in terms of potency and selectivity. These compounds were able to inhibit the proliferation of epimastigotes and were toxic for *T. cruzi* but displayed low cytotoxicity towards host cells. Though compounds **4h** and **4l** both have hydrophobic and bulky substituents, other substituents containing similar properties, such as *tert*-butyl or phenoxy, did not produce active antiparasitic agents. This implies that there are unknown structural requirements involved in **4h** and **4l** that provide the observed antiparasitic activity.

Moreover, we observed that only **4n** (piperidinyl) and **4p** (thiomorpholinyl) inhibited cruzain activity whereas other derivatives did not. The literature describes some diastereoisomers with different cruzain inhibitory properties.^[40] However, the isomeric ratios for **4n** and **4p** are not different from the

rest of the chemical series. Therefore, the observed inhibitory properties for cruzain are likely due to the substituents present in **4n** and **4p**. For compounds **4n** and **4p**, the attachment of a piperidinyl or thiomorpholinyl produced compounds with inhibitory property against cruzain; however, this was abolished when a morpholinyl substituent was attached. In fact, cruzain docking of **4n** showed that the piperidinyl group is oriented in a hydrophobic pocket with the participation of π - π T-shaped interactions. The same is not observed for compounds **4b** and **4o**, which explains their lack of inhibitory activity against cruzain.

Compound **4h** was selected as an anti-*T. cruzi* lead compound because it exhibited the highest selectivity among the thiazolidinones studied here. Under **4h** treatment, in vitro parasite development and invasion in host cells was substantially reduced. This activity was more pronounced even than that observed with benznidazole-treated parasites. Moreover, the treatment with this compound caused alterations in the Golgi apparatus and the ER morphology of *T. cruzi*, whereas little or no effects were observed in the kinetoplast and cell nucleus morphology. Therefore, this compound exerts its antiparasitic activity by altering organelle morphology, which ultimately destroys parasite cells, similar to the mode of action of a parasitocidal agent. In agreement to this, we observed that **4h** caused parasite cell death through a necrotic process.

With regard to the activity in infected mice during the acute phase, **4h** reduced the blood parasitemia in a dose-dependent manner and exhibited a potency similarly to that observed in benznidazole-receiving mice. When compared to untreated infected mice, thiazolidinone **4h** reduced 97% of blood parasitemia, while at the same dose, the reduction observed for the previously reported thiazolidinone **18** was 89%.^[24] Therefore, a potency enhancement of the in vivo antiparasitic activity was achieved from the first-generation thiazolidinone **18** to the new generation described here (**4h**). Regarding toxicity in mice, **4h** was not lethal in doses up to 600 mg kg⁻¹, which is several times higher than the dose used to reduce blood parasitemia. Altogether, these results reinforced the notion that thiazolidinone **4h** is a selective anti-*T. cruzi* agent. A pharmacokinetic analysis as well as identification of its mechanism of action should be determined in the course of further investigation. However, our preliminary results already show that the combination of thiazolidinone **4h** plus benznidazole is additive in reducing in vitro *T. cruzi* infection. This finding indicates that thiazolidinone **4h** could be a suitable partner for anti-Chagas drug combinations. This is an important parameter for new anti-Chagas drug candidates, since an effective treatment will likely contain a drug combination to improve the efficacy of the treatment and to reduce the chance of developing parasite resistance.^[41]

Conclusions

Thiazolidinones are a family of well-known antiparasitic compounds. Here, we prepared a series of new thiazolidinones **4a–p**, which were designed to be potential anti-*Trypanosoma cruzi* compounds targeting the trypanosomal protease cruzain. In

fact, we found these compounds are antiparasitic agents and have a high degree of selectivity. Our structure–activity relationship (SAR) studies revealed structural determinants for antiparasitic activity and led to the identification of thiazolidinone derivatives, which displayed similar potencies to benznidazole. Specifically, we demonstrated that thiazolidinone **4h** has strong antiparasitic activity, low cytotoxicity toward host cells and achieves its anti-*T. cruzi* activity as a parasitocidal agent. Most thiazolidinones, including active compound **4h**, did not inhibit cruzain activity, but these compounds affected the Golgi apparatus as well as ER morphology and produced atypical cytosolic vacuoles, which ultimately is followed by a necrotic parasite cell death. Consistent with in vitro antiparasitic activity, thiazolidinone **4h** reduced parasitemia in a mice model of acute infection. Importantly, this compound displayed low toxicity in mice and exhibited additive antiparasitic activity when combined with benznidazole.

Experimental Section

Chemistry

Synthetic protocols and spectral data for compounds are described in the Supporting Information.

Docking

The structures of all compounds were obtained by application of the RM1 method,^[42] available as part of the SPARTAN 08' program,^[43] using internal default settings for convergence criteria. Some of these new molecules were synthesized as racemic mixtures; therefore, the molecular modeling treated the two isomers (*R* and *S*) independently, when appropriate, and the docking procedure used both isomers for each compound. Docking calculations and analysis were carried using the structure of *T. cruzi* cruzain (PDBID: 3IUT) as the target, which is composed of a co-crystallized complex with inhibitor (referred as "KB2").^[13] The active site was defined as all atoms within a radius of 6.0 Å from the co-crystallized ligand. Residues Gln19, Cys25, Ser61, Leu67, Met68, Asn70, Asp161, His162, Trp184 and Glu208 were treated as flexible during the calculations, using a conformation library for each one. The GOLD 5.1 program^[44] was used for docking calculations, followed by Binana program,^[45] which was used to analyze the molecular interactions present in the best docking solutions, using default setting, except for hydrogen bond distance, which was changed to a maximum of 3.5 Å. Figures were generated with Pymol (version 1.3r1 edu).^[46]

Biology

Animals: Female BALB/c mice, aged 6–8 weeks, were supplied by the animal house of Centro de Pesquisas Gonçalo Moniz (Fundação Oswaldo Cruz, Bahia, Brazil) and Centro de Pesquisas Aggeu Magalhães (Fundação Oswaldo Cruz, Pernambuco, Brazil). Mice were maintained in sterilized cages under a controlled environment, receiving a balanced diet for rodents and water ad libitum. All experiments were carried out in accordance with the recommendations of ethical guidelines and were approved by the local Animal Ethics Committee.

Cell culture: Epimastigotes of a Dm28c strain (discrete typing unit I) were maintained at 26 °C in liver infusion tryptose (LIT) medium (Life Technologies, Carlsbad, CA, USA) supplemented with 10% fetal bovine serum (FBS, Life Technologies), 1% hemin (Sigma–Aldrich, St. Louis, MO, USA), 1% R9 medium (Sigma–Aldrich), and 50 µg mL⁻¹ gentamycin (Novafarma, Anápolis, GO, Brazil). Metacyclic trypomastigotes of Y strain (discrete typing unit II) were obtained from the supernatant of infected LLC-MK2 cells and maintained in RPMI-1640 medium (Sigma–Aldrich) supplemented with 10% FBS and 50 µg mL⁻¹ gentamycin at 37 °C and 5% CO₂. Splenocytes were collected from BALB/c mice and cultivated in RPMI-1640 medium supplemented with 10% FBS and 50 µg mL⁻¹ gentamycin. Peritoneal exudate macrophages were elicited by intraperitoneal injection of sodium thioglycollate in BALB/c mouse.

Cytotoxicity in splenocytes: Splenocytes of BALB/c mice (200 µL) were placed into 96-well plates at 5 × 10⁶ cells/well. Compounds were added in a serial dilution (1.1, 3.3, 11, 33 and 100 µg mL⁻¹) in triplicate. To each well, an aliquot of compound suspended in dimethyl sulfoxide (DMSO) was added. Negative (untreated) and positive (saponin, Sigma–Aldrich) controls were measured in each plate, which was incubated for 24 h at 37 °C and 5% CO₂. After incubation, [³H]-thymidine (1.0 µCi mL⁻¹, PerkinElmer, Waltham, MA, USA) was added to each well, and the plate was returned to the incubator. Cells were then transferred to a filter paper using a cell harvester and measured using a liquid scintillation counter (WALLAC 1209, Rackbeta Pharmacia, Stockholm, Sweden). [³H]-Thymidine incorporation [%] was measured, and the highest noncytotoxic concentration was determined using triplicates.

Antiproliferative activity for epimastigotes: Epimastigotes were counted in a hemocytometer, and 200 µL were dispensed into 96-well plates at 10⁶ cells/well. Compounds were added in a serial dilution (1.1, 3.3, 11, 33 and 100 µg mL⁻¹) in triplicate. The plate was incubated for 5 days at 26 °C, and aliquots of each well were collected for counting the number of viable parasites using a Neubauer chamber. The percentage of inhibition was calculated in relation to untreated cultures. IC₅₀ values were calculated using nonlinear regression on Prism 4.0 (GraphPad). Results are from one single experiment.

Toxicity for trypomastigotes: Trypomastigotes were collected from the supernatant of LLC-MK2 cells, and 200 µL were aliquoted into 96-well plate in an axenic media at 4 × 10⁵ cells/well. Compounds were added in a serial dilution (1.1, 3.3, 11, 33 and 100 µg mL⁻¹) in triplicate. The plate was incubated for 24 h at 37 °C and 5% of CO₂. Aliquots of each well were collected, and the number of viable parasites, based on parasite motility, was counted in a Neubauer chamber. The percentage of inhibition was calculated in relation to untreated cultures. CC₅₀ calculation was also carried out using nonlinear regression with Prism 4.0 (GraphPad). Two independent experiments were performed.

Intracellular parasite development: Macrophages were seeded at 2 × 10⁵ cells/well for 24 h in a 24-well plate with rounded coverslips on the bottom in RPMI-1640 medium supplemented with 10% FBS. Macrophages were infected with trypomastigotes at a ratio of 10 parasites per macrophage for 2 h. Unbound trypomastigotes were removed by successive washes with saline. Each compound was dissolved in 5% DMSO and saline in a serial dilution, in triplicate. Compounds remained on the cell culture for 6 h prior to removal and addition of fresh media. The plate was incubated for 4 days at 37 °C and 5% CO₂. Cells were fixed in MeOH, stained with Giemsa and manual counting of at least 100 cells per slide was done using an optical microscope (Model CX41, Olympus, Tokyo, Japan). The

percentages of infected macrophages and mean numbers of amastigotes per 100 infected macrophages were determined. To calculate IC_{50} values, the percentage of infected macrophages in comparison to untreated infected macrophages was used.

Drug combination evaluation: The combination of thiazolidinone **4h** plus benznidazole was evaluated in the in vitro infection assay (described above). To this end, compounds were tested in the same concentration of their IC_{50} values as well as in higher concentrations.

Parasite invasion: Macrophages (10^5 cells mL^{-1}) were plated onto 13 mm glass coverslips in a 24-well plate and maintained for 24 h. Y strain trypomastigotes were added at 10^7 cells mL^{-1} , followed by addition of compound **4h**. Amphotericin B (Fungizone, Life Technologies) and benznidazole (Lafepe, Recife, PE, Brazil) were used as reference compounds. The plate was incubated for 2 h at $37^\circ C$ and 5% CO_2 . Unbound parasites were then removed by successive washes with saline, and the RPMI medium was replaced. After 2 h of incubation, the number of infected cells was counted by optical microscopy using standard Giemsa staining.

Inhibition of cruzain activity: Recombinant cruzain was kindly provided by Dr. Anna Tochowicz and Dr. James H. McKerrow from the University of California, San Francisco (CA, USA). Cruzain activity was measured by monitoring the cleavage of the fluorogenic substrate Z-Phe-Arg-aminomethylcoumarin (Z-FR-AMC, Sigma-Aldrich) using a Synergy 2 microplate reader (Biotek) from the Center of Flow Cytometry and Fluorimetry in the Biochemistry and Immunology Department (UFMG, Brazil) with filters for $\lambda = 340$ nm (excitation) and $\lambda = 440$ nm (emission). All assays were performed in 0.1 M NaOAc (pH 5.5) and in the presence of 5 mM dithiothreitol. The final concentration of cruzain was 0.5 nM, and the substrate concentration was 2.5 μM ($K_m = 1.0 \mu M$). Assays were conducted in presence of 0.01% Triton X-100. Compounds were screened at 100 μM , after pre-incubation for 10 min with the enzyme prior to the addition of Z-FR-AMC. In all assays, fluorescence was monitored for 5 min after addition of the substrate and activity was calculated in relation to DMSO control. If the cruzain inhibition was higher than 70% at 100 μM , IC_{50} values were determined by using at least seven inhibitor concentrations. Each compound concentration was tested in triplicate and data were analyzed with Prism 5.0 (GraphPad).

Electron microscopy analysis: Trypomastigotes (3×10^7 cells mL^{-1}) were treated with **4h** (4.0 μM) for 24 h. Parasites were fixed in 2% formaldehyde and 2.5% glutaraldehyde (Electron Microscopy Sciences, Philadelphia, PA, USA) in sodium cacodylate buffer (0.1 M, pH 7.2) for 1 h at RT, washed $3 \times$ with sodium cacodylate buffer (0.1 M, pH 7.2), and post-fixed with a 1% solution of osmium tetroxide (Sigma-Aldrich) for 1 h. After dehydration with acetone, trypomastigotes were embedded in Poly/Bed (PolyScience, Dallas, TX, USA), sectioned, stained with uranyl acetate and lead citrate and analyzed using a JEOL TEM-1230 transmission electron microscope (Acworth, GA, USA). Mouse macrophages were infected with Y strain trypomastigotes. Cell cultures were washed with saline to remove unbound parasites, followed by the addition of **4h** (5.0 μM) and incubation for 6 h at RT. Cell cultures were processed as described above for collecting TEM images.

Flow cytometry analysis: Trypomastigotes (10^7 cells mL^{-1}) were treated with **4h** (4.0, 8.0 and 12 μM) and incubated for 72 h at $37^\circ C$. Aliquots were collected in the intervals of 24–72 h and incubated for 45 min with propidium iodide (PI) and annexin V using the annexin V-FITC apoptosis detection kit (BioLegend, San Diego, CA, USA) according to the manufacturer instructions. Data acquisi-

tion and analyses were performed using FACS Calibur flow cytometer (Becton Dickinson, San Jose, CA, USA) and FlowJo software (Tree Star, Ashland, OR, USA), respectively. A total of 20000 events were acquired. Two independent experiments were performed.

Acute toxicity in mice: Uninfected BALB/c mice (female, 7–9 weeks old) were randomly divided in groups ($n = 3$). Oral administration of **4h** was given by gavage in one single dose of 150, 300 or 600 $mg\ kg^{-1}$ in 20% DMSO/saline as vehicle. After treatment, survival was monitored for 14 days. The same experiment was repeated using $n = 6$ per group. Heparinized blood samples were collected 24 h after treatment for biochemical analysis of serum components. Readings were performed in an Analyst platform (Hemagen Diagnostics, Colombia, MD, USA) for 16 biochemical components. Biochemical readings were compared to negative control (received vehicle only).

Infection in mice: BALB/c mice (female, 6–8 weeks old) were infected with bloodstream trypomastigotes (Y strain) by intraperitoneal injection of 10^4 parasites in 100 μL of saline solution. Mice were randomly divided in groups ($n = 6$ per group). After day 5 of post-infection, treatment with **4h** was given orally by gavage once a day for five consecutive days. For the positive control group, benznidazole was given orally. As recommended by standard protocols, infection was monitored daily by counting the number of motile parasites in 5 μL of fresh blood sample drawn from the lateral tail vein.^[47] Mortality was recorded daily until day 30 after the end of treatment.

Statistical analysis: To determine the statistical significance of each group in the in vitro and in vivo experiments, the one-way ANOVA test and the Bonferroni for multiple comparisons were used. A p value < 0.05 was considered significant.

Supporting Information

Please see the Supporting Information for synthetic protocols, spectral data for compounds and a table with toxicological results. CCDC 936127 contains the supplementary crystallographic data (**4q**) of this paper. These data can be obtained free of charge from The Cambridge Crystallographic Data Centre (Cambridge, UK) via www.ccdc.cam.ac.uk.

Acknowledgements

This study was supported by the Brazilian agencies Fundação de Amparo à Pesquisa do Estado da Bahia (FAPESB, Brazil), Conselho Nacional de Desenvolvimento Científico e Tecnológico (CNPq, Brazil), Fundação de Amparo à Pesquisa do estado de Minas Gerais (FAPEMIG, Brazil) and the European Union consortium ChemBioFight. A.C.L.L., M.B.P.S., C.A.S. and M.Z.H. are CNPq fellows. D.R.M.M. and C.S.M. hold a FAPESB scholarship. We thank the Physics Institute, University of Sao Paulo (Brazil) for allowing the use of the diffractometer and the Mass Spectrometry Unit of the Centro de Pesquisas Gonçalo Moniz (CPqGM). The authors acknowledge Dr. Phillippe J. Eugster (University of Lausanne, Switzerland) for recording mass spectra and Dr. Kyan J. Allahdadi (Hospital São Rafael, Brazil) for proofreading the manuscript. R.S.F. is thankful to Dr. Anna Tochowicz (University of California, San Francisco (UCSF), USA) for providing recombinant cruzain.

Keywords: antiprotozoal agents · biological activity · hydrazones · medicinal chemistry · thiazolidinones · *Trypanosoma cruzi*

- [1] J. A. Urbina, *Clin. Infect. Dis.* **2009**, *49*, 1685–1687.
- [2] M. P. Barrett, R. J. Burchmore, A. Stich, J. O. Lazzari, A. C. Frasch, J. J. Cazzulo, S. Krishna, *Lancet* **2003**, *362*, 1469–1480.
- [3] A. Rassi, A. Rassi, Jr., J. A. Marin-Neto, *Lancet* **2010**, *375*, 1388–1402.
- [4] F. S. Machado, L. A. Jelicks, L. V. Kirchoff, J. Shirani, F. Nagajyothi, S. Mukherjee, R. Nelson, C. M. Coyle, D. C. Spray, A. C. de Carvalho, F. Guan, C. M. Prado, M. P. Lisanti, L. M. Weiss, S. P. Montgomery, H. B. Tanowitz, *Cardiol. Rev.* **2012**, *20*, 53–65.
- [5] S. Gupta, X. Wan, M. P. Zago, V. C. Sellers, T. S. Silva, D. Assiah, M. Dhiman, S. Nuñez, J. R. Petersen, J. C. Vázquez-Chagoyán, J. G. Estrada-Franco, N. J. Garg, *PLoS Neglected Trop. Dis.* **2013**, *7*, e2018.
- [6] M. B. P. Soares, R. S. Lima, B. S. F. Souza, J. F. Vasconcelos, L. L. Rocha, R. R. Dos Santos, S. Iacobs, R. C. Goldenberg, M. P. Lisanti, D. A. Iacobs, H. B. Tanowitz, D. C. Spray, A. C. Campos de Carvalho, *Cell Cycle* **2011**, *10*, 1448–1455.
- [7] S. G. Macambira, J. F. Vasconcelos, C. R. Costa, W. Klein, R. S. Lima, P. Guimarães, D. T. Vidal, L. C. Mendez, R. Ribeiro-Dos-Santos, M. B. P. Soares, *FASEB J.* **2009**, *23*, 3843–3850.
- [8] R. A. Cutrullis, T. J. Poklépovich, M. Postan, H. L. Freilij, P. B. Petray, *Int. Immunopharmacol.* **2011**, *11*, 1024–1031.
- [9] J. M. Kraus, H. B. Tatipaka, A. S. McGuffin, N. K. Chennamaneni, M. Karimi, J. Arif, C. L. Verlinde, F. S. Buckner, M. H. Gelb, *J. Med. Chem.* **2010**, *53*, 3887–3898.
- [10] A. Gerpe, G. Alvarez, D. Benítez, L. Boiani, M. Quiroga, P. Hernández, M. Sortino, S. Zacchino, M. González, H. Cerecetto, *Bioorg. Med. Chem.* **2009**, *17*, 7500–7509.
- [11] S. P. Fricker, R. M. Mosi, B. R. Cameron, I. Baird, Y. Zhu, V. Anastassov, J. Cox, P. S. Doyle, E. Hansell, G. Lau, J. Langille, M. Olsen, L. Qin, R. Skerlj, R. S. Wong, Z. Santucci, J. H. McKerrrow, *J. Inorg. Biochem.* **2008**, *102*, 1839–1845.
- [12] M. E. Caputto, A. Ciccarelli, F. Frank, A. G. Moglioni, G. Y. Moltrasio, D. Vega, E. Lombardo, L. M. Finkielstein, *Eur. J. Med. Chem.* **2012**, *55*, 155–163.
- [13] K. Brak, I. D. Kerr, K. T. Barrett, N. Fuchi, M. Debnath, K. Ang, J. C. Engel, J. H. McKerrrow, P. S. Doyle, L. S. Brinen, J. A. Ellman, *J. Med. Chem.* **2010**, *53*, 1763–1773.
- [14] P. S. Doyle, C. K. Chen, J. B. Johnston, S. D. Hopkins, S. S. Leung, M. P. Jacobson, J. C. Engel, J. H. McKerrrow, L. M. Podust, *Antimicrob. Agents Chemother.* **2010**, *54*, 2480–2488.
- [15] F. S. Buckner, M. T. Bahia, P. K. Suryadevara, K. L. White, D. M. Shackelford, N. K. Chennamaneni, M. A. Hulverson, J. U. Laydbak, E. Chatelain, I. Scandale, C. L. Verlinde, S. A. Charman, G. I. Lepesheva, M. H. Gelb, *Antimicrob. Agents Chemother.* **2012**, *56*, 4914–4921.
- [16] F. Villalta, M. C. Dobish, P. N. Nde, Y. Y. Kleshchenko, T. Y. Hargrove, C. A. Johnson, M. R. Waterman, J. N. Johnston, G. I. Lepesheva, *J. Infect. Dis.* **2013**, *208*, 504–511.
- [17] X. Du, C. Guo, E. Hansell, P. S. Doyle, C. R. Caffrey, T. P. Holler, J. H. McKerrrow, F. E. Cohen, *J. Med. Chem.* **2002**, *45*, 2695–2707.
- [18] D. C. Greenbaum, Z. Mackey, E. Hansell, P. Doyle, J. Gut, C. R. Caffrey, J. Lehrman, P. J. Rosenthal, J. H. McKerrrow, K. Chibale, *J. Med. Chem.* **2004**, *47*, 3212–3219.
- [19] A. C. L. Leite, R. S. de Lima, D. R. M. Moreira, M. V. O. Cardoso, A. C. G. Brito, L. M. F. Santos, M. Z. Hernandez, A. C. Kiperstok, R. S. de Lima, M. B. P. Soares, *Bioorg. Med. Chem.* **2006**, *14*, 3749–3457.
- [20] J. M. dos Santos Filho, A. C. L. Leite, B. G. de Oliveira, D. R. M. Moreira, M. S. Lima, M. B. P. Soares, L. F. C. C. Leite, *Bioorg. Med. Chem.* **2009**, *17*, 6682–6891.
- [21] J. M. dos Santos Filho, D. R. M. Moreira, C. A. de Simone, R. S. Ferreira, J. H. McKerrrow, C. S. Meira, E. T. Guimarães, M. B. P. Soares, *Bioorg. Med. Chem.* **2012**, *20*, 6423–6433.
- [22] A. C. L. Leite, D. R. M. Moreira, M. V. O. Cardoso, M. Z. Hernandez, V. R. A. Pereira, R. O. Silva, A. C. Kiperstok, M. S. Lima, M. B. P. Soares, *ChemMedChem* **2007**, *2*, 1339–1345.
- [23] M. Z. Hernandez, M. M. Rabello, A. C. L. Leite, M. V. O. Cardoso, D. R. M. Moreira, D. J. Brondani, C. A. Simone, L. C. Reis, M. A. Souza, V. R. A. Pereira, R. S. Ferreira, J. H. McKerrrow, *Bioorg. Med. Chem.* **2010**, *18*, 7826–7835.
- [24] D. R. M. Moreira, S. P. Costa, M. Z. Hernandez, M. M. Rabello, G. B. O. Filho, C. M. de Melo, L. F. da Rocha, C. A. de Simone, R. S. Ferreira, J. R. Fradico, C. S. Meira, E. T. Guimarães, R. M. Srivastava, V. R. A. Pereira, M. B. P. Soares, A. C. L. Leite, *J. Med. Chem.* **2012**, *55*, 10918–10936.
- [25] C. L. Donnici, M. H. Araújo, H. S. Oliveira, D. R. M. Moreira, V. R. A. Pereira, M. A. Souza, M. C. Castro, A. C. L. Leite, *Bioorg. Med. Chem.* **2009**, *17*, 5038–5043.
- [26] M. Ishikawa, Y. Hashimoto, *J. Med. Chem.* **2011**, *54*, 1539–1554.
- [27] E. J. Barreiro, A. E. Kümmerle, C. A. M. Fraga, *Chem. Rev.* **2011**, *111*, 5215–5246.
- [28] Ö. Ö. Güven, *ARKIVOC* **2007**, 142–147.
- [29] G. M. Allan, N. Vicker, H. R. Lawrence, H. J. Tutill, J. M. Day, M. Huchet, E. Ferrandis, M. J. Reed, A. Purohit, B. V. Potter, *Bioorg. Med. Chem.* **2008**, *16*, 4438–4456.
- [30] P. Vicini, A. Geronikaki, K. Anastasia, M. Incerti, F. Zani, *Bioorg. Med. Chem.* **2006**, *14*, 3859–3864.
- [31] M. H. Bolli, S. Abele, C. Binkert, R. Bravo, S. Buchmann, D. Bur, J. Gatzfeld, P. Hess, C. Kohl, C. Mangold, B. Mathys, K. Menyhart, C. Müller, O. Naylor, M. Scherz, G. Schmidt, V. Sippel, B. Steiner, D. Strasser, A. Treiber, T. Weller, *J. Med. Chem.* **2010**, *53*, 4198–4211.
- [32] A. P. Liesen, T. M. de Aquino, C. S. Carvalho, V. T. Lima, J. M. de Araújo, J. G. de Lima, A. R. de Faria, E. J. de Melo, A. J. Alves, E. W. Alves, A. Q. Alves, A. J. S. Góes, *Eur. J. Med. Chem.* **2010**, *45*, 3685–3691.
- [33] R. S. Ferreira, C. Bryant, K. K. Ang, J. H. McKerrrow, B. K. Shoichet, A. R. Renslo, *J. Med. Chem.* **2009**, *52*, 5005–5058.
- [34] M. A. Vannier-Santos, S. L. De Castro, *Curr. Drug Targets* **2009**, *10*, 246–260.
- [35] C. Pizzo, C. Saiz, A. Talevi, L. Gavernet, P. Palestro, C. Bellera, L. B. Blanch, D. Benítez, J. J. Cazzulo, A. Chidichimo, P. Wipf, S. G. Mahler, *Chem. Biol. Drug Des.* **2011**, *77*, 166–177.
- [36] H. E. Cummings, J. Barbi, P. Reville, S. Oghumu, N. Zorko, A. Sarkar, T. L. Keiser, B. Lu, T. Rückle, S. Varikuti, C. Lezama-Davila, M. D. Wewers, C. Whitacre, D. Radzioch, C. Rommel, S. Seveau, A. R. Satskar, *Proc. Natl. Acad. Sci. USA* **2012**, *109*, 1251–1256.
- [37] N. Zelisko, D. Atamanyuk, O. Vasylenko, P. Grellier, R. Lesyk, *Bioorg. Med. Chem. Lett.* **2012**, *22*, 7071–7074.
- [38] T. L. de B. Moreira, A. F. S. Barbosa, P. Veiga-Santos, C. Henriques, A. Henriques-Pons, S. L. Galdino, M. C. de Lima, I. R. Pitta, W. de Souza, T. M. de Carvalho, *Int. J. Antimicrob. Agents* **2013**, *41*, 183–187.
- [39] T. Mendgen, C. Steuer, C. D. Klein, *J. Med. Chem.* **2012**, *55*, 743–753.
- [40] N. C. Romeiro, G. Aguirre, P. Hernández, M. González, H. Cerecetto, I. Aldana, S. Pérez-Silanes, A. Monge, E. J. Barreiro, L. M. Lima, *Bioorg. Med. Chem.* **2009**, *17*, 641–652.
- [41] S. Cengic, N. Coltel, C. Truyens, Y. Carlier, *Int. J. Antimicrob. Agents* **2012**, *40*, 527–532.
- [42] G. B. Rocha, R. O. Freire, A. M. Simas, J. J. Stewart, *J. Comput. Chem.* **2006**, *27*, 1101–1111.
- [43] Spartan '08 Tutorial and User's Guide; Wavefunction: Irvine, CA, **2008**: <http://www.wavefun.com/products/spartan.html> (accessed: August 2013).
- [44] Gold software, version 5.1, Cambridge Crystallographic Data Centre: <http://www.ccdc.cam.ac.uk> (accessed: August 2013).
- [45] J. D. Durrant, J. A. Mccammon, *J. Mol. Graphics Modell.* **2011**, *29*, 888–893.
- [46] W. L. DeLano. The PyMOL Molecular Graphics System, DeLano Scientific, San Carlos, CA, **2002**: <http://www.pymol.org> (accessed: August 2013).
- [47] A. J. Romanha, S. L. Castro, M. N. Soeiro, J. Lannes-Vieira, I. Ribeiro, A. Talvani, B. Bourdin, B. Blum, B. Olivieri, C. Zani, C. Spadafora, E. Chiari, E. Chatelain, G. Chaves, J. E. Calzada, J. M. Bustamante, L. H. Freitas-Junior, L. I. Romero, M. T. Bahia, M. Lotrowska, M. B. Soares, S. G. Andrade, T. Armstrong, W. Degraive, Z. A. Andrade, *Mem. Inst. Oswaldo Cruz* **2010**, *105*, 233–238.

Received: September 4, 2013

Published online on November 7, 2013